Shedding light on kidney electrolyte physiology: Na^+, Ca^{2+}, and Mg^{2+} in health and disease

Chao Ma

Shedding light on kidney electrolyte physiology: Na^+, Ca^{2+}, and Mg^{2+} in health and disease

Chao Ma

The research presented in this thesis was performed at the department of Physiology, Radboud Institute for Molecular Life Sciences (RIMLS), Radboud university medical center (Radboudumc), The Netherlands. The works in the thesis were financially supported by the RIMLS.

ISBN: 978-94-6421-107-8
Print: Ipskamp Printing, Enschede
Design: Douwe Oppewal, www.oppewal.nl

Shedding light on kidney electrolyte physiology: Na^{+}, Ca^{2+}, and Mg^{2+} in health and disease

Proefschrift

ter verkrijging van de graad van doctor
aan de Radboud Universiteit Nijmegen
op het gezag van de Rector Magnificus prof. dr.,
volgens besluit van het College van decanen
in het openbaar te verdedigen op vrijdag 11 december 2020
om 16.30 uur precies

door

Chao Ma
geboren op 17 oktober 1988
te Jilin, China

Promotor
Prof. dr. J.G.J. Hoenderop

Copromotoren
Dr. J.H.F. de Baaij
Dr. J.A.J van der Wijst

Manuscriptcommissie
Prof. dr. J. van der Vlag
Dr. J. Zhou
Prof. dr. M.G. Vervloet (UMC Amsterdam)

"Everything has beauty, but not everyone sees it"

Confucius (551-479 B.C.)

Table of contents

1

An introduction to Na^+, Ca^{2+}, and Mg^{2+} in health and disease

Tour along the nephron

The kidney controls body fluid volume and osmolality

Sodium (Na^+), calcium (Ca^{2+}) and magnesium (Mg^{2+}) play crucial roles in the normal functioning of cells and organs [1-3]. Careful maintenance and regular monitoring of these electrolyte levels is essential for proper function of cells. Na^+, Ca^{2+} and Mg^{2+} balances are tightly maintained by regulating their absorption in the intestine, exchange from bone, and reabsorption and secretion by the kidneys [4-6].

The functional unit of the kidney is the nephron, which consists of the corpuscle and tubule [7]. A renal corpuscle functions as the blood-filtering component and is build up by the glomerulus and Bowman's capsule [8]. Small molecules, water, and metabolic waste can be filtered through the glomerulus, but large molecules like proteins (>45 kDa) will remain in the blood. The filtrate flows through the renal tubule where electrolytes will be reabsorbed or secreted. Nearly 97% of the filtered Na^+, Ca^{2+} and Mg^{2+} will be reabsorbed along the nephrons. They consist of several distinct functional and anatomical parts where all of the Na^+, Ca^{2+} and Mg^{2+} reabsorption take place: the proximal tubule (PT); the thick ascending limb of loop of Henle (TAL); the distal convoluted tubule (DCT); the connecting tubule (CNT), and collecting duct (CD) (Figure 1).

Segments along the nephron

The proximal tubule

The PT is the first segment of the nephron and is also the major site for Na^+ and Ca^{2+} reabsorption [9, 10]. It is divided into three parts, S1, S2 and S3. In the early PT (S1 and S2), large amounts of filtered amino acids, phosphate, glucose, lactate, and citrate will be reabsorbed [11, 12]. Approximately 65% of the Na^+ will be reabsorbed in the PT, mainly through passive paracellular or active transcellular pathways [13]. The sodium-glucose transporter (SGLT), sodium-dependent phosphate cotransport protein (NaPi-2a) and sodium–hydrogen exchanger 3 (NHE3) are the predominant apical transporters that are responsible for the transport of Na^+ in the PT [14-18]. The intracellular Na^+ concentration must be kept low to facilitate Na^+-coupled co-transport. The basolateral sodium/potassium ATPase (Na^+/K^+-ATPase) pumps three Na^+ ions out of the cell and transports two K^+ ions back into the cell [19]. Nearly 60-70% of the filtered Ca^{2+} will also be reabsorbed in the PT [20]. Na^+ reabsorption coincides with passive water reabsorption. The Na^+-driven water movement can increase the concentration of Ca^{2+} in the lumen, which will drive passive Ca^{2+} diffusion through the tight junctions of epithelial cells into the renal interstitium. Only 10-25% of filtered Mg^{2+} is reclaimed in the PT [21] (Figure 1).

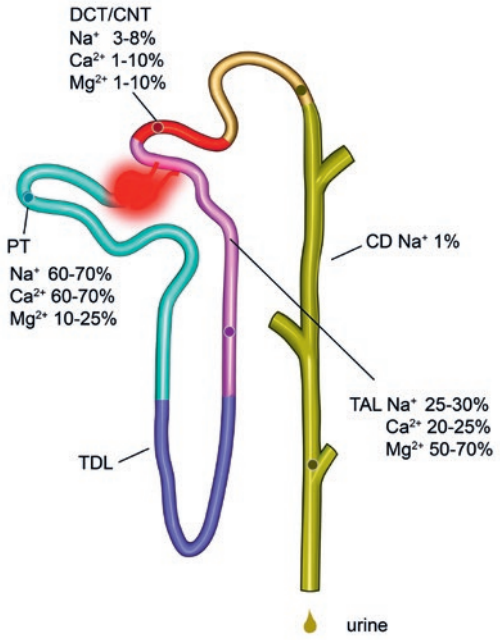

Figure 1. Na^+, Ca^{2+} and Mg^{2+} reabsorption along the nephron.

Around 95-99% of Na^+, Ca^{2+} and Mg^{2+} in the filtered pro-urine is reabsorbed along the nephron in the proximal tubule (PT), thick ascending limb of loop of Henle (TAL), distal convoluted tubule (DCT), connecting tubule (CNT), and the collecting duct (CD). The remaining Na^+, Ca^{2+}, and Mg^{2+} will be excreted with urine. TDL, the descending loop of Henle.

The loop of Henle

The loop of Henle consists of a descending limb and an ascending limb (Figure 1). The descending loop of Henle (TDL) is permeable to water because of the water channel aquaporin 1 (AQP1), but impermeable to electrolytes [22-24]. Vice versa, the TAL is impermeable to water, but it is permeable to electrolytes [25]. The TAL is responsible for roughly 25% of the filtered Na^+ reabsorption. In addition, it is also a crucial segment for Mg^{2+} and Ca^{2+} reabsorption [4, 26, 27], taking in about 20-25% of filtered Ca^{2+}, and 50%-70% of filtered Mg^{2+} by paracellular processes [28, 29].

The PT reabsorbs bulk of filtrated Ca^{2+} via the paracellular pathway. Subsequently, Ca^{2+} is passively reabsorbed in the TAL. Here, the driving force for paracellular cation transport is a lumen-positive transepithelial voltage, which is mainly generated by the sodium-potassium-chloride cotransporter (NKCC2) and the renal outer medullary potassium channel (ROMK) [27]. The calcium sensing receptor (CaSR) can regulate this transport without changing the transepithelial voltage [30]. Studies have shown that CaSR can regulate Ca^{2+} reabsorption by inhibiting the activity of ROMK or by affecting tight junction permeability [31, 32]. Impaired regulation of Ca^{2+} transport in the TAL can result in several diseases, such as hypocalcemia, hypercalcemia, or kidney stone disease.

The reabsorption of the divalent cations such as Mg^{2+} and Ca^{2+} mainly depends on tight junction permeability in this segment. Claudin proteins are the crucial constituents of the tight junction complexes [33]. The claudin family has 24 members. Some claudin family members play fundamental roles in forming impermeable barriers, while others modulate the permeability to small molecules and electrolytes [34-36]. Claudins 3, 10b, 11, 14, 16, and 19 are specifically localized in the TAL [36-38]. The tight junctions formed by claudins 16 and 19 are highly permeable to Mg^{2+} and Ca^{2+} [39], while the tight junctions made by claudin 10b are highly permeable to Na^+ [40, 41]. Mutations in *CLDN16* (claudin 16) and *CLDN19* (claudin 19) can result in familial hypomagnesemia with hypercalciuria and nephrocalcinosis (FHHNC) [42-45]. Recently, several studies showed that increased plasma Ca^{2+} and Mg^{2+} levels can alter the tight junctions by causing them to incorporate claudin 14 in the structure which will shift the preference from divalent cations such as Ca^{2+} and Mg^{2+} towards monovalent ions like Na^+ [31, 46].

The distal convoluted tubule connecting tubule

The DCT is responsible for 3–8% of Na^+ reabsorption [47]. It has two parts, namely an early segment and a late segment, also known as DCT1 and DCT2, respectively [48]. The key player in Na^+ reabsorption is the thiazide-sensitive sodium-chloride co-transporter (NCC) on the apical side of DCT1 cells [49]. Additionally, the epithelial sodium channel (ENaC) also participates in Na^+ reabsorption in DCT2 and CNT [50].

Approximately 1-10 % of filtered Mg^{2+} is reabsorbed in the DCT1 [50]. The transient receptor potential cation channel subfamily M, member 6 (TRPM6) plays a crucial role in epithelial Mg^{2+} transport in the kidney [51]. Recessive *TRPM6* mutations cause disturbances in intestinal Mg^{2+} absorption and urinary Mg^{2+} wasting which lead to severe hypomagnesemia [52, 53]. Several other proteins may play roles in transporting Mg^{2+} across the basolateral membrane, such as solute carrier family 41 member 1 (SLC41A1) and solute carrier family 41 member 3 (SLC41A3). Knocking down slc41a1 caused renal Mg^{2+} wasting in zebrafish larvae [54]. In another study, *Slc41a3* knockout mice exhibit low serum Mg^{2+} levels [55].

The DCT2 and CNT reabsorb nearly 10% of the filtered Ca^{2+} [50]. Unlike other segments of the nephron, Ca^{2+} reabsorption in the DCT and CNT occurs by active transcellular mechanisms. The apical transient receptor potential channel subfamily V member 5 (TRPV5) plays a key role in transepithelial Ca^{2+} transport [56]. *Trpv5* knockout mice exhibited urinary Ca^{2+} wasting [56]. In addition, Ca^{2+}-binding protein calbindin-D_{28K}, which is used to buffer intracellular Ca^{2+} levels [57], carries Ca^{2+} to the basolateral surface. Then, the plasma membrane calcium-ATPase (PMCA) and type 1 sodium/calcium exchanger (NCX1) work together to extrude Ca^{2+} to the extracellular space [58].

The collecting duct

The CD is the final part of the kidney to regulate the fluid balance and electrolytes [59, 60]. The CD extends all the way from the cortex to the medulla section of the kidney and the

DCT and the ureter are connected by the CD. Nearly 1% of filtered Na^+ is reabsorbed in the collecting duct. The CD plays a very minimal role in the reabsorption of Ca^{2+} and Mg^{2+} [61]. Under normal conditions, CD is slightly permeable to Na^+. Filtered Na^+ is diffused through the apical side of CD by ENaC. Then, the Na^+-K^+-ATPase on the basolateral side will extrude the Na^+ to the interstitial space [62-64]. Any remaining Na^+, Ca^{2+} and Mg^{2+} will be excreted in the urine by the kidney.

Na^+ handling in diabetes and hypertension

Na^+ transport in the proximal tubule

Disturbed Na^+ and glucose reabsorption in the PT typically leads to Na^+ and glucose disorders and subsequent hypertension and diabetes, since the PT is the main segment for Na^+ and glucose reabsorption in the kidney. SGLT2 is a key transporter for Na^+ and glucose reabsorption in the PT [65].

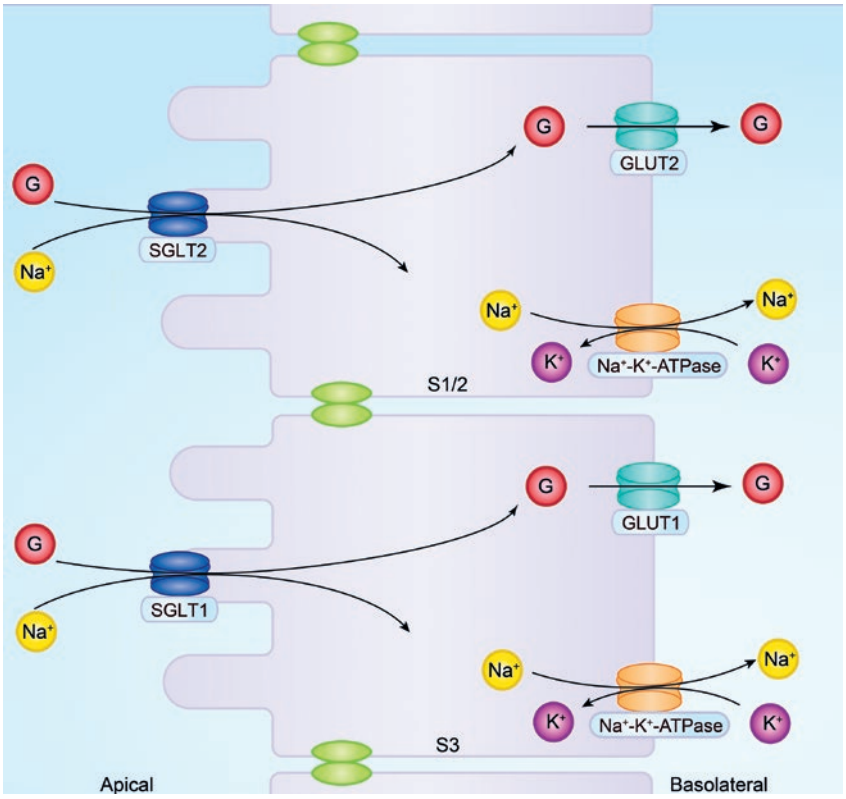

Figure 2. Glucose and Na^+ reabsorption in the proximal tubule.

Na^+ and glucose reabsorption through SGLT2 in the proximal tubule epithelial cell. G, glucose; SGLT1, sodium-glucose co-transporter 1; GLUT1, glucose transporter 1; SGLT2, sodium-glucose co-transporter 2; GLUT2, glucose transporter 2; S1/2, segment 1/2; S3, segment 3.

Na^+ and glucose transport in the proximal tubule in diabetes and hypertension

Type 2 diabetes is characterized by increasing blood glucose levels [66] due to insulin resistance. It is a worldwide epidemic and the number of people affected is projected to rise beyond 600 million in the next 25 years, which equals over 10% of the adult population, with equal rates in both men and women [67]. Type 2 diabetes is also the leading cause of nephropathy [68, 69]. In humans, the kidneys filter approximately 180 grams of D-glucose from plasma each day, and this is normally reabsorbed in the kidney [70]. SGLT1 (*SLC5A1*) and SGLT2 (*SLC5A2*), which are encoded by genes from the solute carrier 5A family, are crucial regulators in intestinal and renal glucose handling [71]. Other transporters that are involved in the glucose maintenance are the facilitative glucose transporters: glucose transporter 1 (GLUT1) and glucose transporter 2 (GLUT2) [72]. SGLT2 reabsorbs approximately 90% of the glucose from the lumen of the S1/S2 segment of the PT [73], while GLUT2 transports glucose across the basolateral membrane (Figure 2) [74]. The remaining glucose is reabsorbed in the S3 segment, through the coordinated actions of SGLT1 and GLUT1 [71]. Mutations in the *Sglt1* gene result in glucose-galactose malabsorption and impaired glucose transport [75]. Mutations in *Sglt2* gene can cause familial renal glycosuria, characterized by decreased renal tubular glucose reabsorption [76, 77]. The *Sglt2* knockout mice exhibited attenuated hyperglycemia and glomerular hyperfiltration [78]. Increased expression and activity of SGLT2 resulted in increased glucose reabsorption, which causes hyperglycemia in diabetes patients [79, 80].

More than two-thirds of patients with type 2 diabetes have concomitant hypertension and salt and water retention [81, 82]. Hypertension in these patients increases their already elevated cardiovascular risks [83, 84]. Recent interest in the kidneys as a target for glucose control in diabetes has important implications for blood pressure management. Na^+ retention has been implicated in the pathophysiology of hypertension in type 2 diabetes and in impaired vasodilatory responsiveness to angiotensin-I-converting enzyme (ACE) inhibition [85, 86]. Pharmacological inhibition of SGLT2 transporters improves glucose control by inducing glucosuria, but these inhibitors also lower blood pressure to a degree comparable with the use of thiazide diuretics [87, 88]. Studies showed that SGLT2 inhibitors increase Na^+ delivery to macula densa, then, juxtaglomerular apparatus sense this increased Na^+ delivery as an elevation in the filtrate volume which leads to afferent vasoconstriction, a reduction in intraglomerular pressure and a suppressed glomerular filtration rate (GFR) [89-91]. Recently, Woods and his colleagues reported that SGLT2 inhibitor canagliflozin decreases mRNA and protein level of renal angiotensinogen and reduced blood pressure in animal models with type 2 diabetes [92]. This suggests that SGLT2 inhibitors may reduce blood pressure through suppressing renin-angiotensin-aldosterone system (RAAS). Co-inhibition of glucose-coupled Na^+ transport may be the driving force behind this blood pressure lowering effect, the effect of which may be mediated by the action of Na^+ transporters located in the local or more distal part of the nephron.

Hypercalciuria in kidney stone disease

Ca^{2+} handling in the Henle's loop

The urinary Ca^{2+} concentration in the loop of Henle is an important factor in the formation of kidney stone. The loop of Henle serves to concentrate pro-urine [93]. Since no water is reabsorbed at this segment, there is a 10-fold or even higher increase in osmolality which results in urinary 'supersaturation' with poorly soluble waste salts such as Ca^{2+}-phosphate (CaP) and Ca^{2+}-oxalate (CaOx). CaP and CaOx are the major components for crystal formation [94]. In this segment, the pathophysiology of kidney stones will be discussed.

Hypercalciuria

Urinary Ca^{2+} excretion greater than 300 milligrams (mg) per day for men and greater than 250 mg per day in women is considered as hypercalciuria [95, 96]. Conditions known to cause hypercalciuria include: *i)* diet, such as excessive dietary intake of Ca^{2+}, Na^{+}, carbohydrates, animal protein, alcohol, and reduced intake of phosphate and potassium, *ii)* increased intestinal Ca^{2+} absorption, *iii)* reduced renal tubular reabsorption of Ca^{2+}, and *iv)* increased osteoclastic bone reabsorption [97-99]. Remarkably, a large percentage of patients have idiopathic hypercalciuria, with no explanation for the increased urinary Ca^{2+} levels [99, 100]. Hypercalciuria is considered a risk factor for Ca^{2+} crystal deposition in the kidneys, which can ultimately result in kidney stone formation (nephrolithiasis). This occurs by at least two mechanisms: first, by increasing the concentration of urinary Ca^{2+} salts (CaP and CaOx), and second, urinary Ca^{2+} binds stone inhibitors such as citrates, leading to a reduction in the activity of this inhibitor [101].

Nephrolithiasis

Nephrolithiasis is a highly widespread urologic disease with prevalence rates ranging from 7-13% in North America, 5-9% in Europe and 1-5% in Asia [102]. The prevalence of kidney stones has increased worldwide over the last four decades, with the prevalence in women rising disproportionately compared to men [103]. This growing trend is considered to be associated with lifestyle changes such as lack of physical activity and altered dietary habits [104]. Medical management of urinary stones includes pharmacological interventions, minor endourological intervention for stone removal, and extracorporeal shock wave lithotripsy [105]. They are highly effective but are associated with some serious side effects and without complete preventing of the recurrence of kidney stones [105]. There is currently no effective drug on the market to cure or prevent kidney stone recurrences. Without proper treatment, the rate of the secondary stone formation ranges from 10% in the first year up to 75% in 20 years [106, 107]. The high prevalence and recurrent nature of kidney stones make it a substantial economic burden. In addition, kidney stone disease is associated with an increased rate of chronic kidney disease, end-stage renal

failure, hypertension, and myocardial infarction [104, 108]. These results suggest that the emphasis should not only be placed on finding new treatments for kidney stones, but also on finding a new method to prevent stone formation in high risk groups and recurrent in kidney stone patients.

Pathophysiology of kidney stones

Biochemically, there are different types of stones depending on the type of abnormalities in urine composition. Ca^{2+} stones are the most common type of renal stones, compromising about 80% of all kidney stones [109]. The formation of kidney stones is a multifactorial process that involves intrinsic factors such as age, sex, genetic predisposition, and extrinsic factors such as geography, diet, and water intake [110]. The pathogenesis of kidney stones is still not completely understood. They often begin from a foundation called Randall's plaque present at the renal papillary surface, but there are several steps involved in the formation of stones [108]. Step 1: Urine supersaturation. In this phase, the supersaturation is the result of the excretion of poorly soluble minerals such as CaP or CaOx in a relatively small volume of urine [108]. Step 2: Nucleation. The free atoms, ions, or molecules in the supersaturated urine begin to form microscopic clusters [104]. Step 3: Crystal growth and crystal aggregation. The preformed crystals stick together and form a hard rock mass. These small hard mass of stones stay together and form a larger stone in a process called crystal aggregation. Crystal aggregation results in more nucleation sites, leading to a snowball effect [104]. Step 4: Crystal-cell interaction. At this stage, the formed crystals adhere to the lining of the epithelial cells in the renal tubules [104]. This process results in oxidative stress leading to cell damage and cell membrane rupture. The damaged cells can then invert their cell membrane, allowing close contact between the anionic side of the cell and the urine. This interaction results in crystal bonding at that location. Step 5: Crystal retention and stone formation. At this stage, the formation of kidney stones depends on the presence of promoting and inhibiting molecules in the urine (Figure 3) [104]. All of the steps are crucial for the formation of stones. Researchers have shown that urine contains small molecules such as citrate and pyrophosphate, and macromolecules such as glycoproteins, glycosaminoglycans, and proteoglycans can alter and inhibit the formation of stones [110-116]. Abnormalities in the structure or function of these molecules have been identified in recurrent kidney stone patients [104, 108]. Theoretically, Ca^{2+}-containing kidney stones can be prevented by increasing physiological inhibitory molecules such as nephrocalcin (NC), Tamm-Horsfall protein (THP), and osteopontin (OPN) or by reducing the urinary Ca^{2+} concentration [117-121]. NC is a Ca^{2+}-binding glycoprotein and one molecule of NC can bind to four molecules of Ca^{2+} [122]. NC is able to inhibit the nucleation phase, Ca^{2+} oxalate monohydrate (COM) crystal growth, crystal aggregation and crystal adherence to renal tubules [120, 122]. THP is a strong crystal aggregation inhibitor that is reported to significantly reduce COM crystal endocytosis [123]. This indicates that THP may prevent the COM crystals uptake by the

distal tubular epithelial cells of the kidney and thereby inhibit renal crystal retention and urolithiasis [124]. OPN plays a crucial role in inhibiting the nucleation step and CaOx crystal growth and aggregation phase [125]. What is more, OPN is able to direct CaOx crystallization to the CaOx dihydrate phase instead of CaOx monohydrate phase [126]. Hypercalciuria is present in about 40 to 60% of all patients with kidney stones [127]. Therefore, targeting urinary Ca^{2+} is an appealing intervention that should be further investigated in the future.

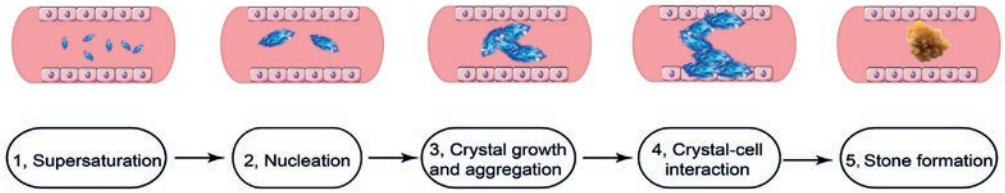

Figure 3. Mechanisms of kidney stone formation.

The process of kidney stone formation includes several steps such as urine supersaturation, nucleation, crystal growth and crystal aggregation, crystal-cell interaction and crystal retention and stone formation.

Fine tuning of Mg^{2+} reabsorption

Mg^{2+} transport in the distal convoluted tubule

The DCT reabsorbs nearly 10% of the filtered Mg^{2+} in the kidney [128]. There is no Mg^{2+} reabsorption beyond the DCT. Mg^{2+} reabsorption is tightly controlled by the Mg^{2+} transporters, channels, and sensors in the DCT [4, 5, 129]. However, it is still not totally understood how these transporters, channels, and sensors mediate the Mg^{2+} influx and efflux. In 2011, patients carrying mutations in *CNNM2*, which encodes cyclin and CBS domain divalent metal cation transport mediators (CNNM2), were found to suffer from hypomagnesemia [130]. Later studies demonstrated that CNNM2 is involved in Mg^{2+} transport in the kidney [131, 132]. In this segment, the structure and molecular function of CNNMs and a novel urinary Mg^{2+} excretion related gene, *Arl15*, will be described.

Domain distribution of CNNMs

CNNM (1-4) proteins are also known as ancient conserved domain proteins (1-4) and share homology with cyclins. However, the function of CNNMs in the cell cycle has not been identified. Structurally, CNNMs possess four different domains that are combined by linkers [132] (Figure 4). The extracellular amino (N)-terminal domain which contains a conserved N residue (N112 in CNNM2, N73 in CNNM3 and N85 in CNNM4) is crucial for glycosylation. This glycosylation site is also important for cell surface expression [132]. After the N-terminal domain is a domain of unknown function-21 (DUF21) that crosses the plasma membrane three times [132]. The cytosolic cystathionine β-synthase (CBS)

domains, known as the 'Bateman module', consist of two consecutive CBS motifs [132]. As with most CBS domain proteins, the Bateman modules of CNNMs interact with each other. The CBS2 domain of CNNMs contains an extended loop that makes this Bateman motif in CNNMs different from the Bateman motifs discovered in other proteins [133-135].

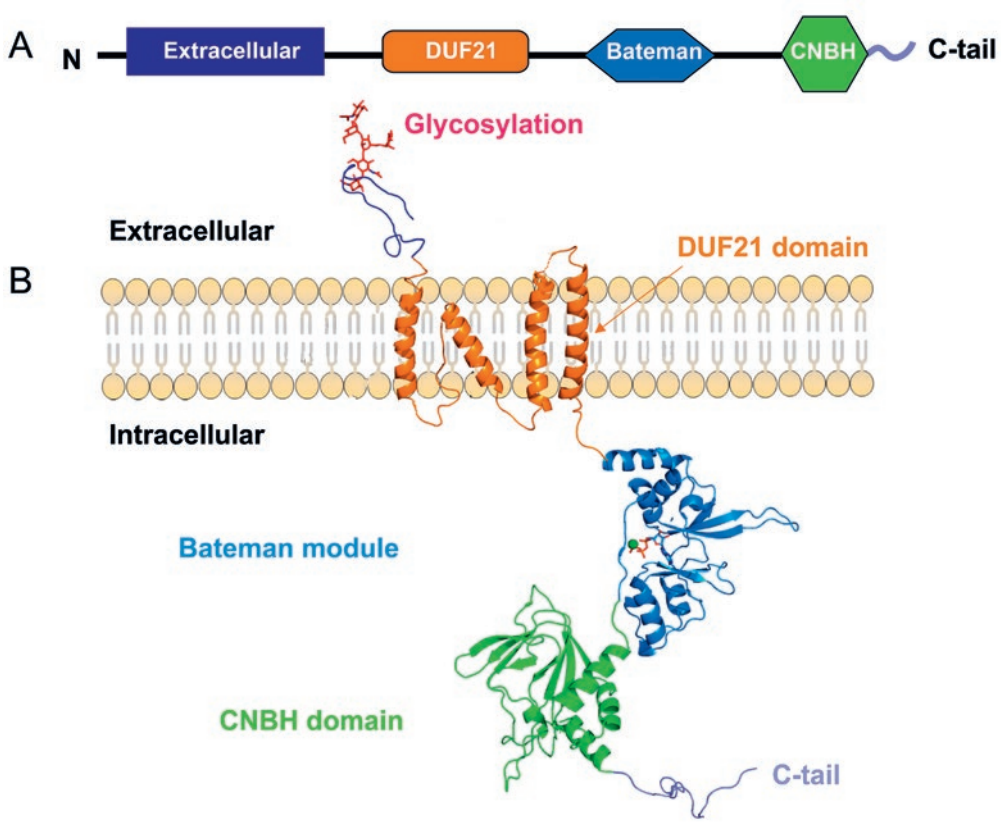

Figure 4. Structural overview of CNNM.

A, Linear model of CNNMs, showing the four color-coded independent domains. Extracellular domain is indicated in dark blue, DUF21 transmembrane domain is indicated in orange, Bateman domain is indicated in light blue and CNBH domain is indicated in light green, the remaining part is the intracellular carboxyl (C)-terminal tail (C-tail). B, Structure of CNNMs, with color-coded domains matching with A. DUF21, domain with unknown function 21. CNBH, cyclic nucleotide monophosphate-binding homology domain (Figure adapted from [135]).

This extended loop plays a crucial role in interacting with other proteins. Studies showed that phosphatase of the regenerating liver (PRLs) bind to the extended loop of the CBS2 domain of CNNM3 to mediate intracellular Mg^{2+} levels [136, 137]. The CBS domains are followed by a cyclic nucleotide monophosphate-binding homology domain (CNBH) and an unstructured carboxyl (C)-tail [132].

Organ distribution and localization of the CNNM protein family

The tissue distribution and expression pattern of the CNNMs are quite diverse [130, 132, 138, 139]. CNNM1 functions as a copper chaperone or storage protein that is mainly expressed in the brain. Northern blots revealed that CNNM1 is moderately expressed in the testis and very low expression levels of CNNM1 have also been detected in the stomach, small intestine, colon, spleen, heart, lungs, liver, kidney, and skeletal muscles [138]. CNNM2 is ubiquitously expressed in the body and is highly expressed in the kidney, brain, liver, and heart. CNNM2 is localized in the TAL and DCT of the kidney [130]. CNNM3 is also ubiquitously present but has the highest expression in the brain, lung, spleen, and heart. It is moderately expressed in the liver, colon, lung, testis, and placenta. However, little expression is detected in skeletal muscles or small intestine [132, 140]. CNNM4 is abundant in the heart, kidney, lung, placenta, testis, and intestinal tract [132, 140]. CNNM4 expression can also be detected in the epididymis and sperm [141].

Importance of CNNM2 in regulating Mg^{2+} homeostasis

In 2011, Stuiver *et al.* reported that renal Mg^{2+} reabsorption is disturbed in patients carrying *CNNM2* mutations [130]. Later, Arjona *et al.* identified five new mutations in *CNNM2* in five families suffering from intellectual disability, seizures, and hypomagnesemia [142]. Interestingly, CNNM2 mutations (except for p.L330F) identified in the hypomagnesemic patients resulted in significantly decreased $^{25}Mg^{2+}$ uptake in HEK293 cells [142]. Cnnm2-knockdown zebrafish exhibited neurodevelopmental impairments, weak touch-evoked escape behavior, and decreased total body Mg^{2+} content [142]. These phenotypes were rescued by injecting mammalian wildtype cnnm2 cRNA [142]. Similar studies investigating the function of CNNM2 in Mg^{2+} homeostasis have also been performed by using *Cnnm2* heterozygous (*Cnnm2*$^{+/-}$) mice and kidney-specific knockout mice [131]. Homozygous *Cnnm2* knockout mice died during embryonic development [131]. Compared with *Cnnm2* wildtype (*Cnnm2*$^{+/+}$) mice, *Cnnm2*$^{+/-}$ mice exhibited lower serum Mg^{2+} levels. However, urinary and fecal Mg^{2+} excretion in *Cnnm2*$^{+/+}$ mice and *Cnnm2*$^{+/-}$ mice did not differ significantly [131]. *Cnnm2* kidney-specific knockout mice demonstrated a decrease in serum Mg^{2+} level [131]. Collectively, all of these results suggest that CNNM2 plays a crucial role in maintaining the Mg^{2+} balance.

Regulation of CNNMs localization and activity by CNNM ligands and interacting partners

Studies have indicated that ligands and CNNM binding partners can modify the cellular localization and activity of CNNM proteins [136, 137, 143]. For example, clathrin adaptor protein (AP) complex-1 mediates the localization of CNNM4 at the basolateral membrane [144]. Mutations of three dileucine motifs (L575/576, L758/759, and L765/766) in the CNBH domain of CNNM4 abrogated CNNM4 basolateral localization and CNNM4's interaction with AP-1A and AP-1B [144].

The activity of CNNMs can also be regulated by either small ligands such as Mg^{2+} and ATP or proteins. Hirata *et al.* first found the direct binding of ATP to the Bateman module of CNNM2 by surface plasmon resonance (SPR) [137]. ATP binding assays demonstrated that this binding is Mg^{2+} dependent since the binding affinity of the CBS domain for ATP is stronger in the presence of Mg^{2+} than the conditions when Mg^{2+} is absent [137].

In 2014, two different groups separately reported that CNNMs interact with the PRLs to regulate intracellular Mg^{2+} concentration [136, 137]. PRL has three members: PRL1, 2, and 3, which are highly expressed in a large number of cancers [145, 146]. Binding between CNNM3 and PRL-2 is important for breast cancer cell proliferation and tumor growth, and inhibition of this binding can hinder human breast cancer cell proliferation [147]. Later studies revealed that all PRL family members bind to CNNMs (CNNM1-4), and truncated CNNM3 mutagenesis studies showed that the CBS domain plays a fundamental role in forming the complex [136, 143]. Moreover, the highly conserved D558 residue, which is localized at the extended loop of the CBS2 motif of CNNM2, was found to play a determinant role in forming the CNNM/PRL complex [134]. This conserved residue act as a pseudosubstrate of PRL and their binding inhibits Mg^{2+} efflux [134, 136].

ARL15 as a novel gene in renal Mg^{2+} handling

ADP ribosylation factor like GTPase 15 (ARL15), which is a member of the GTP-binding proteins, plays a crucial role in renal Mg^{2+} handling [148]. Recently, Corre *et al.* reported that ARL15 influences renal Mg^{2+} reabsorption through regulating the activity of the epithelial Mg^{2+} channel TRMP6 [148]. The T46N ARL15 mutant, which was predicted to possess a dominant negative nature, failed to increase TRPM6 channel activity [148]. Immunohistochemistry results indicated that ARL15 is highly expressed in the TAL and DCT [148]. In their zebrafish model, arl15 knockdown resulted in increased urinary Mg^{2+} excretion. ARL15 is shown to be mainly localized in the Golgi, but it is also expressed in the plasma membrane and intracellular vesicles in 3T3-L1 cells [149]. This indicates that ARL15 might be involved in vesicular trafficking and posttranslational modification [149].

A genome-wide association study (GWAS) showed that ARL15 is associated with low serum adiponectin levels, lipid levels, fasting insulin levels, and type 2 diabetes [150]. Rocha *et al.* reported that the *Arl15* mRNA expression level was significantly increased with the process of adipogenesis in 3T3-L1 adipocytes. Knocking down Arl15 expression significantly impaired 3T3-L1 preadipocyte differentiation and droplet formation [149]. Moreover, decreased mRNA expression levels of adiponectin and reduced secretion of adiponectin in 3T3-L1 adipocytes were demonstrated in Arl15 knockdown cells [149]. However, Arl15 knockdown does not affect insulin-signaling and glucose uptake, suggesting that the function of ARL15 may be restricted to adiponectin secretion and adiponectin vesicle trafficking [149].

Outline of this thesis

The aim of this thesis is to get insight into the role of Na^+, Ca^{2+}, and Mg^{2+} transporters in diseases such as diabetes, hypertension, kidney stone disease, hypomagnesemia, and renal carcinoma. Although much is known about the (patho) physiology of these diseases, little is known about the molecular mechanisms underlying these transport disorders in the kidney. **Chapter 2** provides new insights into renal Na^+-glucose handling. Diabetic mice were treated with dapagliflozin, an SGLT2 inhibitor, and the expression of Na^+ transporters in the kidney was investigated. This study will help us to better understand the effect of dapagliflozin treatment on the local and downstream Na^+ transporters in the kidney. In **Chapter 3**, we studied an out-of-the-box idea to prevent kidney stone formation. Based on the literature on the Ca^{2+}-binding loop of EF-hand proteins, several small peptides (20-30 residues) were developed and analyzed for their Ca^{2+}-binding affinity. To assess the efficacy of such peptides *in vivo*, we aimed to generate a kidney stone mouse model. This study provides the first step towards testing a novel approach to the treatment and prevention of kidney stones. In **Chapter 4,** we investigated the role of ARL15 in Mg^{2+} homeostasis. ARL15 expression and tissue distribution were investigated. *Arl15*$^{+/-}$ mice were generated to investigate its role in renal Mg^{2+} handling by analyzing urine and serum Mg^{2+} levels, as well as the expression of renal Mg^{2+}-related genes. In **Chapter 5,** the functional relevance of binding between ARL15 and CNNMs was outlined. Proximity-dependent biotin identification, affinity-purification/mass spectrometry, and co-immunoprecipitation were used to investigate the binding of ARL15 to CNNMs proteins. Furthermore, ARL15-mediated CNNMs' cell surface expression and Mg^{2+} transport activities were studied in various types of renal cell carcinoma cell lines. These findings revealed a novel regulatory mechanism of Mg^{2+} transport within the DCT, which will help to understand the regulation of Mg^{2+} handling in this segment. Finally, the findings from the studies of this thesis are discussed and summarized in **Chapter 6 and 7.**

References

1. Arruda, A.P. and G.S. Hotamisligil, *Calcium Homeostasis and Organelle Function in the Pathogenesis of Obesity and Diabetes.* Cell Metab, 2015. **22**(3): p. 381-97.
2. Long, S. and A.M. Romani, *Role of Cellular Magnesium in Human Diseases.* Austin J Nutr Food Sci, 2014. **2**(10).
3. Patel, S., *Sodium balance-an integrated physiological model and novel approach.* Saudi J Kidney Dis Transpl, 2009. **20**(4): p. 560-9.
4. Blaine, J., M. Chonchol, and M. Levi, *Renal control of calcium, phosphate, and magnesium homeostasis.* Clin J Am Soc Nephrol, 2015. **10**(7): p. 1257-72.
5. de Baaij, J.H., J.G. Hoenderop, and R.J. Bindels, *Magnesium in man: implications for health and disease.* Physiol Rev, 2015. **95**(1): p. 1-46.
6. Klahr, S. and E. Slatopolsky, *Renal regulation of sodium excretion. Function in health and in edema-forming states.* Arch Intern Med, 1973. **131**(6): p. 780-91.
7. Layton, A.T., *Mathematical modeling of kidney transport.* Wiley Interdiscip Rev Syst Biol Med, 2013. **5**(5): p. 557-73.
8. Scott, R.P. and S.E. Quaggin, *Review series: The cell biology of renal filtration.* J Cell Biol, 2015. **209**(2): p. 199-210.
9. Zhuo, J.L. and X.C. Li, *Proximal nephron.* Compr Physiol, 2013. **3**(3): p. 1079-123.
10. Tojo, A. and S. Kinugasa, *Mechanisms of glomerular albumin filtration and tubular reabsorption.* Int J Nephrol, 2012. **2012**: p. 481520.
11. Boron, W.F., *Acid-base transport by the renal proximal tubule.* J Am Soc Nephrol, 2006. **17**(9): p. 2368-82.
12. Curthoys, N.P. and O.W. Moe, *Proximal tubule function and response to acidosis.* Clin J Am Soc Nephrol, 2014. **9**(9): p. 1627-38.
13. Aronson, P.S., *Role of ion exchangers in mediating NaCl transport in the proximal tubule.* Kidney Int, 1996. **49**(6): p. 1665-70.
14. Horiba, N., et al., *Na(+)-dependent fructose transport via rNaGLT1 in rat kidney.* FEBS Lett, 2003. **546**(2-3): p. 276-80.
15. Magagnin, S., et al., *Expression cloning of human and rat renal cortex Na/Pi cotransport.* Proc Natl Acad Sci U S A, 1993. **90**(13): p. 5979-83.
16. Werner, A., et al., *Cloning and expression of cDNA for a Na/Pi cotransport system of kidney cortex.* Proc Natl Acad Sci U S A, 1991. **88**(21): p. 9608-12.
17. Noonan, W.T., et al., *Blood pressure maintenance in NHE3-deficient mice with transgenic expression of NHE3 in small intestine.* Am J Physiol Regul Integr Comp Physiol, 2005. **288**(3): p. R685-91.
18. Biemesderfer, D., et al., *NHE3: a Na+/H+ exchanger isoform of renal brush border.* Am J Physiol, 1993. **265**(5 Pt 2): p. F736-42.
19. Pirahanchi, Y. and N.R. Aeddula, *Physiology, Sodium Potassium Pump (Na+ K+ Pump)*, in *StatPearls*. 2019: Treasure Island (FL).
20. Suki, W.N., *Calcium transport in the nephron.* Am J Physiol, 1979. **237**(1): p. F1-6.
21. Houillier, P., *Mechanisms and regulation of renal magnesium transport.* Annu Rev Physiol, 2014. **76**: p. 411-30.
22. Agre, P., *Homer W. Smith award lecture. Aquaporin water channels in kidney.* J Am Soc Nephrol, 2000. **11**(4): p. 764-77.
23. Agre, P., et al., *Aquaporin water channels--from atomic structure to clinical medicine.* J Physiol, 2002. **542**(Pt 1): p. 3-16.
24. Mount, D.B., *Thick ascending limb of the loop of Henle.* Clin J Am Soc Nephrol, 2014. **9**(11): p. 1974-86.
25. Knepper, M.A., et al., *Regulation of thick ascending limb transport by vasopressin.* J Am Soc Nephrol, 1999. **10**(3): p. 628-34.
26. Zacchia, M. and G. Capasso, *The importance of uromodulin as regulator of salt reabsorption along the thick ascending limb.* Nephrol Dial Transplant, 2015. **30**(2): p. 158-60.

27. Zacchia, M., et al., *The importance of the thick ascending limb of Henle's loop in renal physiology and pathophysiology.* Int J Nephrol Renovasc Dis, 2018. **11**: p. 81-92.
28. Hoenderop, J.G., B. Nilius, and R.J. Bindels, *Calcium absorption across epithelia.* Physiol Rev, 2005. **85**(1): p. 373-422.
29. Shareghi, G.R. and Z.S. Agus, *Magnesium transport in the cortical thick ascending limb of Henle's loop of the rabbit.* J Clin Invest, 1982. **69**(4): p. 759-69.
30. Loupy, A., et al., *PTH-independent regulation of blood calcium concentration by the calcium-sensing receptor.* J Clin Invest, 2012. **122**(9): p. 3355-67.
31. Gong, Y., et al., *Claudin-14 regulates renal Ca(+)(+) transport in response to CaSR signalling via a novel microRNA pathway.* EMBO J, 2012. **31**(8): p. 1999-2012.
32. Riccardi, D. and G. Valenti, *Localization and function of the renal calcium-sensing receptor.* Nat Rev Nephrol, 2016. **12**(7): p. 414-25.
33. Van Itallie, C.M. and J.M. Anderson, *Claudin interactions in and out of the tight junction.* Tissue Barriers, 2013. **1**(3): p. e25247.
34. Gunzel, D. and A.S. Yu, *Claudins and the modulation of tight junction permeability.* Physiol Rev, 2013. **93**(2): p. 525-69.
35. Findley, M.K. and M. Koval, *Regulation and roles for claudin-family tight junction proteins.* IUBMB Life, 2009. **61**(4): p. 431-7.
36. Rajasekaran, S.A., K.W. Beyenbach, and A.K. Rajasekaran, *Interactions of tight junctions with membrane channels and transporters.* Biochim Biophys Acta, 2008. **1778**(3): p. 757-69.
37. Milatz, S., et al., *Mosaic expression of claudins in thick ascending limbs of Henle results in spatial separation of paracellular Na+ and Mg2+ transport.* Proc Natl Acad Sci U S A, 2017. **114**(2): p. E219-E227.
38. Seker, M., et al., *Mouse Models of Human Claudin-Associated Disorders: Benefits and Limitations.* Int J Mol Sci, 2019. **20**(21).
39. Hou, J., et al., *Claudin-16 and claudin-19 interact and form a cation-selective tight junction complex.* J Clin Invest, 2008. **118**(2): p. 619-28.
40. Breiderhoff, T., et al., *Deletion of claudin-10 (Cldn10) in the thick ascending limb impairs paracellular sodium permeability and leads to hypermagnesemia and nephrocalcinosis.* Proc Natl Acad Sci U S A, 2012. **109**(35): p. 14241-6.
41. Klar, J., et al., *Altered paracellular cation permeability due to a rare CLDN10B variant causes anhidrosis and kidney damage.* PLoS Genet, 2017. **13**(7): p. e1006897.
42. Kausalya, P.J., et al., *Disease-associated mutations affect intracellular traffic and paracellular Mg2+ transport function of Claudin-16.* J Clin Invest, 2006. **116**(4): p. 878-91.
43. Konrad, M., et al., *CLDN16 genotype predicts renal decline in familial hypomagnesemia with hypercalciuria and nephrocalcinosis.* J Am Soc Nephrol, 2008. **19**(1): p. 171-81.
44. Konrad, M., et al., *Mutations in the tight-junction gene claudin 19 (CLDN19) are associated with renal magnesium wasting, renal failure, and severe ocular involvement.* Am J Hum Genet, 2006. **79**(5): p. 949-57.
45. Angelow, S., et al., *Renal localization and function of the tight junction protein, claudin-19.* Am J Physiol Renal Physiol, 2007. **293**(1): p. F166-77.
46. Dimke, H., et al., *Activation of the Ca(2+)-sensing receptor increases renal claudin-14 expression and urinary Ca(2+) excretion.* Am J Physiol Renal Physiol, 2013. **304**(6): p. F761-9.
47. Hierholzer, K. and M. Wiederholt, *Some aspects of distal tubular solute and water transport.* Kidney Int, 1976. **9**(2): p. 198-213.
48. McCormick, J.A. and D.H. Ellison, *Distal convoluted tubule.* Compr Physiol, 2015. **5**(1): p. 45-98.
49. Gamba, G., *The thiazide-sensitive Na+-Cl- cotransporter: molecular biology, functional properties, and regulation by WNKs.* Am J Physiol Renal Physiol, 2009. **297**(4): p. F838-48.
50. Subramanya, A.R. and D.H. Ellison, *Distal convoluted tubule.* Clin J Am Soc Nephrol, 2014. **9**(12): p. 2147-63.
51. Voets, T., et al., *TRPM6 forms the Mg2+ influx channel involved in intestinal and renal Mg2+ absorption.* J Biol Chem, 2004. **279**(1): p. 19-25.

52. Schlingmann, K.P., et al., *Hypomagnesemia with secondary hypocalcemia is caused by mutations in TRPM6, a new member of the TRPM gene family.* Nat Genet, 2002. **31**(2): p. 166-70.
53. Walder, R.Y., et al., *Mutation of TRPM6 causes familial hypomagnesemia with secondary hypocalcemia.* Nat Genet, 2002. **31**(2): p. 171-4.
54. Arjona, F.J., et al., *SLC41A1 is essential for magnesium homeostasis in vivo.* Pflugers Arch, 2019. **471**(6): p. 845-860.
55. de Baaij, J.H., et al., *Identification of SLC41A3 as a novel player in magnesium homeostasis.* Sci Rep, 2016. **6**: p. 28565.
56. Hoenderop, J.G., et al., *Renal Ca2+ wasting, hyperabsorption, and reduced bone thickness in mice lacking TRPV5.* J Clin Invest, 2003. **112**(12): p. 1906-14.
57. Hemmingsen, C., *Regulation of renal calbindin-D28K.* Pharmacol Toxicol, 2000. **87 Suppl 3**: p. 5-30.
58. Magyar, C.E., et al., *Plasma membrane Ca2+-ATPase and NCX1 Na+/Ca2+ exchanger expression in distal convoluted tubule cells.* Am J Physiol Renal Physiol, 2002. **283**(1): p. F29-40.
59. Stein, J.H. and H.J. Reineck, *The role of the collecting duct in the regulation of excretion of sodium and other electrolytes.* Kidney Int, 1974. **6**(1): p. 1-9.
60. Eladari, D., R. Chambrey, and J. Peti-Peterdi, *A new look at electrolyte transport in the distal tubule.* Annu Rev Physiol, 2012. **74**: p. 325-49.
61. Bengele, H.H., E.A. Alexander, and C.P. Lechene, *Calcium and magnesium transport along the inner medullary collecting duct of the rat.* Am J Physiol, 1980. **239**(1): p. F24-9.
62. Ahn, Y.J., et al., *Cloning and functional expression of the mouse epithelial sodium channel.* Am J Physiol, 1999. **277**(1): p. F121-9.
63. Canessa, C.M., et al., *Expression cloning of the epithelial sodium channel.* Kidney Int, 1995. **48**(4): p. 950-5.
64. Weixel, K.M., et al., *Resveratrol inhibits the epithelial sodium channel via phopshoinositides and AMP-activated protein kinase in kidney collecting duct cells.* PLoS One, 2013. **8**(10): p. e78019.
65. Vallon, V., et al., *SGLT2 mediates glucose reabsorption in the early proximal tubule.* J Am Soc Nephrol, 2011. **22**(1): p. 104-12.
66. American Diabetes, A., *Diagnosis and classification of diabetes mellitus.* Diabetes Care, 2009. **32 Suppl 1**: p. S62-7.
67. Unnikrishnan, R., et al., *Type 2 Diabetes: Demystifying the Global Epidemic.* Diabetes, 2017. **66**(6): p. 1432-1442.
68. Aldukhayel, A., *Prevalence of diabetic nephropathy among Type 2 diabetic patients in some of the Arab countries.* Int J Health Sci (Qassim), 2017. **11**(1): p. 1-4.
69. Ritz, E., *Nephropathy in type 2 diabetes.* J Intern Med, 1999. **245**(2): p. 111-26.
70. Cersosimo, E., P. Garlick, and J. Ferretti, *Renal glucose production during insulin-induced hypoglycemia in humans.* Diabetes, 1999. **48**(2): p. 261-6.
71. Wright, E.M., *Renal Na(+)-glucose cotransporters.* Am J Physiol Renal Physiol, 2001. **280**(1): p. F10-8.
72. Zhao, F.Q. and A.F. Keating, *Functional properties and genomics of glucose transporters.* Curr Genomics, 2007. **8**(2): p. 113-28.
73. Kanai, Y., et al., *The human kidney low affinity Na+/glucose cotransporter SGLT2. Delineation of the major renal reabsorptive mechanism for D-glucose.* J Clin Invest, 1994. **93**(1): p. 397-404.
74. Ghezzi, C., D.D.F. Loo, and E.M. Wright, *Physiology of renal glucose handling via SGLT1, SGLT2 and GLUT2.* Diabetologia, 2018. **61**(10): p. 2087-2097.
75. Lam, J.T., et al., *Missense mutations in SGLT1 cause glucose-galactose malabsorption by trafficking defects.* Biochim Biophys Acta, 1999. **1453**(2): p. 297-303.
76. van den Heuvel, L.P., et al., *Autosomal recessive renal glucosuria attributable to a mutation in the sodium glucose cotransporter (SGLT2).* Hum Genet, 2002. **111**(6): p. 544-7.
77. Santer, R., et al., *Molecular analysis of the SGLT2 gene in patients with renal glucosuria.* J Am Soc Nephrol, 2003. **14**(11): p. 2873-82.

78. Vallon, V., et al., *Knockout of Na-glucose transporter SGLT2 attenuates hyperglycemia and glomerular hyperfiltration but not kidney growth or injury in diabetes mellitus.* Am J Physiol Renal Physiol, 2013. **304**(2): p. F156-67.
79. Rahmoune, H., et al., *Glucose transporters in human renal proximal tubular cells isolated from the urine of patients with non-insulin-dependent diabetes.* Diabetes, 2005. **54**(12): p. 3427-34.
80. Vestri, S., et al., *Changes in sodium or glucose filtration rate modulate expression of glucose transporters in renal proximal tubular cells of rat.* J Membr Biol, 2001. **182**(2): p. 105-12.
81. Rizvi, A.A., *Addressing Hypertension in the Patient with Type 2 Diabetes Mellitus: Pathogenesis, Goals, and Therapeutic Approach.* Eur Med J Diabetes, 2017. **5**(1): p. 84-92.
82. Ferrannini, E. and W.C. Cushman, *Diabetes and hypertension: the bad companions.* Lancet, 2012. **380**(9841): p. 601-10.
83. Wu, C.Y., et al., *High Blood Pressure and All-Cause and Cardiovascular Disease Mortalities in Community-Dwelling Older Adults.* Medicine (Baltimore), 2015. **94**(47): p. e2160.
84. Drozdz, D. and K. Kawecka-Jaszcz, *Cardiovascular changes during chronic hypertensive states.* Pediatr Nephrol, 2014. **29**(9): p. 1507-16.
85. Lastra, G., et al., *Type 2 diabetes mellitus and hypertension: an update.* Endocrinol Metab Clin North Am, 2014. **43**(1): p. 103-22.
86. Beevers, G., G.Y. Lip, and E. O'Brien, *ABC of hypertension: The pathophysiology of hypertension.* BMJ, 2001. **322**(7291): p. 912-6.
87. Lytvyn, Y., et al., *Sodium Glucose Cotransporter-2 Inhibition in Heart Failure: Potential Mechanisms, Clinical Applications, and Summary of Clinical Trials.* Circulation, 2017. **136**(17): p. 1643-1658.
88. Kimura, T., et al., *Switching from low-dose thiazide diuretics to sodium-glucose cotransporter 2 inhibitor improves various metabolic parameters without affecting blood pressure in patients with type 2 diabetes and hypertension.* J Diabetes Investig, 2018. **9**(4): p. 875-881.
89. Zou, H., B. Zhou, and G. Xu, *SGLT2 inhibitors: a novel choice for the combination therapy in diabetic kidney disease.* Cardiovasc Diabetol, 2017. **16**(1): p. 65.
90. Cherney, D.Z., et al., *Renal hemodynamic effect of sodium-glucose cotransporter 2 inhibition in patients with type 1 diabetes mellitus.* Circulation, 2014. **129**(5): p. 587-97.
91. Vallon, V., R.C. Blantz, and S. Thomson, *Glomerular hyperfiltration and the salt paradox in early [corrected] type 1 diabetes mellitus: a tubulo-centric view.* J Am Soc Nephrol, 2003. **14**(2): p. 530-7.
92. Burns, K.D. and D. Cherney, *Renal Angiotensinogen and Sodium-Glucose Cotransporter-2 Inhibition: Insights from Experimental Diabetic Kidney Disease.* Am J Nephrol, 2019. **49**(4): p. 328-330.
93. de Rouffignac, C., *Editorial: Physiological role of the loop of henle in urinary concentration.* Kidney Int, 1972. **2**(6): p. 297-303.
94. Miller, N.L. and J.E. Lingeman, *Management of kidney stones.* BMJ, 2007. **334**(7591): p. 468-72.
95. Leslie, S.W., H. Sajjad, and K. Bashir, *24-Hour Urine Testing for Nephrolithiasis Interpretation*, in *StatPearls*. 2019: Treasure Island (FL).
96. Hodgkinson, A. and L.N. Pyrah, *The urinary excretion of calcium and inorganic phosphate in 344 patients with calcium stone of renal origin.* Br J Surg, 1958. **46**(195): p. 10-8.
97. Camus, J.P. and M. Joublin, *[Idiopathic hypercalciuria and its treatment].* Therapeutique, 1970. **46**(2): p. 175-6.
98. Job, J.C., M. Ribierre, and J. Radoual, *[Hypercalcemia, Hypercalciuria and Diminution of the Concentrating Power of the Kidney in the Course of Treatment of Congenital Hypothyroidism].* Arch Fr Pediatr, 1963. **20**: p. 1033-50.
99. Henneman, P.H., et al., *Idiopathic hypercaicuria.* N Engl J Med, 1958. **259**(17): p. 802-7.
100. Albright, F., et al., *Idiopathic hypercalciuria: a preliminary report.* Proc R Soc Med, 1953. **46**(12): p. 1077-81.
101. Pak, C.Y., et al., *The hypercalciurias. Causes, parathyroid functions, and diagnostic criteria.* J Clin Invest, 1974. **54**(2): p. 387-400.
102. Sorokin, I., et al., *Epidemiology of stone disease across the world.* World J Urol, 2017. **35**(9): p. 1301-1320.
103. Scales, C.D., Jr., et al., *Changing gender prevalence of stone disease.* J Urol, 2007. **177**(3): p. 979-82.

104. Alelign, T. and B. Petros, *Kidney Stone Disease: An Update on Current Concepts*. Adv Urol, 2018. **2018**: p. 3068365.
105. Barnela, S.R., et al., *Medical management of renal stone.* Indian J Endocrinol Metab, 2012. **16**(2): p. 236-9.
106. Trinchieri, A., et al., *A prospective study of recurrence rate and risk factors for recurrence after a first renal stone.* J Urol, 1999. **162**(1): p. 27-30.
107. Sutherland, J.W., J.H. Parks, and F.L. Coe, *Recurrence after a single renal stone in a community practice.* Miner Electrolyte Metab, 1985. **11**(4): p. 267-9.
108. Khan, S.R., et al., *Kidney stones.* Nat Rev Dis Primers, 2016. **2**: p. 16008.
109. Coe, F.L., A. Evan, and E. Worcester, *Kidney stone disease.* J Clin Invest, 2005. **115**(10): p. 2598-608.
110. Moe, O.W., *Kidney stones: pathophysiology and medical management.* Lancet, 2006. **367**(9507): p. 333-44.
111. Favazza, T., et al., *Factors influencing bladder stone formation in patients with spinal cord injury.* J Spinal Cord Med, 2004. **27**(3): p. 252-4.
112. Meyer, J.L. and L.H. Smith, *Growth of calcium oxalate crystals. II. Inhibition by natural urinary crystal growth inhibitors.* Invest Urol, 1975. **13**(1): p. 36-9.
113. Shah, O., D.G. Assimos, and R.P. Holmes, *Genetic and dietary factors in urinary citrate excretion.* J Endourol, 2005. **19**(2): p. 177-82.
114. Kok, D.J., et al., *Modulation of calcium oxalate monohydrate crystallization kinetics in vitro.* Kidney Int, 1988. **34**(3): p. 346-50.
115. Ryall, R.L., R.M. Harnett, and V.R. Marshall, *The effect of urine, pyrophosphate, citrate, magnesium and glycosaminoglycans on the growth and aggregation of calcium oxalate crystals in vitro.* Clin Chim Acta, 1981. **112**(3): p. 349-56.
116. Sidhu, H., et al., *Inhibition of calcium oxalate monohydrate (COM) crystal growth by pyrophosphate, citrate and rat urine.* Urol Res, 1986. **14**(6): p. 299-303.
117. Ryall, R.L., et al., *Effects of chondroitin sulphate, human serum albumin and Tamm-Horsfall mucoprotein on calcium oxalate crystallization in undiluted human urine.* Urol Res, 1991. **19**(3): p. 181-8.
118. Nakagawa, Y., et al., *Urine glycoprotein crystal growth inhibitors. Evidence for a molecular abnormality in calcium oxalate nephrolithiasis.* J Clin Invest, 1985. **76**(4): p. 1455-62.
119. Nakagawa, Y., V. Abram, and F.L. Coe, *Isolation of calcium oxalate crystal growth inhibitor from rat kidney and urine.* Am J Physiol, 1984. **247**(5 Pt 2): p. F765-72.
120. Coe, F.L., et al., *Role of nephrocalcin in inhibition of calcium oxalate crystallization and nephrolithiasis.* Miner Electrolyte Metab, 1994. **20**(6): p. 378-84.
121. Giachelli, C.M., et al., *Evidence for a role of osteopontin in macrophage infiltration in response to pathological stimuli in vivo.* Am J Pathol, 1998. **152**(2): p. 353-8.
122. Mustafi, D. and Y. Nakagawa, *Characterization of calcium-binding sites in the kidney stone inhibitor glycoprotein nephrocalcin with vanadyl ions: electron paramagnetic resonance and electron nuclear double resonance spectroscopy.* Proc Natl Acad Sci U S A, 1994. **91**(24): p. 11323-7.
123. Hess, B., *Tamm-Horsfall glycoprotein--inhibitor or promoter of calcium oxalate monohydrate crystallization processes?* Urol Res, 1992. **20**(1): p. 83-6.
124. Kumar, S. and A. Muchmore, *Tamm-Horsfall protein--uromodulin (1950-1990).* Kidney Int, 1990. **37**(6): p. 1395-401.
125. Worcester, E.M. and A.M. Beshensky, *Osteopontin inhibits nucleation of calcium oxalate crystals.* Ann N Y Acad Sci, 1995. **760**: p. 375-7.
126. Wesson, J.A., et al., *Control of calcium oxalate crystal structure and cell adherence by urinary macromolecules.* Kidney Int, 1998. **53**(4): p. 952-7.
127. Taylor, E.N. and G.C. Curhan, *Determinants of 24-hour urinary oxalate excretion.* Clin J Am Soc Nephrol, 2008. **3**(5): p. 1453-60.
128. Xi, Q., J.G. Hoenderop, and R.J. Bindels, *Regulation of magnesium reabsorption in DCT.* Pflugers Arch, 2009. **458**(1): p. 89-98.
129. Schaffers, O.J.M., et al., *The rise and fall of novel renal magnesium transporters.* Am J Physiol Renal Physiol, 2018. **314**(6): p. F1027-F1033.

130. Stuiver, M., et al., *CNNM2, encoding a basolateral protein required for renal Mg2+ handling, is mutated in dominant hypomagnesemia.* Am J Hum Genet, 2011. **88**(3): p. 333-43.
131. Funato, Y., D. Yamazaki, and H. Miki, *Renal function of cyclin M2 Mg2+ transporter maintains blood pressure.* J Hypertens, 2017. **35**(3): p. 585-592.
132. de Baaij, J.H., et al., *Membrane topology and intracellular processing of cyclin M2 (CNNM2).* J Biol Chem, 2012. **287**(17): p. 13644-55.
133. Gulerez, I., et al., *Phosphocysteine in the PRL-CNNM pathway mediates magnesium homeostasis.* EMBO Rep, 2016. **17**(12): p. 1890-1900.
134. Gimenez-Mascarell, P., et al., *Structural Basis of the Oncogenic Interaction of Phosphatase PRL-1 with the Magnesium Transporter CNNM2.* J Biol Chem, 2017. **292**(3): p. 786-801.
135. Gimenez-Mascarell, P., et al., *Current Structural Knowledge on the CNNM Family of Magnesium Transport Mediators.* Int J Mol Sci, 2019. **20**(5).
136. Hardy, S., et al., *The protein tyrosine phosphatase PRL-2 interacts with the magnesium transporter CNNM3 to promote oncogenesis.* Oncogene, 2015. **34**(8): p. 986-95.
137. Hirata, Y., et al., *Mg2+-dependent interactions of ATP with the cystathionine-beta-synthase (CBS) domains of a magnesium transporter.* J Biol Chem, 2014. **289**(21): p. 14731-9.
138. Alderton, A., et al., *Ancient conserved domain protein-1 binds copper and modifies its retention in cells.* J Neurochem, 2007. **103**(1): p. 312-21.
139. Chandran, U., et al., *Expression of Cnnm1 and Its Association with Stemness, Cell Cycle, and Differentiation in Spermatogenic Cells in Mouse Testis.* Biol Reprod, 2016. **95**(1): p. 7.
140. Wang, C.Y., et al., *Molecular cloning and characterization of a novel gene family of four ancient conserved domain proteins (ACDP).* Gene, 2003. **306**: p. 37-44.
141. Yamazaki, D., et al., *The Mg2+ transporter CNNM4 regulates sperm Ca2+ homeostasis and is essential for reproduction.* J Cell Sci, 2016. **129**(9): p. 1940-9.
142. Arjona, F.J., et al., *CNNM2 mutations cause impaired brain development and seizures in patients with hypomagnesemia.* PLoS Genet, 2014. **10**(4): p. e1004267.
143. Funato, Y., et al., *Membrane protein CNNM4-dependent Mg2+ efflux suppresses tumor progression.* J Clin Invest, 2014. **124**(12): p. 5398-410.
144. Hirata, Y., Y. Funato, and H. Miki, *Basolateral sorting of the Mg(2)(+) transporter CNNM4 requires interaction with AP-1A and AP-1B.* Biochem Biophys Res Commun, 2014. **455**(3-4): p. 184-9.
145. Dumaual, C.M., et al., *Tissue-specific alterations of PRL-1 and PRL-2 expression in cancer.* Am J Transl Res, 2012. **4**(1): p. 83-101.
146. Kato, H., et al., *High expression of PRL-3 promotes cancer cell motility and liver metastasis in human colorectal cancer: a predictive molecular marker of metachronous liver and lung metastases.* Clin Cancer Res, 2004. **10**(21): p. 7318-28.
147. Kostantin, E., et al., *Inhibition of PRL-2.CNNM3 Protein Complex Formation Decreases Breast Cancer Proliferation and Tumor Growth.* J Biol Chem, 2016. **291**(20): p. 10716-25.
148. Corre, T., et al., *Genome-Wide Meta-Analysis Unravels Interactions between Magnesium Homeostasis and Metabolic Phenotypes.* J Am Soc Nephrol, 2018. **29**(1): p. 335-348.
149. Rocha, N., et al., *The metabolic syndrome- associated small G protein ARL15 plays a role in adipocyte differentiation and adiponectin secretion.* Sci Rep, 2017. **7**(1): p. 17593.
150. Richards, J.B., et al., *A genome-wide association study reveals variants in ARL15 that influence adiponectin levels.* PLoS Genet, 2009. **5**(12): p. e1000768.

2

Effect of dapagliflozin treatment on the expression of renal Na^+ transporters/ channels on high fat diet diabetic mice

Chao Ma[1], Jeroen HF de Baaij[1], Paul J Millar[3], Victor A Gault[3], Bastiaan E de Galan[2], René JM Bindels[1], Joost GJ Hoenderop[1]

[1]Department of Physiology and [2]Internal Medicine, Radboud Institute for Molecular Life Sciences, Radboud university medical center, Nijmegen, The Netherlands. [3]SAAD Centre for Pharmacy and Diabetes, School of Biomedical Sciences, University of Ulster, Coleraine BT52 1SA, Northern Ireland, UK.

Nephron Clin Pract. 2019 May; 142(1): 51–60

Abstract

Inhibition of the sodium/glucose co-transporter 2 (SGLT2) is a new therapeutic strategy for diabetes. It is unclear how proximal loss of sodium (Na^+) (and glucose) affects the subsequent Na^+ transporters in the proximal tubule (PT), thick ascending limb of loop of Henle (TAL), distal convoluted tubule (DCT), and collecting duct (CD). Mice on a high fat diet were administered 3 doses streptozotocin (STZ) 6 days prior to oral dapagliflozin administration or vehicle for 18 days. A control group of lean mice were also included. Body weight and glucose were recorded at regular intervals during treatment. The expression of renal Na^+ transporters in nephron segments were analyzed by RT-qPCR and Western blot. Dapagliflozin treatment resulted in a significant reduction in body weight and blood glucose compared to vehicle treated controls. mRNA results showed that sodium-hydrogen antiporter 3 (*Nhe3*), solute carrier family 34 member 1 (*Slc34a1*) and sodium channel epithelial 1 subunit alpha (*Scnn1a)* expression was increased, Solute carrier family 8 member 1 (*Slc18a1*), sodium channel epithelial 1 subunit beta (*Scnn1b)* and sodium channel epithelial 1 subunit gamma (*Scnn1g)* expression declined, respectively, in dapagliflozin-treated mice when compared with saline vehicle mice. Solute carrier family 12 member 1 (*Slc12a1*) and solute carrier family 12 member 3 (*Slc12a3*) mRNA expression were not affected by dapagliflozin treatment. ATPase, sodium-potassium transporting, beta 1 polypeptide (*Atp1b1*) expression was also increased significantly by dapagliflozin treatment, but it did not affect ATPase, sodium-potassium transporting, alpha 1 polypeptide (*Atp1a1)* and solute carrier family 2 member 2 (*Slc2a2*) expression. Western blot analysis showed that sodium-phosphate cotransporter (NaPi-2a), NHE3 and sodium-potassium-ATPase subunit beta 1 (Na^+-K^+-ATPase β1) expression was up-regulated in dapagliflozin-treated diabetic mice when compared with saline vehicle mice. Our findings suggest that dapagliflozin treatment augments compensatory changes in the renal PT in diabetic mice.

Introduction

Type 2 diabetes mellitus (T2DM) is a major health problem affecting 415 million people worldwide [1, 2]. This represents 8.3% of the adult population, with equal rates in women and men [3]. From 2012 to 2015, approximately 1.5 to 5.0 million deaths each year resulted from diabetes [4]. Diabetes and hypertension frequently occur together [5]. Hypertension in these patients further increases their already elevated cardiovascular risks, yet is difficult to manage. Indeed, in about half of the diabetic population, blood pressure targets are not met despite the use of multiple blood pressure lowering drugs, including diuretics [6-8].

Recently, dapagliflozin, a SGLT2 (SLC5A2) inhibitor, was introduced as a novel class of glucose-lowering agents for the treatment of type 2 diabetes. As SGLT2 is responsible for approximately 90% of the filtered glucose reabsorption in the PT segment 1 and 2 (S1/2) [9-11], its inhibition reduces renal glucose and Na^+ reabsorption, leading to urinary glucose excretion and a reduction in blood glucose levels [12]. Therefore, dapagliflozin is considered to be an efficient and novel drug to treat patients with T2DM [13-16].

Some studies have also demonstrated that SGLT2 inhibitors exhibit an impressive diuretic effect and consequent blood pressure reduction, whereas others described modest effects on volume status [17-20]. SGLT2 inhibition reduces Na^+ reabsorption in the PT and thereby increases the distal tubular Na^+ load, which inhibits the renin-angiotensin-aldosterone system (RAAS) activation [21]. The kidneys efficiently reabsorb 99% of filtered Na^+ by the combined action of: *i)* the PT where 60-70% is reabsorbed via NHE3, SGLT1 and SGLT2 [22]; *ii)* the TAL that is responsible for 15-25% reabsorption via paracellular routes and NKCC2; *iii)* the DCT that reabsorbs 15-25% via the thiazide-sensitive NCC [23]; *iv)* the CD where the Epithelial sodium channel (ENaC) facilitates the reabsorption of the remaining 1-2% [10, 24].

A recent study has found that treatment with an SGLT2 inhibitor increases the expression of medullary transport proteins [1]. However, a systematic analysis of the compensatory mechanisms that regulate renal Na^+ reabsorption after SGLT2 treatment is lacking. Knowledge of which nephron segment compensates for proximal Na^+ loss is of great fundamental and clinical interest, as this would provide the major pharmacological target for antihypertensive treatment.

Therefore, the purpose of this study was to identify the compensatory impact of proximal Na^+ wasting by the SGLT2 inhibitor, dapagliflozin, on renal Na^+ transporters in high fat diabetic mice.

Methods and materials

Animal model

Adult male Swiss mice (Harlan, Oxon, UK) at 16 weeks of age were housed in an air-conditioned room at 22±2°C with 12:12 h light/dark cycle. Mice had free access to high fat diet (45% AFE Fat; Special Diet Services, Witham, UK; total energy 26.15 kJ/g). An additional lean group had free access to standard rodent chow (Teklad Global 18% Protein Rodent Diet; Harlan, UK; total energy 13.0 kJ/g). All animals were free to access drinking water and respective diet, and no adverse effects were observed during the entire experimental study. All experiments were performed according to the principles of Laboratory Animal Care (NIH publication no. 86-23, revised 1985) and UK Home Office Regulations (UK Animals Scientific Procedures Act 1986).

Experimental treatments

Mice commenced high fat diet on day -20 and remained on this diet for the duration of the study. On day -6, streptozotocin (50 mg/kg; i.p; Sigma-Aldrich, Dorset, UK) freshly prepared in ice-cold 0.1 M Na^+ citrate buffer (HCl/pH 4.5) was administered 3 doses in total over a period of 6 days to induce diabetes. On day 0, one group of high fat mice (n=8) commenced daily treatment with dapagliflozin (1 mg/kg; p.o.; Stratech Scientific Ltd.,Suffolk, UK) for 18 days whereas high fat control group (n=8) received saline vehicle (0.9% w/v NaCl; p.o.) once-daily for the same time period. The volume for the oral gavage was 100 µL. A diagrammatic representation of the experimental design is shown in Figure 1.

Quantitative analyses of gene expression

At study termination, total RNA was extracted from mouse kidney tissues with Trizol (Invitrogen, Carlsbad, CA, USA) in accordance with the manufacturer's protocol.

Subsequently, mouse RNA samples were subjected to DNase treatment (Invitrogen, Breda, The Netherlands) to prevent genomic DNA contamination and the reverse transcriptase reaction was subsequently performed to synthesize cDNA [25]. mRNA levels of the target genes were determined by relative RT-qPCR following the MIQE guidelines 20 with a CFX96TM real-time PCR detection system (Bio-Rad Laboratories, Hercules, CA, USA) using iQTM SYBR Green Supermix (Bio Rad) detection of single PCR product accumulation. Each group had 8 kidneys and RT-qPCR experiments were commenced in triplicate. All primers for *Slc5a2, Slc5a1, Nhe3, Slc34a1, Slc12a1, Slc12a3, Slc18a1, Scnn1a, Scnn1b, Scnn1g, Atp1a1, Atp1b1, Slc2a2,* and *Gapdh* were purchased from Biolegio BV (Nijmegen, Netherlands). In this study, gene expression levels were normalized to the expression levels of the standard species-specific reference genes glyceraldehyde 3-phosphate dehydrogenase (*Gapdh*). Relative mRNA expression was analyzed using the Livak method ($2^{-\Delta\Delta Ct}$). Primer sequences are shown in Table 1.

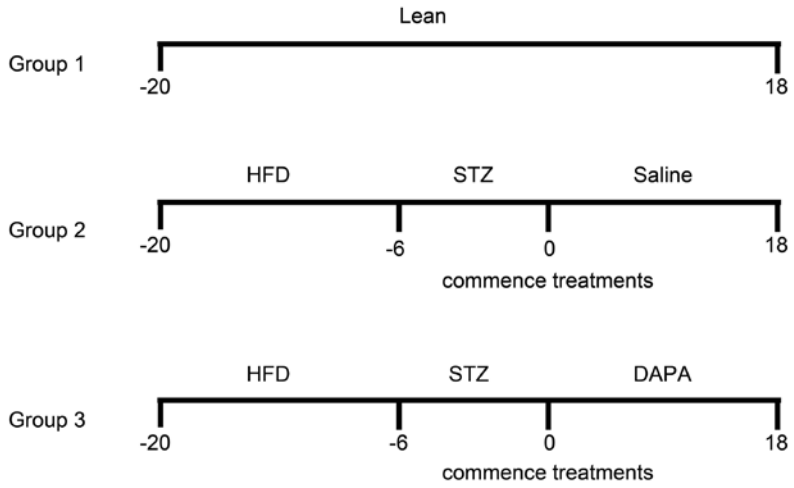

Figure 1. Timeline for the experimental study.

Group 1 (lean control), lean mice on normal diet for 38 days. Group 2 (high fat controls), mice commenced a high fat diet on day -20 and subsequently received STZ treatment on day -6. At day 0, saline vehicle was administered for 18 days. Group 3 (high fat dapagliflozin), mice commenced high fat diet on day -20 and subsequently received STZ on day -6. At day 0, dapagliflozin was administered for 18 days. STZ, streptozotocin; Lean, lean control mice; HFD, high fat diet treatment mice; DAPA, dapagliflozin treated mice.

Table 1. Primer sequences used for real-time quantitative RT-PCR.

Gene	Forward primer	Reverse primer
Slc5a2	5′-ATGGAGCAACACGTAGAGGC-3′	5′-ACATAGACCACAAGCCAACACC-3′
Slc5a1	5′-TCTGTAGTGGCAAGGGGAAG-3′	5′-ACAGGGCTTCTGTGTCTTGG-3′
Slc34a1	5′-AGGTGAGCTCCGCCATTCCGA-3′	5′-CCCTGCAAAAGCCCGCCTGA-3′
Slc12a1	5′-GGCTTGATCTTTGCTTTTGC-3′	5′-CCATCATTGAATCGCTCTCC-3′
Slc12a3	5′-CTTCGGCCACTGGCATTCTG-3′	5′-GATGGCAAGGTAGGAGATGG-3′
Slc18a1	5′-TCCCTACAAAACTATTGAAGGCACA-3′	5′-TTTCTCATACTCCTCGTCATCGATT-3′
Scnn1a	5′-GCTCAACCTTGACCTAGACCT-3′	5′-GCGGTGGAACTCGATCAGT-3′
Scnn1b	5′-GTCATCGGAACTTCACGCCTAT-3′	5′-TCCTCCTGACCGATGTCCAG-3′
Scnn1g	5′-TGACCTGCTTCTTCGATGGG-3′	5′-TTGCAGACCATACTCACTGCC-3′
Nhe3	5′-GGAACAGAGGCGGAGGAGCAT-3′	5′-GAAGTTGTGTGCCAGATTCTC-3′
Atp1a1	5′-GGGGTTGGACGAGACAAGTAT-3′	5′-CGGCTCAAATCTGTTCCGTAT-3′
Atp1b1	5′-ATCTCCTTCCGTCCTAATGACC-3′	5′-CTCGAAAATCATGTCGTCCTTCT-3′
Slc2a2	5′-AGAAGACAAGATCACCGGAACC-3′	5′-TCACACCGATGTCATAGCCG-3′
Gapdh	5′-TAACATCAAATGGGGTGAGG-3′	5′-GGTTCACACCCATCACAAAC-3′

Slc5a1, Solute carrier family 5 member 1; *Slc5a2*, Solute carrier family 5 member 2; *Slc34a1*, Solute carrier family 34 member 1; *Slc12a1*, Solute carrier family 12 member 1; *Slc12a3*, Solute carrier family 12 member 3; *Slc18a1*, Solute carrier family 8 member 1; *Scnn1 (a, b, g)*, Sodium channel epithelial 1 subunit (alpha, beta, gamma); Nhe3, Sodium-hydrogen antiporter 3; *Atp1a1*, ATPase, sodium-potassium transporting, alpha 1 polypeptide; *Atp1b1*, sodium-potassium transporting, beta 1 polypeptide; *Slc2a2*, Solute carrier family 2 member 2; *Gapdh*, Glyceraldehyde 3-phosphate dehydrogenase.

Buffers

Lysis buffer: 150 mM NaCl, 50 mM Tris-HCl (pH 7.5), 1 mM EDTA, 1 mM EGTA, 1 mM sodium-orthovanadate, 1% (v/v) Triton X-100, 10 mM sodium-glycerophosphate, 50 mM sodium fluoride, 0.27 M sucrose, 10 mM sodium pyrophosphate, containing freshly added tablet of complete protease inhibitor cocktail (Roche, Basel, Switzerland) and 0.1% (v/v) β-mercaptoethanol. SDS-PAGE sample buffer: 5x 10% (w/v) SDS, 10 mM β-mercaptoethanol, 50% (v/v) glycerol, 0.3 M Tris-HCl (pH 7.5), 0.05% (w/v) bromophenol blue. TBS-T (Tris-buffered saline, 0.1% (v/v) Tween 20): Tris-HCl (200 mM, pH 7.5), 0.15 M NaCl, and 0.2% (v/v) Tween-20.

Immunoblotting

Kidney tissues were isolated from mice and homogenized in ice cold lysis buffer. The kidney lysates were clarified by centrifugation at 4°C for 15 minutes at 16, 110 g and supernatants were stored at -80°C. Protein concentrations were measured by performing a Bicinchoninic acid protein assay (BCA) (Fisher Scientific, Hampton, NH, USA) and 20 µg of protein was used for western blot. Blots were then incubated in primary antibody overnight rolling at 4 °C. The following primary antibodies were used: sodium-chloride cotransporter (NCC) (Millipore, Billerica, MA, USA), sodium-potassium-chloride cotransporter (NKCC2) (Millipore, Billerica, MA, USA) [26], NaPi-2a (kind gift of Dr. Jürg Biber [27]), NHE3 (Millipore, Billerica, MA, USA) [28], Na^+-K^+-ATPase β1 (Merck KGaA, Darmstadt, Germany) [29], β-actin (Sigma-Aldrich, St. Louis, MO, USA). Next day, the blots were washed with TBS-T to remove unbound primary antibody and incubated with secondary antibodies for 1 hour at room temperature. Secondary antibodies were as follows: peroxidase conjugated goat anti-rabbit (Sigma Aldrich, Zwijndrecht, The Netherlands); peroxidase conjugated sheep anti-mouse (Jackson ImmunoResearch Laboratories Inc., West Grove, PA, USA). After subsequent washes, the protein was visualized with chemiluminescent reagent (SuperSignal West femto/pico; Thermo Scientific, Waltham, MA, USA). Photos were made with Chemidoc (Bio-Rad Laboratories Inc, Hercules, CA, USA).

Statistical analysis

Parametric data were analyzed using a one-way analysis of variance with Tukey's *post hoc* test to correct for multiple comparisons using GraphPad Prism software 5.0 (GraphPad, CA, USA). One-way ANOVA followed by Scheffe's test was used to examine the differences among groups. All data were shown as mean ± SEM. Differences were considered to be significant if $P<0.05$.

Results

Effects of high fat feeding and dapagliflozin on body weight and blood glucose

Mice receiving the high fat diet increased in body weight from day -20 to day 0 more than those receiving normal chow. From day 0 to 18, high fat control mice displayed a further modest increase in body weight, whereas mice treated with dapagliflozin exhibited a significant reduction in body weight. Body weight of lean mice did not differ during the study. High fat control mice displayed increased blood glucose concentrations from day 0 to 18. In contrast, high fat mice treated with dapagliflozin exhibited a marked reduction in blood glucose. Glucose concentrations were unchanged in lean mice. Results are shown in Table 2.

Table 2. Effects of high fat feeding and dapagliflozin on body weight and blood glucose.

Parameter	lean (n=8)		HF+saline (n=8)		HF+DAPA (n=8)	
	d0	d18	d0	d18	d0	d18
Body weight (g)	37.6±5.2	36.0±2.3	45.7±4.2	50.2±4.3[a]	43.5±5.7	37.6±5.2[b]
Blood glucose (mM)	5.2±0.9	5.8±0.4	18.5±3.7	22.3±4.1[a]	17.6±1.7	7.6±2.1[b]

Lean, lean control mice; HF + saline, high fat diet fed mice receiving saline vehicle; HF + DAPA, high fat diet fed mice receiving dapagliflozin (1mg/kg). d0, day 0, saline vehicle or DAPA were administered; d18, day 18, saline vehicle or DAPA were administered for 18 days; [a]$P<0.05$ vs. lean, [b]$P<0.05$ vs. HF + saline.

The effect of dapagliflozin on Na^+ transporter expression in the proximal tubule

RT-qPCR was performed to analyze the renal expression of *Slc5a1*, *Slc5a2*, *Nhe3*, and *Slc34a1* in the dapagliflozin-treated and control group mice. Gene expression of *Nhe3* and *Slc34a1* was increased significantly by 33% and 34%, respectively, in the dapagliflozin-treated mice compared to high fat control group (Figure 2C and Figure 2D).In contrast, there were no significant differences in the expression of *Slc5a1* and *Slc5a2* between dapagliflozin-treated group and vehicle control group (Figure 2A and Figure 2B). Protein expression level of NaPi-2a and NHE3 was further investigated by Western blot analysis (Figure 2E). The expression of NHE3 and NaPi-2a (Slc34a1) was increased by 55% and 139% in dapagliflozin treatment group when compared with saline vehicle diabetic mice ($P<0.05$) (Figure 2F and Figure 2G).

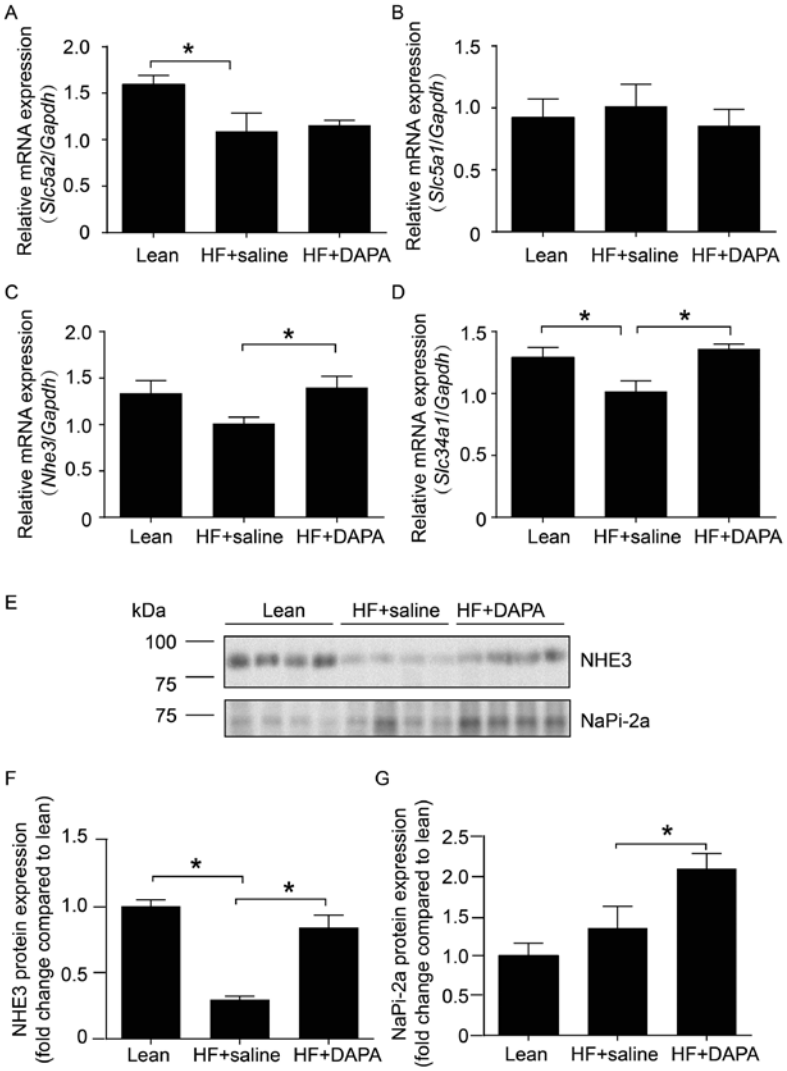

Figure 2. Effect of dapagliflozin on the expression of the Na^+ transporters in the proximal tubule.

A, B, C, and D, Quantitative RT-PCR analyses for the expression of *Slc5a1, Slc5a2, Nhe3,* and *Slc34a1* in the proximal tubule. E, Immunoblot analysis of NaPi-2a (~70 kDa), NHE3 (~93 kDa) in mice fed the indicated diet. F and G, Histograms for NaPi-2a, NHE3 Western blots results and normalized for β-actin expression. *P<0.05. Lean, lean control mice; HF + saline, high fat diet fed mice receiving saline vehicle; HF + DAPA, high fat diet fed mice receiving dapagliflozin (1mg/kg).

The effect of dapagliflozin on Na+ transporter expression in thick ascending limb of loop of Henle and distal convoluted tubule

In order to study the effect of dapagliflozin on the expression of the Na+ transporters in the TAL and DCT, the expression of *Slc12a1*, *Slc12a3*, and *Slc18a1* was analyzed by RT-qPCR. The expression of *Slc12a1* and *Slc12a3* tended to increase by 23% and 17%, respectively, in the dapagliflozin treatment group (P<0.05) (Figure 3A and Figure 3B). However, these changes did not reach statistical significance. The expression of *Slc18a1* was shown to decrease by 27% in the dapagliflozin treatment group when compared with saline vehicle control group (P<0.05) (Figure 3C). Dapagliflozin treatment did not alter the protein abundance of NCC and NKCC2 when compared with saline vehicle treated diabetic mice (Figure 3D-F)

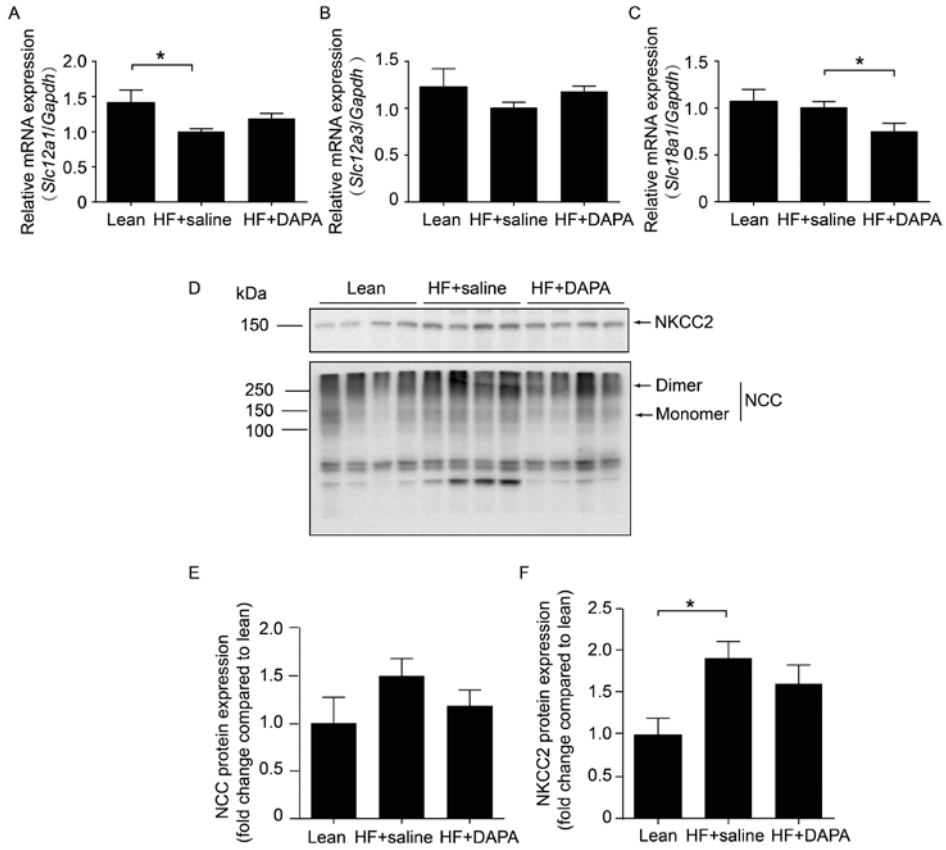

Figure 3. Effect of dapagliflozin on the expression of the Na+ transporters in the loop of Henle and distal convoluted tubule.

A, B, and C, Quantitative RT-PCR analyses for the expression of *Slc12a1, Slc12a3*, and *Slc18a1* in the loop of Henle and distal convoluted tubule. D, Immunoblot analysis of NKCC2 (~150 kDa), NCC (~120 kDa) in mice fed the indicated diet. E, Histograms for NCC Western blot results and normalized for β-actin expression. F, Histograms for NKCC2 Western blot results and normalized for β-actin expression. *P<0.05. Lean, lean control mice; HF + saline, high fat diet fed mice receiving saline vehicle; HF + DAPA, high fat diet fed mice receiving dapagliflozin (1mg/kg).

The effect of dapagliflozin on the expression of Na^+ channels in the collecting duct

To further investigate the effect of proximal Na^+ loss on the Na^+ transporters in the CD, we tested the expression of the *Scnn1* (*a*, *b* and *g*) by RT-qPCR. Dapagliflozin treatment increased the expression of *Scnn1a* by 29% when compared with vehicle control mice (Figure 4A). In addition, the expression of *Scnn1b* and *Scnn1g* declined significantly by 13% and 26%, respectively, in dapagliflozin-treated group compared to vehicle controls (Figure 4B and Figure 4C).

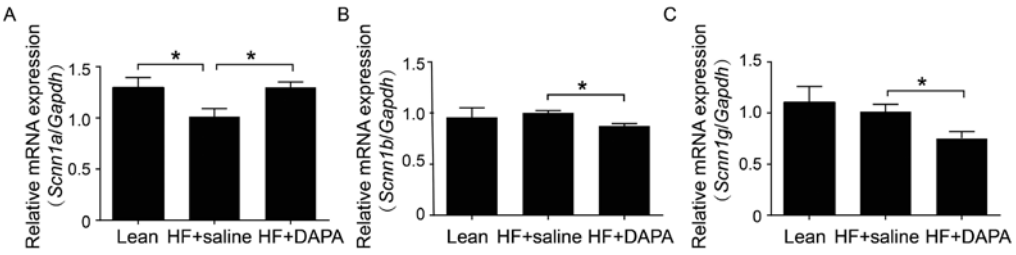

Figure 4. Effect of dapagliflozin on the expression of the Na^+ transporters in the collecting duct.

A, B, and C, Quantitative RT-PCR analyses for the expression of *Scnn1a, Scnn1b,* and *Scnn1g*, in the collecting duct. *P<0.05. Lean, lean control mice; HF + saline, high fat diet fed mice receiving saline vehicle; HF + DAPA, high fat diet fed mice receiving dapagliflozin (1mg/kg).

The effect of dapagliflozin on the expression of Na^+-K^+-ATPase and glucose transporter 2

We also evaluated the effect of dapagliflozin on *Slc2a2* and *Na^+-K^+-ATPase* transporters by RT-qPCR. The expression of *Atp1b1* was significantly increased by 32% in the dapagliflozin-treated mice compared to the vehicle control group (Figure 5B). The expression of *Atp1a1* was not changed in the dapagliflozin-treated group (Figure 5A). Dapagliflozin treatment caused a slight reduction in the expression of *Slc2a2* compared to vehicle control group, but this effect failed to reach statistical significance (Figure 5C). Western blot analysis was further used to investigate the protein expression level of Na^+-K^+-ATPase β1. Na^+-K^+-ATPase β1 expression was increased by 123% in dapagliflozin treatment group when compared with saline vehicle diabetic mice (Figure 5D-E).

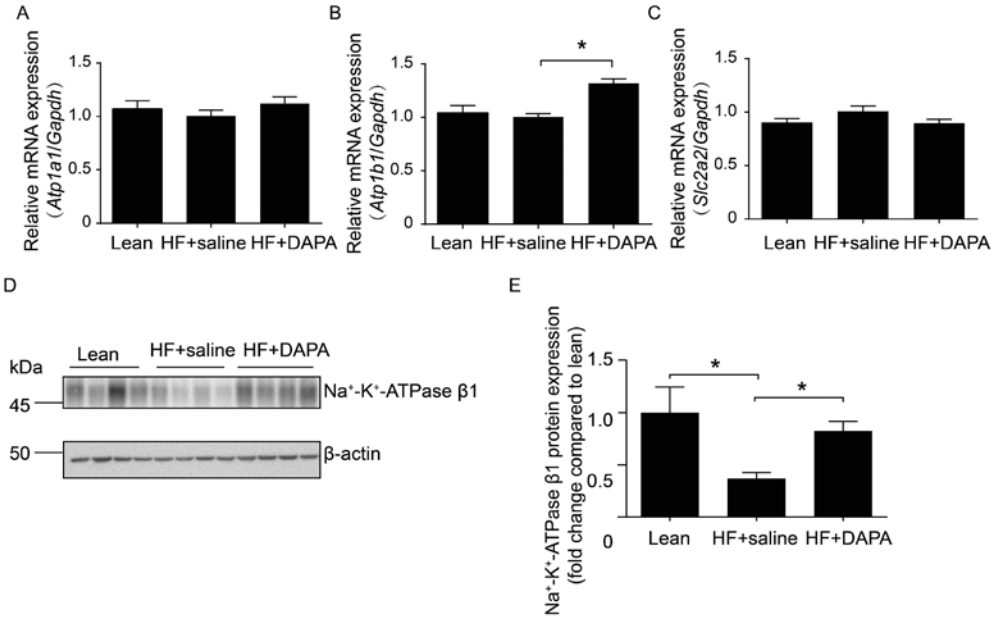

Figure 5. Effect of dapagliflozin on Na⁺-K⁺-ATPase and Slc2a2.

A, B, and C, Quantitative RT-PCR analyses for the expression of *Atp1a1*, *Atp1b1*, and Slc2a2. D, Immunoblot analysis of Na⁺-K⁺-ATPase β1 (~50 kDa) in mice fed the indicated diet. E, Histogram for Na⁺-K⁺-ATPase β1 Western blots results and normalized for β-actin expression. *P<0.05. Lean, lean control mice; HF + saline, high fat diet fed mice receiving saline vehicle; HF + DAPA, high fat diet fed mice receiving dapagliflozin (1mg/kg).

Discussion

In this study, we demonstrated that inhibition of SGLT2 increased the mRNA expression level of *Nhe3*, *Slc34a1*, and *Scnn1a*. Western blotting results showed that the protein expression level of NHE3 and NaPi-2a was increased in dapagliflozin-treated mice. Moreover, Na⁺-K⁺-ATPase β1 protein expression level was also increased. Our findings demonstrated that proximal inhibition of Na⁺ reabsorption via SGLT2 is compensated by increased expression of local Na⁺ transporters in the PT but not in the TAL, DCT and CD.

The kidneys reabsorb large amounts of filtered glucose to clear urinary glucose, primarily through the SGLT2 in the S1 segment of the PT. Inhibitors of SGLT2 are newly developed anti-diabetic agents and interfere with the pathway of physiological glucose reabsorption in the kidney. In this study, high fat and STZ induction significantly increased blood glucose when compared with lean group mice. In the dapagliflozin treatment group, we found that the blood glucose levels decreased significantly when compared with the vehicle control group. In our study, STZ-induced diabetes decreased SGLT2 expression. María F *et al.* have also demonstrated that STZ decreased SGLT2 expression and activity [30]. In contrast, SGLT2 expression was increased in Akita mice

[31], humans [32] with type 2 diabetes, and alloxan-induced diabetic rats [33]. Indeed, the use of different diabetic models may, therefore, result in different SGLT2 expression. However, despite lower SGLT2 expression in STZ-induced mice, dapagliflozin treatment reduced blood glucose levels. We, therefore, expect that in other studies with higher SGLT2 expression, the observed effects may even be larger. Moreover, dapagliflozin treatment did not change SGLT2 expression in our experiment. The expression of SGLT2 does not necessarily alter upon dapagliflozin treatment. Other studies also found that pharmacological SGLT2 inhibition does not affect the expression of SGLT2 [31, 34]. Given the reduction of blood glucose concentrations in the dapagliflozin-treated group at day 18 when compared with saline vehicle mice, the unchanged SGLT2 expression did not impair the effects of dapagliflozin treatment. Therefore, we do not expect that this has a major impact on our results.

The management of hypertension in diabetes is not without controversy [17]. Hence, the precise level at which anti-hypertensive therapy should be initiated and what the target blood pressure should be, remain difficult issues. Many patients with type 2 diabetes receive multiple drugs to treat both hyperglycemia and hypertension. The new class of SGLT2 inhibitors also induces renal Na^+ wasting and, therefore, will have blood pressure reducing properties. However, some studies report an impressive diuretic effect and consequent reduction in blood pressure, others described modest effects on volume status [17, 35]. It is known that the compensatory capacity of the kidney is immense [36]. Inhibition of Na^+ reabsorption in the PT will turn on compensatory systems in local or more distally located segments to counteract the proximal Na^+ loss.

In this study, dapagliflozin treatment significantly increased the mRNA expression level of *Nhe3*, *Slc34a1* and *Scnn1a*. In line with the mRNA expression level, Western blot results showed that NHE3, NaPi-2a also increased in the dapagliflozin treatment group when compared with saline vehicle mice. Therefore, our results suggest that the inhibition of SGLT2 in the PT can turn on the local Na^+ compensatory systems. Increased reabsorption of Na^+ may result in Na^+ retention and elevate blood pressure in type 2 diabetes [37-39]. Wang *et al*. showed that changed expression of Na^+ transport in renal PT can be compensated by changes in more distal tubule in nephron, by tubuloglomerular feedback and also by glomerular filtration rate adjustments. Nevertheless, extracellular fluid volume and consequently blood pressure can also be affected by the changed expression of Na^+ transport in the PT. Na^+ reabsorption initially happens at the PT apical membrane, therefore resulting in making apical Na^+ transport critical in adjusting the extracellular fluid volume and ultimately blood pressure control [38]. Indeed, in polygenic human essential hypertension, the increase in Na^+ transport occurs at the PT and TAL [40-42] rather than in more distal nephron segments [43]. Unfortunately, there were no plasma and urine electrolytes results in this study. Therefore, further studies are needed to better understand of the compensatory mechanisms of the Na^+ transporters on adjusting blood pressure control.

SGLT2 is located in the S1 segment and accounts for 90% of the glucose reabsorption [44-47]. Na^+ reabsorption across the cell membrane creates an energy gradient that in turn allows the reabsorption of glucose. On the other side of the cell, Na^+ is extruded through Na^+-K^+-ATPase into the bloodstream [48-50]. Slc2a2 is responsible for transporting glucose into bloodstream [51-53]. In order to evaluate if the increased expression of Na^+ transporters in the PT influenced the expression of Na^+-K^+-ATPase and Slc2a2, we furthermore tested the expression of *Atp1a1*, *Atp1b1*, and *Slc2a2* transporters by RT-qPCR. The results revealed that the expression of *Atp1b1* increased significantly in the dapagliflozin-treated group, however, the expression of *Atp1a1* and *Slc2a2* did not change. Furthermore, Na^+-K^+-ATPase β1 protein expression level was also increased in the dapagliflozin-treated group. The increased expression of Na^+-K^+-ATPase β1 may facilitate Na^+ to be transported into the bloodstream, which could lead to salt retention and hypertension. These effects may blunt the potential blood pressure-lowering effects of the SGLT2 inhibitor.

In conclusion, we demonstrated that the SGLT2 inhibitor, dapagliflozin, increased NHE3, NaPi-2a expression in the PT. Furthermore, Na^+-K^+-ATPase β1 was also up-regulated which may facilitate the transport of the Na^+ into the bloodstream. Our findings provide insights that dapagliflozin treatment augments compensatory changes in the renal PT in diabetic mice.

Acknowledgements

This work was financially supported by grants from the Netherlands Organization for Scientific Research (NWO Veni 016.186.012 and VICI 016.130.668) and was supported by grants from the Radboud Institute for Molecular Life Science. The authors thank Caro Bos for her excellent technical assistance.

References

1. Chen, L., et al., *Effect of Dapagliflozin Treatment on Fluid and Electrolyte Balance in Diabetic Rats.* Am J Med Sci, 2016. **352**(5): p. 517-523.
2. Shi, Y. and F.B. Hu, *The global implications of diabetes and cancer.* Lancet, 2014. **383**(9933): p. 1947-8.
3. Vos, T., et al., *Years lived with disability (YLDs) for 1160 sequelae of 289 diseases and injuries 1990-2010: a systematic analysis for the Global Burden of Disease Study 2010.* Lancet, 2012. **380**(9859): p. 2163-96.
4. *Death rates fall for 8 of 10 top causes; Alzheimer's up to no. 6.* Hosp Health Netw, 2008. **82**(7): p. 127.
5. Campbell, N.R., et al., *Hypertension in people with type 2 diabetes: Update on pharmacologic management.* Can Fam Physician, 2011. **57**(9): p. 997-1002, e347-53.
6. Cheung, B.M. and C. Li, *Diabetes and hypertension: is there a common metabolic pathway?* Curr Atheroscler Rep, 2012. **14**(2): p. 160-6.
7. Canale, M.P., et al., *Obesity-related metabolic syndrome: mechanisms of sympathetic overactivity.* Int J Endocrinol, 2013. **2013**: p. 865965.
8. Oliva, R.V. and G.L. Bakris, *Blood pressure effects of sodium-glucose co-transport 2 (SGLT2) inhibitors.* J Am Soc Hypertens, 2014. **8**(5): p. 330-9.
9. Gorboulev, V., et al., *Na(+)-D-glucose cotransporter SGLT1 is pivotal for intestinal glucose absorption and glucose-dependent incretin secretion.* Diabetes, 2012. **61**(1): p. 187-96.
10. Vrhovac, I., et al., *Localizations of Na(+)-D-glucose cotransporters SGLT1 and SGLT2 in human kidney and of SGLT1 in human small intestine, liver, lung, and heart.* Pflugers Arch, 2015. **467**(9): p. 1881-98.
11. Wright, E.M., D.D. Loo, and B.A. Hirayama, *Biology of human sodium glucose transporters.* Physiol Rev, 2011. **91**(2): p. 733-94.
12. Plosker, G.L., *Dapagliflozin: a review of its use in type 2 diabetes mellitus.* Drugs, 2012. **72**(17): p. 2289-312.
13. Ptaszynska, A., et al., *Safety profile of dapagliflozin for type 2 diabetes: pooled analysis of clinical studies for overall safety and rare events.* Drug Saf, 2014. **37**(10): p. 815-29.
14. Wilding, J.P., et al., *Dapagliflozin in patients with type 2 diabetes receiving high doses of insulin: efficacy and safety over 2 years.* Diabetes Obes Metab, 2014. **16**(2): p. 124-36.
15. Kaku, K., et al., *Efficacy and safety of dapagliflozin as a monotherapy for type 2 diabetes mellitus in Japanese patients with inadequate glycaemic control: a phase II multicentre, randomized, double-blind, placebo-controlled trial.* Diabetes Obes Metab, 2013. **15**(5): p. 432-40.
16. Ferrannini, E., et al., *Dapagliflozin monotherapy in type 2 diabetic patients with inadequate glycemic control by diet and exercise: a randomized, double-blind, placebo-controlled, phase 3 trial.* Diabetes Care, 2010. **33**(10): p. 2217-24.
17. Lovshin, J.A. and R.E. Gilbert, *Are SGLT2 inhibitors reasonable antihypertensive drugs and renoprotective?* Curr Hypertens Rep, 2015. **17**(6): p. 551.
18. Group, S.R., et al., *A Randomized Trial of Intensive versus Standard Blood-Pressure Control.* N Engl J Med, 2015. **373**(22): p. 2103-16.
19. Kohan, D.E., et al., *Long-term study of patients with type 2 diabetes and moderate renal impairment shows that dapagliflozin reduces weight and blood pressure but does not improve glycemic control.* Kidney Int, 2014. **85**(4): p. 962-71.
20. Osorio, H., et al., *Effect of treatment with losartan on salt sensitivity and SGLT2 expression in hypertensive diabetic rats.* Diabetes Res Clin Pract, 2009. **86**(3): p. e46-9.
21. Vallon, V. and S.C. Thomson, *Renal function in diabetic disease models: the tubular system in the pathophysiology of the diabetic kidney.* Annu Rev Physiol, 2012. **74**: p. 351-75.
22. Fujimoto, M., K. Naito, and T. Kubota, *Electrochemical profile for ion transport across the membrane of proximal tubular cells.* Membr Biochem, 1980. **3**(1-2): p. 67-97.
23. Cadnapaphornchai, M.A., et al., *Urinary concentrating defect in hypothyroid rats: role of sodium, potassium, 2-chloride co-transporter, and aquaporins.* J Am Soc Nephrol, 2003. **14**(3): p. 566-74.

24. Palmer, L.G. and G. Frindt, *Amiloride-sensitive Na channels from the apical membrane of the rat cortical collecting tubule.* Proc Natl Acad Sci U S A, 1986. **83**(8): p. 2767-70.
25. de Baaij, J.H., et al., *P2X6 Knockout Mice Exhibit Normal Electrolyte Homeostasis.* PLoS One, 2016. **11**(6): p. e0156803.
26. van der Wijst, J., et al., *Effects of a high-sodium/low-potassium diet on renal calcium, magnesium, and phosphate handling.* Am J Physiol Renal Physiol, 2018. **315**(1): p. F110-F122.
27. Custer, M., et al., *Expression of Na-P(i) cotransport in rat kidney: localization by RT-PCR and immunohistochemistry.* Am J Physiol, 1994. **266**(5 Pt 2): p. F767-74.
28. de Groot, T., et al., *Acetazolamide Attenuates Lithium-Induced Nephrogenic Diabetes Insipidus.* J Am Soc Nephrol, 2016. **27**(7): p. 2082-91.
29. Gottardi, C.J. and M.J. Caplan, *Delivery of Na+,K(+)-ATPase in polarized epithelial cells.* Science, 1993. **260**(5107): p. 552-4; author reply 554-6.
30. Albertoni Borghese, M.F., et al., *Expression and activity of SGLT2 in diabetes induced by streptozotocin: relationship with the lipid environment.* Nephron Physiol, 2009. **112**(3): p. p45-52.
31. Vallon, V., et al., *SGLT2 inhibitor empagliflozin reduces renal growth and albuminuria in proportion to hyperglycemia and prevents glomerular hyperfiltration in diabetic Akita mice.* Am J Physiol Renal Physiol, 2014. **306**(2): p. F194-204.
32. Quinn, P.G. and D. Yeagley, *Insulin regulation of PEPCK gene expression: a model for rapid and reversible modulation.* Curr Drug Targets Immune Endocr Metabol Disord, 2005. **5**(4): p. 423-37.
33. Freitas, H.S., et al., *Na(+) -glucose transporter-2 messenger ribonucleic acid expression in kidney of diabetic rats correlates with glycemic levels: involvement of hepatocyte nuclear factor-1alpha expression and activity.* Endocrinology, 2008. **149**(2): p. 717-24.
34. Gembardt, F., et al., *The SGLT2 inhibitor empagliflozin ameliorates early features of diabetic nephropathy in BTBR ob/ob type 2 diabetic mice with and without hypertension.* Am J Physiol Renal Physiol, 2014. **307**(3): p. F317-25.
35. List, J.F., et al., *Sodium-glucose cotransport inhibition with dapagliflozin in type 2 diabetes.* Diabetes Care, 2009. **32**(4): p. 650-7.
36. Roth, K.S., *Diagnosis of renal tubular transport disorders. A guide for the clinician.* Clin Pediatr (Phila), 1988. **27**(10): p. 463-70.
37. Pratt, J.H., *Central role for ENaC in development of hypertension.* J Am Soc Nephrol, 2005. **16**(11): p. 3154-9.
38. Wang, X., et al., *The regulation of proximal tubular salt transport in hypertension: an update.* Curr Opin Nephrol Hypertens, 2009. **18**(5): p. 412-20.
39. Xu, L., et al., *Effects of angiotensin II on NaPi-IIa co-transporter expression and activity in rat renal cortex.* Biochim Biophys Acta, 2004. **1667**(2): p. 114-21.
40. Doris, P.A., *Renal proximal tubule sodium transport and genetic mechanisms of essential hypertension.* J Hypertens, 2000. **18**(5): p. 509-19.
41. Ortiz, P.A. and J.L. Garvin, *Intrarenal transport and vasoactive substances in hypertension.* Hypertension, 2001. **38**(3 Pt 2): p. 621-4.
42. Staessen, J.A., et al., *Blood pressure and renal sodium handling in relation to genetic variation in the DRD1 promoter and GRK4.* Hypertension, 2008. **51**(6): p. 1643-50.
43. Ji, W., et al., *Rare independent mutations in renal salt handling genes contribute to blood pressure variation.* Nat Genet, 2008. **40**(5): p. 592-599.
44. Fujita, Y. and N. Inagaki, *Renal sodium glucose cotransporter 2 inhibitors as a novel therapeutic approach to treatment of type 2 diabetes: Clinical data and mechanism of action.* J Diabetes Investig, 2014. **5**(3): p. 265-75.
45. Santer, R. and J. Calado, *Familial renal glucosuria and SGLT2: from a mendelian trait to a therapeutic target.* Clin J Am Soc Nephrol, 2010. **5**(1): p. 133-41.
46. Kanai, Y., et al., *The human kidney low affinity Na+/glucose cotransporter SGLT2. Delineation of the major renal reabsorptive mechanism for D-glucose.* J Clin Invest, 1994. **93**(1): p. 397-404.
47. Nomura, S., *Renal sodium-dependent glucose cotransporter 2 (SGLT2) inhibitors for new anti-diabetic agent.* Curr Top Med Chem, 2010. **10**(4): p. 411-8.

48. Avner, E.D., et al., *Sodium-potassium ATPase activity mediates cyst formation in metanephric organ culture.* Kidney Int, 1985. **28**(3): p. 447-55.
49. Ernst, S.A., *Transport ATPase cytochemistry: ultrastructural localization of potassium-dependent and potassium-independent phosphatase activities in rat kidney cortex.* J Cell Biol, 1975. **66**(3): p. 586-608.
50. Landon, E.J., N. Jazab, and L. Forte, *Aldosterone and sodium-potassium-dependent ATPase activity of rat kidney membranes.* Am J Physiol, 1966. **211**(4): p. 1050-6.
51. Poudel, R.R., *Renal glucose handling in diabetes and sodium glucose cotransporter 2 inhibition.* Indian J Endocrinol Metab, 2013. **17**(4): p. 588-93.
52. Leloup, C., et al., *Glucose transporter 2 (GLUT 2): expression in specific brain nuclei.* Brain Res, 1994. **638**(1-2): p. 221-6.
53. Thorens, B., *Molecular and cellular physiology of GLUT-2, a high-Km facilitated diffusion glucose transporter.* Int Rev Cytol, 1992. **137**: p. 209-38.

3

Development of Ca^{2+}-binding peptides to control urinary Ca^{2+} concentration to prevent kidney stone formation

Chao Ma[1], Sanédy Simon[1], Caro Bos[1], Joost GJ Hoenderop[1], Jenny van der Wijst[1]

[1]Department of Physiology, Radboud Institute for Molecular Life Sciences, Radboud university medical center, Nijmegen, The Netherlands.

In preparation

Abstract

The incidence of nephrolithiasis has been increasing worldwide in recent decades. Although medical therapies have significantly improved nephrolithiasis treatment, the recurrence rate is still very high after 5 years. Thus, an improved, possibly preventive treatment is needed. Our study aims to develop a novel drug to prevent kidney stone formation, based on our body's calcium (Ca^{2+}) regulation. We developed several Ca^{2+}-binding peptides, analyzed their Ca^{2+}-binding affinity by circular dichroism and tested their safety on renal proximal tubule cells. Results showed a Ca^{2+}-induced change in ellipticity at 220 nm for peptide 4 (Ac-DKNGDGYIDAAE-NH_2). This peptide did not induce cell toxicity and exhibited cellular uptake in Human Kidney-2 (HK-2) cells. To ultimately investigate the biological function of these peptides *in vivo*, we aimed to establish a mouse model of nephrolithiasis. 20 male C57BL/6J mice were given 1% (v/v) ethylene glycol (EG) via drinking water and were administrated either a normal Ca^{2+} diet (0.92% w/w) or a high Ca^{2+} diet (2% w/w) for 28 days. Blood and 24 hours urine were collected on day 1, 7, 14, 21, and 28 for electrolyte analysis. Serum Ca^{2+} concentrations and urinary Ca^{2+} excretions were similar between the two groups, except for day 21 on which serum Ca^{2+} concentration was significantly higher in the high Ca^{2+} diet group. Ca^{2+} crystal deposits were not detected in the kidneys by Von Kossa staining. Together, our study indicated that peptide 4 (Ac-DKNGDGYIDAAE-NH_2) may have the potential to serve as a peptide with low Ca^{2+}-binding affinity in future studies in the kidney stone mouse model. So far, we did not establish such a model as we demonstrated that 1% (v/v) EG administration in drinking water supplied with a high Ca^{2+} diet cannot cause kidney stones in C57BL/6J mice.

Introduction

Nephrolithiasis (kidney stone disease) is a major medical problem with a prevalence ranging from 7-13% in North America, 1-5% in Asia and 5-9% in Europe, and the incidence is predicted to rise in the next decades [1, 2]. This growing trend is generally considered to be due to changes in our lifestyle such as lack of physical activity and poor dietary habits [3]. Kidney stone disease is linked to an increased rate of chronic kidney disease, end-stage renal failure, hypertension, and myocardial infarction [4]. Medical treatment of kidney stones includes dietary management, pharmacological interventions, extracorporeal shock wave lithotripsy, and minor endourological intervention for stone removal [5, 6]. These treatments can result in severe side effects, such as shock wave lithotripsy that may cause acute renal damage [7]. Although medication and minimally invasive surgery have significantly improved acute stone management, the recurrence rate can be up to 14% after 1 year and 35% after 5 years [8]. These data suggest the need for finding a more effective approach to prevent stone recurrence.

Two main predisposing factors for kidney stone formation are hyperoxaluria and hypercalciuria, with the majority of kidney stones being Ca^{2+} oxalate (CaOx) stones [9]. An estimated 40-60% of kidney stone patients have an increased urinary Ca^{2+} excretion [10-12]. Most of these patients have idiopathic hypercalciuria, meaning that the exact underlying mechanism responsible for their hypercalciuria remains unknown [13, 14].

The pathogenesis of nephrolithiasis is a complicated process that is still not entirely elucidated. In general, stone formation includes a cascade of events: urinary supersaturation, nucleation, crystal growth, crystal aggregation, and crystal retention [3, 8]. The pro-urine becomes increasingly concentrated towards the loop of Henle. The osmolality in this segment can increase 10-fold or even higher as a result of the 180-degree turn of the limb of Henle's loop and the minimal reabsorption of water at this segment. This hyperosmolar microenvironment, although crucial for the function of kidney, leads to urinary 'supersaturation' with poorly soluble waste salts such as Ca^{2+} phosphate (CaP) and CaOx, which are the main components for crystal formation [15]. The inability to excrete crystalline material results in the onset of nucleation and is highly appropriate for accumulating Ca^{2+}-binding proteins that promote crystal growth and aggregation [3].

In this study, we aimed to develop a Ca^{2+}-binding peptide with supersaturation-specific Ca^{2+}-buffering capacity that may ultimately be used to investigate the peptide's safety and efficacy by repeated administration in a kidney stone mouse model. Therefore, we used the peptide sequence of the so-called EF-hand protein domain [16]. The structure of an EF-hand is a helix-loop-helix motif linked by a loop of 12 amino acids that are key for Ca^{2+} binding (Figure 2A) [17]. Yap *et al*. compared 90 EF-hand motif structures in 31 EF-hand containing proteins, and found that variations in the amino acids of the Ca^{2+}-binding loop can lead to a wide range of Ca^{2+}-binding affinities [18]. Based on this knowledge, we synthesized several small EF-hand peptides (around 20-30 residues) and tested their Ca^{2+}-

binding affinity. In addition, the present study aimed to establish a kidney stone mouse model. Wildtype (C57BL/6J) mice were treated with 1% (v/v) ethylene glycol (EG) for 28 days via their drinking water while simultaneously placed on either a high-Ca^{2+} (2% w/w) diet or normal Ca^{2+} diet (0.92% w/w) in order to induce Ca^{2+} crystal deposition in the kidney.

Methods and materials

Ethical approval of the study protocol

This study has been approved by the Dutch Central Commission for Animal Experiments (CCD; AVD1030020186805) and the Animal Ethics Board of Radboud University Nijmegen (RU-DEC2018-0030; Nijmegen, The Netherlands).

Chemicals

The EG was provided by Merck Schuchardt OHG and was diluted to 1% (v/v) EG in demi water. Peptides were purchased from EMC Microcollections (Tübingen, Germany), with peptide sequences depicted in Figure 2. All of the peptides in the figure were amino (N)-terminus acetylated (Ac) and carboxy (C)-terminus amidated (NH_2).

Cell culture

HK-2 cells were cultured in Dulbeccos Modified Eagles Medium (DMEM; Gibco, Thermo Fisher Scientific, Waltham, MA, USA) supplemented with Hams-F12 (GE Healthcare, Chicago, USA), HEPES (20 mM) (Gibco, Thermo Fisher Scientific), 1% (v/v) penicillin-streptomycin (Gibco, Thermo Fisher Scientific), 10% (v/v) fetal bovine serum and non-essential amino acids (Lonza Westburg, Arnhem, The Netherlands). The cells were incubated at 37 °C a humidity-controlled incubator with 5% (v/v) CO_2 atmosphere.

Resazurin assay

The resazurin assay (Sigma Aldrich, Zwijndrecht, The Netherlands), staining mitochondrial viability, is used as a measure of cell viability upon exposure of increasing concentrations of peptide to HK-2 cells. At the start of the experiment, 10,000 cells per well were seeded into 96-well plates. After 24 hours, the medium was replaced by a series of peptide concentrations (0-1 mM, dissolved in 50 mM HEPES, pH 8.0 adjusted with NaOH), with peptide diluted in the cell culture medium. Cells were incubated with the peptide for 2, 4, and 24 hours at 37 °C. At the indicated time points, the peptide solution was removed from the cells and 50 µl resazurin (0.1 mg/ml, diluted in medium) was added to the cells and incubated for 4 hours at 37 °C. Subsequently, the quantity of resorufin production (colorimetric change) was measured on a microplate fluorometer (Gibco, Thermo Fisher Scientific) using 540 nm excitation and 620 nm emission wavelength. As controls, three wells were added to each plate with only resazurin (no cells), cells without resazurin, and

100% cell death (1% (v/v) Triton-X-100 (Sigma Aldrich)). All measurements were performed in duplo (1 mM peptide) and triplo (0, 0.01, and 0.1 mM peptide).

Circular dichroism spectroscopy

Circular dichroism (CD) experiments were conducted by using a Jasco J-810 spectropolarimeter (Jasco, Dunmow, United Kingdom) at 20 °C in the wavelength range from 250 to 200 nm. The experiments were done according to Jasco J-810 Spectropolarimeter manual. The measurement was acquired at a scanning speed of 50 nm/min, a bandwidth of 1 nm, a 0.1 nm data pitch and a 2 seconds data integration time were used. Peptide concentration was 250 µM (dissolved in 500 mM HEPES, pH 8.0 adjusted with NaOH) and Ca^{2+} concentrations were 0, 0.5, 1, 5 and 10 mM (dissolved in Milli-Q). Samples were placed in High Precision Cell (Hellma Analytics, College Park, USA) for absorbance measurements.

Proximal tubule cellular peptide uptake

To investigate the potential cellular uptake of the peptide, fluorescence activated cell sorting (FACS) was performed. Cy5-labeled peptides were dissolved in 50 mM HEPES, pH 8.0 NaOH. One day prior to the FACS measurements, 20,000 HK-2 cells per well were seeded in a 96-well plate. After 24 hours, cells were incubated for 15 minutes at 37 °C with different concentration of cy5-labeled peptide (0, 0.01, 0.05, and 0.1 mM, diluted in DMEM) and penetratin-cy5 (0.01 mM) was used as a positive control. Subsequently, cells were washed 3 times with ice cold PBS followed by trypsinization. The cell pellet was resuspended in DMEM and cellular uptake was measured by BD FACSMelody™ cell sorter (Becton Dickinson, Heidelberg, Germany). Cy5-positive cells were excited at a wavelength of 633 nm and emitted at a wavelength of 643–714 nm. The results were analyzed by using FlowJo™ v10.6.1 software (ACEA Biosciences, San Diego, USA).

Animal study

20 healthy 8 weeks-old male C57BL/6J mice were obtained from Charles River Laboratories (Wilmington, MA, USA). All mice had 2 weeks to adjust to the new environment (Animal Research Facility of the Radboud University in Nijmegen, The Netherlands) and their pelleted food (Ssniff Spezialdiäten, Soest, Germany). Next, the animals were placed on a synthetic chow (Ssniff Spezialdiäten) for another 2 weeks. Throughout the whole experiment, the mice were kept in a temperature-controlled room, had free access to water and food, and were exposed to 12 hours dark-light cycles. The mice were randomly grouped in 4 cages (Eurostandard Type II, Amersfoort, The Netherlands) with 5 animals in each cage. During the follow-up period, the animals were kept in their initial cage till the day of their sacrifice.

The cages were randomly divided into two groups: 10 mice were placed on a high Ca^{2+} (HC) diet (2% (w/w) Ca^{2+}) while receiving 1% (v/v) EG via their drinking water, and

the other 10 mice continued on the normal Ca^{2+} (NC) (0.92% (w/w) Ca^{2+}) and received 1% (v/v) EG in their water. Both the animal conductor and the researchers were blinded for the experimental diets. The EG-containing water was changed each week to prevent potential breakdown over time.

The mice were placed in individual metabolic cages (Techniplast, Amersfoort, The Netherlands) to collect 24 hour urine on day 1, 7, 14, 21, and 28 (D1, D7, D14, D21, and D28) (Figure 1). To prevent evaporation, 100 µl of mineral oil (Sigma-Aldrich) was added to the urine collecting tubes in the metabolic cage. After each metabolic cage period, two mice from each group were anesthetized with 4% (v/v) isoflurane and sacrificed. Both kidneys were harvested for subsequent analysis. Blood was collected from the retro-orbital sinus bleeding in the sacrificed mice and from the submandibular vein in the mice that were still part of the experiment (Figure 1).

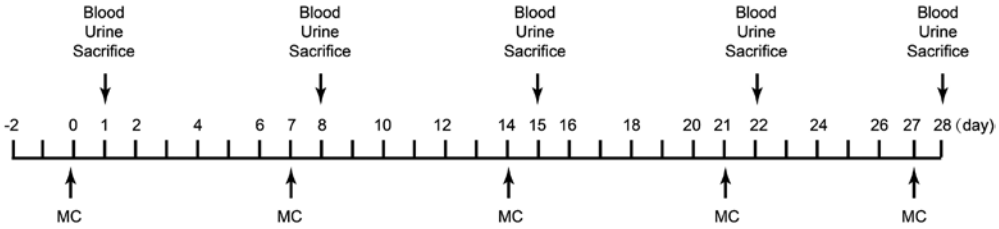

Figure 1. Timeline for the experimental study (days).

At day 0 of the experiment and every following week, the mice were placed in individual metabolic cages. After each metabolic cage period, blood and 24 hours urine were collected from all the mice and two mice from each experimental group were sacrificed and kidneys were harvested, the remaining mice were kept for longer time points. MC, metabolic cage.

Von Kossa staining

The kidney tissues were fixed in 4% (v/v) (neutral) buffered formalin for 24 hours. The kidneys were subsequently put in a descending series of ethanol concentrations (from 100 to 50% (v/v)), cleared in xylene, and embedded in paraffin wax. The paraffin blocks were cut in 5 µm thick sections. Subsequently, 1% (w/v) aqueous silver nitrate solution (Sigma-Aldrich) was added to these samples and they were exposed to 365 nm ultraviolet (UV) light for 30 minutes. The unreacted silver nitrate was removed with 5% (w/v) sodium thiosulfate (Sigma-Aldrich), rinsed in distilled water, and counterstained with 0.1% (w/v) nuclear fast red (Sigma-Aldrich). Subsequently, the slides were dehydrated in an ascending series of ethanol concentrations (from 50-100% (v/v)) and cleared in xylene and mounted with pertex (Histolab, Gothenburg, Sweden). The presence of Ca^{2+} crystal deposits in the kidney tissue was analyzed by using the light microscope Axio Imager M.2 (Carl Zeiss, Oberkochen, Germany) with 10x magnification. Images of the samples were taken using the ZEISS ZEN microscope software (Carl Zeiss).

Serum and urine analysis

Blood was collected on D1, D7, D14, D21, and D28 in microvette tubes (Sarstedt Inc, North Carolina, USA) and was allowed to solidify at room temperature for 30 minutes. Serum was separated from plasma by centrifugation at 1,792 *g* for 5 minutes and an additional 5 minutes at 11,200 *g*. Urinary pH was measured with the SCHOTT pH meter CG 840 (Thermo Fisher Scientific). The serum and urinary magnesium (Mg^{2+}) concentrations were measured by using a xylidyl blue colorimetric assay kit in accordance with the manufacturer's protocol (Roche Diagnostics, Woerden, The Netherlands). In short, 5 µl of standard, precinorm, and diluted samples were added to a 96-well plate. Next, 100 µl Tris-buffered EGTA pH 11.25 (Roche Diagnostics GmbH, Mannheim, Germany) was added to each well followed by 100 µl xylidyl blue (Roche Diagnostics GmbH). The results were determined by a VictorX multilabel plate reader (PerkinElmer, Waltham, MA, USA) set to 600 nm. For the serum and urinary Ca^{2+} measurements, a colorimetric assay kit was used in accordance with the manufacture's protocol (Roche Diagnostics, Woerden, The Netherlands). Serum and urinary Ca^{2+} values were measured by using a VictorX multilabel plate reader (PerkinElmer, Waltham, MA, USA) set to 570 nm. Sodium (Na^{+}), potassium (K^{+}), chloride (Cl^{-}), oxalate, and citrate measurements were performed at the laboratory for diagnostics on an automated system in accordance with the manufacturer's protocol (Abbott Diagnostics, Belgium) at Radboudumc, Nijmegen, The Netherlands.

Statistical analysis

All data were analyzed using Graphpad Prism 7.0 (Graphpad Software, La Jolla, CA, USA), and results were presented as means ± SEM. Unpaired T-test was used to analyze the difference between the two experimental groups. One-way ANOVA was used to analyze the data within the same group but at the various time points. $P<0.05$ was considered as statistically significant.

Results

Peptides and Ca^{2+}-binding stoichiometry

In order to design our low-affinity Ca^{2+}-binding peptides, we used the EF-hand domain as a template. The structure of an EF-hand is comprised of two alpha helices connected by a 12-residue Ca^{2+}-binding loop (Figure 2A). This conserved structural motif is present in many protein families and is reported to be important for Ca^{2+}-binding [19]. Therefore, several variations in these residues of the Ca^{2+}-binding loop were designed and showed in Figure 2B. The Ca^{2+}-binding affinity of designed peptides was measured using CD which is able to detect the secondary conformation change of the peptides upon binding of Ca^{2+}. A Ca^{2+}-induced change in ellipticity at 220 nm was detected upon the addition of Ca^{2+} (from 0 mM to 10 mM) (Figure 2C) for peptide 4, while peptide 1-3 remained unchanged.

Peptide toxicology test

In the CD study, peptide 4 was selected based on its Ca^{2+}-binding affinity. To further investigate the potential toxicity of this peptide on living cells, increasing concentrations of peptide 4 (0-1 mM) were added to HK-2 cells for 2, 4 and 24 hours. A resazurin assay was performed to assess cell viability at these time points. As shown in Figure 3, none of the peptide concentrations resulted in a decreased number of viable HK-2 cells over time, compared to 0 mM peptide, suggesting that peptide 4 is not toxic to the cells. Of note, 1% (v/v) Triton-X100 resulted in significant cell death (Figure 3).

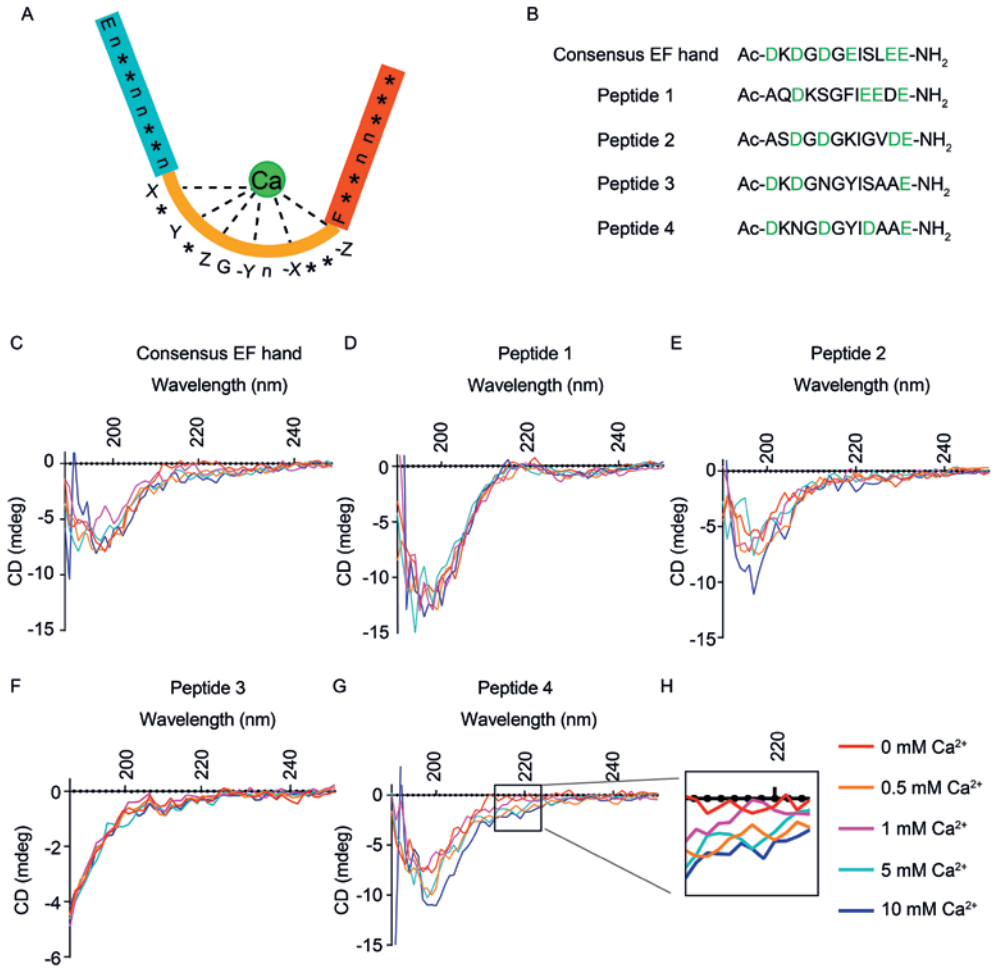

Figure 2. Circular dichroism monitored Ca^{2+} and peptide binding.

A, Schematic figure of a consensus EF hand and Ca^{2+}-binding motif in orange color (figure adapted from [20]). The blue and red colors depict the flanking regions of the binding motif. B, The sequence for designed peptides and consensus EF-hand motif. Negative charged amino acids that bind with Ca^{2+} were marked in dark green color. C-G, Circular dichroism detection for indicated peptides to assess conformational changes upon Ca^{2+}-binding under different concentrations of Ca^{2+}. H, zoom in image from figure G. The data is an average of three measurements in one experiment, with the experiment performed once. CD, Circular dichroism.

Cellular peptide uptake in HK2 cells

In order to detect whether peptide 4 can be taken up by the proximal tubule cells, HK2 proximal tubular cells were incubated with increasing concentrations of Cy5-labelled peptide 4 and Cy5-labelled penetratin as positive control for 15 minutes at 37 °C. FACS results showed that the Cy5 signal increased with a higher concentration of peptide 4. Yet, the Cy5-labelled signal of 0.01 mM penetratin was 9.5 and 1.5 times higher than the Cy5-labelled signal of 0.01 mM and 0.1 mM peptide, respectively (Figure 4).

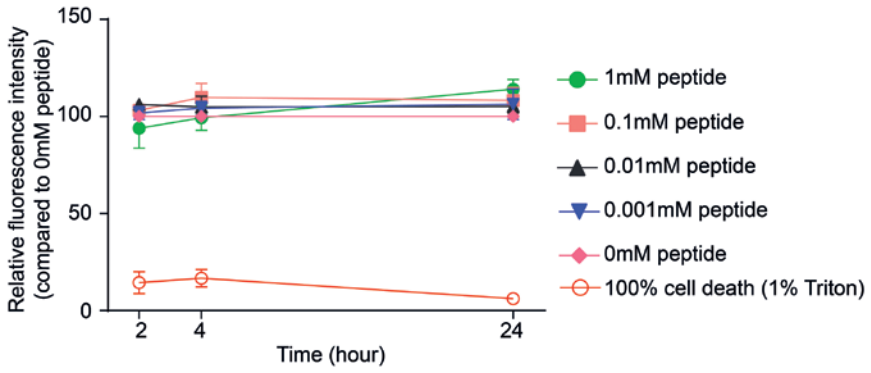

Figure 3. Resazurin assay for testing the cell viability by adding peptide 4 in HK-2 cells.

Increasing concentrations (0-1 mM) of peptide 4 were added to HK-2 cells and incubated for 2, 4, and 24 hours. Resorufin production was measured after 4 hours of incubation with resazurin. The red line represents the condition in which all the HK-2 cells are dead. This experiment was performed twice in triplicate.

Metabolic parameters in mice

In order to investigate crystal deposition in mouse kidney, C57BL/6J mice were placed on a high Ca^{2+} (HC) or normal Ca^{2+} (NC) diet while receiving 1% (v/v) EG via their drinking water for 28 days. Body weight, food intake, water intake were measured and were not statistically different between the groups throughout the whole experiment (Table 1). Of note, the water intake in the group of mice treated with the NC diet was significantly higher on D14 and D21 compared to D1. Blood and 24 hours urine were collected after each metabolic cage period. In line with an increased water intake, urine volume in the NC group was higher on D21 compared to D1, D7, and D14. The 24 hours urine volume in the HC diet group was also significantly increased on D21 compared to D1 (Table 1).

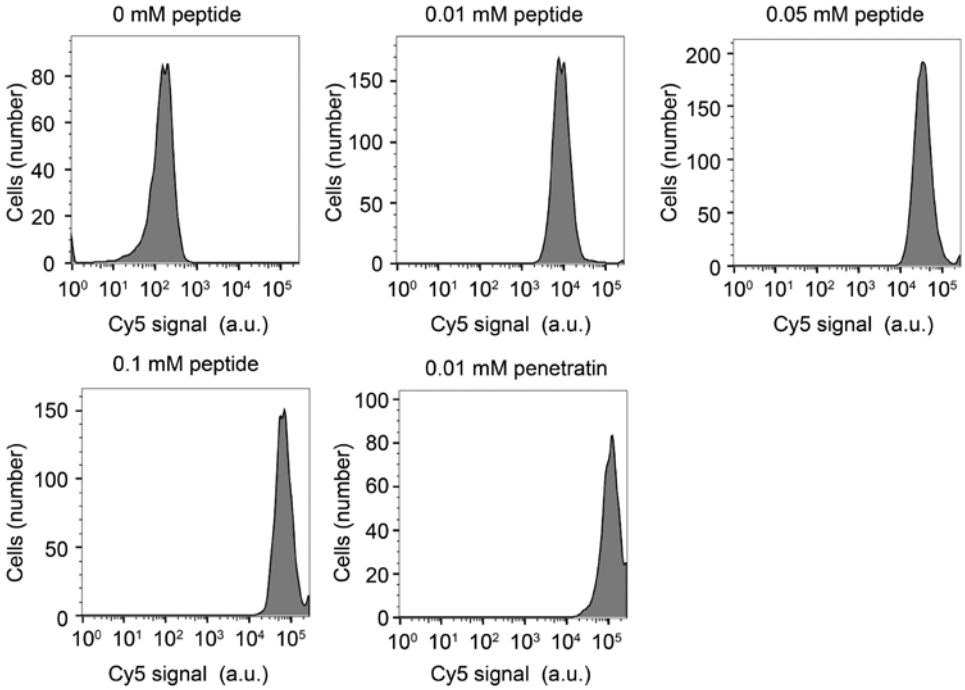

Figure 4. Peptide 4 exhibited cellular uptake in HK-2 cells.

Increasing concentrations of peptide 4 (0-0.1 mM) and penetratin as positive control were added to HK-2 cells for 15 minutes. After cell lysis, cellular uptake of the cy5-labeled peptides was counted by FACS with Cy5 fluorescence. This experiment was performed twice in triplicate.

Serum and urinary electrolyte handling in mice

To investigate the effect of EG and the diets on electrolyte handling, serum, and 24 hours urine electrolyte levels were analyzed. Serum Ca^{2+} concentrations and urinary Ca^{2+} excretion were similar between NC and HC groups, except on D21 where the serum Ca^{2+} concentration was significantly higher in the HC group (2.6±0.1 mmol/L) compared to the NC group (2.3±0.1 mmol/L) (Table 2-3). Other serum values (Na^+, K^+, Cl^-, and Mg^{2+}) did not differ significantly between HC and NC groups (Table 3). The urinary values were also similar between groups, except for two conditions. The urinary Na^+ excretion on D7 increased by 14% in the HC group compared to the NC group. The urinary Mg^{2+} excretion on D14 decreased by 19% in the NC group compared to the HC group (Table 2).

However, we observed changes in urinary electrolyte excretion within either group over the time course of the experiment. Within the NC groups, the urinary Na^+, Cl^- and K^+ concentrations were significantly higher on D21 compared to D1, D7, and D14 (Table 2). While urinary Ca^{2+} levels on day 21 in the NC group were higher compared to all other days (D1, D7, D14), urinary Ca^{2+} excretion in the HC group was only higher on D21 compared to D1. Moreover, there was no significant difference in urinary Mg^{2+} levels over time in the NC group and higher urinary Mg^{2+} levels were detected on D21 in the HC group compared to D1 and D14 (Table 2).

Table 1. **Metabolic parameters of mice under normal Ca^{2+} (NC) and high Ca^{2+} (HC) diet.**

Metabolic parameters	D1		D7		D14		D21		D28	
	NC	HC	NC	HC	NC	HC	NC	HC	NC	HC
Body weight (g)	26.0±0.4	24.2±0.7	27.2±1.2	24.9±0.3	27.0±0.3	26.2±0.3	26.9±0.3	26.5±0.3	26.9±0.7	26.8±0.3
Water intake (ml)	5.5±0.3	4.8±0.5	9.7±1.4	7.1±1.6	13.2±3.0[a]	7.6±1.9	14.6±2.6[a]	9.2±2.3	7.7±2.0	9.2±5.2
Food intake (g)	3.6±0.1	3.2±0.2	3.1±0.5	3.4±0.2	3.4±0.2	3.3±0.2	3.4±0.4	2.7±0.1	2.9±0.1	3.2±0.2
Urine volume (ml)	1.7±0.3	1.6±0.4	2.6±0.3	2.0±0.5	3.2±0.6	2.2±0.5	5.8±1.3[a,b,c]	4.2±0.7[a]	4.0±0.9	4.5±1.8

Body weight, water intake, food intake, and urine volume have been investigated after placing the mice in metabolic cages for 24 hours on day 1 (D1), day 7 (D7), day 14 (D14), day 21 (D21), and day 28 (D28). n=10 for each group on D1, n=8 for each group on D7, n=6 for each group on D14, n=4 for each group on D21, and n=2 for each group on D28. Numbers represent the mean ± SEM. Statistical significance ($p<0.05$) is indicated as a, compared to D1 within the respective group; b, compared to D7 within the respective group; c, compared to D14 within the respective group; d, compared to D28 within the respective group. NC, normal Ca^{2+}; HC, high Ca^{2+}.

Table 2. Urinary electrolyte excretion of mice under normal Ca^{2+} (NC) and high Ca^{2+} (HC) diet.

Urine parameter	D1		D7		D14		D21		D28	
	NC	HC	NC	HC	NC	HC	NC	HC	NC	HC
Ca^{2+} (µmol/24h)	2.2±0.3	2.3±0.6	3.3±0.4	2.7±0.6	3.1±0.2	2.5±0.8	8.3±2.0^{a,b,c,d}	6.0±1.2^{a}	2.7±0.2	3.1±0.5
Mg^{2+} (µmol/24h)	68.0±8.6	61.2±10.2	68.7±6.6	81.2±8.3	75.8±4.1	61.1±2.9^{e}	88.6±16.5	137.2±38.8^{a,c}	102.9±3.1	87.8±23.1
Na^{+} (µmol/24h)	110.6±10.6	118.0±16.4	86.3±7.5	98.6±14.4^{e}	64.5±7.4	86.5±14.9	57.23±5.7^{a,b,c}	76.8±10.4	84.5±13.5	69.5±22.5
K^{+} (µmol/24h)	136.4±12.2	161.0±24.1	98.5±11.0	136.6±20.3	77.0±7.7	125.5±18.7	64.78±7.5^{a,b,c}	100.8±17.5^{m}	83.5±15.5	92.5±37.5
Cl^{-} (µmol/24h)	61.4±6.8	76.6±14.7	41.0±4.6	59.9±9.2	34.0±3.7	52.5±7.8	27.5±2.7^{a,b,c}	43.8±7.2	34.0±5.0	40.5±16.5

24 hours urine on day 1 (D1), day 7 (D7), day 14 (D14), day 21 (D21) and day 28 (D28) were collected from mice on the normal Ca^{2+} (NC) and the high Ca^{2+} (HC) diet. Urinary Ca^{2+}, Mg^{2+}, Na^{+}, K^{+}, and Cl^{-} excretion has been investigated after placing the mice in metabolic cages for 24 hours. n=10 for each group on D1, n=8 for each group on D7, n=6 for each group on D14, n=4 for each group on D21, and n=2 for each group on D28. Numbers represent the mean ± SEM. Statistical significance ($p<0.05$) is indicated as a, compared to D1 within the respective group; b, compared to D7 within the respective group; c, compared to D14 within the respective group; d, compared to D28 within the respective group; e, compared to the normal Ca^{2+} group at the same time point.

Table 3. **Serum electrolyte concentrations of mice under normal Ca^{2+} (NC) and high Ca^{2+} (HC) diet.**

Serum parameter		D7		D14		D21		D28	
		HC	NC	HC	NC	HC	NC	HC	NC	HC
Ca^{2+} (mmol/L)	2.4±0.1	2.2±0.2	2.4±0.03	2.5±0.1	2.6±0.3	2.0±0.3	2.3±0.1	2.6±0.1[a]	2.9±0.5	2.6±0.1
Mg^{2+} (mmol/L)	1.7±0.1	1.6±0.1	1.5±0.02	1.5±0.1	1.4±0.3	1.0±0.3	1.6±0.1	1.7±0.2	1.5±0.2	1.2±0.02
Na^{+} (mmol/L)	150.0±0.0	150.5±1.5	148.0±0.0	152.0±0.0	149.5±0.5	151.0±0.0	150.5±0.5	150.0±1.0	147.0±1.0	146.5±0.5
K^{+} (mmol/L)	4.5±0.1	4.9±0.2	4.9±0.2	4.7±0.0	4.9±0.4	5.1±0.2	5.1±0.1	4.9±0.1	4.7±0.1	4.6±0.0
Cl^{-} (mmol/L)	102.0±0.0	101.0±1.0	100.5±1.5	103.0±0.0	101.5±0.5	102.0±1.0	103.5±0.5	100.0±1.0	103.5±0.5	100.5±1.5

Serum was collected on day 1 (D1), day 7 (D7), day 14 (D14), day 21 (D21) and day 28 (D28) after placing the mice in metabolic cages for 24 hours. Serum Na^{+}, K^{+}, and Cl^{-} levels were measured. n=2 for each group on D1, D7, D14, D21, and D28. Serum Ca^{2+} and Mg^{2+} levels were measured. n=10 for each group on D1, n=8 for each group on D7, n=6 for each group on D14, n=4 for each group on D21, and n=2 for each group on D28. Numbers represent the mean ± SEM. a, compared to the normal Ca^{2+} group at the same time point. NC, normal Ca^{2+}; HC, high Ca^{2+}.

Measurement of urinary citrate and urinary oxalate excretion and the urinary pH in mice

Urinary citrate and oxalate levels were measured at the beginning and end of the experimental time frame. On day 28, urinary citrate excretion was increased by 37% in the HC group compared to the NC group (Figure 5A). In the HC group, the oxalate excretion was nearly 6.3 folds and 5.9 folds higher than mice fed the NC diet at D1 and D28, respectively (Figure 5B). The urinary pH was similar between the NC and HC groups (Figure 5C).

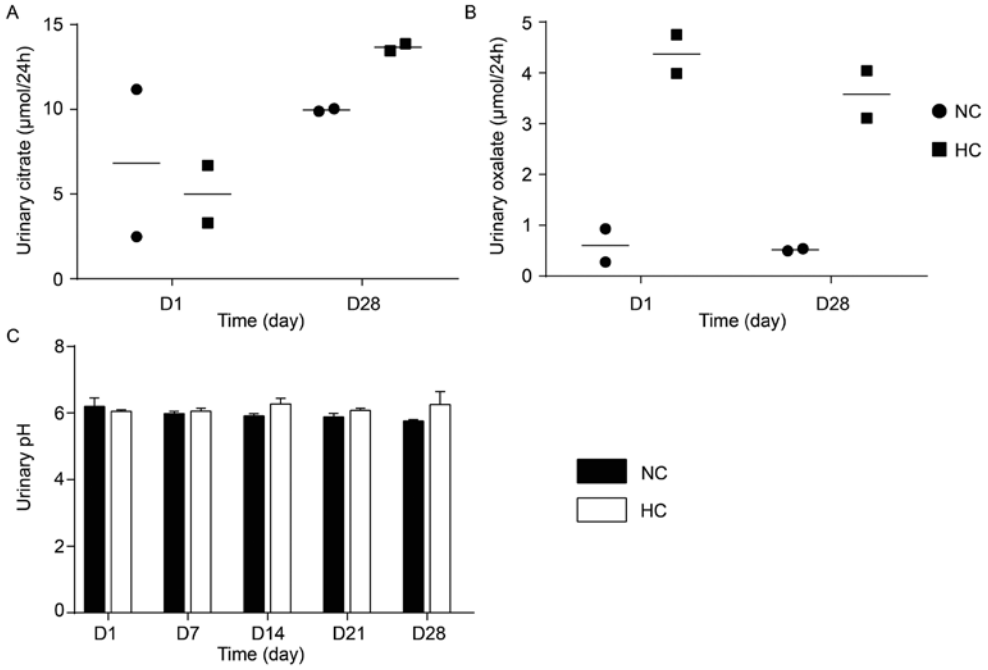

Figure 5. Urinary citrate and oxalate excretion and pH of mice under normal Ca^{2+} (NC) and high Ca^{2+} (HC) diet.

(A-C) Urinary citrate (A) and oxalate (B) excretion and pH (C) were investigated after placing the mice in metabolic cages for 24 hours. n=2 for each group for urinary citrate and oxalate measurement. For urinary pH measurement, n=10 for each group on D1, n=8 for each group on D7, n=6 for each group on D14, n=4 for each group on D21 and n=2 for each group on D28. D represents day.

Von kossa staining for Ca^{2+} deposit in mice kidney

In order to assess whether 1% (v/v) EG was able to induce crystal deposition in the kidneys of the mice, Von kossa staining was conducted on kidney tissue. The trachea from *Klotho* knockout mice were used as positive control since they develop CaP precipitates [21, 22]. Von Kossa staining results showed that Ca^{2+} deposits were not observed by using 1% (v/v) EG administration in drinking water combined with a HC diet for 28 days (Figure 6).

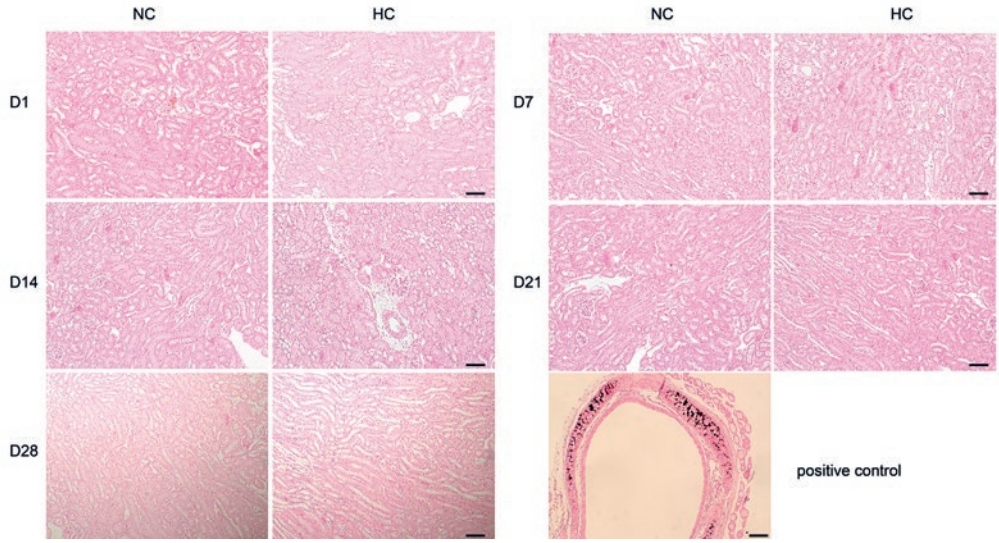

Figure 6. Von Kossa staining for Ca^{2+} deposits in mice kidney.

Representative staining of kidney tissue from each experimental group (normal Ca^{2+} (NC) and high Ca^{2+} (HC) diets) on day 1 (D1), day 7 (D7), day 14 (D14), day 21 (D21) and day 28 (D28). Trachea from *Klotho* knockout mice was used as a positive control. n=2 for each group. Size bar represents 25 µm.

Discussion

In this study, several shortened EF-hand peptides with altered sequences were analyzed for their Ca^{2+}-binding capacity. The aim was to identify a peptide with low binding affinity for Ca^{2+} (2-5 mM range). Our preliminary results suggest that peptide 4 (Ac-DKNGDGYIDAAE-NH_2) has the potential to serve as such a peptide. Moreover, this peptide did not induce cellular toxicity but did show mild cellular uptake in HK-2 cells. To ultimately evaluate the efficacy of this peptide *in vivo*, we aimed to generate a nephrolithiasis mouse model by administrating 1% (v/v) EG via drinking water in combination with either a normal or a high Ca^{2+} diet. However, no Ca^{2+} crystal deposits were observed in the kidney tissues of mice on either diet.

Previously, Reid *et al.* developed a Ca^{2+}-binding peptide (α-helix-DKNGDGYISAAE-α-helix) with a Ca^{2+}-binding affinity in the micromolar range (Kd=59 µM) [23]. We used the Ca^{2+}-binding loop (DKNGDGYISAAE) as template and changed the amino acid residue at position 9 from S to D. The CD spectra of the peptide showed a Ca^{2+}-induced change in ellipticity at 220 nm upon the incremental addition of Ca^{2+} in the millimolar range, which suggested that the Ca^{2+}-binding affinity of this peptide is decreased compared to the study by Reid *et al.* With the alteration from S to D, our peptide had 3 acidic side chains. In contrast to what we found, the acid pair hypothesis suggests that more acidic

side chains (within four) in the loop lead to a higher Ca^{2+}-binding affinity [24]. In addition, D is negatively charged and exhibits increased binding affinity to Ca^{2+} compared to S in the study of Reid *et al* [23]. We suspect that the decreased binding affinity to Ca^{2+} in our peptide is due to the removal of the flanking α-helices, compared to the Ca^{2+}-binding peptide developed by Reid *et al*. This is in line with the idea proposed by Lakowski *et al*. that the absence of the flanking helix of the EF-hand loop reduces Ca^{2+}-binding affinity [25].

Preliminary results from our study demonstrated that this peptide is not toxic. The presence of residues like C, H, N, and P was shown to be higher in toxic peptides compared to non-toxic peptides [26]. In agreement with their findings, the peptide we designed had only one N residue. Moreover, FACS results showed that the amount of peptide cellular uptake increased at higher concentrations, but remained lower than the uptake of the cell-penetrating peptide penetratin. This indicated that the peptide (Ac-DKNGDGYIDAAE-NH_2) exhibited cellular uptake, which might be caused by the high concentrations of peptide added to the cells. In general, receptor-mediated endocytosis plays a crucial role in the reabsorption of low molecular weight proteins in the proximal tubule [27]. Megalin, which is expressed in the apical side of the PT, interacts with its associated protein such as cubilin, and contributes significantly in the receptor-mediated endocytosis process [28-30]. Therefore, megalin and cubilin may also play a role in the reabsorption of the peptide we designed. Although these peptide *in vitro* experiments are very encouraging, more repeats still need to be performed due to some of them were conducted less than three times.

In contrast to our *in vivo* study, other studies have successfully induced nephrolithiasis in mice and rats by administrating EG. A study in rats showed that intraperitoneal injection with EG led to the development of CaOx crystal deposits after 2-4 weeks [31]. This suggests that the absence of crystal deposition in the renal tissue of the mice in our study may be due to species differences. Other studies have successfully used Swiss albino mice to induce crystal formation by administering 0.75% (v/v) EG via the drinking water for 28 days [32]. The difference in susceptibility to stone formation between C57BL/6J mice and Swiss albino mice may lie in the genetic background of these animals [32]. Though, C57BL/6J mice have been used previously to study nephrolithiasis, with variation in genetically modified models, the agents that were used, and the method of administering. In 2007, Okada *et al*. successfully detected kidney stones in male C57BL/6J (wildtype) mice by intraabdominal glyoxylate injection [33]. Here, they found that the expression of osteopontin (OPN), which is an important kidney stone-related protein, was significantly increased [33]. OPN expression was not measured in our study. In addition, Jiang *et al*. demonstrated that mice lacking solute carrier family 26 member 6 (*Slc26a6*), which is a Cl^--oxalate exchanger [34], are more prone to develop CaOx nephrolithiasis compared to wildtype mice [35]. In their later study, they demonstrated that only the *Slc26a6* knockout mice with hypercalciuria develop crystal deposits in the kidney, which

suggests that hypercalciuria plays a very important role in forming kidney stones [34]. This is substantiated by a study by Khan *et al.* concluding that hyperoxaluria alone is not enough to induce CaOx crystal deposits, both hypercalciuria and hyperoxaluria are required in mice [36]. Importantly, hypercalciuria was not detected in the mice of our study, which could explain the fact that we did not observe crystal deposits.

The fact that a HC diet did not induce changes in serum and/or urinary Ca^{2+} levels might be due to the compensatory loss in the gastrointestinal tract. Under high Ca^{2+} intake conditions, Ca^{2+} is passively absorbed by the paracellular process in the jejunum and ileum leading to lower fractional absorption of Ca^{2+} and loss of Ca^{2+} in the feces [37]. Thus, it is necessary to measure the Ca^{2+} levels in the feces in order to elucidate whether the normal serum Ca^{2+} levels are caused by fecal Ca^{2+} loss in the mice treated with HC diets.

And finally, it is important to note a few limitations of this pilot study. While EG is not expected to affect serum and urinary parameters, a control group (without EG) would be optimal. Moreover, we sacrificed 2 animals per time point, leaving only 2 mice per group at day 28. Therefore, it is not possible to draw any significant conclusions on urinary markers after day 21. Also, this resulted in more variability of the measured electrolyte levels, limiting statistical testing. On this note, the significantly higher water intake in the NC diet treated mice on D14 and D21 was due to one extreme value (mice) that we could not omit because of the small sample size.

Taken together, our *in vitro* study revealed that peptide 4 (Ac-DKNGDGYIDAAE-NH_2) can be potentially used for single or repeated injection in a kidney stone mouse model. Our *in vivo* study showed that the EG administration in drinking water supplied with a HC diet is not sufficient for nephrolithiasis induction in C57BL/6J mice. For future studies, it might be interesting to use Swiss albino mice or rats to induce kidney stone disease. When the kidney stone model is set up, we can investigate if the peptide can be served as the first step towards the development of a new therapeutic intervention for kidney stone recurrence.

Acknowledgements

This work was financially supported by grants from the Netherlands Organization for Scientific Research (NWO VICI 016.130.668), from the Radboud Institute for Molecular Life Sciences, and the Netherlands Organization for Health Research and Development (Off Road Grant 451001 004). The authors thank Dr. Roland Brock and Sander van Asbeck for their suggestions in the peptide work and excellent technical assistance.

References

1. Romero, V., H. Akpinar, and D.G. Assimos, *Kidney stones: a global picture of prevalence, incidence, and associated risk factors.* Rev Urol, 2010. **12**(2-3): p. e86-96.
2. Edvardsson, V.O., et al., *Incidence of kidney stone disease in Icelandic children and adolescents from 1985 to 2013: results of a nationwide study.* Pediatr Nephrol, 2018. **33**(8): p. 1375-1384.
3. Khan, S.R., et al., *Kidney stones.* Nat Rev Dis Primers, 2016. **2**: p. 16008.
4. Rule, A.D., et al., *Kidney stones and the risk for chronic kidney disease.* Clin J Am Soc Nephrol, 2009. **4**(4): p. 804-11.
5. Sorokin, I. and M.S. Pearle, *Medical therapy for nephrolithiasis: State of the art.* Asian J Urol, 2018. **5**(4): p. 243-255.
6. Barnela, S.R., et al., *Medical management of renal stone.* Indian J Endocrinol Metab, 2012. **16**(2): p. 236-9.
7. Lingeman, J.E., et al., *Shock wave lithotripsy: advances in technology and technique.* Nat Rev Urol, 2009. **6**(12): p. 660-70.
8. Alelign, T. and B. Petros, *Kidney Stone Disease: An Update on Current Concepts.* Adv Urol, 2018. **2018**: p. 3068365.
9. Heilberg, I.P. and N. Schor, *Renal stone disease: Causes, evaluation and medical treatment.* Arq Bras Endocrinol Metabol, 2006. **50**(4): p. 823-31.
10. Hussein, N.S., et al., *Twenty-four-hour urine constituents in stone formers: a study from the northeast part of Peninsular Malaysia.* Saudi J Kidney Dis Transpl, 2013. **24**(3): p. 630-7.
11. Mittal, R.D., et al., *Stone composition, metabolic profile and the presence of the gut-inhabiting bacterium Oxalobacter formigenes as risk factors for renal stone formation.* Med Princ Pract, 2003. **12**(4): p. 208-13.
12. Kumar, R., et al., *Evaluation of urinary abnormalities in urolithiasis patients: A study from North India.* Indian J Clin Biochem, 2003. **18**(2): p. 209-15.
13. Albright, F., et al., *Idiopathic hypercalciuria: a preliminary report.* Proc R Soc Med, 1953. **46**(12): p. 1077-81.
14. Henneman, P.H., et al., *Idiopathic hypercaicuria.* N Engl J Med, 1958. **259**(17): p. 802-7.
15. Miller, N.L. and J.E. Lingeman, *Management of kidney stones.* BMJ, 2007. **334**(7591): p. 468-72.
16. Nakayama, S., *[Evolution of EF-hand proteins].* Seikagaku, 1995. **67**(2): p. 131-7.
17. Kretsinger, R.H. and C.E. Nockolds, *Carp muscle calcium-binding protein. II. Structure determination and general description.* J Biol Chem, 1973. **248**(9): p. 3313-26.
18. Yap, K.L., et al., *Diversity of conformational states and changes within the EF-hand protein superfamily.* Proteins, 1999. **37**(3): p. 499-507.
19. Nakayama, S. and R.H. Kretsinger, *Evolution of the EF-hand family of proteins.* Annu Rev Biophys Biomol Struct, 1994. **23**: p. 473-507.
20. Zhou, Y., T.K. Frey, and J.J. Yang, *Viral calciomics: interplays between Ca2+ and virus.* Cell Calcium, 2009. **46**(1): p. 1-17.
21. Alexander, R.T., et al., *Klotho prevents renal calcium loss.* J Am Soc Nephrol, 2009. **20**(11): p. 2371-9.
22. Ter Braake, A.D., et al., *Magnesium prevents vascular calcification in Klotho deficiency.* Kidney Int, 2019.
23. Reid, R.E., *Synthetic fragments of calmodulin calcium-binding site III. A test of the acid pair hypothesis.* J Biol Chem, 1990. **265**(11): p. 5971-6.
24. Reid, R.E., *A synthetic 33-residue analogue of bovine brain calmodulin calcium binding site III: synthesis, purification, and calcium binding.* Biochemistry, 1987. **26**(19): p. 6070-3.
25. Lakowski, T.M., et al., *Calcium-induced folding of a fragment of calmodulin composed of EF-hands 2 and 3.* Protein Sci, 2007. **16**(6): p. 1119-32.
26. Gupta, S., et al., *In silico approach for predicting toxicity of peptides and proteins.* PLoS One, 2013. **8**(9): p. e73957.
27. De, S., S. Kuwahara, and A. Saito, *The endocytic receptor megalin and its associated proteins in proximal tubule epithelial cells.* Membranes (Basel), 2014. **4**(3): p. 333-55.

28. Leheste, J.R., et al., *Megalin knockout mice as an animal model of low molecular weight proteinuria.* Am J Pathol, 1999. **155**(4): p. 1361-70.
29. Amsellem, S., et al., *Cubilin is essential for albumin reabsorption in the renal proximal tubule.* J Am Soc Nephrol, 2010. **21**(11): p. 1859-67.
30. Ahuja, R., et al., *Interactions of cubilin with megalin and the product of the amnionless gene (AMN): effect on its stability.* Biochem J, 2008. **410**(2): p. 301-8.
31. Oh, S.Y., et al., *A comparative study of experimental rat models of renal calcium oxalate stone formation.* J Endourol, 2011. **25**(6): p. 1057-61.
32. Alenzi, M., S. Rahiman, and B.A. Tantry, *Antiurolithic effect of olive oil in a mouse model of ethylene glycol-induced urolithiasis.* Investig Clin Urol, 2017. **58**(3): p. 210-216.
33. Okada, A., et al., *Successful formation of calcium oxalate crystal deposition in mouse kidney by intraabdominal glyoxylate injection.* Urol Res, 2007. **35**(2): p. 89-99.
34. Aronson, P.S., *Role of SLC26A6-mediated Cl(-)-oxalate exchange in renal physiology and pathophysiology.* J Nephrol, 2010. **23 Suppl 16**: p. S158-64.
35. Jiang, Z., et al., *Calcium oxalate urolithiasis in mice lacking anion transporter Slc26a6.* Nat Genet, 2006. **38**(4): p. 474-8.
36. Khan, S.R. and P.A. Glenton, *Experimental induction of calcium oxalate nephrolithiasis in mice.* J Urol, 2010. **184**(3): p. 1189-96.
37. Sorensen, M.D., *Calcium intake and urinary stone disease.* Transl Androl Urol, 2014. **3**(3): p. 235-40.

4

Arl15 heterozygous mice exhibit normal electrolyte homeostasis

Chao Ma[1], Ying Bai[2], Liz Bentley[2], René JM Bindels[1], Roger D Cox[2], Joost GJ Hoenderop[1], Jeroen HF de Baaij[1]

[1]Department of Physiology, Radboud Institute for Molecular Life Sciences, Radboud university medical center, Nijmegen, The Netherlands. [2]MRC Harwell Institute, Mammalian Genetics Unit, Harwell Campus, Oxfordshire, United Kingdom.

In preparation

Abstract

Magnesium (Mg^{2+}) homeostasis is maintained by intestinal absorption and renal excretion. Genome wide association studies (GWAS) investigated genetic loci associated with urinary Mg^{2+} excretion in 9099 individuals and identified ADP-ribosylation factor-like GTPase 15 (*ARL15*). Moreover, it was shown that ARL15 can regulate Mg^{2+} reabsorption by regulating the channel activity of TRPM6 in the kidney, but the function of ARL15 in the kidney is still unknown. The objective of this study was to further characterize ARL15 and its role in Mg^{2+} homeostasis in the kidney by using *Arl15* heterozygous (*Arl15*$^{+/-}$) mice. The *ARL15* gene has 795 bp encoding a protein of 265 amino acids. Iterative Threading ASSEmbly Refinement (I-TASSER) prediction showed that the secondary structure of ARL15 consists of 8 alpha-helixes, 7 beta-strands and belongs to the small GTPase superfamily. Furthermore, Mg^{2+} is predicted to bind to ARL15. Tissue distribution indicated that ARL15 is ubiquitously expressed in mouse tissue, with the highest abundance in the lung, inguinal fat, epididymal fat, spleen, testes, and kidney. Differences in serum Mg^{2+} concentration and 24 hours urinary Mg^{2+} excretion were not detected between *Arl15* wildtype (*Arl15*$^{+/+}$) and *Arl15*$^{+/-}$ mice on the high fat and low fat diets. Furthermore, on the low fat diet, water intake of male *Arl15*$^{+/-}$ mice was significantly increased by 60% compared to male *Arl15*$^{+/+}$ mice. On the high fat diet, body weight of female *Arl15*$^{+/-}$ mice significantly decreased by 12% compared to female *Arl15*$^{+/+}$ mice. However, food intake and 24 hours urine volume did not significantly differ between the groups on the high fat and low fat diets. Quantitative real-time PCR analysis showed that the mRNA expression levels of Mg^{2+}-related genes, metabolism-related genes, and membrane trafficking-related genes are not affected in the kidney of *Arl15*$^{+/-}$ mice. Thus, our results suggest that ARL15 does not play a role in the regulation of renal electrolyte transport.

Introduction

Magnesium (Mg^{2+}) plays an important role in the synthesis, folding, and stability of biomolecules and it works as a cofactor for various enzymatic reactions [1]. Mg^{2+} also plays an essential role in stabilization of the cell membrane, cardiac excitability, regulation of blood pressure, glucose-insulin metabolism, and muscle contraction [2, 3]. An adult human body contains approximately 22-26 grams (g) of Mg^{2+} [4]. Only 1% of the total Mg^{2+} in the body is found in the extracellular space, which is primarily in blood [1].

The kidney plays a key role in the regulation of blood Mg^{2+} concentration. Around 95-99% of the filtered Mg^{2+} is reabsorbed in the proximal tubule (PT), the thick ascending limb (TAL), and the distal convoluted tubule (DCT) of the kidney [5]. Although the DCT reabsorbs only 5-10% of the filtered Mg^{2+} [6], it is the last segment to determine the final Mg^{2+} concentration in urine since no Mg^{2+} reabsorption takes place beyond this segment [5, 6]. Transient receptor potential cation channel subfamily M member 6 (TRPM6) is the gatekeeper of transcellular Mg^{2+} reabsorption in the DCT [6, 7]. Its importance in Mg^{2+} homeostasis is highlighted by the fact that mutations in the *TRPM6* gene lead to hypomagnesemia with secondary hypocalcemia (HSH) [8].

Recently, a GWAS identified ADP-ribosylation factor-like protein 15 (ARL15) to be associated with urinary Mg^{2+} wasting [9]. ARL15 belongs to the ADP-ribosylation factor (ARF) family [9]. Immunohistochemical studies demonstrated its localization in the TAL and DCT of the kidney [9], but the function of this protein has not yet been clarified. A recent study proposed that ARL15 may be involved in the regulation of intracellular vesicle trafficking [9]. In line with this, Corre *et al.* found that TRPM6 channel activity is significantly increased in the presence of ARL15, and knockdown of *Arl15* in zebrafish resulted in urinary Mg^{2+} wasting [9]. Thus, this set of experiments suggests that ARL15 is a key protein in maintaining Mg^{2+} homeostasis.

Additional GWAS showed a strong association between *ARL15* locus variants and several metabolic and cardiovascular traits including risk of diabetes mellitus type 2, elevated fasting insulin concentration, hemoglobin A1C (HbA1c) levels and pancreatic beta cell proliferation [8, 10-14]. Indeed, Rocha *et al.* demonstrated that knockdown of *Arl15* significantly impaired the adipogenesis and adiponectin secretion of 3T3-L1 cells [11].

The aim of this study was, therefore, to characterize the role of ARL15 in renal Mg^{2+} handling and metabolic traits. For this purpose, *Arl15* heterozygous knockout (*Arl15*$^{+/-}$) mice were analyzed for electrolyte homeostasis and renal abnormalities. Furthermore, by challenging the mice with high fat diets, the mRNA expression of Mg^{2+}-related, metabolism-related and membrane trafficking related-genes was investigated by quantitative real-time-PCR (RT-qPCR).

Methods and materials

Ethical approval of the study protocol

All mice models used in this experiment were approved by animal ethics board of Radboud University (Nijmegen, The Netherlands) and the MRC Harwell Institute of Animal Welfare and Ethical Review Committee. All procedures were performed in accordance with the Home Office license 30/3146 and 30/3070 under the Animal (Scientific Procedures) Act 1986 which is issued by the Medical Research Council.

Mice were kept under a 12:12 hour light/dark cycle (lights on 7 am and off 7 pm), at a temperature of 21±2°C and a humidity of 55±10% conditions. Mice had free access to water (9–13 ppm chlorine) and were maintained *ad libitum* on either a high fat diet (D12492, Research Diets, New Brunswick, NJ, U.S.A.) or low fat diet (D12450J, Research Diets, New Brunswick, NJ, U.S.A.) for 24 weeks from weaning.

Expression profiling and quantitative real time PCR

Three 12-weeks old wildtype C57BL/6 mice were sacrificed. Brain, retina, aorta, lung, heart, stomach, caecum, duodenum, jejunum, ileum, colon-ascend, colon-descend, rectum, brown fat, inguinal fat, epididymal fat, thigh muscle, spleen, adrenal gland, kidney, and testes were collected. 10 *Arl15*$^{+/-}$ mice and *Arl15*$^{+/+}$ littermate controls with C57BL/6NTac background were sacrificed in the end of experiment. Total RNA was extracted from above described tissues with Trizol (Invitrogen, Carlsbad, CA, USA) according to the manufacturer's protocol. Subsequently, RNA samples were subjected to DNase (Invitrogen, Breda, The Netherlands) treatment to prevent genomic DNA contamination and the reverse transcriptase reaction was performed for 1 hour at 37°C to synthesize cDNA. mRNA levels of the target genes were determined with a CFX96TM Real-Time PCR Detection System (Bio-Rad Laboratories, Hercules, CA) using iQTM SYBR Green Supermix (Bio-Rad) detection of single PCR product accumulation. All RT-qPCR experiments were executed in triplicate. Gene expression levels were normalized to the expression levels of the standard reference gene glyceraldehyde 3-phosphate dehydrogenase (*Gapdh*). Relative mRNA expression was analyzed using the Livak method ($2^{-\Delta\Delta Ct}$). All primers were purchased from Biolegio BV (Nijmegen, Netherlands). Primer sequences are shown in Table 1.

Table 1. Primer sequences used for real-time quantitative RT-PCR

Gene	Forward primer	Reverse primer
Slc5a1	5′-ATGGAGCAACACGTAGAGGC-3′	5′-ACATAGACCACAAGCCAACACC-3′
Slc5a2	5′-TCTGTAGTGGCAAGGGGAAG-3′	5′-ACAGGGCTTCTGTGTCTTGG-3′
Cldn16	5′-GTTGCAGGGACCACATTAC-3′	5′-GAGGAGCGTTCGACGTAAAC-3′
Cnnm2	5′-GTCTCGCACCTTTGTTGTCA-3′	5′-GTCGCTCCGACTGAGAGAAT-3′
Fxyd2	5′-TCAGCCTTTCTTGTGACTGG-3′	5′-GGTCTTCCTGTGGCCTCTACT-3′
Slc41a1	5′-CATCCCACACGCCTTCCTGC-3′	5′-CGGCTGGCCTGCACAGCCAC-3′
Slc41a3	5′-CTTCGGCCACTGGCATTCTG-3′	5′-GATGGCAAGGTAGGAGATGG-3′
Trpm6	5′-CTTCACAATGAAAACCTGCCC-3′	5′-AAAGCCATGCGAGTTATCAGC-3′
Cpt1	5′-GTGAGCCTGGCCTCGCC-3′	5′-TGAGTGGTGACCGAGTCTGC-3′
Pepck1	5′-CCTAGTGCCTGTGGGAAGAC-3′	5′-AGCCCTTAAGTTGCCTTGGG-3′
Ardb2	5′-TCCGTCGTCTTCTGTGTAGC-3′	5′-GCCATCAAACCTGTTGAGCG-3′
Cpt2	5′-GTATCTGCAGCACAGCATCG-3′	5′-GTTTAGGGATAGGCAGCCTGG-3′
Arf6	5′-GGTGGGCTTCAACGTGGAG-3′	5′-CGGTGTAGTAATGCCGCAG-3′
Adipor1	5′-TTTGCCACTCCCAAGCAC-3′	5′-ACACCACTCAAGCCAAGTCC-3′
Adipor2	5′-TCTCAGTGGGACATGTTTGC-3′	5′-AGGCCTAAGCCCACGAAC-3′
Arf1	5′-TGGGCGAAATTGTGACCACC-3′	5′-TCCACTACGAAGATCAAGCCT-3′
Arfgef-1	5′-TCACTGCGGTAAGTAAAGCCT-3′	5′-GACTGGCAGGGCTCCAGATA-3′
Arfgef-2	5′-ACATCCCCACACATTGAAATCC-3′	5′-CGGTGGTTTGATTGATGAGGT-3′
Arl15	5′-TGCAGCGAAAGCCCGGAGAA-3′	5′-CCGGATATTGTCAGCTCTCAAGT-3′
Gapdh	5′-TAACATCAAATGGGGTGAGG-3′	5′-GGTTCACACCCATCACAAAC-3′

Slc5a1, Solute carrier family 5 member 1; *Slc5a2*, Solute carrier family 5 member 2; *Cldn16,* Claudin-16; *Cnnm2,* Cyclin and CBS domain divalent metal cation transport mediator 2; *Fxyd2,* FXYD domain containing ion transport regulator 2; *Slc41a1,* Solute carrier family 41 member 1; *Slc41a3,* Solute carrier family 41 member 3; *Trpm6,* Transient receptor potential cation channel subfamily M member 6; *Cpt 1,* Carnitine palmitoyltransferase I; *Cpt 2,* Carnitine palmitoyltransferase 2; *Afr6*, ADP ribosylation factor 6; *Afr1*, ADP ribosylation factor 1; *Adipor1*, Adiponectin receptor 1; *Adipor2*, Adiponectin receptor 2; *Pepck 1,* Phosphoenolpyruvate carboxykinase; *Arfgef-1*, ADP ribosylation factor guanine nucleotide exchange factor 1; *Arfgef-2*, ADP ribosylation factor guanine nucleotide exchange factor 2; *Arl15*, ADP-ribosylation factor-like GTPase 15; *Gapdh*, Glyceraldehyde 3-phosphate dehydrogenase.

Bioinformatics analysis

To further understand ARL15 protein function, bioinformatics analysis was performed. Gene structure analysis, homologous alignment, signal peptide and protein conserved domain prediction was performed using the following sources: https://blast.ncbi.nlm.nih.gov/Blast.cgi, and https://zhanglab.ccmb.med.umich.edu/I-TASSER/.

Serum and urinary Mg^{2+} measurements

Serum and urinary total Mg^{2+} concentrations were measured by a colorimetric xylidyl-II blue assay kit (Roche Diagnostics, Woerden, The Netherlands), according to the protocol provided by the manufacturer. Urine volume was measured in order to calculate 24 hours Mg^{2+} excretion.

Immunohistochemistry

Adrenal gland, kidney, testes, and fat tissue were fixed in 4% (w/v) paraformaldehyde for 24 hours, and embedded in paraffin. Subsequently, 5 µm sections were cut and serial 5 µm paraffin-embedded tissue sections were deparaffinned and rehydrated. Endogenous peroxidase activity was inhibited by incubating the sections in 3.0% (v/v) hydrogen peroxide (H_2O_2) (Avantor, Arnhem, The Netherlands). After blocking the sections with 20% (v/v) goat serum in phosphate-buffered saline (PBS), the sections were incubated overnight at 4°C with ARL15 antibody (Abcam, Cambridge, The UK). Then, the sections were incubated with the swine anti-rabbit secondary antibody (Abcam, Cambridge, UK). Sections were imaged by using the light microscope Axio Imager M.2 (Carl Zeiss, Oberkochen, Germany). Blinded analysis of positive immunostained sections were performed using Image Pro Plus (Media Cybernetics, Warrendale, Pennsylvania).

Statistical analysis

All data were analyzed using Graphpad Prism 7.0 (Graphpad Software, La Jolla, CA, USA), and results were presented as means ± SEM. Results are statistically analyzed by performing a two-way ANOVA followed by Tukey as post-test. $P<0.05$ was considered as statistically significant.

Results

Identification of *ARL15* gene and protein comparison

ARL15 has an open reading frame of 795 bp encoding a protein of 265 amino acids. The protein sequence is highly conserved and comparison analysis showed that human and mouse ARL15 share 74% similarity in amino acid sequence. In order to elucidate the function of ARL15, secondary protein analysis was performed. Structure prediction indicated that ARL15 consists of 8 alpha-helices and 7 beta-strands. I-TASSER prediction

for the tertiary structure of ARL15 showed that it belongs to the small GTPase superfamily (Figure 1A). Interestingly, Mg^{2+} is shown to interact with the surrounding T107 and T124 residues of ARL15 (Figure 1B and C).

Analysis of *Arl15* expression in different mouse tissues

To investigate the tissue distribution of *Arl15*, RNA was isolated from various tissues of adult mice and gene expression was analyzed by RT-qPCR. *Arl15* mRNA was highly expressed in lung, inguinal fat, epididymal fat, spleen, testes, and kidney, followed by the retina, stomach, duodenum, ileum (Figure 2A). It was weakly detectable in brain, aorta, liver, heart, caecum, jejunum, colon, rectum, adrenal gland, brown fat, and thigh-muscle (Figure 2A). Protein expression of ARL15 in adrenal gland, brown fat, kidney, and testes in adult mice was further investigated by immunohistochemistry. ARL15 was highly expressed in the cortex and medulla of the adrenal gland (Figure 2B, panel a). In the kidney, ARL15 was present in the TAL and DCT (Figure 2B, panel b). There was a robust expression in the adipocytes in inguinal fat (Figure 2B, panel c). Moreover, ARL15 was highly expressed in the spermatoblast and interstitial cells in testes (Figure 2A, panel d).

Normal metabolic parameters in *Arl15*$^{+/-}$ *mice*

The function of ARL15 *in vivo* was further investigated in *Arl15*$^{+/+}$, *Arl15*$^{+/-}$ and *Arl15*$^{-/-}$ mice (kindly provided by Dr. Roger Cox). The importance of ARL15 for metabolism was indicated by the fact that *Arl15*$^{-/-}$ mice, generated via CRISPR/Cas9 germline knockout, died after birth (unpublished data from Roger Cox's group). The *Arl15*$^{+/+}$ *and Arl15*$^{+/-}$ mice are viable (unpublished data from Roger Cox's group) and were subjected to low and high fat diets for 24 weeks after weaning. At the end of the experiments, mice were placed in metabolic cages for 24 hours to collect blood and 24 hours urine for further analysis.

A

B

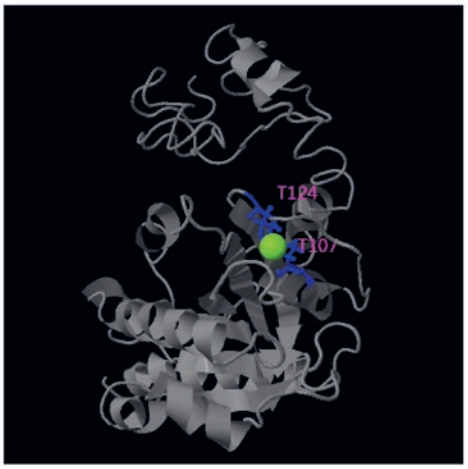

C

Rank	C-score	Cluster size	PDB Hit	Lig Name	Ligand biding site residues
1	0.79	684	4c4pA	GNP	102 103 104 105 106 107 108 118 119 120 121 123 124 145 146 203 204 206 207 237 238 239
2	0.02	15	1ksgA	MG	107 124
3	0.02	24	1tadB	ALF	102 103 106 121 123 124 144 145 146 147
4	0.00	1	3NKVA	3NKVA01	30 31 32 76 79 127 129 157
5	0.00	1	1R2QA	1R2QA03	190 191 192

Figure 1. I-TASSER prediction for the tertiary structure of *Arl15* and potentially binding of Mg^{2+}.

A, Predicted tertiary structure of ARL15 by using a model for compact volume of truncated monomeric cytohesin-3 (Grp1; amino acids 63-399) E161A 6GS Arf6 Q67L fusion protein. Different domains of the protein were color coded. B, Detail of the Mg^{2+} binding region. Mg^{2+} is shown in green in this model. Mg^{2+} interacts with the surrounding T107 and T124 residues with side chains highlighted in dark blue. C, Top 5 binding ligands of ARL15 and annotations on ligand binding site. C-score: The confidence score for evaluating the quality of the model. Lig Name: the name of the ligands that bind to ARL15.

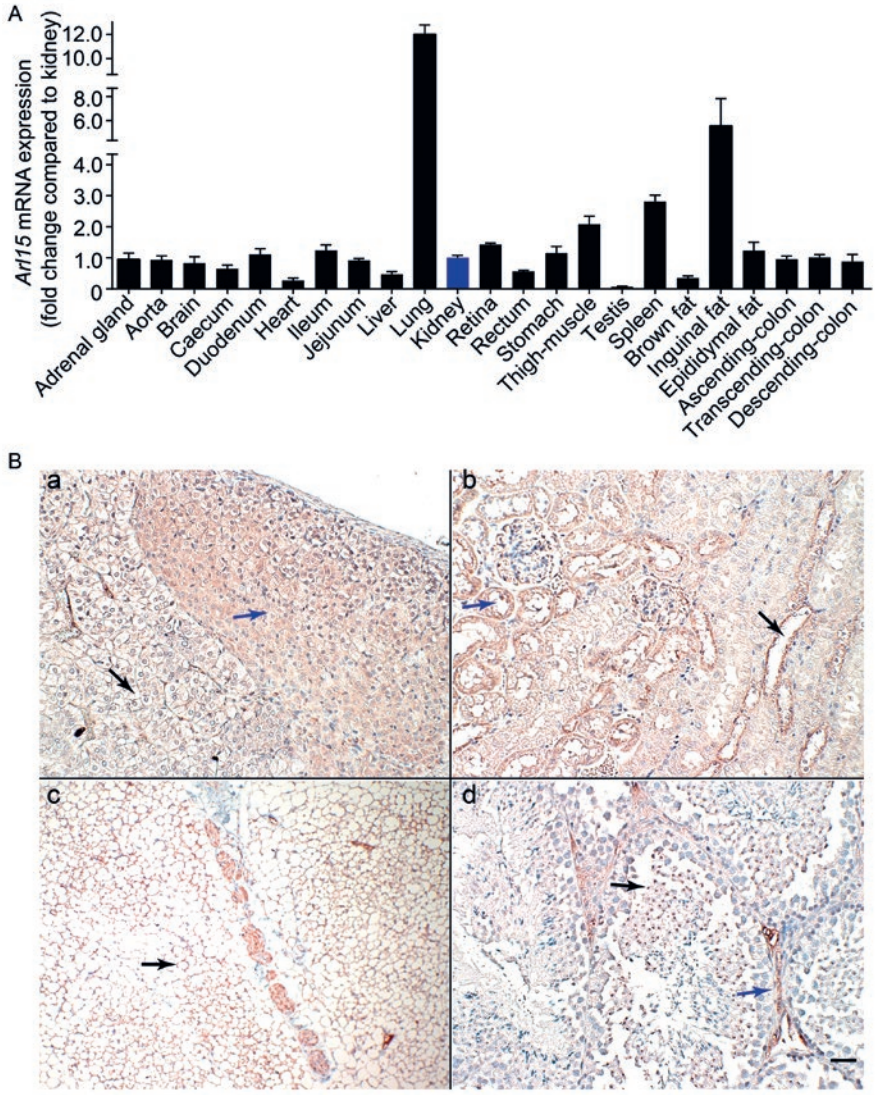

Figure 2. Gene and protein expression of *Arl15* in a panel of mouse tissues.

A, *Arl15* mRNA expression of the indicated mouse tissues, normalized for *Gapdh*. Data represent the mean of three individual mice ± SEM and were expressed as the fold change relative to total kidney gene expression. B, Immunohistochemical staining of ARL15 in different regions in the adrenal gland (a), kidney (b), inguinal fat (c) and testes (d). Blue arrow in panel a represents cortex of the adrenal gland, black arrow in panel a represents medulla of the adrenal gland, black arrow in panel b represents distal convoluted tubule of the kidney, blue arrow in panel b represents thick ascending loop of Henle of the kidney, black arrow in panel c represents adipocytes, black arrow in panel d represents testis spermatoblast, blue arrow in panel d represents interstitial cells. Size bar represents 25 µm.

On the low fat diet, water intake of male *Arl15*$^{+/-}$ mice was significantly increased by 60% compared to male *Arl15*$^{+/+}$ mice (Table 2). On the high fat diet, body weight of female *Arl15*$^{+/-}$ mice was significantly decreased by 12% compared to female *Arl15*$^{+/+}$ mice (Table 2). However, food intake and urine volume did not significantly differ between the groups on the respective diets (Table 2).

Table 2. Metabolic parameters of *Arl15*$^{+/-}$ Mice

Male	Low fat diet		High fat diet	
	***Arl15*$^{+/+}$**	***Arl15*$^{+/-}$**	***Arl15*$^{+/+}$**	***Arl15*$^{+/-}$**
Weight (g)	35.2 ± 1.5	33.3 ± 1.1	45.4 ± 0.6	43.6 ± 1.7
Food intake (g)	4.7 ± 0.5	4.4 ± 0.5	1.5 ± 0.2	1.2 ± 0.2
Water intake (mL)	2.2 ± 0.3	3.6 ± 0.5[a]	1.9 ± 0.2	1.7 ± 0.2
Urine volume (mL)	1.2 ± 0.2	1.2 ± 0.1	0.9 ± 0.1	1.0 ± 0.1

Female	Low fat diet		High fat diet	
	***Arl15*$^{+/+}$**	***Arl15*$^{+/-}$**	***Arl15*$^{+/+}$**	***Arl15*$^{+/-}$**
Weight (g)	26.6 ± 0.8	27.8 ± 0.8	46.6 ± 1.5	41.8 ± 1.4[b]
Food intake (g)	5.0 ± 0.5	4.4 ± 0.3	0.7 ± 0.2	0.9 ± 0.2
Water intake (mL)	4.1 ± 1.2	3.1 ± 0.3	1.2 ± 0.1	1.3 ± 0.2
Urine volume (mL)	0.7 ± 0.1	0.6 ± 0.2	0.6 ± 0.1	0.5 ± 0.1

Arl15$^{+/+}$ and *Arl15*$^{+/-}$ mice were kept on low fat and high fat diets for 24-weeks. During the last 24 hours, the mice were placed in metabolic cages to collect blood and 24 hours urine. Numbers represent mean ± SEM. a represents a significant difference compared to *ARL15*$^{+/+}$ mice on low fat diet; b indicates a significant difference compared to *ARL15*$^{+/+}$ mice on high fat diet. +/+, *Arl15* wildtype mice, +/-, *Arl15* heterozygous mice.

Effects of low and high fat diets on Mg^{2+} handling in *Arl15*$^{+/+}$ and *Arl15*$^{+/-}$ mice

To investigate the role of ARL15 in Mg^{2+} handing, serum Mg^{2+} concentration and 24 hours urinary Mg^{2+} excretion were measured in male and female *Arl15*$^{+/+}$ and *Arl15*$^{+/-}$ mice. Mg^{2+} excretion was nearly 3 folds lower in female *Arl15*$^{+/+}$ mice on high fat diets compared to female *Arl15*$^{+/+}$ mice fed low fat diets (Figure 3D). However, serum Mg^{2+} concentration and 24 hours urinary Mg^{2+} excretion did not alter significantly between the other groups (Figure 3A-D).

The expression of Mg^{2+}-related genes in the kidney of *Arl15*$^{+/+}$ and *Arl15*$^{+/-}$ mice

To further study the role of ARL15 in renal Mg^{2+} handling, the expression of Mg^{2+}-related genes in the kidney of *Arl15*$^{+/+}$ and *Arl15*$^{+/-}$ mice fed low fat or high fat diets were evaluated by RT-qPCR. While the expression of *Cldn16* did not change between male *Arl15*$^{+/-}$ mice on high fat and low fat diets (Figure 4A), *Cldn16* expression in female *Arl15*$^{+/+}$ mice treated with high fat diets was significantly decreased compared to female *Arl15*$^{+/+}$ mice fed

with low fat diets (Figure 4G). *Fxyd2* expression in both male and female *Arl15*$^{+/-}$ mice on high fat diets was significantly higher compared to the mice fed low fat diets (Figure 4B, H). Expression of *Cnnm2*, *Slc41a1*, *Slc41a3*, and *Trpm6* was not affected between the conditions (Figure 4C- F, I-L).

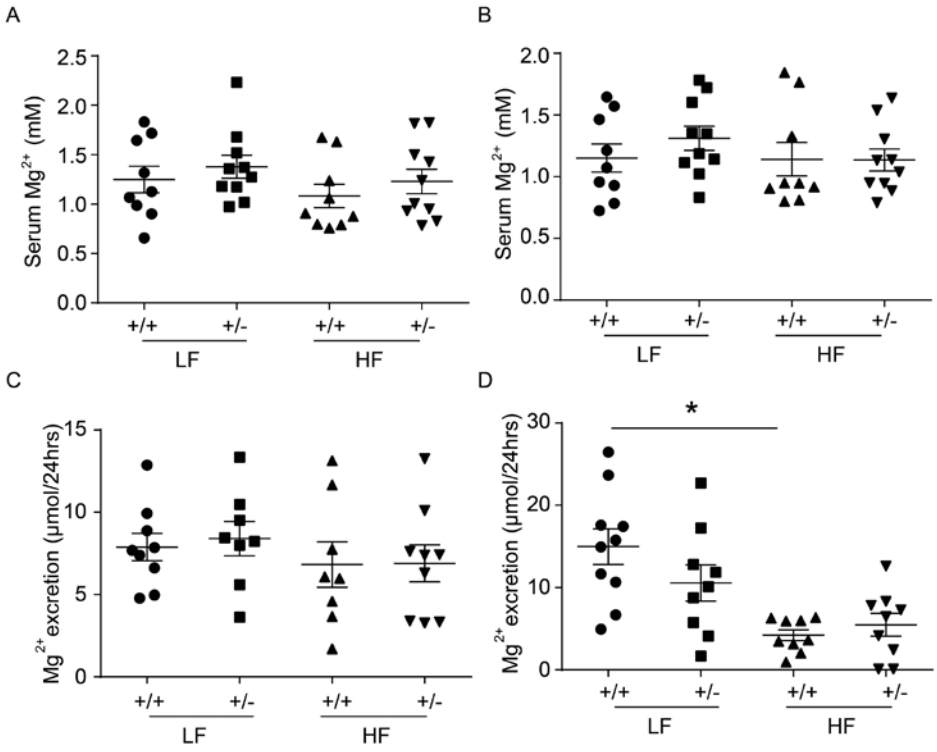

Figure 3. *Arl15*$^{+/-}$ mice exhibit normal serum Mg^{2+} concentrations and urinary Mg^{2+} excretions.

A, B, Serum Mg^{2+} concentrations of male (A) and female (B) *Arl15*$^{+/+}$ and *Arl15*$^{+/-}$ mice fed with either low fat or high fat diets. C, D, 24 hours urinary Mg^{2+} excretion of male (C) and female (D) *Arl15*$^{+/+}$ and *Arl15*$^{+/-}$ mice treated with either low fat or high fat diets. Values were presented as single data points with means ± SEM. +/+, *Arl15* wildtype mice, +/-, *Arl15* heterozygous mice, LF, low fat diets, HF, high fat diets.

The expression of metabolism-related genes in the kidney of *Arl15*$^{+/+}$ and *Arl15*$^{+/-}$ mice

GWAS showed that variants of ARL15 were associated with serum adiponectin levels, fasting insulin levels, and triglyceride concentrations [12, 15]. Therefore, RT-qPCR was commenced to analyze the expression of metabolism-related genes in the kidney of *Arl15*$^{+/+}$ and *Arl15*$^{+/-}$ mice fed with low fat and high fat diets.

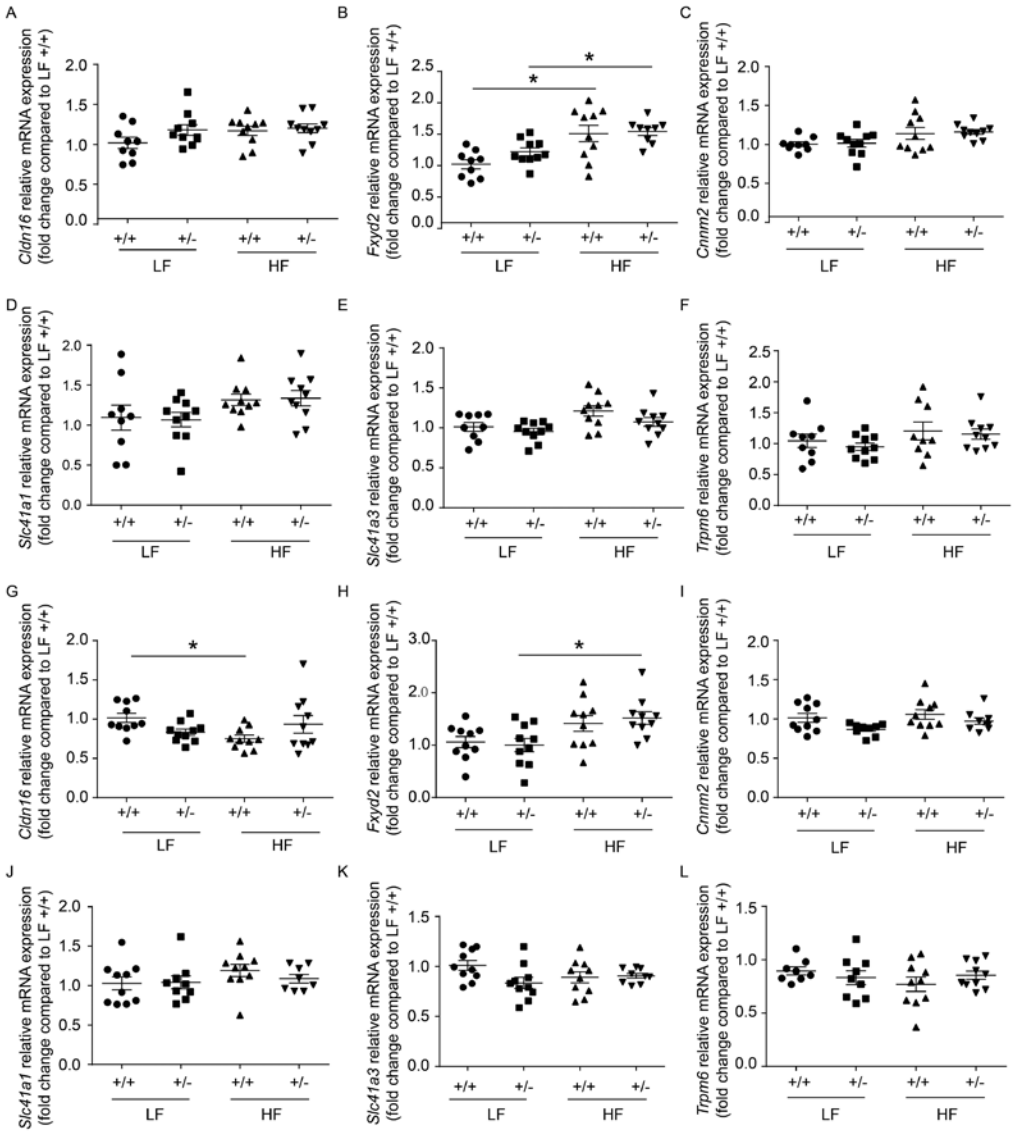

Figure 4. Mg^{2+}-related gene expression did not alter between *Arl15*$^{+/+}$ and *Arl15*$^{+/-}$ mice.

The mRNA expression levels of *Cldn16*, *Cnnm2*, *Fxyd2*, *Slc41a1*, *Slc41a3*, and *Trpm6* in the kidney of male (A-F) and female (G-L) *Arl15*$^{+/+}$ and *Arl15*$^{+/-}$ mice fed with either low fat diets (LF) or high fat (HF) diets were measured by RT-qPCR. Results were normalized to *Gapdh* expression (reference gene). * $P < 0.05$ indicates statistical significance. *Cldn16,* Claudin-16; *Cnnm2,* Cyclin and CBS domain divalent metal cation transport mediator 2; *Fxyd2,* FXYD domain containing ion transport regulator 2; *Slc41a1,* Solute carrier family 41 member 1; *Slc41a3,* Solute carrier family 41 member 3; *Trpm6,* Transient receptor potential cation channel subfamily M member 6; *Gapdh*, Glyceraldehyde 3-phosphate dehydrogenase. +/+, *Arl15* wildtype mice, +/-, *Arl15* heterozygous mice.

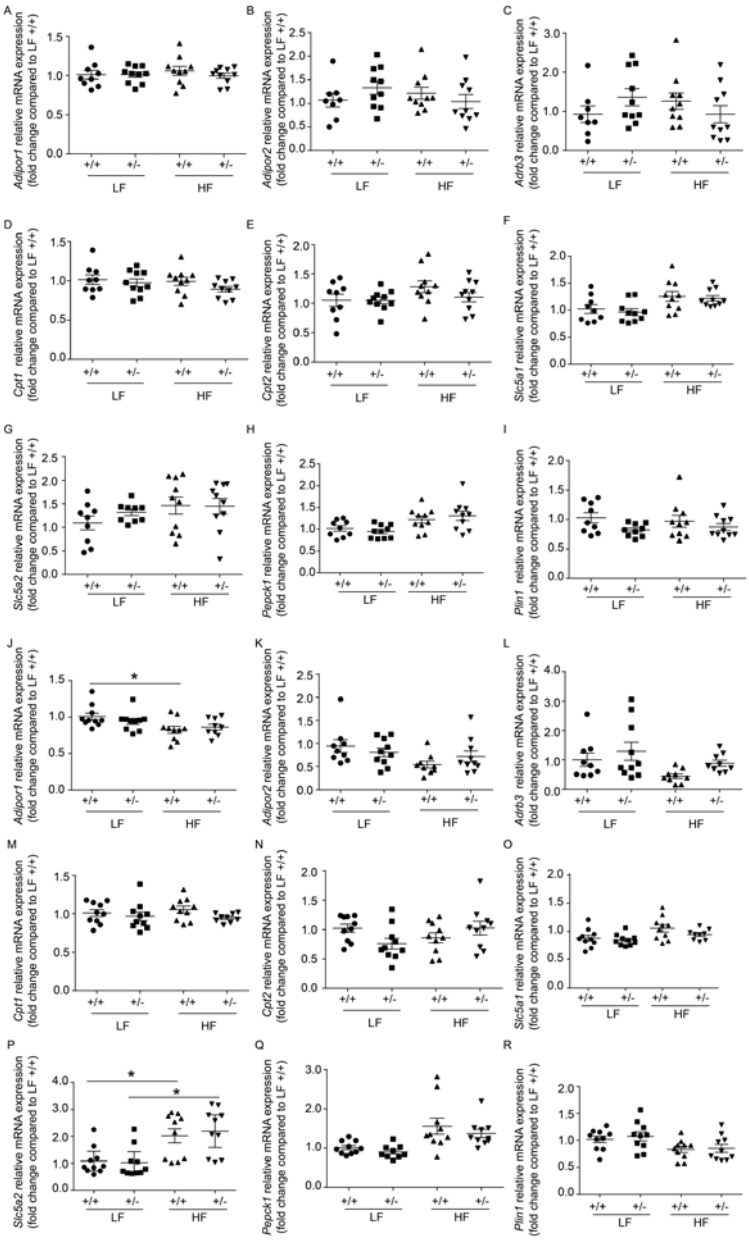

Figure 5. Metabolism-related gene expression did not change between *Arl15*$^{+/+}$ and *Arl15*$^{+/-}$ mice.

The mRNA expression levels of *Adipor1*, *Adipor2*, *Adrb3*, *Cpt1*, *Cpt2*, *Slc5a1*, *Slc5a2*, *Pepck1*, and *Plin1* in the kidney of male (A-I) and female (J-R) *Arl15*$^{+/+}$ and *Arl15*$^{+/-}$ mice fed with low fat or high fat diets were measured by RT-qPCR. Results were normalized to *Gapdh* expression (reference gene). Data represent means ± SEM and are expressed as fold difference compared to *Arl15*$^{+/+}$ mice on low fat diets. * $P < 0.05$ indicates a statistically significance. +/+, *Arl15* wildtype mice, +/-, *Arl15* heterozygous mice, LF, low fat diet, HF, high fat diet. *Adipor1*, Adiponectin receptor 1; *Adipor2*, Adiponectin receptor 2; *Adrb3,* Beta-3 adrenergic receptor; *Cpt1*, Carnitine palmitoyltransferase 1; *Cpt2,* Carnitine palmitoyltransferase 2; *Fabp1*, Fatty acid-binding protein 1; *Slc5a1*, Solute carrier family 5 member 1; *Slc5a2*, Solute carrier family 5 member 2; *Pepck,* Phosphoenolpyruvate carboxykinase; *Plin1,* Perilipin 1.

Gene expression of *Adipor1*, *Adipor2*, *Adrb3*, *Cpt1*, *Cpt2*, *Slc5a1*, *Slc5a2, Pepck and Plin1* were analyzed. Gene expression of *Adipor1* was significantly lower in female *Arl15*$^{+/+}$ mice on high fat diets compared to the mice treated with low fat diets (Figure 5J). Gene expression of *Adipor1* was not affected in male *Arl15*$^{+/+}$ mice on either diet (Figure 5A). The expression of *Slc5a2* in female *Arl15*$^{+/+}$ or *Arl15*$^{+/-}$ mice fed with low fat diets were lower than female *Arl15*$^{+/+}$ or *Arl15*$^{+/-}$ mice fed with high fat diets respectively (Figure 5P). However, the expression of *Slc5a2* in male *Arl15*$^{+/+}$ or *Arl15*$^{+/-}$ mice was not changed with either diet (Figure 5G). The expression of other genes, such as *Adipor2*, *Ardb3*, *Cpt1*, *Cpt2, Slc5a1*, *Pepck1* and *Plin1* were not affected in male or female *Arl15*$^{+/+}$ or *Arl15*$^{+/-}$ mice exposed to the high fat or low fat diets (Figure 5B-F, H, I, K-N, Q, and R).

Expression of membrane trafficking-related genes in the kidney of *Arl15*$^{+/+}$ and *Arl15*$^{+/-}$ mice

ARL15 was predicted to be a small GTPase and protein-protein interaction prediction showed that ARL15 interacts with vesicular trafficking genes [9]. In order to examine whether reduced ARL15 expression was compensated by other small GTPase involved in intracellular vesicle trafficking, the expression of *Arf1*, *Arfgef-1*, *Arfgef-2*, and *Arf6* was measured by RT-qPCR in the kidney of *Arl15*$^{+/+}$ and *Arl15*$^{+/-}$ mice fed with low fat and high fat diets. However, the results indicated that expression of *Arf1*, *Arfgef-1*, *Arfgef-2*, and *Arf6* in male or female *Arl15*$^{+/+}$ or *Arl15*$^{+/-}$ mice treated with high fat and low fat diets did not change significantly (Figure 6A-H).

Discussion

This study demonstrated that *Arl15*$^{+/-}$ mice have a normal phenotype, and exhibit no changes in serum Mg^{2+} concentration or urinary Mg^{2+} excretion. Furthermore, there was no altered expression of Mg^{2+}-related, metabolism-related, and membrane trafficking-related genes in *Arl15*$^{+/-}$ mice compared to *Arl15*$^{+/+}$ mice. Taken together, these findings showed that partial loss of ARL15 does not impair renal Mg^{2+} handling and metabolism. Other models may be required to study the role of ARL15 in the kidney.

ARL15 was predicted to be a small GTPase that was associated with plasma adiponectin, insulin, and high-density lipoprotein (HDL) cholesterol levels, obesity, and coronary atherosclerosis [15, 16]. However, its function is still unknown. Our tertiary analysis indicated that ARL15 belongs to the small GTPase superfamily. Subfamilies like Rab and Arf GTPase were reported to be involved in endomembrane trafficking, from the endoplasmic reticulum (ER) to the Golgi in many studies [17-19]. Immunostaining results showed that ARL15 was predominantly localized in the Golgi apparatus [11]. Together with our tertiary analysis, this supports the idea that ARL15 may be involved in endomembrane trafficking. In line with this, Corre *et al.* proposed that ARL15 can influence the channel activity of the Mg^{2+} channel TRPM6, possibly by affecting channel trafficking [9].

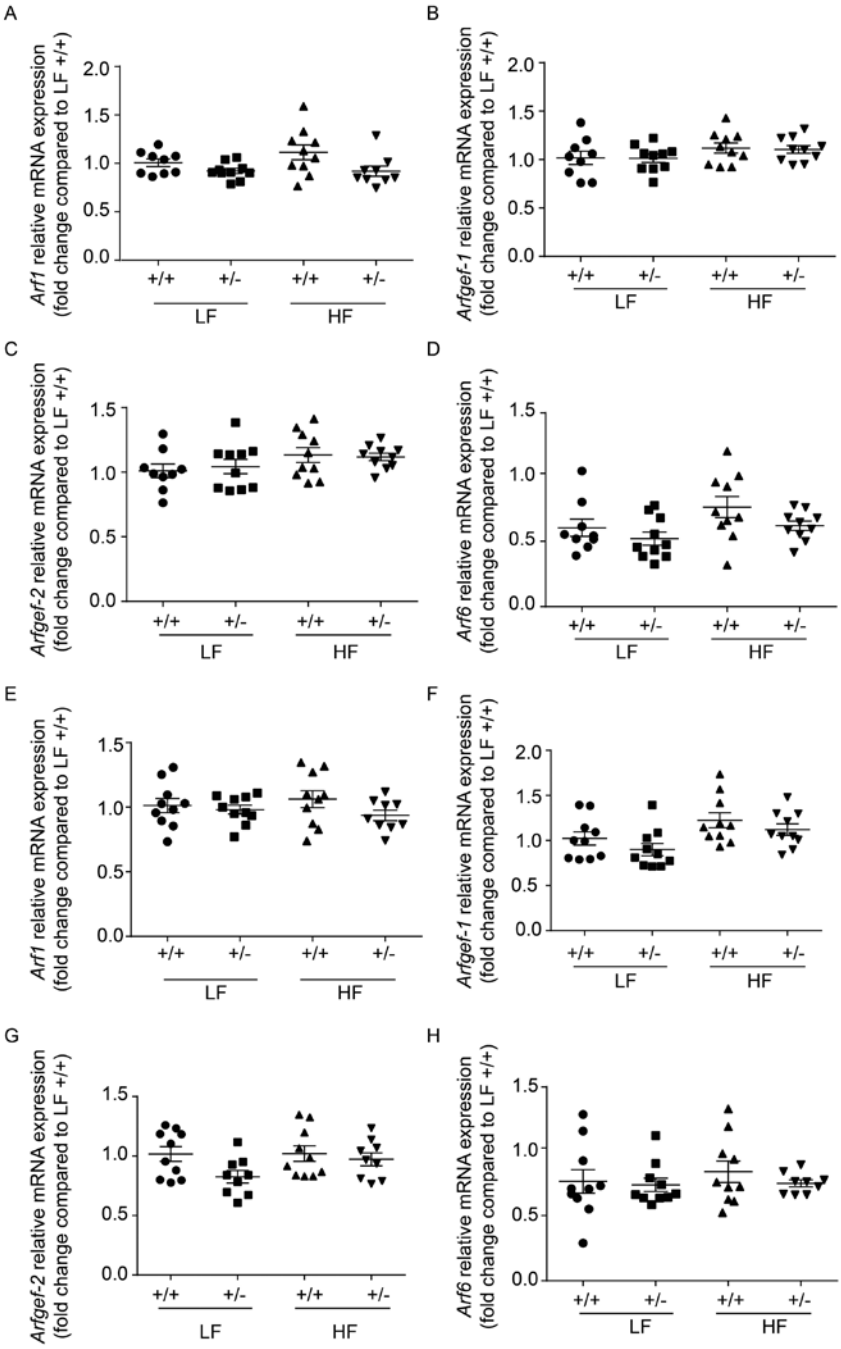

Figure 6. Membrane trafficking-related genes expression did not change in *Arl15*$^{+/-}$ mice.

The mRNA expression levels of *Arf1*, *Arfgef-1*, *Arfgef-2*, and *Arf6* in the kidney of male (A-D) and female (E-H) *Arl15*$^{+/+}$ (+/+) and *Arl15*$^{+/-}$ (+/-) mice fed with low fat diets (LF) or high fat diets (HF) were measured by RT-qPCR. Results were normalized to *Gapdh* expression (reference gene). *Afr1*, ADP ribosylation factor 1; *Afr6*, ADP ribosylation factor 6; *Arfgef-1*, ADP ribosylation factor guanine nucleotide exchange factor 1; *Arfgef-2*, ADP ribosylation factor guanine nucleotide exchange factor 2.

In this study, we demonstrated that *Arl15* mRNA was widely expressed in mice. *Arl15* was highly abundant in white adipose tissue. The white adipose tissue was responsible for adiponectin secretion, which plays an important role in modulating the level of blood glucose and the breakdown of fatty acid [20, 21]. It had been shown that *Arl15* knockdown in differentiated adipocytes resulted in decreased adiponectin secretion and impaired adipogenesis in pre-adipocytes [11]. Together, this suggests that ARL15 was directly or indirectly involved in the regulation of adiponectin function [11]. However, In contrast to the positive correlation of *Arl15* and *Adiponectin* in 3T3-L1 cells [11], our study did not observe changes in mRNA expression level of *Adiponectin* or other metabolism-related genes in *Arl15*$^{+/-}$ mice compare to *Arl15*$^{+/+}$ mice. This may due to the fact that certain signal pathways and/or compensatory mechanisms can be activated to counteract the heterozygous knockout of ARL15.

A recent GWAS analysis demonstrated that ARL15 was associated with urinary Mg^{2+} excretion [9]. Knockdown of *arl15b* expression in zebrafish larvae decreased the Mg^{2+} content compared with controls, which was suggestive of renal Mg^{2+} wasting [9]. Nevertheless, serum and urinary Mg^{2+} levels were normal in *Arl15*$^{+/-}$ mice. A compensatory network may be activated to counteract Mg^{2+} wasting in *Arl15*$^{+/-}$ mice. Although this could not be detected by RT-qPCR, changes in protein expression or function cannot be excluded. For instance, Mg^{2+} reabsorption by TRPM6 in the DCT may be altered by heterozygous knockout of ARL15, given the role of ARL15 in TRPM6 channel function [9]. Therefore, further studies on the protein level and function level should be performed to better understand potential compensatory mechanisms. Alternatively, *Arl15*$^{+/-}$ mice could be faced with low Mg^{2+} diets in order to challenge potential compensation. Corre *et al.* reported that the mRNA expression of *arl15b* increased nearly 70% to deal with Mg^{2+} deficiency in zebrafish [9]. Additionally, ARL15 kidney-specific knockout could be generated to understand more about the function of ARL15 in the kidney.

Taken together, our studies demonstrated that *Arl15*$^{+/-}$ mice possess a normal physiological behavior and no disturbances in Mg^{2+} handling. Thus, to determine whether ARL15 is involved in renal Mg^{2+} handling, additional studies are warranted. Future research should focus on generating ARL15 kidney-specific knockout mice and challenging the mice with low Mg^{2+} diets to further elucidate the physiological and pathological role of ARL15 in Mg^{2+} homeostasis.

Acknowledgements

This work was financially supported by grants from the Netherlands Organization for Scientific Research (NWO Veni 016.186.012 and VICI 016.130.668) and a grant from the Radboud Institute for Molecular Life Sciences. Ying Bai, Liz Bentley, and Roger D. Cox were funded by the UK Medical Research Council (MC_U142661184). The authors thank Sidra Kashif for her excellent technical assistance.

References

1. Jahnen-Dechent, W. and M. Ketteler, *Magnesium basics.* Clin Kidney J, 2012. **5**(Suppl 1): p. i3-i14.
2. Grober, U., J. Schmidt, and K. Kisters, *Magnesium in Prevention and Therapy.* Nutrients, 2015. **7**(9): p. 8199-226.
3. Volpe, S.L., *Magnesium in disease prevention and overall health.* Adv Nutr, 2013. **4**(3): p. 378S-83S.
4. DiNicolantonio, J.J., J. Liu, and J.H. O'Keefe, *Magnesium for the prevention and treatment of cardiovascular disease.* Open Heart, 2018. **5**(2): p. e000775.
5. Houillier, P., *Mechanisms and regulation of renal magnesium transport.* Annu Rev Physiol, 2014. **76**: p. 411-30.
6. Xi, Q., J.G. Hoenderop, and R.J. Bindels, *Regulation of magnesium reabsorption in DCT.* Pflugers Arch, 2009. **458**(1): p. 89-98.
7. Schlingmann, K.P., et al., *TRPM6 and TRPM7--Gatekeepers of human magnesium metabolism.* Biochim Biophys Acta, 2007. **1772**(8): p. 813-21.
8. Walder, R.Y., et al., *Mutation of TRPM6 causes familial hypomagnesemia with secondary hypocalcemia.* Nat Genet, 2002. **31**(2): p. 171-4.
9. Corre, T., et al., *Genome-Wide Meta-Analysis Unravels Interactions between Magnesium Homeostasis and Metabolic Phenotypes.* J Am Soc Nephrol, 2018. **29**(1): p. 335-348.
10. Taneera, J., et al., *Silencing of the FTO gene inhibits insulin secretion: An in vitro study using GRINCH cells.* Mol Cell Endocrinol, 2018. **472**: p. 10-17.
11. Rocha, N., et al., *The metabolic syndrome- associated small G protein ARL15 plays a role in adipocyte differentiation and adiponectin secretion.* Sci Rep, 2017. **7**(1): p. 17593.
12. Richards, J.B., et al., *A genome-wide association study reveals variants in ARL15 that influence adiponectin levels.* PLoS Genet, 2009. **5**(12): p. e1000768.
13. Willer, C.J., et al., *Discovery and refinement of loci associated with lipid levels.* Nat Genet, 2013. **45**(11): p. 1274-1283.
14. Thomsen, S.K., et al., *Systematic Functional Characterization of Candidate Causal Genes for Type 2 Diabetes Risk Variants.* Diabetes, 2016. **65**(12): p. 3805-3811.
15. Scott, R.A., et al., *Large-scale association analyses identify new loci influencing glycemic traits and provide insight into the underlying biological pathways.* Nat Genet, 2012. **44**(9): p. 991-1005.
16. Teslovich, T.M., et al., *Biological, clinical and population relevance of 95 loci for blood lipids.* Nature, 2010. **466**(7307): p. 707-13.
17. Nielsen, E., A.Y. Cheung, and T. Ueda, *The regulatory RAB and ARF GTPases for vesicular trafficking.* Plant Physiol, 2008. **147**(4): p. 1516-26.
18. Stenmark, H. and V.M. Olkkonen, *The Rab GTPase family.* Genome Biol, 2001. **2**(5): p. REVIEWS3007.
19. Pereira-Leal, J.B. and M.C. Seabra, *Evolution of the Rab family of small GTP-binding proteins.* J Mol Biol, 2001. **313**(4): p. 889-901.
20. Palanivel, R., et al., *Globular and full-length forms of adiponectin mediate specific changes in glucose and fatty acid uptake and metabolism in cardiomyocytes.* Cardiovasc Res, 2007. **75**(1): p. 148-57.
21. Halleux, C.M., et al., *Secretion of adiponectin and regulation of apM1 gene expression in human visceral adipose tissue.* Biochem Biophys Res Commun, 2001. **288**(5): p. 1102-7.

5

ARL15 modulates Mg^{2+} homeostasis through N-glycosylation of CNNMs

Chao Ma*[1], Yevgen Zolotarov*[2,3], Irene Gonzalez-Recio[4], Serge Hardy[2,3], Gijs Franken[1], Elie Kostantin[2,3], Femke Latta[1], Noriko Uetani[2,3], Jean-François Côté[5], Irene Díaz Moreno[5], Antonio Díaz Quintana[5], Joost GJ Hoenderop[1], Luis Alfonso Martínez-Cruz[4], Michel L. Tremblay*[2,3], Jeroen HF de Baaij*[1]

[1] Department of Physiology, Radboud Institute for Molecular Life Sciences, Radboud university medical center, 6500HB, Nijmegen, The Netherlands.
[2] Rosalind and Morris Goodman Cancer Research Centre, McGill University, Montréal, QC, Canada H3A 1A3.
[3] Department of Biochemistry, McGill University, Montréal, QC, Canada H3G 1Y6.
[4] Liver Disease Laboratory, Center for Cooperative Research in Biosciences (CIC bioGUNE), Basque Research and Technology Alliance (BRTA), Bizkaia Technology Park, Building 801A, 48160 Derio, Spain.
[5] Montreal Clinical Research Institute (IRCM), Montréal, QC, Canada H2W 1R7.
*The authors contributed equally to this work.

Submitted

Abstract

Cyclin M (CNNM1-4) proteins maintain cellular and body magnesium (Mg^{2+}) homeostasis. Here, we identified using various biochemical approaches that members of the CNNM family are direct interacting partners of ADP-ribosylation factor-like GTPase 15 (ARL15). ARL15 interacts with CNNMs at their carboxyl-terminal conserved cytosolic cystathionine β-synthase (CBS) domains. *In silico* modeling of the interaction using the reported structures of both CNNM2 and ARL15 supports that the small GTPase specifically binds the CBS1 domain. Immunohistochemistry and immunocytochemistry experiments demonstrated that CNNM2 and ARL15 co-localize in the kidney, with both proteins showing subcellular localization in the Golgi-apparatus. Towards understanding the role of this interaction, we found that overexpression of ARL15 in human embryonic kidney 293 (HEK293) cells resulted in complex N-glycosylation of CNNMs. Moreover, Mg^{2+} uptake experiments with stable isotopes demonstrate that there is a significant increase of $^{25}Mg^{2+}$ uptake upon knockdown of ARL15 in multiple kidney cancer cell lines. Altogether, our results establish ARL15 as a novel negative regulator of Mg^{2+} homeostasis by promoting the N-glycosylation of CNNMs.

Introduction

Mg^{2+} is an essential cation for all living organisms. As co-factor of ATP, Mg^{2+} is involved in over 600 enzymatic reactions and as such it plays important roles in a plethora of biological mechanisms such as DNA transcription, protein synthesis and energy metabolism [1]. Approximately 1% of the body Mg^{2+} content is present in the blood, indicating that the great majority of Mg^{2+} is stored intracellularly in soft tissues and in the hydroxyapatite structure of the bone [2]. Decreased intracellular Mg^{2+} levels suppress cell cycle progression and are consequently associated with cell growth impairment [3]. Recent studies therefore have focused on the regulation of intracellular Mg^{2+} concentration as a central mechanism for cellular metabolism and proliferation [4].

Among the various mechanisms of Mg^{2+} sensing and transport, proteins of the CNNM family were shown to play an important role in the intracellular sensing of the Mg^{2+} availability [5, 6]. The CNNM family has 4 members, which are highly conserved but have different tissue distribution [4-7]. CNNM3 shows a ubiquitous expression pattern, whereas CNNM1, CNNM2, and CNNM4 have the highest expression levels in the brain, kidney, and intestine, respectively [8]. All CNNMs interact with phosphates of the regenerating liver (PRL1-3) via the CBS domain of CNNMs [9, 10]. CNNMs and PRLs have been associated with the progression of breast and colon cancers [10, 11]. Although the exact molecular function of CNNM proteins is under debate [12, 13], it has been shown that engineered and naturally occurring mutations in CNNMs result in decreased Mg^{2+} transport in both cell and animal models [10, 14]. Notably, mutations in *CNNM2* result in renal Mg^{2+} wasting [14].

Recently, a large genome wide association study (GWAS) identified the *ARL15* locus to be associated with urinary Mg^{2+} excretion [15]. ARL15 is structurally similar to Ras-related GTP-binding proteins, which regulate intracellular vesicle trafficking [16, 17]. Within the kidney, ARL15 is highly expressed in the thick ascending limb (TAL) and distal convoluted tubule (DCT), like CNNM2, where Mg^{2+} reabsorption is tightly regulated [15]. However, the exact function of ARL15 and the mechanism by which ARL15 regulates Mg^{2+} homeostasis is still unknown.

In this study, we identified CNNMs as direct interacting partners of ARL15 by binding to the CBS1 domain of CNNM2. We demonstrate that ARL15 is a negative regulator of cellular Mg^{2+} homeostasis through its modulation of CNNMs glycosylation and the direct correlation of its expression to levels of intracellular Mg^{2+}.

Methods and materials

DNA constructs

Human *CNNM2* cDNA with an in-frame HA tag before CNNM2 stop codon and an *XhoI* restriction site after *CNNM2* stop codon was amplified using Phusion

polymerase (New England Biolabs, Ipswich, MA, USA) and then the product was cloned into the pCINeo-IRES-GFP vector using *NheI* and *XhoI* (New England Biolabs). To obtain truncated *CNNM2* plasmids, primers (Forward:5'-CGGCTAGCGCCACCATGA TTGGCTGTGGCGCTTG-3' and Reverse 1 (full-length *CNNM2*:05'-CCCTCGAGCTATGCG TAGTCTGGCACGTCGTATGGGTAACCGGTGATGGCGCCTTCGTTG-3'), Reverse 2 (*CNNM2* transmembrane region: 5'-CCACCGGTCACGTCCTCCACCGTC-3'), Reverse 3 (*CNNM2* transmembrane+CBS1 region: 5'-CCACCGGTGTCATCGGGATCCAC-3'), Reverse 4 (*CNNM2* transmembrane+CBS1+link region: 5'-CCACCGGTGTGGTTATAAAATTTGGTGATG-3') or Reverse 5 (*CNNM2* transmembrane+CBS1+link+CBS2 region: 5'-CGGCTAGCGCCACCATGATTGGCTGTGGCGCTTG-3') were synthesized. All primers were purchased from Biolegio BV (Nijmegen, Netherlands). The PCR product was purified using a NucleoSpin® Gel and PCR Clean up kit (Macherey Nagel, Düren, Germany). Subsequently, the truncated *CNNM2* PCR products were cloned into the pCINE-IRES-GFP vector by digestion with restriction enzymes *NheI* (New England Biolabs) and *XhoI* (New England Biolabs).

To obtain C-terminal FLAG-tagged ARL15 and CNNM constructs, human coding sequences were amplified with appropriate primers containing attB1 and attB2 recombination site overhangs. Amplification was carried out with KAPA HiFi polymerase using GC buffer (Kapa Biosystems, Wilmington, MA, USA). Amplicons were gel purified and Gateway cloning was used to first recombine the amplicon into pDONR221 vector and then, pDEST26 (Addgene #79275) vector, using Gateway BP or LR Clonase II enzyme mix, respectively (Thermo Fisher Scientific, Waltham, MA, US). Chemically competent DH5α *E. coli* were transformed with pDONR221 and pDEST26 vectors. All constructs were verified by sequence analysis.

Cell culture, transfection and transduction

HEK293 cells were grown in Dulbecco's Modified Eagle Medium (DMEM) (Biowhittaker Europe, Vervier, Belgium) supplemented with 10% (v/v) fetal calf serum (PAA Laboratories, Linz, Austria), non-essential amino acids, and 2 mM L-glutamine at 37 °C in a humidified incubator with 5% (v/v) CO_2 (New Brunswick Galaxy 170s). Cells were seeded 6 hours before transient transfection with Lipofectamine 2,000 (Invitrogen, Breda, The Netherlands), the ratio of DNA: Lipofectamine 2,000 was 1:2.

ACHN, Caki-1, HeLa, RCC4 and SK-RC-39 cells were grown in DMEM, high glucose (Thermo Fisher Scientific) supplemented with 10% fetal bovine serum (FBS) (Thermo Fisher Scientific) and 2 mM GlutaMAX at 37 °C in a humidified incubator with 5% (v/v) CO_2.

For lentivirus production, HEK293T/17 cells were transfected with a 4:2:1 ratio of lentiviral construct of interest: PAX2: VSV-G. 24 hours later, the media was changed. 48 hours later, the media was collected and filtered through a 0.45 µm filter. To infect the cells, media was substituted with HEK293T/17 supernatant containing virus with 8 µg/ml polybrene. 48 hours later, the media was changed to fresh media containing a selection reagent and the selection was carried out for 7 days.

Site-directed mutagenesis

To mutate asparagine 73 (N73) that was predicted to be the site of N-glycosylation of CNNM3 into alanine (A), pDONR221-CNNM3 carrying the wild-type sequence without a stop codon was amplified using a single primer PCR. Amplification was carried out with KAPA HiFi polymerase using GC buffer (Kapa Biosystems, Wilmington, MA, USA). The following primer was used: 5'-GGCCCGGGCTTCGCCgcCAGCTCTTGGTCCTGGGTGG-3', indicating the nucleotides necessary to introduce the mutation in lower-case letters. After amplification, the original plasmid was digested with *DpnI* (New England Biolabs) for 2 hours at 37 °C, which was followed by transformation of chemically competent DH5α E. coli. The construct was verified by sequencing.

Pull down assay

A pull down assay was performed to determine which proteins of mice DCT interact with CNNM2. pGEX-mCNNM2 c-tail-GST was inserted in bacteria to be able to multiply the protein. Afterwards, bacteria were lysed with lysis buffer (150mM NaCl, 5mM EGTA, Triton 1% (v/v), 1mg/ml pepstatin, 1mM PMSF, 5mg/ml leupeptin, 5mg/ml aproptinin, 50mM Tris/HCl, pH 7.5). Glutathione beads (Thermo Fisher, Rockford, IL, USA) were used to purify the samples to obtain only CNNM2 c-tail. The beads were washed with pull down buffer (20mM Tris-HCL pH 7.4, 140mM NaCl, 1 mM $CaCl_2$, 0.2% (v/v) triton-x-100, 0.2% (v/v) NP-40, 1:1000 pepstatin, 1:1000 Aprotinin, 1:400 Leupeptin, 1:100 PMSF) and bacterial lysate was added to the beads followed by an incubation of 3 hours at 4 °C. After incubation, beads were transferred into a new tube and washed with pull down buffer. For kidney tissue, kidneys of 8 PV-GFP mice were dissected and minced in small pieces. The DCT was selected and dissolved in pull down buffer followed by homogenizing of the mixture using ultra turrax. After 30 minutes of incubation on ice, aliquots were taken and centrifuged. Supernatant was added to the beads followed by an incubation overnight rotating at 4 °C. After incubation, beads were washed with pull down buffer, Laemmli and DTT were added, and Western blot was performed. Migration was stopped when the sample was 1 cm in the running gel. Then samples were cut out and measured with mass spectrometry.

Biotin identification (BioID)

BioID was performed as previously described [18]. The graph of ARL15 interacting partners was generated using ProHits-viz [19]. Gene ontology overrepresentation analysis was performed using PANTHER 15.0 [20].

ARL15 model

A model of the structure of ARL15 was generated by simulated annealing as implemented in Modeller [21] using as templates the X-ray diffraction coordinates of the complex between human ARL2 and BART (pdb code 3DOE chain A; 36.3 identity) complex

between murine ARL2 and PDEδ (pdb code 1KSG chain A; 36.3 identity) murine ARF6 (pdb code 6BBQ; 35.67% identity) human ARF6 (pdb code 2A5G; 35.67% identity). Results were monitored in UCSF Chimera [22]. A single structure, displaying the lowest zDOPE [23] score (-0.58) and an RMSD value of 3.54 Å with respect to the closest template, out of 100 results were selected. This structure was subjected to energy minimization using the Amber 14SB force field [24]. A final check was performed with Coot [25] before deposition and the ModelArchive server.

CNNM models

To generate alternative linker conformations, in addition to completing sidechains from a SAXS model, simulated annealing computations were carried out using Modeller 9.3 [21]. 100 conformations were generated, arranged according to their zDOPE scores and tested for collisions with other subunits with UCSF Chimera. At the end, three different conformations were tested. A model of the cytosolic domains of CNNM3 was also generated using the full precursor sequence (NCBI accession code 060093.3) and the XRD coordinates of the CNNM2 cytosolic domains in their flat conformation [26].

Docking models

Docking computations were carried out with benchtop HEX [27] and compared with Brownian dynamics (BD) computations. Hex computations included shape evaluation, in vacuo electrostatics and Decoys As a Reference State (DARS) potentials [28]. In every simulation, 20,000 structures were generated, clustered using a RMSD cut-off value of 3 Å and arranged according to their energies. First 100 were selected for analysis. Post-processing consisted in a short Optimized Potentials for Liquid Simulations (OPLS) energy minimization as implemented in the software.

Brownian dynamics

Docking modeling was complemented with BD computations using the WebSDA server [29] to test if results could be reproduced by other methods. The force-field grids used in BD included all electrostatics and desolvation [30, 31] grids. Charges were added with PDB2PQR tool [32].

200 trajectories of BD computations were run in docking mode. A total of 500 non-redundant complexes were recorded along the computations. Table 1 displays the summary of the clustering analysis of the distinct complexes found. First cluster corresponds to binding to cyclic nucleotide monophosphate-binding homology (CNBH) domains at regions nearby missing structure, so they are considered artefactual. Cluster 2, however, showed the highest population and—on average— displayed lowest energies, and the lowest dispersion of conformations, according to RMSD values with respect to the representative structure.

Glycosidase and tunicamycin treatment

20 ug of protein from SK-RC-39 cells were treated with N-glycosidase F (PNGase F) and Endoglycosidase H (Endo H) (New England Biolabs) according to the manufacturer's instructions. Briefly: protein was denatured at 100 °C for 10 minutes, 1 unit/ul of a glycosidase was added with appropriate buffers and digested at 37 °C for 1 hour. SK-RC-39 cells grown in DMEM were treated with tunicamycin (Sigma-Aldrich, St. Louis, MO, USA) at 1 ug/ml for 8 hours to inhibit N-glycosylation.

Immunohistochemistry

5 µm kidney frozen sections were fixed with formalin and washed with TN buffer (0.1 M Tris/HCl (pH7.6) 0.15 M NaCl). Then, the sections were permeabilized in TN-Triton (TN with 0.1% Triton X-100) for 30 minutes. After incubation, the sections were washed and blocked with TN with 0.5% (w/v) blocking reagent TSA fluorescein system (Perkin Elmer, Waltham, MA, USA) for 30 minutes. The sections were incubated overnight at 4 °C with the following primary antibodies: guinea pig anti-CNNM2 (kindly received from Dr. Muller), rabbit anti-ARL15 (Sigma-Aldrich, St. Louis, MO, USA). For detection, kidney sections were incubated with Alexa Fluor 488 conjugated goat anti-rabbit and Alexa Fluor 596 conjugated goat anti-guinea pig IgG secondary antibodies (Thermo Fisher, Rockford, IL, USA). Images were visualized using AxioCam cameras (Zeiss, Oberkochen, Germany) and AxioVision software (Zeiss).

Immunocytochemistry

HEK293 cells were seeded at a low density on 0.01% (w/v) poly-L-lysine (Sigma, St Louis, MO, USA) coated coverslips and were transfected the subsequent day using Lipofectamine 2000 (Invitrogen, Breda, The Netherlands). Then, the following constructs: pCINEO-CNNM2-HA-IRES-GFP, pLenti6-CNNM3-V5, pDEST26-ARL15-FLAG, and mCherry-Golgi-7 were transfected. 24 hours after transfection, cells were washed with PBS, followed by fixation for 10 minutes using 4% (w/v) methanol-free formaldehyde (ThermoFisher, Waltham, MA, USA) in PBS. Afterwards, cells were permeabilized for 10 minutes in 0.1% (v/v) Triton-X100 and 0.3% (w/v) bovine serum albumin (BSA) (ThermoFisher, Waltham, MA, USA) solution. Subsequently, cells were treated with 50 mM NH_4Cl in PBS in order to reduce the background. Thereafter, cells were washed in PBS followed by blocking in 16% (v/v) normal goat serum (Merck Millipore, Burlington, MA, USA) supplemented with 0.1% (v/v) Triton-X100 for 30 minutes in room temperature. Then, cells were probed with primary antibody diluted in blocking buffer overnight at 4 °C, washed three times and incubated in secondary antibodies for 45 minutes at room temperature in the dark. Cells were washed three times with PBS and subsequently mounted using mounting medium supplemented with 4', 6-diamidino-2-phenylindole (DAPI; Southern Biotech, Birmingham, AL, USA). Images were made using the Zeiss LSM880 (Oberkochen, Germany) and analyzed using the freely available Fiji software [33]. The following antibodies were

used: mouse monoclonal anti-HA (Sigma-Aldrich, St. Louis, MO, USA), mouse monoclonal anti-V5 (Thermo Fisher, Rockford, IL, USA) and rabbit polyclonal anti-FLAG (Sigma-Aldrich, St. Louis, MO, USA), Alexa Fluor 488 conjugated goat anti-rabbit and Alexa Fluor 647 conjugated goat anti-mouse (Thermo Fisher, Rockford, IL, USA).

Western blot

Cells were lysed with lysis buffer containing 1mg/ml pepstatin, 1mM PMSF, 5mg/ml leupeptin, 5mg/ml aproptinin protease inhibitors. The lysis buffer contained 50mM Tris-HCl (pH 7.5), 1mM EDTA, 1mM EGTA, 150mM NaCl, 1mM sodium-orthovanadate, 10mM sodium-glycerophosphate, 50mM sodium fluoride, 0.27M sucrose, 10mM sodium pyrophosphate, 1% (v/v) Triton X-100. Protein concentrations were measured by performing a Bicinchoninic Acid protein assay (BCA) (Fisher Scientific, Hampton, NH, USA) and 20 µg protein were used for Western blot. Blots were then incubated in primary antibody overnight rolling at 4 °C. Primary antibodies were diluted in 1% (w/v) milk diluted in Tris-Buffered Saline and Tween 20 (TBST) as following; anti-HA (Cell Signaling technology, Leiden, The Netherlands), anti-FLAG (Sigma-Aldrich, St. Louis, MO, USA), anti-V5 (Thermo Fisher, Rockford, IL, USA), anti-β-actin (Sigma-Aldrich, St. Louis, MO, USA), all are raised in mice. After washing with TBST, blots were incubated for 1 hour rolling at room temperature (RT) in secondary antibody which was sheep anti-mouse antibody (Sigma-Aldrich, St. Louis, MO, USA). Then, proteins were visualized with Chemidoc (Bio-Rad Laboratories Inc, Hercules, CA, USA). Subsequent analysis was done using Image J [33].

Co-Immunoprecipitation

HEK293 or HeLa cells were seeded and transfected in petri dishes, 24 to 48 hours after transfection, cells were lysed with lysis buffer. BCA assay was performed to determine the protein concentration of the lysates. Input samples were taken to be able to check transfection efficiency by performing Western blot. For co-immunoprecipitation samples, 30 µl/sample protein A/G plus agarose beads (Santa Cruz Biotechnology, CA, USA) were washed with PBS. And 1.5 µl/sample in mouse raised antibody for human HA (Sigma-Aldrich, St. Louis, MO, USA) was added to the beads. For negative control, no antibody was added to the beads. Samples were then incubated for 2 hours rotated at 4 °C. Unbound antibodies were removed by washing with PBS. Then, lysates with the same amount of proteins (as calculated with the BCA test) were added to the beads and incubated overnight rotated at 4 °C. After incubation, lysates and beads were washed with lysis buffer. Then, Laemmli and Dithiothreitol (DTT) were added, and Western blot was performed. For FLAG-tagged protein immunoprecipitation, for each sample, 20 ug of Anti-FLAG M2 affinity agarose gel (Sigma-Aldrich, St. Louis, MO, US) were pre-blocked with 5% (w/v) BSA and 300 ug of total cell lysate (TCL) was pre-cleared with 20 ug of protein A/G agarose mix, for 2 hours at 4°C on a rotator. TCL supernatant was collected and incubated with pre-blocked FLAG beads for 2 hours at 4 °C on a rotator.

ATP production

5,000 kidney cancer cells were plated per well in a 96-well plate and ATP production was measured after growing overnight. CellTiter-Glo 2 kit (Promega) was used in accordance with manufacturer's instructions.

CRISPR-Cas9 experiments

Guide RNA (sgRNAs) targeting ARL15 were cloned into lentiCRISPRv2 plasmid (Addgene #52961) using Golden-Gate Assembly with the Esp3I endonuclease following the standard protocol [34]. For lentivirus production, HEK293T/17 cells were transfected using Lipofectamine 2000 (Invitrogen, Breda, The Netherlands) with 4:2:1 ratio of lentiCRISPRv2:PAX2: VSV-G. 24 hours later, the media was changed. 48 hours later, the media was collected and filtered through a 0.45 µm filter. To transduce the cells, media was substituted with HEK293T/17 supernatant containing virus with 8 µg/ml polybrene. 48 hours later, the media was changed to fresh media containing puromycin and the selection was carried out for 7 days.

$^{25}Mg^{2+}$ uptake

ACHN, Caki-1, RCC4 and SK-RC-39 cells were seeded into 12-well plates. Two days after transfection, cells were washed once with basic uptake buffer without Mg^{2+} (125 mM NaCl, 5 mM KCl, 0.5 mM $CaCl_2$, 0.5 mM Na_2HPO_4, 0.5 mM Na_2SO_4, 15 mM HEPES/NaOH, pH 7.5), followed by incubation for 0 or 15 minutes at 37°C with basic uptake buffer containing 1 mM $^{25}Mg^{2+}$ (Cortecnet, Voisins Le Bretonneux, France). After incubation, the basic uptake buffer containing $^{25}Mg^{2+}$ was removed and cells were washed with ice cold PBS. Then cells were lysed with 1 ml nitric acid (Sigma Aldrich, St. Louis, MO, USA) which was then diluted in Milli-Q until a nitric acid concentration of 10%. Samples were analyzed with inductively coupled plasma mass spectrometry (ICP-MS).

Cell surface biotinylation

Petri dishes were coated with poly-L-lysine before seeding and transfection. Two days after transfection the cells were washed with PBS-CM (100 ml 10x PBS, 1 mM $MgCl_2$, 0.5 mM $CaCl_2$, pH 8.0 adjusted with NaOH, Milli-Q until total volume of 1,000 ml) followed by adding 0.5 mg/ml Sulfo-NHS-LC-LC-biotin (Thermo fisher scientific, Rockford, USA). After 30 minutes incubation, cells were washed with 0.1% (w/v) PBS-CM BSA and PBS. Cells were then lysed with lysis buffer, and protein concentration was measured with a BCA test. Input samples were taken to be able to check transfection efficiency by performing Western blot. Then, lysates with the same amount of proteins (as calculated with the BCA test) were added with the neutravidin agarose beads (Thermo fisher scientific, Rockford, USA) and incubated overnight rotated at 4°C. After incubation, protein lysates were washed with lysis buffer. Then, Laemmli and DTT buffer were added to samples and incubated at 37°C for 30 minutes before loading the protein samples on SDS-PAGE.

Statistical analysis

Results are expressed as mean ± standard error of the mean (SEM). Biotinylation, Co-Immunoprecipitation and ATP production results are statistically analyzed by performing one-way ANOVA followed by Tukey as post-test. $^{25}Mg^{2+}$ uptake results are statistically analyzed by performing a two-way ANOVA followed by Tukey as post-test. Differences with $P<0.05$ were regarded as statistically significant.

Results

ARL15 is a new binding partner of CNNMs

To identify CNNM2 protein interactions, pull down of mouse CNNM2 carboxyl-terminal region was performed using DCT-enriched kidney lysates, followed by mass spectrometry (Figure 1A). Twenty-four interacting partners of CNNM2 were detected, including ARL15 (Figure 1B). Since ARL15 has been shown to be involved in urinary Mg^{2+} excretion [15], we decided to further explore this particular interacting partner. To confirm the interaction between ARL15 and CNNMs, BioID of ARL15 was performed and we identified 221 proteins as potential interacting partners of ARL15 and CNNM2, CNNM3 and CNNM4 were among them (Figure 1F). Gene ontology (GO) biological process overrepresentation analysis indicated that Mg^{2+} ion homeostasis was one of the most highly enriched processes (Figure 1C). Immunoprecipitation demonstrated that CNNM3 and ARL15 interact endogenously (Figure 1D). To further confirm this association, co-immunoprecipitation assays were performed with overexpressed ARL15 and the four members of the CNNM family. ARL15 binding was observed to a similar extent for each CNNM protein (Figure 1E). Endogenous PRL-1 and PRL-2, which are well described interacting partners of CNNMs that regulate Mg^{2+} flux [10, 11], also co-precipitated with CNNMs and ARL15 (Figure 1E). The above data indicate that ARL15 is a novel interacting partner of the four members of the CNNM family of Mg^{2+} modulators.

ARL15 interacts with CNNM2 cytoplasmic region

The topology for CNNMs consists of a signal peptide, three transmembrane domains (TM) and an intracellular C-carboxyl containing the CBS and a CNBH domain (Figure 2A) [8]. To determine which domain of CNNM2 is important for the interaction with ARL15, truncated CNNM2 proteins were co-immunoprecipitated with ARL15. The presence of the CBS domains is essential for the binding of ARL15 to CNNM2. The interaction of the proteins decreases by 36% when the CBS2 domain is removed (Figure 2B and 2C). No interaction with the transmembrane domain was observed. These results show that ARL15 interacts with the cytoplasmic portion of CNNM2 and that the interaction is enhanced by the presence of the complete C-terminal region of the protein.

To determine whether the interaction between ARL15 and CNNMs was dependent on Mg^{2+} or not, ARL15 and CNNM were immunoprecipitated in the presence or absence of Mg^{2+} in the lysis buffer. Results showed that adding 1mM Mg^{2+} in the lysis buffer does not affect the association between ARL15 and CNNM2 compared to the condition of the lysis buffer without Mg^{2+} (Figure 2D). In line with this, the binding between ARL15 and CNNM3 was similar in both conditions (Figure 2E).

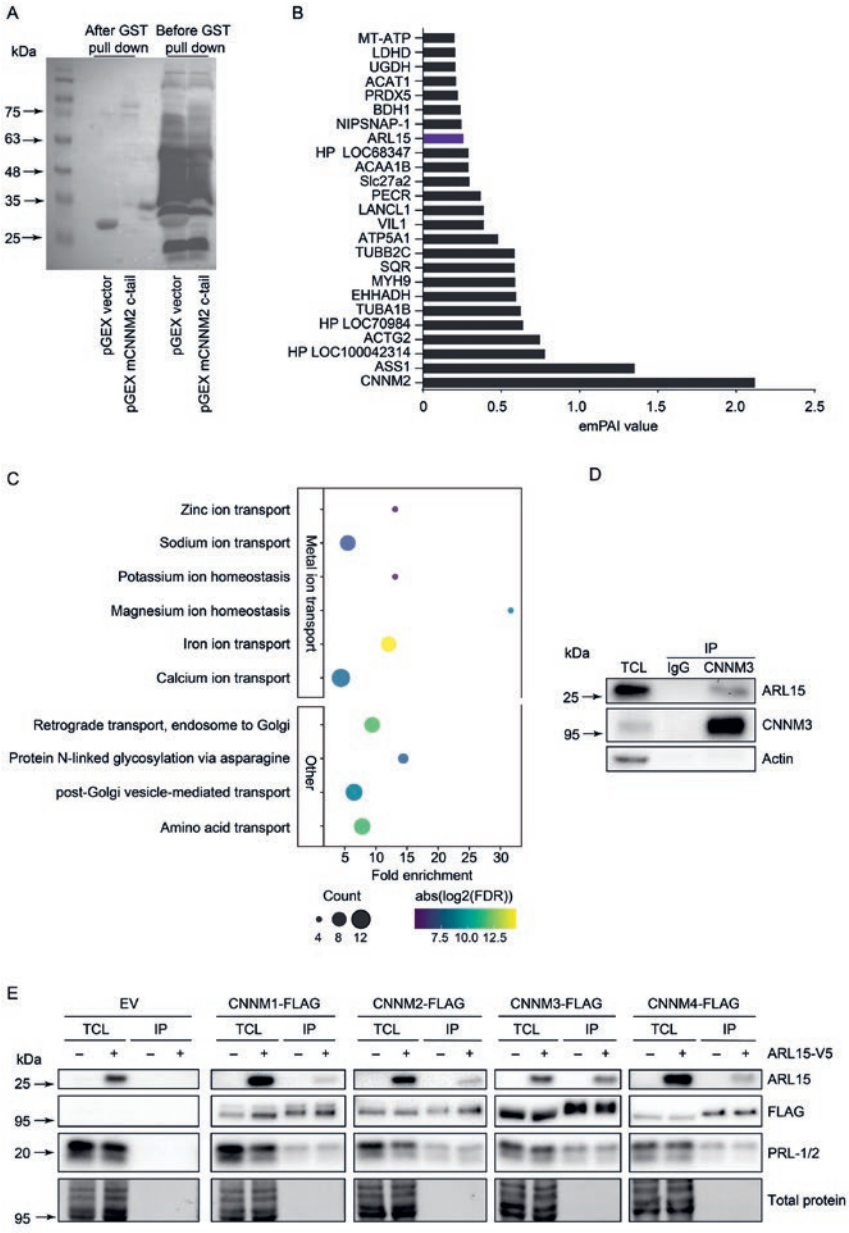

Figure 1. **Part 1**

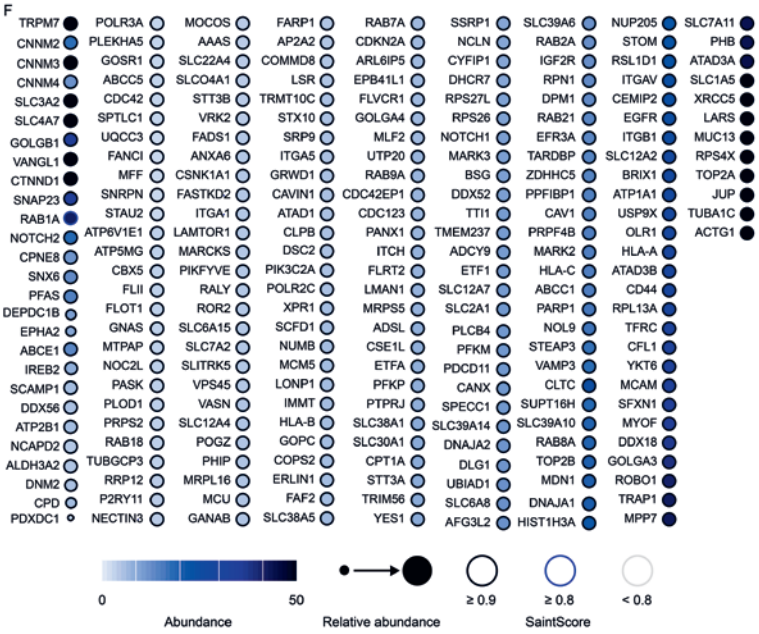

Figure 1. ARL15 interacts with CNNMs

A, Immunoblot of GST-mCNNM2 c-tail pGex and empty pGex was used as control. The C-tail of mCNNM2 is purified and bind to glutathione beads. The DCT enriched fraction from 8 parvalbumin GFP mice were added to the bead. B, List of binding proteins to mCNNM2 C-tail (emPAI value). C, Representative pathways related to metal ion transport and Golgi-trafficking identified using gene ontology biological process overrepresentation analysis with ARL15 interacting partners. D, Endogenous CNNM3 was immunoprecipitated from HEK293 lysates and endogenous ARL15 co-immunoprecipitated with it. IgG antibody of the same subclass as CNNM3 antibody was used as negative control. E, Anti-FLAG beads were used to immunoprecipitate overexpressed FLAG-tagged CNNM1-4 proteins. The blots show that ARL15 interacts with CNNM1-4, as well as endogenous PRL-1 and PRL-2. F, List of ARL15 interacting partners identified through BioID. emPAI, Exponentially modified protein abundance index; TCL, Total cell lysate; IP, Immunoprecipitation; GST, Glutathione-S-transferase; ARL5, ADP ribosylation factor like GTPase 15; CNNM, Cyclin M.

Docking models of the CNNM-ARL15 interaction

To assess the role of the various cytoplasmic CNNM2 cytosolic domains as targets of ARL15, docking computations were carried out. The coordinates of the flexible linker joining the Bateman and CNBH domains were modelled onto the available X-ray diffraction data of the CNNM2 cytosolic domains. Figure 3 displays the domain arrangement of CNNM2 cytosolic domains (Figure 3A) as well as the electrostatic potential on their surface (Figure 3B). Notably, the linkers joining the Bateman domain to the CNBH display a stretch of basic residues. Best score solutions displayed ARL15 interacting with both CNNM2 monomers. ARL15 was partly inserted into the cleft between the Bateman domains and the CNBH domains (Figure 3C-D). In each of the two symmetric solutions, the total buried solvent accessible surface per partner was 2,175.7 Å^2, 1,830.8 Å^2 (932.6 Å^2 from CBS1, 262.3 Å^2 from the linker and 344.9 Å^2 from the CNBH domain) with one of the two CNNM2

monomers and 344.9 $Å^2$ (190.6 $Å^2$ from CBS1* and 154.3 $Å^2$ from CNBH*) for the interaction with the second CNNM2 monomer. Such values are typical of rather stable complexes, and in the upper limit of non-obligate interactions [35]. In addition, the complex displays complementarity of charges at the rim of the interface, as shown in Figure 3D.

As pointed out, the Bateman CBS1 domains contacted with ARL15, in particular that of the first monomer with a surface region defined between α–helix A, the β1-β2 hairpin loop and α-helix H1 in one of them, but also contacting the second monomer. Figure 3C shows the lowest energy solution found in different simulations. Other solutions with low energies corresponded to the hydrophobic surface of H0 helix pair, which interacts with the lipid bilayer, and spots of the CNBH domains in which the absence of coordinates from the nearby unstructured regions disclosed an artifactual interaction site, otherwise concealed. Notably, BD computations (Figure 3 E-G, Table 1) yielded results very similar to those displayed herein. Thus, the interaction model herein is compatible with a 1:1 CNNM2:ARL15 stoichiometry. Other sets of solutions targeted the same region, but displayed different orientations of ARL15 towards CNNM2 surface, and were not found in all simulations. The result in Figure 3, however, was hardly dependent on the modelled conformation of the linker—residues 525 to 546 (Figure 3D). Nevertheless, in most simulations several positive residues of the linker mapped near the interface. As CNNM3 has been reported to bind ARL15 with an affinity higher than that for CNNM2, HEX docking simulations were also performed using a CNNM3 model (Figure 3 E-G). Notably, ARL15 targeted the same site in CNNM3 as does in CNNM2, though the orientation differs by a slight rotation of ARL15.

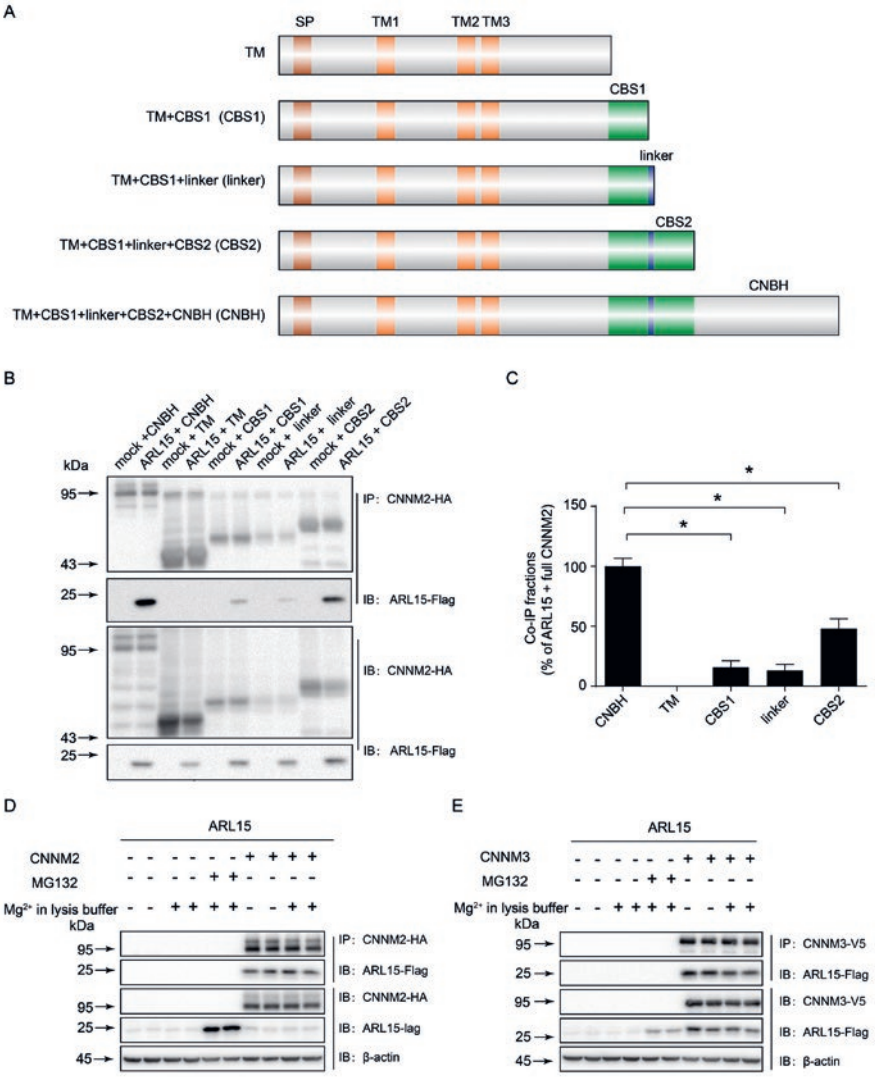

Figure 2. ARL15 interacts with CNNM2 cytoplasmic region.

A, Schematic overview of CNNM2 constructs including the predicted protein domains and truncations. B, HEK293 cells were co-transfected with truncated CNNM2-HA and ARL15-Flag. The upper two blots show the detection of the Flag-tagged proteins in anti-HA precipitated cell lysates. The lower two blots show input controls of HA-tagged and Flag-tagged proteins respectively. C, Quantification of ARL15/CNNM2 binding between the different truncated CNNM2 proteins. Results are the mean ± SEM of 3 independent experiments. * indicate significant differences compared to CNNM2 + ARL15 transfected cells ($P<0.05$). D, Co-immunoprecipitation of HEK293 cells transfected with ARL15-FLAG and HA-CNNM2 treated with or without 1mM Mg^{2+} in lysis buffer. The upper two blots show the detection of the FLAG-tagged proteins in anti-HA precipitated cell lysates. The lower two blots show input controls of HA-tagged and Flag-tagged proteins respectively. E, Co-immunoprecipitation of HEK293 cells transfected with ARL15-FLAG and V5-CNNM3 treated with or without 1mM Mg^{2+} in lysis buffer. The upper two blots show the detection of the FLAG-tagged proteins in anti-V5 precipitated cell lysates. The lower two blots show input controls of V5-tagged and FLAG-tagged proteins respectively. The figure shows a representative blot of 3 independent experiments. SP, Signal peptide; TM, Transmembrane; CBS, Cytosolic cystathionine β-synthase; CNBH, Cyclic nucleotide monophosphate-binding homology; ARL5, ADP ribosylation factor like GTPase 15; CNNM, Cyclin M; TCL, Total cell lysate; IP, Immunoprecipitation; IB, Immunoblotting;

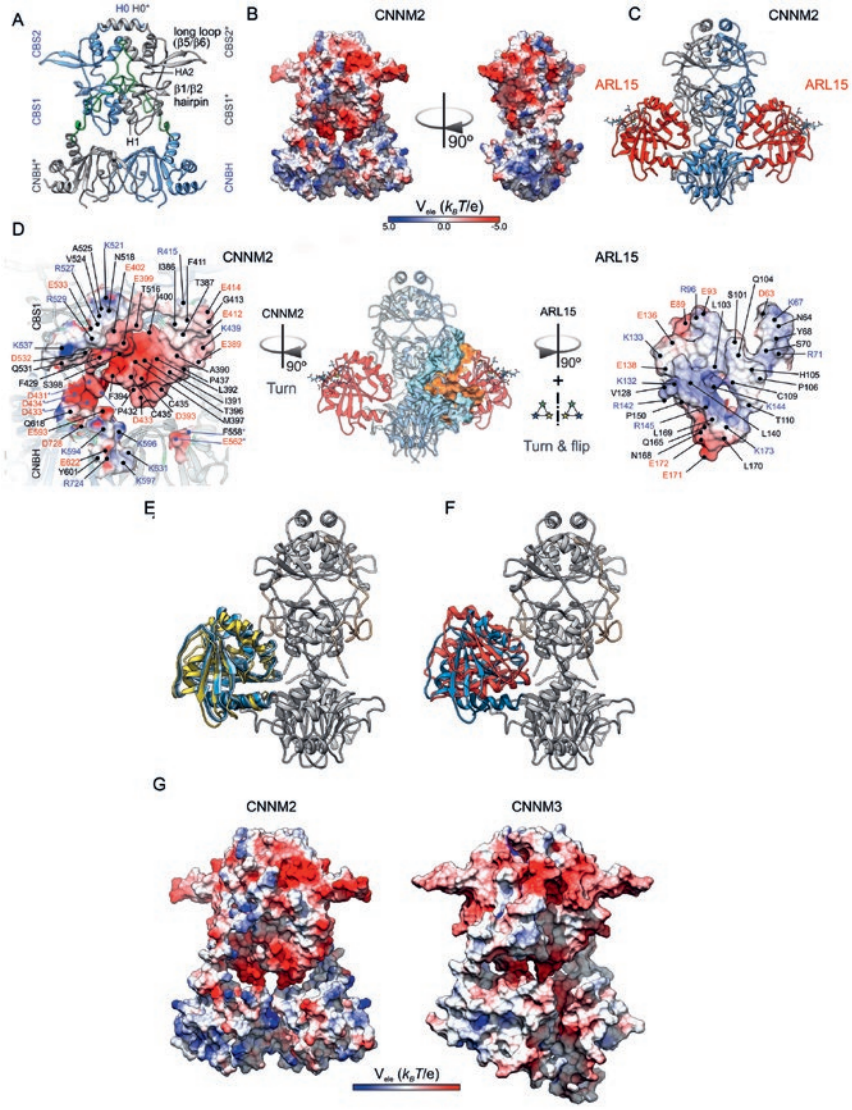

Figure 3. Model of the interaction between the CNNM2 cytosolic domains and ARL15.

A, Richardson (ribbon) diagram of the cytosolic CNNM2 dimer domains. Each monomer is in a different color, and the model of flexible linker joining the Bateman domains to the CNBH ones are in light green. B, Electrostatic potentials at the surface of CNNM2 cytosolic domains. Electrostatic grids were generated with APBS 3.0 [36] at 150 mM ionic strength. C, Best solution of ARL15 (red ribbons) docking to CNNM2 computations. D, Dissection of the interface between ARL15 and CNNM2 (middle) illustrating both the surface and charge complementarity between the two partners. E, Overlay of two solutions (dark and light cyan) from different HEX docking computations with the representative structure of the most populated cluster (yellow) from Brownian dynamics computations. F, Overlay of the results from HEX docking computations between Arl15 and CNNM2 and CNNM3. CNNM3 was aligned to CNNM2—which is shown. The ARL15 bound to CNNM3 is in red ribbons. G, Comparison of CNNM2 and CNNM3 electrostatic potentials at the surface. CBS, Cystathionine β-synthase; CNBH, Cyclic nucleotide monophosphate-binding homology; ARL5, ADP ribosylation factor like GTPase 15; CNNM, Cyclin M.

Table 1: Brownian Dynamics data

No	Size	Repr	ReprE	ClAE	CLAED	ElE	ElDesE	HyDesE	Spread	Stddev	Max
1	61257	141	-25.858	-25.609	0.743	-7.640	3.766	-21.984	28.666	15.109	44.108
2	**63258**	277	**-25.069**	**-26.597**	1.261	**-7.960**	**6.939**	**-24.048**	19.155	7.041	32.403
3	13185	200	-25.504	-26.276	0.600	-4.104	2.758	-24.158	9.718	16.588	46.429
4	32649	363	-24.803	-26.204	1.889	-1.591	4.212	-27.424	17.866	11.585	29.227
5	9200	484	-24.473	-25.335	0.439	-3.661	3.750	-24.562	4.455	8.879	28.354

No, Cluster Number; Size, Number of representative entries for the cluster; Repr, Representative chosen; ReprE, Total interaction energy of the chosen Representative; ClAE, Average total energy of all cluster members weighted with number of representatives; CLAED, Weighted standard deviation of total energy of cluster entries in the complexes (f55) file; Ele, Electrostatic energy of the representative complex; ElDesE, Electrostatic desolvation energy of the representative complex; HyDesE, Hydrophobic desolvation energy of the representative complex; Spread, arithmetic average of rmsd's of each cluster member from the representative, weighted by occupancy; Stddev, Stddev of the rmsd's for a given cluster, weighted by occupancy; Max, Maximum rmsd within one cluster from the representative.

ARL15 and CNNM co-localize in the perinuclear region and in kidney DCTs

The subcellular localization for the ARL15-CNNM complex was determined by immunocytochemistry in HEK293 cells. Overexpression of the mCherry-tagged Golgi-marker Beta-1,4-Galactosyltransferase 1 (B4GALT1) showed co-localization with ARL15 and CNNM2 in HEK293 cells, suggesting that the function of ARL15 is exerted within the perinuclear region containing the endoplasmic reticulum (ER) and the Golgi-apparatus (Figure 4A). Similar results were obtained with ARL15 and CNNM3, confirming that the proteins predominantly co-localize in Golgi (Figure 4B).

Since CNNM2 has been implicated in Mg^{2+} transport in the DCT segment of the kidney [8], we investigated whether ARL15 co-localizes with CNNM2 in this segment of the nephron (Figure 4C). Immunostaining results showed that CNNM2 staining was concomitant with ARL15 staining in mouse kidney sections. One of the ARL15 interacting partners identified using BioID was RPN1 (ribophorin I) (Figure 1F). RPN1 is part of the oligosaccharyltransferase complex that is involved in N-glycosylation and is found in the ER [37]. To confirm the interaction, co-immunoprecipitation assays with overexpressed CNNM3, ARL15, and RPN1 were performed (Figure 4D). CNNM3 interacted with RPN1 and ARL15, corroborating the localization of the three proteins to the ER as well (Figure 4D).

CNNM3 N-glycosylation is modulated by ARL15 and Mg^{2+}

CNNM2 has been previously shown to have an N-glycosylation site close to its amino (N)-terminus [8]. Using NetNGlyc [38], N-glycosylation sites were predicted in CNNM1, CNNM2, CNNM3, and CNNM4. The N-glycosylation site is conserved on their extracellular domain (CNNM1 N97, CNNM2 N112, CNNM3 N73, and CNNM4 N85). To confirm that CNNM3 does indeed have an N-glycosylation site similar to CNNM2, the predicted N73 was mutated to A (N73A mutant). Compared to wild-type CNNM3, the N73A mutant migrated further down the gel, which is indicative for the loss of N-glycosylation (Figure 5A). Endo H and

PNGase F were used to characterize the type of glycans attached to CNNM3 (Figure 5B). When wild-type CNNM3 was treated with Endo H, which cleaves oligomannose glycans, the bottom band of the doublet shifted further. Cleavage with PNGase F shifted all bands of CNNM3 to a lower molecular mass, indicating that the top band represents the hybrid/complex glycoform (Figure 5A).

Since one of the enriched GO biological processes identified in ARL15 BioID was "Protein N-linked glycosylation via asparagine" (Figure 1C), we aimed to assess the effect of ARL15 on CNNM3 N-glycosylation. To this end, four different kidney cancer cell lines were used: Caki-1 and RCC4 as well as ACHN and SK-RC-39, belonging to renal clear cell carcinoma and papillary renal cell carcinoma, respectively. ARL15 was stably overexpressed in these four cell lines and the pattern of endogenous CNNM3 bands was evaluated.

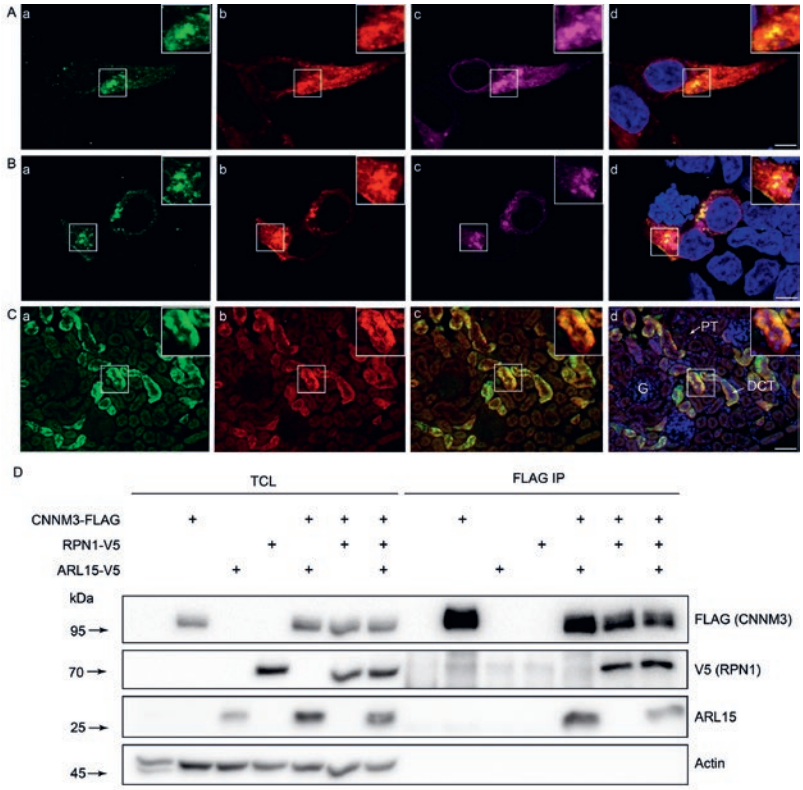

Figure 4. ARL15 and CNNMs co-localize in the Golgi system

A, Immunocytochemistry of HEK293 overexpressing ARL15 (a), CNNM2 (b), and mCherry-tagged Golgi-apparatus marker, B4GALT1 (c). Nuclei are stained with DAPI (d). B, Immunocytochemistry of HEK293 overexpressing ARL15 (a), CNNM3 (b), and mCherry-tagged Golgi-apparatus marker, B4GALT1 (c). Nuclei are stained with DAPI (d). C, Mouse kidneys were permeabilized and co-immunostained with (a) anti-ARL15 (in green) and (b) anti-CNNM2 (in red). (c) Merged picture of ARL15 in green and CNNM2 in red. (d) Merged picture stained for ARL15 in green, CNNM2 in red, and DAPI (nuclei) in blue. Bar in figure A and B represents 5 µm, bar in figure C represents 50 µm. Representative image presented of three independent experiments with triplicates. G, Glomerulus, PT, Proximal tubule, DCT, Distal convoluted tubule. D, CNNM3 was immunoprecipitated from HeLa lysate with overexpression of ARL15-V5 and RPN1-V5. TCL, Total cell lysate; IP, Immunoprecipitation; ARL5, ADP ribosylation factor like GTPase 15; CNNM, Cyclin M; RPN1, Ribophorin I.

In all four cell lines, overexpression of ARL15 resulted in the increase of hybrid/complex glycoform and a decrease in oligomannose glycoform of CNNM3 (Figure 5C). Using SK-RC-39 cells, an interplay between ARL15 expression and Mg^{2+} concentration in the growth media was observed (Figure 5D). Lack of Mg^{2+} resulted in an increase of oligomannose CNNM3 glycoform. Additionally, CRISPR knockout of ARL15 led to a decrease of complex glycoform of CNNM3 as can be seen in the last two lanes (Figure 5D).

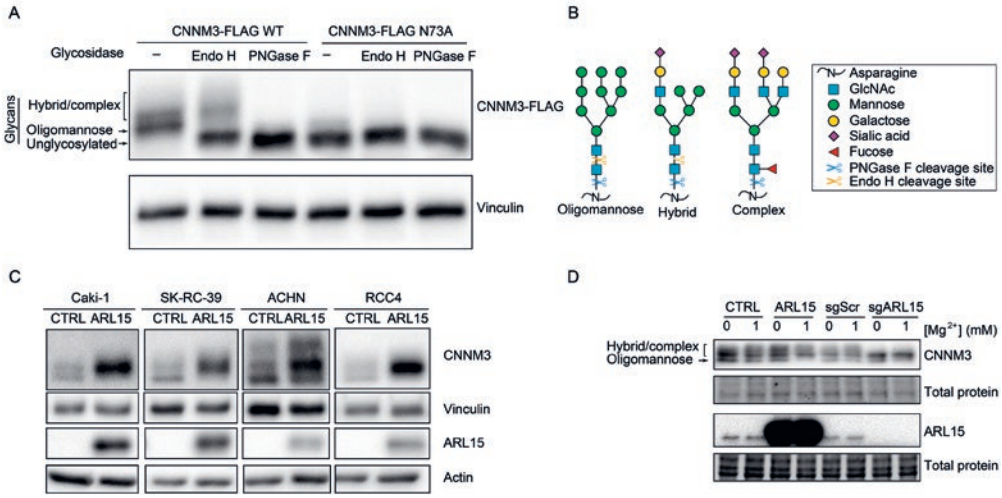

Figure 5. CNNM3 N-glycosylation is modulated by ARL15 and Mg^{2+}.

A, Wild-type and N-glycosylation mutant CNNM3 were treated with PNGase F and Endo H glycosidases to assess the presence of different glycoforms of CNNM3 and to confirm N73 as the site of glycosylation. B, Schematic representation of different types of glycans. C, Overexpression of ARL15 increases complex CNNM3 N-glycosylation in kidney cancer cells. D, SK-RC-39 cells were grown in the presence or absence of Mg^{2+} in the media and the status of CNNM3 glycoforms was assessed using Western blotting. CTRL, Control; sg, Single guide; Scr, Sccramble; ARL5, ADP ribosylation factor like GTPase 15; CNNM, Cyclin M; PNGase F, N-glycosidase F; Endo H, Endoglycosidase H.

ARL15 affect Mg^{2+} flux and ATP production

To study whether ARL15 regulates CNNM-dependent Mg^{2+} transport, its effect on Mg^{2+} transport capacity was determined using the stable $^{25}Mg^{2+}$ isotope. Stably transduced kidney cancer cells with overexpression or CRISPR-mediated knockout of ARL15 were used. Overexpression of ARL15 decreased $^{25}Mg^{2+}$ uptake, while ARL15 knockout increased $^{25}Mg^{2+}$ significantly, more than 3-fold in RCC4 and SKRC39 cells (Figure 6A).

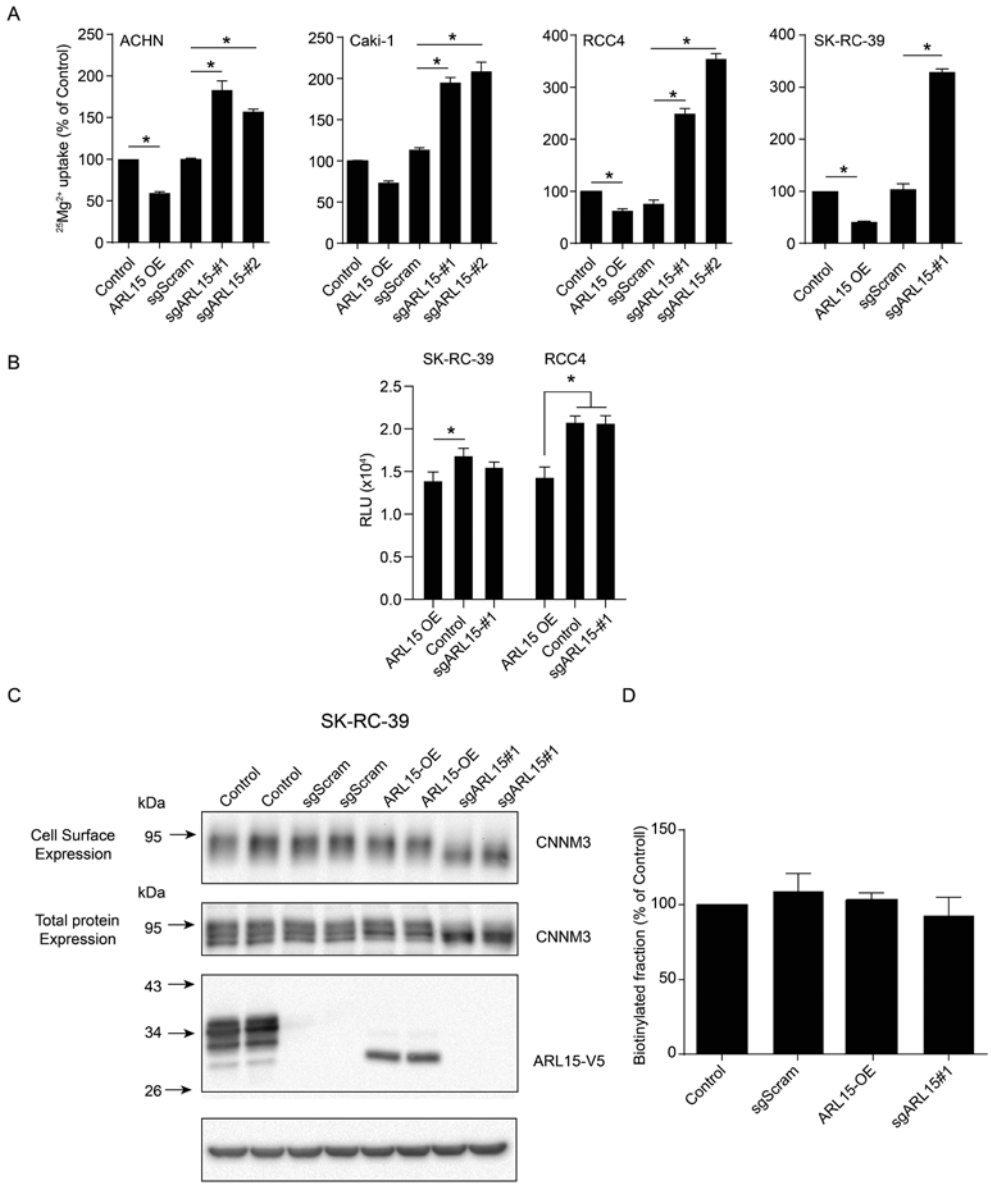

Figure 6. ARL15 affects Mg^{2+} flux and ATP production.

A, $^{25}Mg^{2+}$ uptake measurements in ARL15 stably overexpressed and knockdown ACHN, Caki-1, RCC4, and SK-RC-39 cells. These various types of renal carcinoma cell lines were incubated with $^{25}Mg^{2+}$ for 15 minutes and results were normalized to 0 minute. Each data represents the mean of 3 independent experiments ± SEM. * indicates significant difference compared to control cells. B, ATP production in ARL15 stably overexpressed and knockdown SK-RC-39 and RCC4 cells. Results are the mean ± SEM of 3 independent experiments. C, Endogenous cell surface expression of CNNM3 was detected in SK-RC-39 cells by biotinylation. The upper immunoblots show CNNM3 cell membrane expression and the lower blot shows the total CNNM3 expression. D, The diagram shows the quantification of cell surface CNNM3 expression corrected for total CNNM3 protein expression. Results are the mean ± SEM of 3 independent experiments. sg, Single guide; Scr, Scramble; OE, Overexpression; ARL5, ADP ribosylation factor like GTPase 15; CNNM, Cyclin M.

Since multiple enzymes involved in ATP production by using Mg^{2+} as a cofactor and ATP is bound to intracellular Mg^{2+} to form Mg-ATP [1], we decided to assess the impact of Mg^{2+} influx on ATP production. In RCC4 and SK-RC-39 cells, overexpressing ARL15 resulted in a significant decrease in ATP production (Figure 6B).

Endogenous cell surface expression of CNNM3 was detected in SK-RC-39 cells with overexpression or CRISPR-mediated knockout of ARL15. The complex N-glycosylated CNNM3 glycoform runs at approximately 95kDa, oligomannose glycoform of CNNM3 runs at around 90kDa. Results demonstrated that plasma membrane expression of CNNM3 was not altered in the presence or absence of ARL15 (Figure 6C and 6D). However, the oligomannose CNNM3 glycoform was observed at the plasma membrane in the ARL15 knockout, compared to the ARL15 scramble group.

Discussion

In this study, we identified ARL15 as a novel interacting partner of CNNMs. ARL15 binds to CNNMs in the ER and regulates their complex N-glycosylation in the Golgi system (Figure 7). Our data suggest that the complex N-glycosylation of CNNMs reduces their activity at the plasma membrane, as reflected in a reduced $^{25}Mg^{2+}$ uptake in renal carcinoma cells. As such, ARL15 may affect cellular Mg^{2+} homeostasis and energy metabolism.

ARL15 is a member of the superfamily of ARF-like (ARL) proteins, which have been functionally characterized as small GTPases. Although ARL15 has been relatively scarcely studied to date, many studies have demonstrated that other ARL and ARF proteins are involved in vesicle trafficking [39]. Our immunocytochemistry results in HEK293 cells demonstrated that ARL15 is predominantly localized in the Golgi system (Figure 4), which is in line with previous reports of ARL15 in 3T3-L1 pre-adipocytes [40]. Moreover, proximity labeling of ARL15 identified many Golgi-specific proteins (Figure 1F).

However, the localization with RPN1, a protein of the oligosaccharyltransferase complex, suggests that the interaction between ARL15 and CNNMs is already formed in the ER. Indeed, several ARF (-like) proteins, e.g. ARF1 and ARF3, have been shown to regulate ER-to-Golgi trafficking [41].

The main finding of our study is that ARL15 binds CNNMs and modulates their activity via N-glycosylation. Biosynthesis of glycoproteins commences in the ER, where a pre-assembled oligosaccharide is bound onto the nascent protein by oligosaccharyltransferases. After passing the ER, a series of reactions further assemble the glycan in the medial-Golgi and maturation takes place in the trans-Golgi. Three different types of N-glycans are commonly present on proteins; oligomannose, hybrid and complex N-glycans. Our results demonstrate that ARL15 stimulates the formation of complex N-glycans on CNNMs. Although ARL15 does not possess the enzymatic capacity to change the glycosylation *per se*, we have identified several proteins of the oligosaccharyltransferase

complex in our BioID experiments (e.g. DPM1, RPN1, LMAN1, STT3A and STT3B) (Figure 1F). Moreover, protein N-glycosylation was among the enriched GO-terms in our analysis. We hypothesize that trans-Golgi trafficking via ARL15 is an essential step in the complex glycosylation of CNNMs. A similar mechanism has been postulated for ADP-ribosylation factor guanine nucleotide-exchange factor 1 (ARFGEF1), which regulates the N-glycosylation and trafficking of integrins [42].

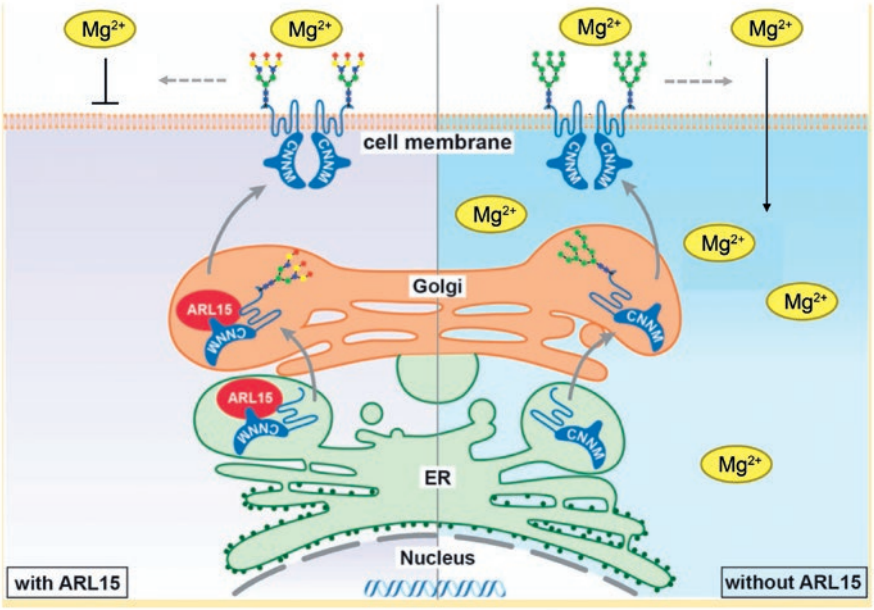

Figure 7. Summary of the effect of ARL15•CNNM complex on Mg^{2+} flux.

In the presence of ARL15, it interacts with CNNMs in the ER and Golgi, resulting in the complex N-glycosylation of CNNMs, which in turn decreases Mg^{2+} uptake. In the absence of ARL15, CNNMs are found in less complex glycoforms, which result in increased Mg^{2+} uptake. ER, Endoplasmic reticulum; ARL5, ADP ribosylation factor like GTPase 15; CNNM, Cyclin M.

The N-glycosylation of CNNMs is essential for their plasma membrane expression. CNNMs contain a single N-glycosylation site in the extracellular N-terminal region [8]. Mutation of the N73 residue to A in CNNM3 completely abrogated its membrane expression (Figure 5A). Similar results were previously obtained for N112 residue in CNNM2 [8]. In this study, we demonstrated that not only the presence of, but also the composition of the glycan is essential for the protein function. ARL15 overexpression resulted in a complex-glycosylation of CNNM3, which was accompanied by a significant reduction of $^{25}Mg^{2+}$ uptake. *Vice versa*, ARL15 downregulation resulted in a high-mannose glycan and increased $^{25}Mg^{2+}$ uptake. Altogether, we propose a model in which the composition of the N-glycan affects CNNM activity.

Multiple roles for N-glycosylation of plasma membrane proteins have been described, ranging from effects on membrane trafficking, membrane stability and protein degradation [43, 44]. In our experiments, neither ARL15 overexpression nor ARL15 downregulation affected the plasma membrane expression of CNNM3 (Figure 6C), suggesting that membrane trafficking of CNNM3 is not affected by ARL15. Consequently, changes in N-glycosylation may directly affect the activity of CNNM3 at the plasma membrane. It has been extensively described that N-glycans interact with glycan-binding proteins in the extracellular spaces, such as lectins. Lectin-glycan interactions are involved in many biological cellular processes such as apoptosis, differentiation as well as regulation of membrane transport [45]. Indeed, binding of lectins and other glycan-binding proteins has been shown to regulate TRPV5-mediated Ca^{2+} transport [46, 47]. Whether the binding of lectins explains the changes in CNNM3 activity remains to be defined.

The interaction model that we developed is compatible with a 1:1 CNNM2:ARL15 stoichiometry. ARL15 interacts with the Bateman CBS1 domains, in particular with a surface region defined between α–helix A, the β1-β2 hairpin loop and α-helix H1. Indeed, co-immunoprecipitation experiments confirmed that the CBS domains are essential for ARL15 binding (Figure 2B). Overall, the interaction surface is small (355 Å, *ca* 700 Å of surface burial) and presents a core of hydrophobic and polar residues surrounded by charged ones. Interestingly, the positive-charged residues present in the CNNM2 docking site is complementarity to the negative-charged surface of ARL15 (Figure 3). Notably, no overlap is observed between the binding site of ARL15 and PRL, which mostly binds CBS2 by its long loop region comprising β5 and β6 [26].

The identification of ARL15 as a novel regulator of CNNM activity is of particular interest in the DCT segment of the kidney. In the DCT, transient receptor potential cation channel subfamily M member 6 (TRPM6) facilitates apical Mg^{2+} transport [48]. Basolateral Mg^{2+} extrusion in the DCT is regulated by CNNM2. Consequently, mutations in *CNNM2* and *TRPM6* have been shown to cause renal Mg^{2+} wasting in patients [14, 49, 50]. Interestingly, the ARL15 locus was recently associated with urinary Mg^{2+} wasting in a GWAS [15]. In the same study, TRPM6 channel activity was shown to be significantly increased in the presence of ARL15 [15]. Our results demonstrate that ARL15 also binds CNNM2, suggesting that both the apical and basolateral Mg^{2+} transport mechanisms are simultaneously regulated. These findings explain how ARL15 determined urinary Mg^{2+} excretion.

Interestingly, overexpression of ARL15 resulted in decreased ATP levels (Figure 6B). Intracellular Mg^{2+} and ATP are closely associated, as ATP must be bound to this cation to be biologically active [1]. Indeed, previous experiments have shown that PRL2 knockdown decreased intracellular Mg^{2+} levels, reduced intracellular ATP levels and regulated cellular metabolism [4]. Given that ARL15 overexpression reduced CNNM-mediated Mg^{2+} uptake, the expression of ARL15 may indirectly regulate cellular metabolism. Indeed, ARL15 has been associated with a wide range of metabolic parameters and diseases

in GWAS, including adiponectin, high-density lipoprotein, diabetes mellitus and body shape [51-56]. As these studies did not analyze Mg^{2+} status as a modifying factor, it cannot be excluded that ARL15 has additional functions that explain these associations. Indeed, ARL15 has been demonstrated to modify the insulin-signaling pathway in myotubes [57].

Overall, our work establishes complex N-glycosylation of CNNMs as an essential process to regulate their activity. This crucial post-translational modification promoted by ARL15 on CNNMs adds to recent mechanisms of CNNMs modulation such as their circadian rhythm expression and their regulation by Mg^{2+}-sensitive translation [4, 58]. The increasing complexity of CNNMs regulation provides a dynamic system to ensure the correct levels of intracellular Mg^{2+} during metabolic changes and cell requirements.

Acknowledgements

We thank Caro Bos, Milou Smits and Shirin Mostert for excellent technical support. This work was financially supported by grants from the European Joint Program for Rare Diseases (EJPRD2019-40), the Netherlands Organization for Scientific Research (NWO Veni 016.186.012. Vici 016.130.668), the Dutch Diabetes Research Foundation (2017.81.014), the Ministry of Science and Innovation (PGC2018-096049-B-I00), European Regional Development Fund (FEDER), and the Andalusian Government (BIO-198, US-1254317 and US-1257019).

References

1. de Baaij, J.H., J.G. Hoenderop, and R.J. Bindels, *Magnesium in man: implications for health and disease.* Physiol Rev, 2015. **95**(1): p. 1-46.
2. Jahnen-Dechent, W. and M. Ketteler, *Magnesium basics.* Clin Kidney J, 2012. **5**(Suppl 1): p. i3-i14.
3. Ryazanova, L.V., et al., *TRPM7 is essential for Mg(2+) homeostasis in mammals.* Nat Commun, 2010. **1**: p. 109.
4. Hardy, S., et al., *Magnesium-sensitive upstream ORF controls PRL phosphatase expression to mediate energy metabolism.* Proc Natl Acad Sci U S A, 2019. **116**(8): p. 2925-2934.
5. Gimenez-Mascarell, P., et al., *Current Structural Knowledge on the CNNM Family of Magnesium Transport Mediators.* Int J Mol Sci, 2019. **20**(5).
6. Yoshida, A., Y. Funato, and H. Miki, *Phosphatase of regenerating liver maintains cellular magnesium homeostasis.* Biochem J, 2018. **475**(6): p. 1129-1139.
7. Gulerez, I., et al., *Phosphocysteine in the PRL-CNNM pathway mediates magnesium homeostasis.* EMBO Rep, 2016. **17**(12): p. 1890-1900.
8. de Baaij, J.H., et al., *Membrane topology and intracellular processing of cyclin M2 (CNNM2).* J Biol Chem, 2012. **287**(17): p. 13644-55.
9. Hardy, S., et al., *Physiological and oncogenic roles of the PRL phosphatases.* FEBS J, 2018. **285**(21): p. 3886-3908.
10. Hardy, S., et al., *The protein tyrosine phosphatase PRL-2 interacts with the magnesium transporter CNNM3 to promote oncogenesis.* Oncogene, 2015. **34**(8): p. 986-95.
11. Funato, Y., et al., *Membrane protein CNNM4-dependent Mg2+ efflux suppresses tumor progression.* J Clin Invest, 2014. **124**(12): p. 5398-410.
12. Funato, Y., et al., *CrossTalk proposal: CNNM proteins are Na(+) /Mg(2+) exchangers playing a central role in transepithelial Mg(2+) (re)absorption.* J Physiol, 2018. **596**(5): p. 743-746.
13. Arjona, F.J. and J.H.F. de Baaij, *CrossTalk opposing view: CNNM proteins are not Na(+) /Mg(2+) exchangers but Mg(2+) transport regulators playing a central role in transepithelial Mg(2+) (re) absorption.* J Physiol, 2018. **596**(5): p. 747-750.
14. Arjona, F.J., et al., *CNNM2 mutations cause impaired brain development and seizures in patients with hypomagnesemia.* PLoS Genet, 2014. **10**(4): p. e1004267.
15. Corre, T., et al., *Genome-Wide Meta-Analysis Unravels Interactions between Magnesium Homeostasis and Metabolic Phenotypes.* J Am Soc Nephrol, 2018. **29**(1): p. 335-348.
16. Downward, J., *The ras superfamily of small GTP-binding proteins.* Trends Biochem Sci, 1990. **15**(12): p. 469-72.
17. Newman, C.M. and A.I. Magee, *Posttranslational processing of the ras superfamily of small GTP-binding proteins.* Biochim Biophys Acta, 1993. **1155**(1): p. 79-96.
18. Bagci, H., et al., *Mapping the proximity interaction network of the Rho-family GTPases reveals signalling pathways and regulatory mechanisms.* Nat Cell Biol, 2020. **22**(1): p. 120-134.
19. Knight, J.D.R., et al., *ProHits-viz: a suite of web tools for visualizing interaction proteomics data.* Nat Methods, 2017. **14**(7): p. 645-646.
20. Mi, H., et al., *Protocol Update for large-scale genome and gene function analysis with the PANTHER classification system (v.14.0).* Nat Protoc, 2019. **14**(3): p. 703-721.
21. Eswar, N., et al., *Protein structure modeling with MODELLER.* Methods Mol Biol, 2008. **426**: p. 145-59.
22. Pettersen, E.F., et al., *UCSF Chimera--a visualization system for exploratory research and analysis.* J Comput Chem, 2004. **25**(13): p. 1605-12.
23. Shen, M.Y. and A. Sali, *Statistical potential for assessment and prediction of protein structures.* Protein Sci, 2006. **15**(11): p. 2507-24.
24. Maier, J.A., et al., *ff14SB: Improving the Accuracy of Protein Side Chain and Backbone Parameters from ff99SB.* J Chem Theory Comput, 2015. **11**(8): p. 3696-713.
25. Emsley, P., et al., *Features and development of Coot.* Acta Crystallogr D Biol Crystallogr, 2010. **66**(Pt 4): p. 486-501.

26. Gimenez-Mascarell, P., et al., *Structural Basis of the Oncogenic Interaction of Phosphatase PRL-1 with the Magnesium Transporter CNNM2.* J Biol Chem, 2017. **292**(3): p. 786-801.
27. Ritchie, D.W. and G.J. Kemp, *Protein docking using spherical polar Fourier correlations.* Proteins, 2000. **39**(2): p. 178-94.
28. Chuang, G.Y., et al., *DARS (Decoys As the Reference State) potentials for protein-protein docking.* Biophys J, 2008. **95**(9): p. 4217-27.
29. Yu, X., et al., *webSDA: a web server to simulate macromolecular diffusional association.* Nucleic Acids Res, 2015. **43**(W1): p. W220-4.
30. Elcock, A.H., et al., *Computer simulation of protein-protein association kinetics: acetylcholinesterase-fasciculin.* J Mol Biol, 1999. **291**(1): p. 149-62.
31. Gabdoulline, R.R. and R.C. Wade, *On the contributions of diffusion and thermal activation to electron transfer between Phormidium laminosum plastocyanin and cytochrome f: Brownian dynamics simulations with explicit modeling of nonpolar desolvation interactions and electron transfer events.* J Am Chem Soc, 2009. **131**(26): p. 9230-8.
32. Dolinsky, T.J., et al., *PDB2PQR: an automated pipeline for the setup of Poisson-Boltzmann electrostatics calculations.* Nucleic Acids Res, 2004. **32**(Web Server issue): p. W665-7.
33. Schneider, C.A., W.S. Rasband, and K.W. Eliceiri, *NIH Image to ImageJ: 25 years of image analysis.* Nat Methods, 2012. **9**(7): p. 671-5.
34. Konermann, S., et al., *Genome-scale transcriptional activation by an engineered CRISPR-Cas9 complex.* Nature, 2015. **517**(7536): p. 583-8.
35. Nooren, I.M. and J.M. Thornton, *Diversity of protein-protein interactions.* EMBO J, 2003. **22**(14): p. 3486-92.
36. Baker, N.A., et al., *Electrostatics of nanosystems: application to microtubules and the ribosome.* Proc Natl Acad Sci U S A, 2001. **98**(18): p. 10037-41.
37. Harada, Y., et al., *Oligosaccharyltransferase: A Gatekeeper of Health and Tumor Progression.* Int J Mol Sci, 2019. **20**(23).
38. Gupta R, e.a., *Prediction of N-glycosylation sites in human proteins.* 2004.
39. Donaldson, J.G. and C.L. Jackson, *ARF family G proteins and their regulators: roles in membrane transport, development and disease.* Nat Rev Mol Cell Biol, 2011. **12**(6): p. 362-75.
40. Rocha, N., et al., *The metabolic syndrome- associated small G protein ARL15 plays a role in adipocyte differentiation and adiponectin secretion.* Sci Rep, 2017. **7**(1): p. 17593.
41. Ben-Tekaya, H., R.A. Kahn, and H.P. Hauri, *ADP ribosylation factors 1 and 4 and group VIA phospholipase A(2) regulate morphology and intraorganellar traffic in the endoplasmic reticulum-Golgi intermediate compartment.* Mol Biol Cell, 2010. **21**(23): p. 4130-40.
42. Shen, X., et al., *BIG1, a brefeldin A-inhibited guanine nucleotide-exchange protein, is required for correct glycosylation and function of integrin beta1.* Proc Natl Acad Sci U S A, 2007. **104**(4): p. 1230-5.
43. Cohen, D.M., *Regulation of TRP channels by N-linked glycosylation.* Semin Cell Dev Biol, 2006. **17**(6): p. 630-7.
44. Dennis, J.W., et al., *Adaptive regulation at the cell surface by N-glycosylation.* Traffic, 2009. **10**(11): p. 1569-78.
45. Gabius, H.J. and K. Kayser, *Introduction to glycopathology: the concept, the tools and the perspectives.* Diagn Pathol, 2014. **9**: p. 4.
46. Leunissen, E.H., et al., *The epithelial calcium channel TRPV5 is regulated differentially by klotho and sialidase.* J Biol Chem, 2013. **288**(41): p. 29238-46.
47. Chang, Q., et al., *The beta-glucuronidase klotho hydrolyzes and activates the TRPV5 channel.* Science, 2005. **310**(5747): p. 490-3.
48. Voets, T., et al., *TRPM6 forms the Mg2+ influx channel involved in intestinal and renal Mg2+ absorption.* J Biol Chem, 2004. **279**(1): p. 19-25.
49. Stuiver, M., et al., *CNNM2, encoding a basolateral protein required for renal Mg2+ handling, is mutated in dominant hypomagnesemia.* Am J Hum Genet, 2011. **88**(3): p. 333-43.
50. Chery, M., et al., *Hypomagnesemia with secondary hypocalcemia in a female with balanced X;9 translocation: mapping of the Xp22 chromosome breakpoint.* Hum Genet, 1994. **93**(5): p. 587-91.

51. Richards, J.B., et al., *A genome-wide association study reveals variants in ARL15 that influence adiponectin levels*. PLoS Genet, 2009. **5**(12): p. e1000768.
52. Teslovich, T.M., et al., *Biological, clinical and population relevance of 95 loci for blood lipids*. Nature, 2010. **466**(7307): p. 707-13.
53. Dastani, Z., et al., *Novel loci for adiponectin levels and their influence on type 2 diabetes and metabolic traits: a multi-ethnic meta-analysis of 45,891 individuals*. PLoS Genet, 2012. **8**(3): p. e1002607.
54. Willer, C.J., et al., *Discovery and refinement of loci associated with lipid levels*. Nat Genet, 2013. **45**(11): p. 1274-1283.
55. Ried, J.S., et al., *A principal component meta-analysis on multiple anthropometric traits identifies novel loci for body shape*. Nat Commun, 2016. **7**: p. 13357.
56. Mahajan, A., et al., *Genome-wide trans-ancestry meta-analysis provides insight into the genetic architecture of type 2 diabetes susceptibility*. Nature Genetics, 2014. **46**(3): p. 234-244.
57. Zhao, J., et al., *ADP-ribosylation factor-like GTPase 15 enhances insulin-induced AKT phosphorylation in the IR/IRS1/AKT pathway by interacting with ASAP2 and regulating PDPK1 activity*. Biochem Biophys Res Commun, 2017. **486**(4): p. 865-871.
58. Uetani, N., et al., *PRL2 links magnesium flux and sex-dependent circadian metabolic rhythms*. JCI Insight, 2017. **2**(13).

6

General discussion

Introduction

Sodium (Na^+), calcium (Ca^{2+}) and magnesium (Mg^{2+}) homeostasis plays a key role in a variety of physiological processes in the human body, such as cellular signal transduction, cell metabolism, bone development, enzymatic activity, neuronal conduction and excitability [1-3]. The final concentration and excretion of these electrolytes in the urine is determined by the kidneys through the reabsorption from the pro-urine into the bloodstream [2]. Paracellular and transcellular transport of electrolytes in the proximal tubule (PT), thick ascending limb of loop of Henle (TAL), distal convoluted tubule (DCT), connecting tubule (CNT), and collecting duct (CD) account for the reabsorption processes [4-6]. In particular, this is facilitated by *i*) cation-selective ion transporters, *ii*) endocrine and paracrine hormones, and *iii*) sensors that are sensitive to intra- or extracellular Na^+, Ca^{2+}, and Mg^{2+} fluctuations [7, 8]. Abnormal regulation of these processes is linked to a variety of diseases such as hypertension, diabetes, kidney stone formation and hypomagnesemia. The purpose of this thesis was to investigate the regulation of Na^+ transporters in the kidney during treatment with sodium-glucose transport protein 2 (SGLT2) inhibitors, to develop Ca^{2+}-binding peptides that may control the urinary Ca^{2+} concentration in hypercalciuria and kidney stone formation, and to study new players involved in renal Mg^{2+} handling.

Na^+ handling in the proximal tubule in diabetes and hypertension

The role of potential Na^+ compensatory mechanisms for SGLT2 inhibitors as cardiovascular protective therapies.

In the last decades, SGLT2 inhibitors have become novel and effective type of anti-hyperglycemic drugs that increase glucosuria and ameliorate glycemic control. In addition to their glucose lowering effect, SGLT2 inhibitors can alleviate blood pressure (BP) by reducing systolic blood pressure (SBP) by 3-5 mmHg [9-11]. While it is likely in part due to associated natriuresis and polyuria, the molecular mechanism behind it is still not well documented. In **Chapter 2,** mice with high fat feeding were administrated the SGLT2 inhibitor dapagliflozin (DAPA) to investigate its effect on renal Na^+ handling. These mice exhibited increased blood glucose levels that were alleviated upon 18-day DAPA treatment. Our results showed that the expression of the sodium-phosphate cotransporter (NaPi-2a) and sodium-hydrogen antiporter 3 (NHE3) is upregulated in the kidneys of DAPA-treated mice.

The influence of SGLT2 inhibitors on the function and expression of NaPi-2a and NHE3 is controversial. In 2018, Blau *et al.* found that the serum phosphorus level is increased in volunteers treated with the SGLT2 inhibitor canagliflozin [12]. This increased level of serum phosphorus was associated with an increased reabsorption of phosphate in the PT [13], which would be in line with the increased expression of NaPi-2a in our study. In contrast to

these findings, Thrailkill *et al.* demonstrated that canagliflozin treated diabetic mice exhibit no altered expression levels of NaPi-2a compared with vehicle treated diabetic mice [14]. The following reasons may explain the difference. First, Thrailkill *et al.* only used streptozotocin (STZ) to induce hyperglycemia [14], while we exposed the mice to a high fat diet prior to STZ administration to induce hyperglycemia. Second, canagliflozin was administrated for 10 weeks to diabetic mice in their study [14], whereas we treated the mice with DAPA for 18 days.

Interestingly, Pessoa *et al.* previously showed that SGLT2 and NHE3 are functionally interdependent [15]. Glucose promotes NHE3-regulated bicarbonate transport in the PT of Wistar rats, which could be inhibited by perfusion with the SGLT inhibitor phlorizin [15]. Immunostaining results showed that NHE3 was co-localized with SGLT2 instead of SGLT1 in the PT [15]. While they performed stationary *in vivo* microperfusion to rat proximal tubules with phlorizin and sugars, and found that phlorizin inhibited NHE3 activity, gene or protein expression levels were not examined [15]. Nevertheless, NHE3 and SGLT2 seem to be directly or indirectly coupled in the PT [15]. In addition, several studies have reported that alterations of renal NHE3 activity and expression are related to BP changes [16-18]. The BP is decreased in *Nhe3* knockout mice compared to their wildtype littermates [16]. Transgenic mice with NHE3 overexpression exhibited elevated BP, together with decreased urinary water and Na^+ excretion [17]. Moreover, the activity and protein levels of NHE3 were found to be significantly increased in spontaneously hypertensive rats compared to Wistar-Kyoto (WKY) rats, which will probably lead to renal Na^+ retention [18]. In line with our results, another study also demonstrated that luseogliflozin treatment increases the protein expression levels of NHE3 in spontaneously hypertensive rats [19]. While there were no plasma or urine Na^+ measurements in our study, it is most likely that increased expression of NHE3 and NaPi-2a functions as compensation for the decreased Na^+ reabsorption by SGLT2, which may lead to Na^+ retention. However, it is still uncertain to which magnitudes the NHE3 and NaPi-2a upregulation influences the urinary Na^+ excretion and urine volume.

Notably, several studies reported that the BP reduction effect of SGLT2 inhibitors always occur in the early phase of the treatment [20, 21]. Indeed, SGLT2 inhibitor-induced natriuresis was observed shortly after the start of the SGLT2 inhibitor treatment in several clinical studies [22-25]. Similarly, canagliflozin has been shown to increase urine volume in type 2 diabetic patients in the beginning of the treatment [24, 26-29]. Though, the diuretic and natriuretic effects of SGLT2 inhibitors seem to be transient [19, 30]. In the beginning of treatment, SGLT2 inhibitors result in natriuresis [31], which will lead to increased distal Na^+ delivery to the macula densa [32, 33]. Then, the decreased hyperfiltration, afferent vasoconstriction, and tubuloglomerular feedback will be triggered, through which the BP is decreased [34-36]. In our study, we found that NHE3 and NaPi-2a expression were upregulated. This will result in the decreased Na^+ delivery to the macula densa, which may inhibit the BP reduction effect of DAPA. In addition, the loss of Na^+ and water will activate the renin-angiotensin-aldosterone system (RAAS) in long term treatment

(Figure 1) [31]. This could explain why SGLT2 inhibitors reduced BP in the early phase of treatment. Therefore, clinical studies can combine SGLT2 inhibitors with RAAS blockade to better decrease BP in type 2 diabetes patients who suffer from hypertension [37, 38]. Weber *et al.* demonstrated that BP was significantly decreased in a combined DAPA and angiotensin-converting enzyme (ACE) inhibitor treated group compared to the placebo and ACE inhibitor treated group [37]. In another study, Kojima and colleagues addressed that combination treatment of luseogliflozin with lisinopril, which is an angiotensin-converting enzyme inhibitor, significantly reduced BP compared to lisinopril alone [38]. The current thought of SGLT2 inhibition on renal Na^+ handling is summarized in Table 1 and 2.

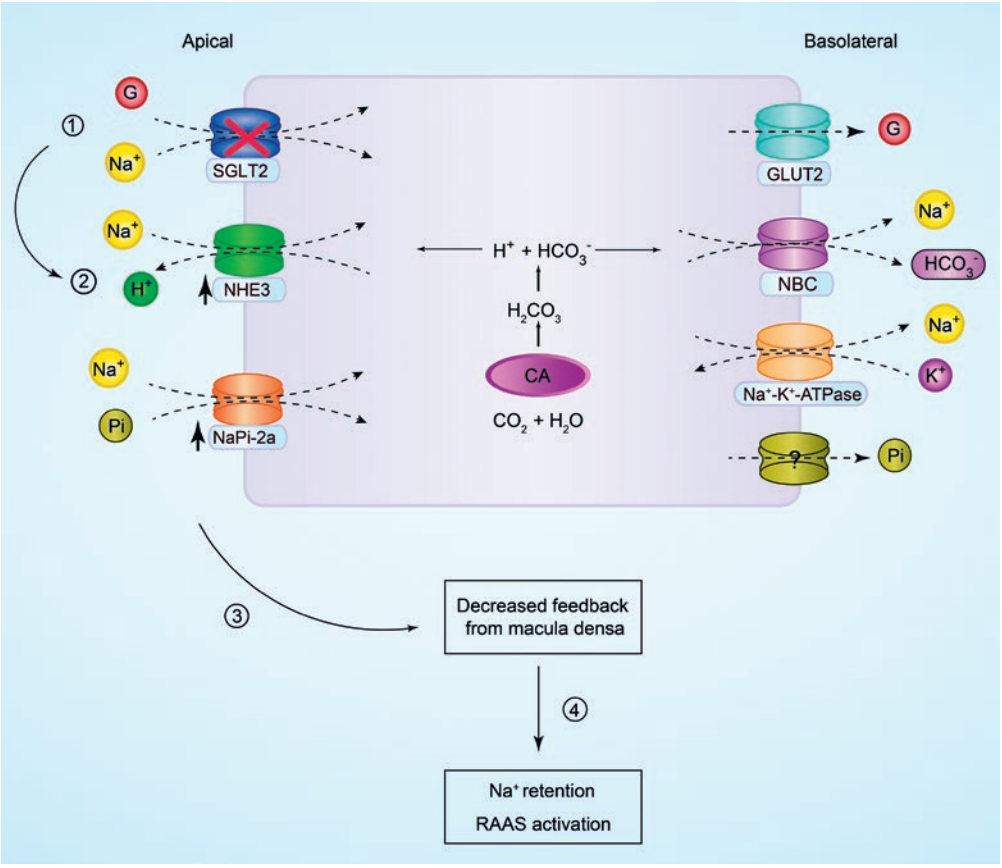

Figure 1. Mechanism of the potential Na^+ compensatory effect in the proximal tubule upon SGLT2 inhibition on the feedback of macula densa.

SGLT2 inhibitor (Dapagliflozin) treatment may lead to reduced Na^+ and glucose reabsorption in the PT (1), which activates the compensatory expression of NHE3 and NaPi-2a in the PT (2). Increased NHE3 and NaPi-2a may partially prevent the Na^+ loss due to SGLT2 inhibition, which results in decreased distal Na^+ delivery to the macula densa and inhibited tubuloglomerular feedback activity (3). Ultimately, this might lead to Na^+ retention, activation of the renin–angiotensin–aldosterone system, and inhibition of the blood pressure reduction effect of dapagliflozin (4). SGLT2, sodium-glucose transport protein 2; G, glucose; NHE3, sodium–hydrogen antiporter 3; NaPi-2a, sodium-coupled phosphate transporter type 2a; GLUT2, glucose transporter 2; NBC, sodium-bicarbonate cotransporter; CA, carbonic anhydrase; RAAS, renin–angiotensin–aldosterone system.

Interestingly, we did not observe changes in the expression of the sodium-potassium-chloride cotransporter (NKCC2), sodium-chloride cotransporter (NCC) and epithelial sodium channel (ENaC) in the TAL, DCT, and CD, respectively. This seems surprising since inhibition of Na^+ reabsorption in the PT is expected to turn on compensatory mechanisms and to activate Na^+ transporters in the more distal parts of the nephron. For example, the expression of NCC is significantly increased in spontaneously hypertensive rats upon 13 weeks of treatment with luseogliflozin [19]. The discrepancy between our studies may due to the fact that DAPA treatment was only 18 days. In response to water loss and reduced Na^+ delivery at the distal tubule in the long term treatment, the expression of Na^+ transporters may increase to compensate for Na^+ loss, and renin release will be increased from the juxtaglomerular cells which can result in the activation of RAAS [39].

Taken together, **Chapter 2** focused on the compensatory expression of Na^+ transporters in the local and downstream segments of the nephron in response to DAPA treatment. In order to better alleviate high BP in type 2 diabetic patients with long-term SGLT2 inhibitor treatment, it is interesting to isolate and analyze exosomes in urine samples to investigate the effect of the treatment with SGLT2 inhibitors on the expression of Na^+ transporters (NKCC2, NCC, and ENaC (α, β, γ)) in the distal part of the nephron. Next, certain inhibitors can be used to block the individual Na^+ transporters that are predominantly (up) regulated in type 2 diabetes patients.

Hypercalciuria in kidney stone disease in Henle's loop

Kidney stone prevention through a novel Ca^{2+}-binding peptide

Kidney stones are mineral and acid salts that are formed in the urinary tract in the kidney [40]. The majority of stones consist of Ca^{2+} oxalate and Ca^{2+} phosphate [41]. Although medical therapy has largely improved kidney stone treatment, the recurrence rate after the first stone formation is still very high [42]. Therefore, we investigated our out-of-the-box idea to develop a potentially better remedy for treatment of kidney stones **in Chapter 3**.

This idea is based on nature's EF-hand motif, which is present in a large number of Ca^{2+}-binding proteins and is involved in intracellular Ca^{2+}-binding [43]. The structure of an EF-hand contains two alpha helices connected by a Ca^{2+}-binding loop of 12 residues (Figure 2B). The Ca^{2+}-binding affinities of various EF hands have been studied in detail, and several variations were made to residues of the Ca^{2+}-binding loop that result in changes in Ca^{2+}-binding affinities [44]. With further optimization, we aimed to generate an EF-hand containing peptide that *i)* exhibits Ca^{2+} binding capacity in the renal supersaturation region (~5-10 mmol/L free Ca^{2+}), namely the limb of Henle's loop, but remains inert in the bloodstream (~1.2 mmol/L free Ca^{2+}); *ii)* is not toxic to cells and has a good biosafety profile for ultimate *in vivo* treatment; and *iii)* exhibits minimal uptake/reabsorption by proximal tubule cells.

Table 1. Current thought on the effect of SGLT2 inhibitors on renal Na^+ handling in animals

Rodent studies						
Animals	**Duration**	**Diet**	**Urine Na^+**	**Urine V**	**SGLTi**	**Ref.**
C57BL/6J mice	16W	HFD	N/A	↑	EMPA	[45]
C57BL/6J mice	14 W	HFD	N/A	↑	CANA	[46]
FLS-ob/ob mice	12W	SD	N/A	↓	IPRA	[47]
$ApoE^{-/-}$ T2D	8 W	WTD	N/A	↓	CANA	[48]
$ApoE^{-/-}$ T2D	12 W	WTD	N/A	↓	CANA	[48]
T1D mice	3 W	No	N/A	↑	IPRA	[49]
STZ-NAM T2D mice	1 D	HFD	N/A	↑	IPRA	[50]
KK/A^y mice	4 W	HFD	N/A	↑	IPRA	[51]
KK/A^y t mice	4W	HFD	N/A	↑	EMPA	[52]
db/db mice	4 W	No	N/A	↑	TOFO	[53]
db/db mice	1 D	No	↑	↑	EMPA	[54]
db/db mice	10 W	No	N/A	↑	EMPA	[55]
T1D rats	70 min	No	↑	↑	Phlorizin	[56]
SD rats	1 D	No	N/A	↑	DAPA	[57]
SD rats	2 h	No	↑	↑	LUSEO	[58]
SHRcp rats	5 W	No	↑	↑	LUSEO	[19]
ZDF rats	1 D	No	N/A	↑	DAPA	[57]
ZDF rats	1 D	No	↑	↑	LUSEO	[59]
OLETF rats	12 h	0.5% NaCl	↑	N/A	EMPA	[60]
OLETF rats	14 W	No	↓	↓	EMPA	[61]
Albino rats	3 D	chow diet	N/A	↑	DAPA	[62]
Wistar rats	6 W	adenine	N/A	N	LUSEO	[63]
WK rats	6 W	adenine	N/A	N	LUSEO	[63]
GK T2DM rats	8 W	CE-2	↓	↑	IPRA	[64]

SGLT2, sodium-glucose cotransporter 2; SGLT2i, SGLT2 inhibitors; T1D, type 1 diabetes; T2D, type 2 diabetes; STZ, streptozotocin; NAM, nicotinamide; FLS-ob/ob mice, fatty liver shionogi-ob/ob mouse; KK/A^y, diabetic KK and lethal yellow (Ay) mice; SD rat, sprague dawley rat; WK, wistar kyoto; GK, goto-kakizaki; SHRcp, metabolic syndrome SHR/NDmcr-cp (+/+); ZDF, zucker diabetic fatty; OLETF, otsuka long-evans tokushima fatty; SD, standard diet; HFD, high fat diet; WTD, western-type diet; N, no change; No, no diet restriction; N/A, not available; IPRA, ipragliflozin; DAPA, dapagliflozin; TOFO, tofogliflozin; LUSEO, luseogliflozin; CANA, canagliflozin; EMPA, empagliflozin; Urine V, urine volume; Ref, reference; min, minutes; h, hour; D, day; W, week; M, month.

Table 2. Current thought on the effect of SGLT2 inhibitors on renal Na^+ handling in patients

Clinical studies						
Patients	**Duration**	**Diet**	**Urine Na^+**	**Urine V**	**SGLTi**	**Ref.**
T2D	12 W	SD	N	↑	DAPA	[20]
T2D	12 W	SD	N/A	↑	DAPA	[65]
T2D	12 W	SRD	↑	↑	CANA	[24]
T2D	1 D	Isocaloric	N/A	↑	CANA	[66]
T2D	2 W	Isocaloric	N/A	N	CANA	[66]
T2D	1 W	SD	N/A	↑	LUSEO	[67]
T2D	4 D	No	↑	↑	IPRA	[68]
T2D	1 D	SD	N	↑	CANA	[25]
T2D	18 D	SD	N	N	CANA	[25]
T2D	1 D	No	↑	↑	CANA	[22]
T2D	5 D	No	N	↑	CANA	[22]
T2D	12 W	SD	N	N	DAPA	[30]
T2D	4 D	SRD	↑	↑	IPRA	[69]
T2D	1 D	No	N	N	DAPA	[70]
T2D	12 W	No	N/A	N	DAPA	[71]
T2D	1 M	No	N	N	TOFO	[72]
T2D	6 M	SD	↑	↑	EMPA	[73]

SGLT2, sodium-glucose cotransporter 2; SGLT2i, SGLT2 inhibitors; T2D, type 2 diabetes; SD, standard diet; SRD, sodium restricted diet; No, no diet restriction; N, no change; N/A, not available; IPRA, ipragliflozin; DAPA, dapagliflozin; TOFO, tofogliflozin; LUSEO, luseogliflozin; CANA, canagliflozin; EMPA, empagliflozin; Urine V, urine volume; Ref, reference; D, day; W, week; M, month.

As such, several small Ca^{2+}-binding peptides (around 20-30 residues) were developed in our study. One peptide, Ac-DKNGDGYIDAAE-NH_2, demonstrated a dose-dependent binding affinity to Ca^{2+} in the millimolar range. This peptide was developed based on the study of Reid *et al.* [74]. These authors developed an amino acid sequence (α-helix-DKNGDGYISAAE-α-helix) which has a micromolar range Ca^{2+}-binding affinity (Kd=58.8 μmol/L) [74]. By using the Ca^{2+}- binding loop (DKNGDGYISAAE) of their amino acid sequence as a template, we changed the amino acid at position 9 from S to D. Hereby, our data is in line with earlier studies showing that acidic residues paired on the x axes in the chelating positions of the loop (in bold in our peptide sequence: **D**KNGDGYI**D**AAE, Figure 2B), together with charged D on the z position are important for determining Ca^{2+}-binding affinity [74, 75]. In comparison with the study of Reid *et al.* [74], the Ca^{2+}-binding affinity of our peptide is decreased. This could be explained by the fact that the peptide in our study is shorter than the Ca^{2+}-binding peptide developed by Reid *et al* [74]. A similar observation has been documented on peptides from EF-hand proteins, showing that absence of the flanking helices reduced Ca^{2+}-binding affinity [76].

Although, the peptide-based treatment has become a promising therapeutic method [77], the potential peptide toxicity remains a bottleneck in the development of peptide-based remedies [78]. Therefore, we tested the toxicity of the designed peptide and demonstrated that cell viability was not affected by this peptide (Ac-DKNGDGYIDAAE-NH_2) in human kidney-2 (HK-2) proximal tubular cells. By calculating and comparing the composition of the amino acid sequence in toxic and non-toxic peptides, Gupta *et al.* demonstrated that the average amino acid composition in toxic peptides contains C in the highest amount, followed by N and P [79]. The average amino acid composition of I, K, L, and R in the toxic peptides are very low [79]. The residues C and P are not present in the peptide we selected. Although residue N is present, it is close to the amino-terminus of the peptide. Gupta *et al.* found that N is frequently present in the carboxyl-terminus of toxic peptides [79]. Interestingly, by counting the cumulative difference between the average amino acid composition of preferred residues in the toxic and non-toxic peptides, A, I, V, and F were shown to be ample in non-toxic peptides [79]. Likewise, A and I are present in the peptide we selected. Together, these suggest that the peptide likely has a good safety profile in terms of toxicity. But success of a peptide in a therapeutic setting depends on many other factors including stabilization, aggregation behavior, circulation time, renal clearance, immunogenicity, which need to be experimentally determined.

Due to the small size, the peptide is expected to be freely filtered. However, it should overcome uptake by proximal tubular cells in order to reach the site of action, the limb of Henle's loop. In our study, we found that the selected peptide exhibited mild cellular uptake in HK-2 cells. In the PT, low molecular weight proteins or peptides can be taken up through multiligand receptors [80-82] or apical endocytic pathway [83]. Vegt and colleagues injected radiolabelled peptides in megalin-deficient mice and addressed that a significantly lower amount of peptide was taken up in the kidneys of megalin-deficient mice compared to wildtype mice [84]. This suggests that megalin plays an important role in the renal peptide reabsorption [84]. HK-2 cells are commonly used since the cellular parameters are rather similar to the physiology of renal proximal tubular cells [85]. Therefore, the peptide uptake in the HK-2 cells provides insight that the peptide we designed may also be taken up by the PT in mice or humans. Though, it has to be considered that the observed dose-dependent uptake of the Ca^{2+}-binding peptide might also be caused by force-feeding cells with high amounts of the peptide. It was significantly less in comparison to a control cell-penetrating peptide that has been reported be taken up through endocytosis [86] or direct translocation [87, 88]. Importantly, Vegt *et al.* demonstrated presence of radiolabelled peptides in the urine of wildtype mice, yet at lower amounts than the megalin-deficient mice. And radioactivity did not differ significantly in the bloodstream and most other organs, except for the kidney between these mice [84]. This study provides evidence that peptides can reach the limb of Henle's loop. Hence, future *in vivo* studies should assess renal clearance in addition to the tissue distribution, immunogenicity, and efficacy of this peptide in animals.

For such future studies, it is crucial to establish a mouse model with kidney stone disease. **Chapter 3** described a first approach by treating healthy male C57BL/6J mice with 1% (v/v) ethylene glycol (EG) via drinking water for 28 days. While EG is known to induce Ca^{2+} deposits in animals [89], these were not present in the mice from our study. This could be due to the fact that hypercalciuria was not induced in high Ca^{2+} diet treated mice, the urinary pH was similar between the normal Ca^{2+} and high Ca^{2+} diet treated groups, or that C57BL/6J mice had the capacity to prevent stone formation in the kidney [90]. Notably, Ca^{2+} deposits were present in Swiss albino mice administrated with 0.75% (v/v) EG in the drinking water for 28 days [91]. A difference in genetic background may explain the discrepancy. Additionally, Okada and co-workers successfully induced Ca^{2+} oxalate crystal deposits in C57BL/6J mice by injecting glyoxylate intra-abdominally [90]. Generating transgenic mouse is another tool to induce kidney stones *in vivo*. In 2004, Wesson and colleagues showed that EG in the drinking water of Tamm-Horsfall protein (THP) knockout mice results in Ca^{2+} deposits in the kidneys, and not in the kidneys of wildtype mice [92]. Finally, rats could also be considered for our future study as kidney stone formation in rats was shown to share similarities with kidney stone formation seen in humans, such as the oxalate metabolism process [93]. Moreover, EG was also widely and successfully used in several rat studies [89, 93, 94]. Upon identifying the optimal kidney stone animal model, injection of the peptide will be performed to investigate its biodistribution, safety, and efficacy by repeated administration in a kidney stone animal model (Figure 2A and C).

Together, our study provided a first step towards developing a Ca^{2+}-binding peptide with supersaturation-specific Ca^{2+} buffering ability and set up a systematic methodology for generating a kidney stone animal model for future testing.

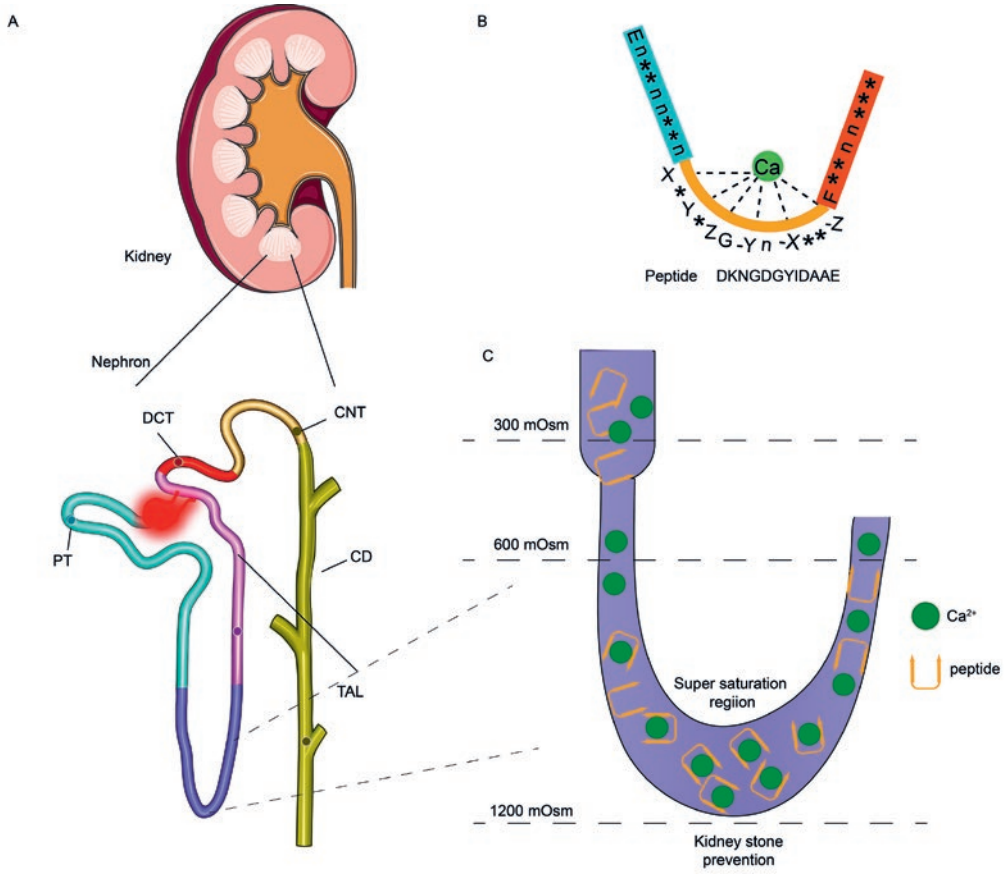

Figure 2. Kidney stone prevention through a novel Ca^{2+}-binding peptide.

A, the kidney consists of ~1 million nephrons as schematically depicted below, with the different segments color-coded. B, schematic representation of the Ca^{2+}-binding EF-hand structure, with the tested peptide sequence underneath. C, proposed assessment for functional consequences of the Ca^{2+}-binding peptide (orange) in the loop of Henle of an animal model that is prone to stone formation. PT, proximal tubule; TAL, thick ascending limb of loop of Henle; DCT, distal convoluted tubule; CNT, connecting tubule; CD, collecting duct.

Fine tuning of Mg^{2+} reabsorption in the distal convoluted tubule

Identification of a novel gene, *ARL15*

Mg^{2+} is one of the most important cations for energy metabolism and multiple enzymatic reactions involved in DNA and protein synthesis [95]. It is filtered by the glomerulus and is mainly reabsorbed in the TAL and DCT of the kidney [96]. A genome-wide association study (GWAS) identified a novel gene, ADP ribosylation factor like GTPase 15 (ARL15), to be associated with urinary Mg^{2+} excretion in seven European cohorts [97]. Other GWAS

demonstrated that variation at the *ARL15* locus is also associated with fasting insulin levels, plasma adiponectin levels, and triglyceride concentrations [98-101]. The role of ARL15 in the regulation of adiponectin and adiponectin receptor I and insulin signaling was confirmed by *in vitro* studies [102, 103]. Interestingly, we found that *Arl15* mRNA and protein levels are most abundant in mouse white adipose tissue, which is the main site of adiponectin secretion [104, 105]. Furthermore, Rocha *et al.* demonstrated that *Arl15* knockdown in differentiated adipocytes results in decreased mRNA levels of *Adiponectin*, and impaired adipogenesis in pre-adipocytes [106]. In contrast, our study in **Chapter 4** did not show changes in mRNA expression of *Adiponectin* or other metabolism- or Mg^{2+}-related genes in *Arl15* heterozygous (*Arl15*$^{+/-}$) mice. Alterations in serum electrolytes levels and 24 hours urinary electrolytes excretion were not found in *Arl15*$^{+/-}$ mice compared to *Arl15* wildtype (*Arl15*$^{+/+}$) mice. Certain compensatory mechanisms may be activated to counteract for the heterozygous knockout of ARL15, since *Arl15* knockout mice are lethal after birth. Although compensatory mechanisms could not be detected by RT-qPCR in our study, we cannot exclude changes in protein expression or activity. A similar study on the ADP-ribosylation factor (ARF)-related protein 1 (ARFRP1), which shares 30.8% similarity to ARL15, showed that heterozygous *Arfrp1* (*Arfrp*$^{+/-}$) mice developed normally whereas homozygous *Arfrp1* knockout (*Arfrp1*$^{-/-}$) mice exhibited embryonic lethality [107]. Interestingly, mice with specific deletion of *Arfrp1* in adipocytes showed a lipodystrophic phenotype and enhanced lipolysis in adipocytes [108]. In light of these studies, additional experiments should focus on investigating protein levels of ARL15-related proteins to better understand the potential compensatory mechanisms. Moreover, adipocyte-specific and kidney-specific *Arl15* knockout mice can be generated and challenged with various diets to explore the role of ARL15 in metabolism and renal electrolyte handling.

Exploring the novel function of ARL15 by BioID

In **Chapter 4**, we studied this novel gene and investigated its potential role in the kidney. I-TASSER tertiary structure prediction confirmed that ARL15 belongs to the small GTPase superfamily. Other members of this superfamily, like Rab and Arf, are known to be involved in vesicle trafficking from the endoplasmic reticulum (ER) to the Golgi [109].

ARL15 shares 33.5% similarity with ARF6, which is localized in the plasma membrane [110] and intracellular compartment [111]. Immunostaining results from our study and Rocha *et al.* proved that ARL15 is localized in the Golgi complex, the plasma membrane and intracellular compartment of 3T3-L1 cells [106]. Other studies demonstrated that ARF6 is involved in endocytic vesicular transport [112] and increased the cell surface expression of transferrin [113]. In accordance with this, Corre *et al.* showed that ARL15 increases the activity of the Mg^{2+} channel transient receptor potential melastatin 6 (TRPM6), probably by influencing its trafficking [97]. In **Chapter 5,** Biotin identification (BioID) results revealed that ARL15 interacts with TRPM7, a close homologue of TRPM6. In agreement with this, Donate-Macián *et al.* discovered that ARL15 interacts with another

TRP family member, TRPV2, by protein-protein interaction prediction [114]. Additionally, ARL15 interacts with amino acid transporters, Ca^{2+} transporters, potassium (K^{+}) transporters, and other metal ion transporters including zinc (Zn^{2+}) transporters (**Chapter 5**). Together, these findings broadened the basic knowledge on the function of ARL15, and strengthened the idea that ARL15 may act as small GTPase to interact and modify various types of transporters [97].

Gene ontology (GO) overrepresentation analysis of ARL15 BioID results suggest that ARL15 is involved in N-linked protein glycosylation. This pathway coincides with those observed in earlier studies evaluating the effects of small GTPase on glycosylation [115]. Protein glycosylation is a crucial and ubiquitous post-translational modification that can influence protein structure, stability, expression, and function [116-118]. Notably, BioID results revealed dolichol-phosphate mannosyltransferase subunit 1 (DPM1), dolichyl-diphospho-oligosaccharide (RPN1), lectin mannose binding 1 (LMAN1), and STT3 oligosaccharyltransferase complex catalytic subunits A and B (STT3A and STT3B) as the glycosylation-related proteins that have the highest relative binding abundance with ARL15. DPM1 transfers mannose from GDP-mannose (GDP-Man) to dolichol mannose (Dol-Man) in the synthesis of dolichol-phosphate mannose (Dol-P-Man) [119]. RPN1, which is exclusively found in the ER, is the component of N-oligosaccharyl transferase complex [120, 121]. This complex attaches high mannose oligosaccharides to N residues found in the nascent polypeptide chain consensus motif, this process is the first step of N-linked glycosylation [120, 121]. The LMAN1 functions as a glycoprotein transport cargo receptor that identifies sugar residues of glycoproteins and plays a crucial role in the transport or recycling of these proteins [122-124]. STT3A and STT3B are important for transferring the oligosaccharide in the process of glycosylation [125]. STT3A conveys glycan chains onto N residues of target proteins in the ER [126, 127]. STT3B is used to attach oligosaccharides onto N residues of target proteins [126, 127]. The binding between ARL15 and DPM1, RPN1, LMAN1, STT3A, and STT3B further support a role for ARL15 in the modification of protein glycosylation from ER to Golgi.

The functional interaction of ARL15 with CNNM proteins

Importantly, our Western blot results demonstrated that ARL15 affects the N-linked glycosylation of cyclin M 3 (CNNM3) (**Chapter 5**). The N-glycosylation of its homologue, CNNM2, is shown to be crucial in regulating CNNM2 plasma membrane expression [128]. Structurally, CNNM2 and CNNM3 have nearly 69% amino acid similarity [129], and the N-glycosylation site is conserved on their extracellular domain (CNNM2 N112 and CNNM3 N73) [128]. Interestingly, our mass spectrometry results identified ARL15 as the binding partner of CNNM2 in the DCT of the mouse kidney. Moreover, co-immunoprecipitation results demonstrated that ARL15 predominantly binds to the CBS2 motif of CNNM2.

Although the exact molecular function of CNNM proteins is still under debate [130, 131], it has been elucidated mutations in *CNNM2* lead to hypomagnesemia and CNNM

protein members are shown to be involved in Mg^{2+} transport [132, 133]. CNNM2 is localized to the basolateral side of the DCT, where is suggested to play a role in Mg^{2+} extrusion [128]. Here, TRPM6 (and TRPM7) channels are responsible for facilitating apical Mg^{2+} transport [134]. Interestingly, our BioID results present that ARL15 interacts with TRPM7. In a previous study by our group, 2-amino-ethoxydiphenyl borate, a non-selective TRPM6/7 inhibitor, was shown to abolish CNNM2-mediated $^{25}Mg^{2+}$ uptake in HEK293 cells [132]. Together, this suggests a connection between apical and basolateral Mg^{2+} transport mechanisms that may be simultaneously regulated by ARL15.

Our functional studies revealed that stable knockdown of ARL15 in various types of renal cell carcinoma cell lines resulted in increased $^{25}Mg^{2+}$ uptake and stable overexpression of ARL15 led to decreased $^{25}Mg^{2+}$ uptake (**Chapter 5**). Notably, in our cell surface expression experiments, neither ARL15 overexpression nor ARL15 knockdown affected the plasma membrane expression of CNNM3, which suggests that membrane trafficking of CNNM3 is not affected by ARL15. However, ARL15 knockdown resulted in disturbed glycosylation of CNNM3, suggesting that glycosylation of CNNM3 is important for its function. As a result of disturbed glycosylation CNNM3 may not be able to monitor or sense the intracellular Mg^{2+} concentration, which could lead to increased Mg^{2+} influx in ARL15 knockdown cells.

Recent studies showed that phosphatase of the regenerating liver (PRLs), which is a sub-family of the protein tyrosine phosphatases (PTP), interact with the extended loop of cystathionine-beta-synthase (CBS) 2 domain of CNNM3 [133, 135]. The binding between PRL2 and CNNM3 was increased under Mg^{2+}-deficient conditions, which led to an increase in the intracellular Mg^{2+} concentration [133]. Interestingly, Western bot results also showed that the expression of PRL2 is decreased in renal carcinoma cells overexpressing ARL15 (data not shown). The decreased expression of PRL2 could explain why ARL15 overexpression leads to decreased Mg^{2+} uptake in renal cell carcinoma cell lines (Figure 3).

Interestingly, ARL15 overexpression also decreased ATP production (**Chapter 5**). Mg^{2+} is used as a cofactor for multiple enzymes involved in ATP production, and ATP is bound to intracellular Mg^{2+} to form Mg-ATP as a biologically active molecule [96]. Hardy *et al*. demonstrated that intracellular ATP production is decreased upon cellular Mg^{2+} depletion, and that PRL expression is increased in response to low Mg^{2+} conditions [136]. In the same study, they addressed that this Mg^{2+}-dependent upregulation of PRL2 was activated by the AMPK/mTORC2 pathway [136], which could regulate cellular energy status [137].

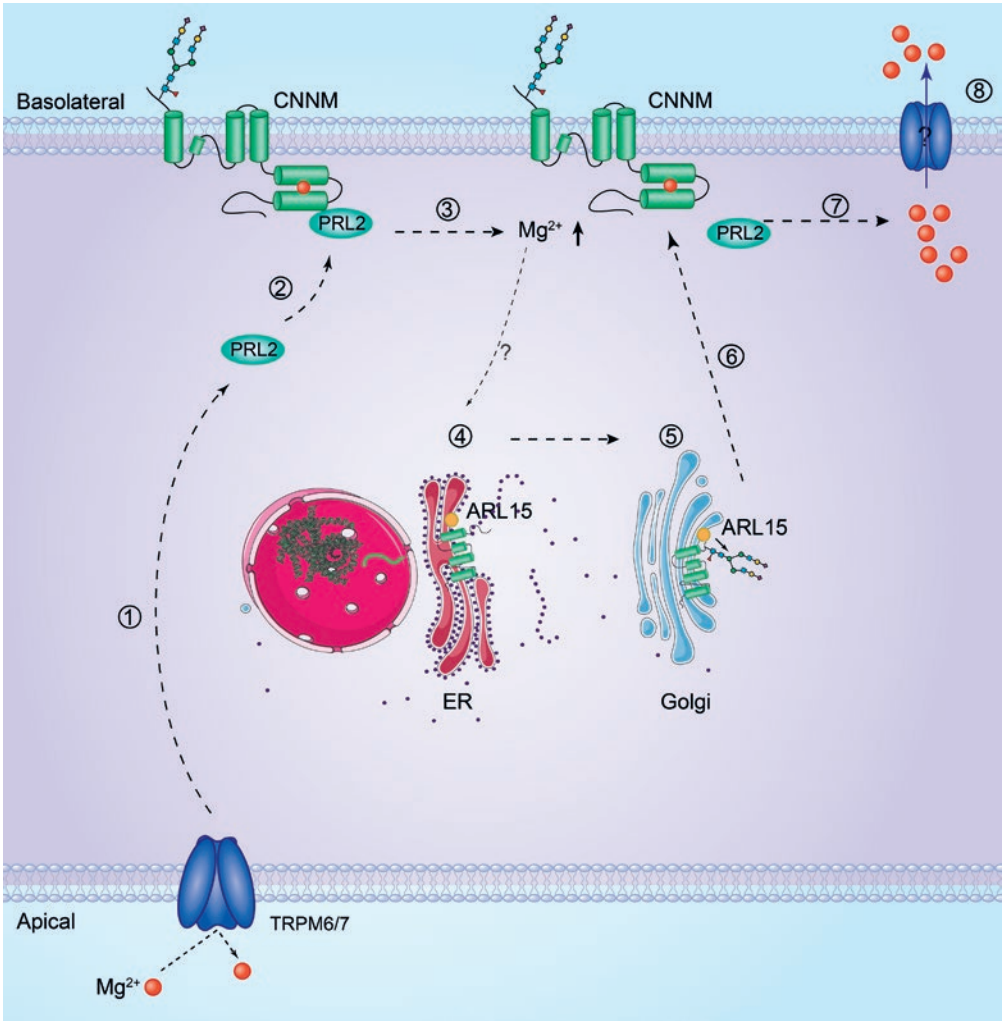

Figure 3. Proposed mechanisms for the ARL15/CNNMs complex regulating Mg^{2+} transport.

In the DCT segment of the kidney, TRPM6/7 channels facilitate apical Mg^{2+} transport. Basolateral Mg^{2+} extrusion is regulated by CNNMs. When TRPM6/7 Mg^{2+} channels are closed, intracellular Mg^{2+} is low which will increase the expression levels of PRL2 (1) and concomitantly its binding to the CBS2 domain of CNNM (2). This will result in an increase of intracellular Mg^{2+} (3). Increased intracellular Mg^{2+} may increase ARL15 expression and/or activity (4), which will facilitate the glycosylation process of CNNM from endoplasmic reticulum (ER) to Golgi (5) to cell membrane (6). Increased intracellular ARL15 may act as negative feedback that decreases PRL2 expression, leading to less binding between CNNM and PRL2 (7), and a subsequent decrease in intracellular Mg^{2+} levels by Mg^{2+} extrusion via a yet unidentified transporter (8). ARL15, ADP ribosylation factor like GTPase 15; TRPM6/7, Transient receptor potential cation channel subfamily M member 6/7; CNNM, Cyclin M. PRL2, phosphatase of the regenerating liver 2.

Reduced Mg^{2+} levels stimulated mTORC2 activity, a downstream target of AMPK, which in turn was responsible for increasing PRL2 protein levels, without affecting mRNA status [136]. Inhibiting mTORC1 had no effect on the Mg^{2+}-dependent increase in PRL2 protein expression, while combined mTORC2 and mTORC1 inhibition decreased the expression

of PRL2 [136]. Given that ARL15 overexpression affected CNNM-mediated Mg^{2+} uptake and ATP production, the expression of ARL15 may indirectly regulate cellular metabolism.

Together, our study established ARL15 as a novel negative regulator of Mg^{2+} homeostasis by modulating the N-glycosylation of CNNMs.

Scientific impact and future perspectives

In **Chapter 2**, we found that DAPA treatment activates compensatory changes in the PT in diabetic mice by upregulating the expression of NaPi-2a and NHE3. This compensatory effect in the PT may lead to an imbalance in renal Na^+ handling in type 2 diabetes patients who suffer from hypertension. Future studies could focus on isolating and investigating urinary exosomes from type 2 diabetes patients to study the effect of SGLT2 inhibitors on BP by analyzing the expression of distal nephron Na^+ transporters such as NKCC2, NCC, and ENaC (α, β, γ). Then, the upregulated Na^+ transporter can be blocked by its inhibitor to improve BP control in type 2 diabetes patients.

In **Chapter 3**, we developed a Ca^{2+}-binding peptide with potential properties for further testing in kidney stone mouse model. A first study was started to induce kidney stone formation in C57BL/6J mice by administrating 1% (v/v) EG in their drinking water combined with a high or normal Ca^{2+} diet. While kidney stones were not observed in these mice, **Chapter 3** provided a solid theoretical basis and methodology reference on the knowledge related to kidney stone formation and the development of a novel treatment to prevent kidney stone disease.

In **Chapter 4,** we identified the novel Mg^{2+}-related *ARL15* gene and tested its function by the characterization of heterozygous knockout mice. *Arl15*$^{+/-}$ mice displayed a normal phenotype, and showed no alterations in serum Mg^{2+} concentrations and 24 hours urinary Mg^{2+} excretion. In addition, the mRNA expression level of renal Mg^{2+}-, metabolism-, and membrane trafficking-related genes was not changed. These results suggest that ARL15 may not be involved in the regulation of renal electrolyte transport in the kidney. Future studies can focus on generating *Arl15* kidney-specific knockout mice and challenge these mice with Mg^{2+}-deficient diets to further reveal the function of ARL15 in the kidney.

In **Chapter 5,** we revealed the importance of ARL15 in maintaining Mg^{2+} homeostasis by interacting with CNNMs at their carboxy-terminal conserved CBS domains. ARL15 was shown to regulate complex N-glycosylation of CNNMs. Knockdown of ARL15 resulted in a significant increase of $^{25}Mg^{2+}$ uptake and ATP production in multiple kidney cancer cell lines. Our work provided new insights on how the interaction between ARL15 and CNNMs regulates N-glycosylation, Mg^{2+} transport, and ATP production. Future studies should reveal the interconnection between these processes, and demonstrate whether the ARL15-CNNM complex may provide new paths towards treating Mg^{2+}-related diseases.

In conclusion, elucidating the mechanisms involved in the maintenance of Na^+, Ca^{2+} and Mg^{2+} homeostasis in both health and disease improves our understanding of their roles in diabetes, hypertension, kidney stones, and hypomagnesemia diseases.

References

1. Ferre, S., J.G. Hoenderop, and R.J. Bindels, *Sensing mechanisms involved in Ca2+ and Mg2+ homeostasis.* Kidney Int, 2012. **82**(11): p. 1157-66.
2. Blaine, J., M. Chonchol, and M. Levi, *Renal control of calcium, phosphate, and magnesium homeostasis.* Clin J Am Soc Nephrol, 2015. **10**(7): p. 1257-72.
3. Llorente-Folch, I., et al., *The regulation of neuronal mitochondrial metabolism by calcium.* J Physiol, 2015. **593**(16): p. 3447-62.
4. Udwan, K., et al., *Dietary sodium induces a redistribution of the tubular metabolic workload.* J Physiol, 2017. **595**(22): p. 6905-6922.
5. Gimenez-Mascarell, P., et al., *Novel Aspects of Renal Magnesium Homeostasis.* Front Pediatr, 2018. **6**: p. 77.
6. Alexander, R.T. and H. Dimke, *Effect of diuretics on renal tubular transport of calcium and magnesium.* Am J Physiol Renal Physiol, 2017. **312**(6): p. F998-F1015.
7. Lockless, S.W., *Determinants of cation transport selectivity: Equilibrium binding and transport kinetics.* J Gen Physiol, 2015. **146**(1): p. 3-13.
8. Hofer, A.M. and E.M. Brown, *Extracellular calcium sensing and signalling.* Nat Rev Mol Cell Biol, 2003. **4**(7): p. 530-8.
9. Zinman, B., J.M. Lachin, and S.E. Inzucchi, *Empagliflozin, Cardiovascular Outcomes, and Mortality in Type 2 Diabetes.* N Engl J Med, 2016. **374**(11): p. 1094.
10. Radholm, K., et al., *Canagliflozin and Heart Failure in Type 2 Diabetes Mellitus: Results From the CANVAS Program.* Circulation, 2018. **138**(5): p. 458-468.
11. Tikkanen, I., R. Chilton, and O.E. Johansen, *Potential role of sodium glucose cotransporter 2 inhibitors in the treatment of hypertension.* Curr Opin Nephrol Hypertens, 2016. **25**(2): p. 81-6.
12. Blau, J.E., et al., *Canagliflozin triggers the FGF23/1,25-dihydroxyvitamin D/PTH axis in healthy volunteers in a randomized crossover study.* JCI Insight, 2018. **3**(8).
13. Blau, J.E. and S.I. Taylor, *Adverse effects of SGLT2 inhibitors on bone health.* Nat Rev Nephrol, 2018. **14**(8): p. 473-474.
14. Thrailkill, K.M., et al., *SGLT2 inhibitor therapy improves blood glucose but does not prevent diabetic bone disease in diabetic DBA/2J male mice.* Bone, 2016. **82**: p. 101-7.
15. Pessoa, T.D., et al., *Functional role of glucose metabolism, osmotic stress, and sodium-glucose cotransporter isoform-mediated transport on Na+/H+ exchanger isoform 3 activity in the renal proximal tubule.* J Am Soc Nephrol, 2014. **25**(9): p. 2028-39.
16. Schultheis, P.J., et al., *Renal and intestinal absorptive defects in mice lacking the NHE3 Na+/H+ exchanger.* Nat Genet, 1998. **19**(3): p. 282-5.
17. Kuro-o, M., et al., *Salt-sensitive hypertension in transgenic mice overexpressing Na(+)-proton exchanger.* Circ Res, 1995. **76**(1): p. 148-53.
18. LaPointe, M.S., et al., *Na+/H+ exchange activity and NHE-3 expression in renal tubules from the spontaneously hypertensive rat.* Kidney Int, 2002. **62**(1): p. 157-65.
19. Rahman, A., et al., *Effects of diuretics on sodium-dependent glucose cotransporter 2 inhibitor-induced changes in blood pressure in obese rats suffering from the metabolic syndrome.* J Hypertens, 2016. **34**(5): p. 893-906.
20. List, J.F., et al., *Sodium-glucose cotransport inhibition with dapagliflozin in type 2 diabetes.* Diabetes Care, 2009. **32**(4): p. 650-7.
21. Yasui, A., et al., *Empagliflozin Induces Transient Diuresis Without Changing Long-Term Overall Fluid Balance in Japanese Patients With Type 2 Diabetes.* Diabetes Ther, 2018. **9**(2): p. 863-871.
22. Tanaka, H., et al., *Factors Affecting Canagliflozin-Induced Transient Urine Volume Increase in Patients with Type 2 Diabetes Mellitus.* Adv Ther, 2017. **34**(2): p. 436-451.
23. Rajasekeran, H., Y. Lytvyn, and D.Z. Cherney, *Sodium-glucose cotransporter 2 inhibition and cardiovascular risk reduction in patients with type 2 diabetes: the emerging role of natriuresis.* Kidney Int, 2016. **89**(3): p. 524-6.

24. Sha, S., et al., *Effect of the sodium glucose co-transporter 2 inhibitor canagliflozin on plasma volume in patients with type 2 diabetes mellitus*. Diabetes Obes Metab, 2014. **16**(11): p. 1087-95.
25. Iijima, H., et al., *Pharmacokinetics, Pharmacodynamics, and Safety of Canagliflozin in Japanese Patients with Type 2 Diabetes Mellitus*. Adv Ther, 2015. **32**(8): p. 768-82.
26. Heise, T., et al., *Safety, tolerability, pharmacokinetics and pharmacodynamics following 4 weeks' treatment with empagliflozin once daily in patients with type 2 diabetes*. Diabetes Obes Metab, 2013. **15**(7): p. 613-21.
27. Weir, M.R., et al., *Effect of canagliflozin on blood pressure and adverse events related to osmotic diuresis and reduced intravascular volume in patients with type 2 diabetes mellitus*. J Clin Hypertens (Greenwich), 2014. **16**(12): p. 875-82.
28. Bode, B., et al., *Efficacy and safety of canagliflozin treatment in older subjects with type 2 diabetes mellitus: a randomized trial*. Hosp Pract (1995), 2013. **41**(2): p. 72-84.
29. Yale, J.F., et al., *Efficacy and safety of canagliflozin in subjects with type 2 diabetes and chronic kidney disease*. Diabetes Obes Metab, 2013. **15**(5): p. 463-73.
30. van Bommel, E.J.M., et al., *The renal hemodynamic effects of the SGLT2 inhibitor dapagliflozin are caused by post-glomerular vasodilatation rather than pre-glomerular vasoconstriction in metformin-treated patients with type 2 diabetes in the randomized, double-blind RED trial*. Kidney Int, 2020. **97**(1): p. 202-212.
31. Li, L., et al., *Effect of a SGLT2 inhibitor on the systemic and intrarenal renin-angiotensin system in subtotally nephrectomized rats*. J Pharmacol Sci, 2018. **137**(2): p. 220-223.
32. Vallon, V., et al., *Glomerular hyperfiltration in experimental diabetes mellitus: potential role of tubular reabsorption*. J Am Soc Nephrol, 1999. **10**(12): p. 2569-76.
33. Skrtic, M. and D.Z. Cherney, *Sodium-glucose cotransporter-2 inhibition and the potential for renal protection in diabetic nephropathy*. Curr Opin Nephrol Hypertens, 2015. **24**(1): p. 96-103.
34. Vallon, V., et al., *SGLT2 mediates glucose reabsorption in the early proximal tubule*. J Am Soc Nephrol, 2011. **22**(1): p. 104-12.
35. Vallon, V., et al., *Knockout of Na-glucose transporter SGLT2 attenuates hyperglycemia and glomerular hyperfiltration but not kidney growth or injury in diabetes mellitus*. Am J Physiol Renal Physiol, 2013. **304**(2): p. F156-67.
36. Monami, M., C. Nardini, and E. Mannucci, *Efficacy and safety of sodium glucose co-transport-2 inhibitors in type 2 diabetes: a meta-analysis of randomized clinical trials*. Diabetes Obes Metab, 2014. **16**(5): p. 457-66.
37. Weber, M.A., et al., *Effects of dapagliflozin on blood pressure in hypertensive diabetic patients on renin-angiotensin system blockade*. Blood Press, 2016. **25**(2): p. 93-103.
38. Kojima, N., et al., *Renoprotective effects of combined SGLT2 and ACE inhibitor therapy in diabetic Dahl S rats*. Physiol Rep, 2015. **3**(7).
39. Nishiyama, A. and H. Kobori, *Independent regulation of renin-angiotensin-aldosterone system in the kidney*. Clin Exp Nephrol, 2018. **22**(6): p. 1231-1239.
40. Han, H., et al., *Nutritional Management of Kidney Stones (Nephrolithiasis)*. Clin Nutr Res, 2015. **4**(3): p. 137-52.
41. Lieske, J.C., et al., *Stone Composition as a Function of Age and Sex*. Clinical Journal of the American Society of Nephrology, 2014. **9**(12): p. 2141-2146.
42. Alelign, T. and B. Petros, *Kidney Stone Disease: An Update on Current Concepts*. Adv Urol, 2018. **2018**: p. 3068365.
43. Nakayama, S., *[Evolution of EF-hand proteins]*. Seikagaku, 1995. **67**(2): p. 131-7.
44. Yap, K.L., et al., *Diversity of conformational states and changes within the EF-hand protein superfamily*. Proteins, 1999. **37**(3): p. 499-507.
45. Xu, L., et al., *SGLT2 Inhibition by Empagliflozin Promotes Fat Utilization and Browning and Attenuates Inflammation and Insulin Resistance by Polarizing M2 Macrophages in Diet-induced Obese Mice*. EBioMedicine, 2017. **20**: p. 137-149.
46. Wei, D., et al., *Canagliflozin ameliorates obesity by improving mitochondrial function and fatty acid oxidation via PPARalpha in vivo and in vitro*. Life Sci, 2020. **247**: p. 117414.
47. Hosokawa, K., et al., *Ipragliflozin Ameliorates Endoplasmic Reticulum Stress and Apoptosis through Preventing Ectopic Lipid Deposition in Renal Tubules*. Int J Mol Sci, 2019. **21**(1).

48. Rahadian, A., et al., *Canagliflozin Prevents Diabetes-Induced Vascular Dysfunction in ApoE-Deficient Mice.* J Atheroscler Thromb, 2020.
49. Salim, H.M., et al., *Glycemic Control with Ipragliflozin, a Novel Selective SGLT2 Inhibitor, Ameliorated Endothelial Dysfunction in Streptozotocin-Induced Diabetic Mouse.* Front Cardiovasc Med, 2016. **3**: p. 43.
50. Tahara, A., et al., *Effects of SGLT2 selective inhibitor ipragliflozin on hyperglycemia, hyperlipidemia, hepatic steatosis, oxidative stress, inflammation, and obesity in type 2 diabetic mice.* Eur J Pharmacol, 2013. **715**(1-3): p. 246-55.
51. Tahara, A. and T. Takasu, *SGLT2 inhibitor ipragliflozin alone and combined with pioglitazone prevents progression of nonalcoholic steatohepatitis in a type 2 diabetes rodent model.* Physiol Rep, 2019. **7**(22): p. e14286.
52. Lu, Y.H., et al., *Empagliflozin Attenuates Hyperuricemia by Upregulation of ABCG2 via AMPK/AKT/CREB Signaling Pathway in Type 2 Diabetic Mice.* Int J Biol Sci, 2020. **16**(3): p. 529-542.
53. Nagata, T., et al., *Tofogliflozin, a novel sodium-glucose co-transporter 2 inhibitor, improves renal and pancreatic function in db/db mice.* Br J Pharmacol, 2013. **170**(3): p. 519-31.
54. Lin, B., et al., *Glycemic control with empagliflozin, a novel selective SGLT2 inhibitor, ameliorates cardiovascular injury and cognitive dysfunction in obese and type 2 diabetic mice.* Cardiovasc Diabetol, 2014. **13**: p. 148.
55. Gallo, L.A., et al., *Once daily administration of the SGLT2 inhibitor, empagliflozin, attenuates markers of renal fibrosis without improving albuminuria in diabetic db/db mice.* Sci Rep, 2016. **6**: p. 26428.
56. O'Neill, J., et al., *Acute SGLT inhibition normalizes O2 tension in the renal cortex but causes hypoxia in the renal medulla in anaesthetized control and diabetic rats.* Am J Physiol Renal Physiol, 2015. **309**(3): p. F227-34.
57. Han, S., et al., *Dapagliflozin, a selective SGLT2 inhibitor, improves glucose homeostasis in normal and diabetic rats.* Diabetes, 2008. **57**(6): p. 1723-9.
58. Ansary, T.M., et al., *Responses of renal hemodynamics and tubular functions to acute sodium-glucose cotransporter 2 inhibitor administration in non-diabetic anesthetized rats.* Sci Rep, 2017. **7**(1): p. 9555.
59. Yamamoto, K., et al., *TS-071 is a novel, potent and selective renal sodium-glucose cotransporter 2 (SGLT2) inhibitor with anti-hyperglycaemic activity.* Br J Pharmacol, 2011. **164**(1): p. 181-91.
60. Takeshige, Y., et al., *A sodium-glucose co-transporter 2 inhibitor empagliflozin prevents abnormality of circadian rhythm of blood pressure in salt-treated obese rats.* Hypertens Res, 2016. **39**(6): p. 415-22.
61. Chung, S., et al., *Empagliflozin Contributes to Polyuria via Regulation of Sodium Transporters and Water Channels in Diabetic Rat Kidneys.* Front Physiol, 2019. **10**: p. 271.
62. Rezq, S., et al., *Doxazosin down-regulates sodium-glucose cotransporter-2 and exerts a renoprotective effect in rat models of acute renal injury.* Basic Clin Pharmacol Toxicol, 2019.
63. Yamazaki, D., et al., *Failure to confirm a sodium-glucose cotransporter 2 inhibitor-induced hematopoietic effect in non-diabetic rats with renal anemia.* J Diabetes Investig, 2019.
64. Masuda, T., et al., *Osmotic diuresis by SGLT2 inhibition stimulates vasopressin-induced water reabsorption to maintain body fluid volume.* Physiol Rep, 2020. **8**(2): p. e14360.
65. Wilding, J.P., et al., *A study of dapagliflozin in patients with type 2 diabetes receiving high doses of insulin plus insulin sensitizers: applicability of a novel insulin-independent treatment.* Diabetes Care, 2009. **32**(9): p. 1656-62.
66. Sha, S., et al., *Pharmacodynamic effects of canagliflozin, a sodium glucose co-transporter 2 inhibitor, from a randomized study in patients with type 2 diabetes.* PLoS One, 2014. **9**(9): p. e110069.
67. Sasaki, T., et al., *Pharmacokinetics, Pharmacodynamics, and Safety of Luseogliflozin in Japanese Patients with Type 2 Diabetes Mellitus: A Randomized, Single-blind, Placebo-controlled Trial.* Adv Ther, 2015. **32**(4): p. 319-40.
68. Takeuchi, T., et al., *Diuretic effects of sodium-glucose cotransporter 2 inhibitor in patients with type 2 diabetes mellitus and heart failure.* Int J Cardiol, 2015. **201**: p. 1-3.
69. Fukuoka, S., et al., *Mechanisms and prediction of short-term natriuretic effect of sodium-glucose cotransporter 2 inhibitor in heart failure patients coexisting type 2 diabetes mellitus.* Heart Vessels, 2020.

70. Kambara, T., et al., *Importance of sodium-glucose cotransporter 2 inhibitor use in diabetic patients with acute heart failure.* Ther Adv Cardiovasc Dis, 2019. **13**: p. 1753944719894509.
71. Ghanim, H., et al., *Dapagliflozin Suppresses Hepcidin And Increases Erythropoiesis.* J Clin Endocrinol Metab, 2020. **105**(4).
72. Higashikawa, T., et al., *Effects of Tofogliflozin on Cardiac Function in Elderly Patients With Diabetes Mellitus.* J Clin Med Res, 2020. **12**(3): p. 165-171.
73. Kawasoe, S., et al., *Mechanism of the blood pressure-lowering effect of sodium-glucose cotransporter 2 inhibitors in obese patients with type 2 diabetes.* BMC Pharmacol Toxicol, 2017. **18**(1): p. 23.
74. Reid, R.E., *Synthetic fragments of calmodulin calcium-binding site III. A test of the acid pair hypothesis.* J Biol Chem, 1990. **265**(11): p. 5971-6.
75. Procyshyn, R.M. and R.E. Reid, *A structure/activity study of calcium affinity and selectivity using a synthetic peptide model of the helix-loop-helix calcium-binding motif.* J Biol Chem, 1994. **269**(3): p. 1641-7.
76. Lakowski, T.M., et al., *Calcium-induced folding of a fragment of calmodulin composed of EF-hands 2 and 3.* Protein Sci, 2007. **16**(6): p. 1119-32.
77. Fosgerau, K. and T. Hoffmann, *Peptide therapeutics: current status and future directions.* Drug Discov Today, 2015. **20**(1): p. 122-8.
78. Baig, M.H., et al., *Peptide based therapeutics and their use for the treatment of neurodegenerative and other diseases.* Biomed Pharmacother, 2018. **103**: p. 574-581.
79. Gupta, S., et al., *In silico approach for predicting toxicity of peptides and proteins.* PLoS One, 2013. **8**(9): p. e73957.
80. Christensen, E.I., et al., *Endocytic receptors in the renal proximal tubule.* Physiology (Bethesda), 2012. **27**(4): p. 223-36.
81. Leheste, J.R., et al., *Megalin knockout mice as an animal model of low molecular weight proteinuria.* Am J Pathol, 1999. **155**(4): p. 1361-70.
82. Cui, S., et al., *Megalin/gp330 mediates uptake of albumin in renal proximal tubule.* Am J Physiol, 1996. **271**(4 Pt 2): p. F900-7.
83. Hatae, T., et al., *Formation of apical tubules from large endocytic vacuoles in kidney proximal tubule cells during absorption of horseradish peroxidase.* Cell Tissue Res, 1986. **246**(2): p. 271-8.
84. Vegt, E., et al., *Renal uptake of different radiolabelled peptides is mediated by megalin: SPECT and biodistribution studies in megalin-deficient mice.* Eur J Nucl Med Mol Imaging, 2011. **38**(4): p. 623-32.
85. Detrisac, C.J., et al., *Tissue culture of human kidney epithelial cells of proximal tubule origin.* Kidney Int, 1984. **25**(2): p. 383-90.
86. Jones, A.T., *Macropinocytosis: searching for an endocytic identity and role in the uptake of cell penetrating peptides.* J Cell Mol Med, 2007. **11**(4): p. 670-84.
87. Matsuzaki, K., et al., *Transbilayer transport of ions and lipids coupled with mastoparan X translocation.* Biochemistry, 1996. **35**(25): p. 8450-6.
88. Pouny, Y., et al., *Interaction of antimicrobial dermaseptin and its fluorescently labeled analogues with phospholipid membranes.* Biochemistry, 1992. **31**(49): p. 12416-23.
89. Bilbault, H. and J.P. Haymann, *Experimental models of renal calcium stones in rodents.* World J Nephrol, 2016. **5**(2): p. 189-94.
90. Okada, A., et al., *Successful formation of calcium oxalate crystal deposition in mouse kidney by intraabdominal glyoxylate injection.* Urol Res, 2007. **35**(2): p. 89-99.
91. Alenzi, M., S. Rahiman, and B.A. Tantry, *Antiurolithic effect of olive oil in a mouse model of ethylene glycol-induced urolithiasis.* Investig Clin Urol, 2017. **58**(3): p. 210-216.
92. Wesson, J.A., et al., *Osteopontin is a critical inhibitor of calcium oxalate crystal formation and retention in renal tubules.* Journal of the American Society of Nephrology, 2003. **14**(1): p. 139-147.
93. Khan, S.R., *Animal models of kidney stone formation: an analysis.* World J Urol, 1997. **15**(4): p. 236-43.
94. Wang, S., et al., *Use of a calcium tracer to detect stone increments in a rat calcium oxalate xenoplantation model.* Experimental and Therapeutic Medicine, 2013. **6**(4): p. 957-960.

95. Feeney, K.A., et al., *Daily magnesium fluxes regulate cellular timekeeping and energy balance.* Nature, 2016. **532**(7599): p. 375-9.
96. de Baaij, J.H., J.G. Hoenderop, and R.J. Bindels, *Magnesium in man: implications for health and disease.* Physiol Rev, 2015. **95**(1): p. 1-46.
97. Corre, T., et al., *Genome-Wide Meta-Analysis Unravels Interactions between Magnesium Homeostasis and Metabolic Phenotypes.* J Am Soc Nephrol, 2018. **29**(1): p. 335-348.
98. Richards, J.B., et al., *A genome-wide association study reveals variants in ARL15 that influence adiponectin levels.* PLoS Genet, 2009. **5**(12): p. e1000768.
99. Teslovich, T.M., et al., *Biological, clinical and population relevance of 95 loci for blood lipids.* Nature, 2010. **466**(7307): p. 707-13.
100. Willer, C.J., et al., *Discovery and refinement of loci associated with lipid levels.* Nat Genet, 2013. **45**(11): p. 1274-1283.
101. Scott, R.A., et al., *Large-scale association analyses identify new loci influencing glycemic traits and provide insight into the underlying biological pathways.* Nat Genet, 2012. **44**(9): p. 991-1005.
102. Shen, J., et al., *ARL15 overexpression attenuates high glucose-induced impairment of insulin signaling and oxidative stress in human umbilical vein endothelial cells.* Life Sci, 2019. **220**: p. 127-135.
103. Kashyap, S., et al., *Functional characterisation of ADP ribosylation factor-like protein 15 in rheumatoid arthritis synovial fibroblasts.* Clin Exp Rheumatol, 2018. **36**(4): p. 581-588.
104. Maeda, K., et al., *cDNA cloning and expression of a novel adipose specific collagen-like factor, apM1 (AdiPose Most abundant Gene transcript 1).* Biochem Biophys Res Commun, 1996. **221**(2): p. 286-9.
105. Arita, Y., et al., *Paradoxical decrease of an adipose-specific protein, adiponectin, in obesity.* Biochem Biophys Res Commun, 1999. **257**(1): p. 79-83.
106. Rocha, N., et al., *The metabolic syndrome- associated small G protein ARL15 plays a role in adipocyte differentiation and adiponectin secretion.* Sci Rep, 2017. **7**(1): p. 17593.
107. Mueller, A.G., et al., *Embryonic lethality caused by apoptosis during gastrulation in mice lacking the gene of the ADP-ribosylation factor-related protein 1.* Mol Cell Biol, 2002. **22**(5): p. 1488-94.
108. Hommel, A., et al., *The ARF-like GTPase ARFRP1 is essential for lipid droplet growth and is involved in the regulation of lipolysis.* Mol Cell Biol, 2010. **30**(5): p. 1231-42.
109. Choy, E., et al., *Endomembrane trafficking of ras: the CAAX motif targets proteins to the ER and Golgi.* Cell, 1999. **98**(1): p. 69-80.
110. Song, J., et al., *Localization of endogenous ARF6 to sites of cortical actin rearrangement and involvement of ARF6 in cell spreading.* J Cell Sci, 1998. **111 (Pt 15)**: p. 2257-67.
111. D'Souza-Schorey, C., et al., *ARF6 targets recycling vesicles to the plasma membrane: insights from an ultrastructural investigation.* J Cell Biol, 1998. **140**(3): p. 603-16.
112. Figueiredo, J., et al., *ADP-ribosylation factor 6 mediates E-cadherin recovery by chemical chaperones.* PLoS One, 2011. **6**(8): p. e23188.
113. D'Souza-Schorey, C., et al., *A regulatory role for ARF6 in receptor-mediated endocytosis.* Science, 1995. **267**(5201): p. 1175-8.
114. Donate-Macian, P., et al., *Trafficking of Stretch-Regulated TRPV2 and TRPV4 Channels Inferred Through Interactomics*. Biomolecules, 2019. **9**(12).
115. Gillingham, A.K. and S. Munro, *The small G proteins of the Arf family and their regulators.* Annu Rev Cell Dev Biol, 2007. **23**: p. 579-611.
116. Walsh, M.T., J.F. Foley, and B.T. Kinsella, *Characterization of the role of N-linked glycosylation on the cell signaling and expression of the human thromboxane A2 receptor alpha and beta isoforms.* J Pharmacol Exp Ther, 1998. **286**(2): p. 1026-36.
117. Casalou, C., A. Faustino, and D.C. Barral, *Arf proteins in cancer cell migration.* Small GTPases, 2016. **7**(4): p. 270-282.
118. Cohen, D.M., *Regulation of TRP channels by N-linked glycosylation.* Semin Cell Dev Biol, 2006. **17**(6): p. 630-7.
119. Kim, S., et al., *Dolichol phosphate mannose synthase (DPM1) mutations define congenital disorder of glycosylation Ie (CDG-Ie).* J Clin Invest, 2000. **105**(2): p. 191-8.
120. Wilson, C.M., Q. Roebuck, and S. High, *Ribophorin I regulates substrate delivery to the oligosaccharyltransferase core.* Proc Natl Acad Sci U S A, 2008. **105**(28): p. 9534-9.

121. Wilson, C.M. and S. High, *Ribophorin I acts as a substrate-specific facilitator of N-glycosylation.* J Cell Sci, 2007. **120**(Pt 4): p. 648-57.
122. Zhang, B., R.J. Kaufman, and D. Ginsburg, *LMAN1 and MCFD2 form a cargo receptor complex and interact with coagulation factor VIII in the early secretory pathway.* J Biol Chem, 2005. **280**(27): p. 25881-6.
123. Segal, A., et al., *A mutation in LMAN1 (ERGIC-53) causing combined factor V and factor VIII deficiency is prevalent in Jews originating from the island of Djerba in Tunisia.* Blood Coagul Fibrinolysis, 2004. **15**(1): p. 99-102.
124. Duellman, T., et al., *LMAN1 (ERGIC-53) is a potential carrier protein for matrix metalloproteinase-9 glycoprotein secretion.* Biochem Biophys Res Commun, 2015. **464**(3): p. 685-91.
125. Hese, K., et al., *The yeast oligosaccharyltransferase complex can be replaced by STT3 from Leishmania major.* Glycobiology, 2009. **19**(2): p. 160-71.
126. Shrimal, S., et al., *Mutations in STT3A and STT3B cause two congenital disorders of glycosylation.* Hum Mol Genet, 2013. **22**(22): p. 4638-45.
127. Lu, H., et al., *Mammalian STT3A/B oligosaccharyltransferases segregate N-glycosylation at the translocon from lipid-linked oligosaccharide hydrolysis.* Proc Natl Acad Sci U S A, 2018. **115**(38): p. 9557-9562.
128. de Baaij, J.H., et al., *Membrane topology and intracellular processing of cyclin M2 (CNNM2).* J Biol Chem, 2012. **287**(17): p. 13644-55.
129. Wang, C.Y., et al., *Molecular cloning and characterization of a novel gene family of four ancient conserved domain proteins (ACDP).* Gene, 2003. **306**: p. 37-44.
130. Funato, Y., et al., *CrossTalk proposal: CNNM proteins are Na(+) /Mg(2+) exchangers playing a central role in transepithelial Mg(2+) (re)absorption.* J Physiol, 2018. **596**(5): p. 743-746.
131. Arjona, F.J. and J.H.F. de Baaij, *CrossTalk opposing view: CNNM proteins are not Na(+) /Mg(2+) exchangers but Mg(2+) transport regulators playing a central role in transepithelial Mg(2+) (re) absorption.* J Physiol, 2018. **596**(5): p. 747-750.
132. Arjona, F.J., et al., *CNNM2 mutations cause impaired brain development and seizures in patients with hypomagnesemia.* PLoS Genet, 2014. **10**(4): p. e1004267.
133. Hardy, S., et al., *The protein tyrosine phosphatase PRL-2 interacts with the magnesium transporter CNNM3 to promote oncogenesis.* Oncogene, 2015. **34**(8): p. 986-95.
134. Voets, T., et al., *TRPM6 forms the Mg2+ influx channel involved in intestinal and renal Mg2+ absorption.* J Biol Chem, 2004. **279**(1): p. 19-25.
135. Gimenez-Mascarell, P., et al., *Structural Basis of the Oncogenic Interaction of Phosphatase PRL-1 with the Magnesium Transporter CNNM2.* J Biol Chem, 2017. **292**(3): p. 786-801.
136. Hardy, S., et al., *Magnesium-sensitive upstream ORF controls PRL phosphatase expression to mediate energy metabolism.* Proc Natl Acad Sci U S A, 2019. **116**(8): p. 2925-2934.
137. Herzig, S. and R.J. Shaw, *AMPK: guardian of metabolism and mitochondrial homeostasis.* Nat Rev Mol Cell Biol, 2018. **19**(2): p. 121-135.

7

Summary

Nederlandse samenvatting

Summary

Sodium (Na^+), magnesium (Mg^{2+}) and calcium (Ca^{2+}) homeostasis is critical for a variety of physiological processes in the human body. The kidney plays a crucial role in the regulation of this electrolyte balance. The concentration of serum Na^+, Mg^{2+}, and Ca^{2+} is determined by the kidneys through the reabsorption of these electrolytes by transporters, ion channels and sensors in the proximal tubule (PT), thick ascending limb of loop of Henle (TAL), distal convoluted tubule (DCT) and connecting duct (CD) of the kidney. A disturbed electrolyte balance is associated with a variety of diseases such as hypertension, diabetes, renal carcinoma, and kidney stones. The aim of this thesis was *I)* to investigate the expression of Na^+ transporters in the kidney upon inhibiting the Na^+-glucose transporter 2 (SGLT2) in the PT; *II)* to identify Ca^{2+}-binding peptides to reduce the urinary Ca^{2+} concentration and potentially prevent kidney stone formation; *III)* to study the novel urinary Mg^{2+}-related gene *ARL15* (ADP ribosylation factor like GTPase 15) in the kidney; and *IV)* to investigate how ARL15 regulates Mg^{2+} transport by interacting with the cyclin and CBS domain divalent metal cation transport mediators (CNNMs) in the kidney.

Potential compensatory mechanisms of Na^+ transporters upon inhibition of SGLT2 in the proximal tubule

SGLT2 inhibitors have progressively attracted attention due to their function in increasing glucose excretion, ameliorating glycemic control and alleviating blood pressure. The latter is possibly due to the fact that SGLT2 inhibitors lead to natriuresis. However, the molecular mechanism is still unknown. In **Chapter 2,** diabetic mice were administrated with the SGLT2 inhibitor dapagliflozin (DAPA) and the expression of renal Na^+ transporters/ion channels was studied. The diabetic mice exhibited increased blood glucose levels upon 18-day DAPA treatment, and mRNA levels of sodium-hydrogen antiporter 3 (*Nhe3*), and sodium-phosphate cotransporter (*Napi-2a*), were upregulated in kidneys of DAPA-treated mice. However, changes in expression of distal Na^+ transporters such as sodium-potassium-chloride cotransporter (NKCC2) and sodium-chloride cotransporter (NCC) in the TAL and DCT, respectively, were not detected. The results of this study proved that DAPA treatment results in compensatory changes in the PT of the kidney in diabetic mice.

Development of Ca^{2+}-binding peptides to prevent kidney stone formation in Henle's loop

Kidney stone disease (nephrolithiasis) is becoming a major medical concern in the world. Although medical therapies have largely improved nephrolithiasis treatment, the recurrence rate is still very high. Therefore, an improved and effective remedy to avoid kidney stone recurrence is needed. In **Chapter 3,** several Ca^{2+}-binding peptides were developed, based on the established Ca^{2+}-binding EF-hand domain. The Ca^{2+}-binding affinities of these peptides were investigated by circular dichroism demonstrating

dose-dependent response to $CaCl_2$ concentrations in the millimolar range for peptide 4 (Ac-DKNGDGYIDAAE-NH_3). This peptide did not result in cellular toxicity and exhibited minimal cellular uptake by proximal tubular human kidney 2 (HK-2) cells. A Ca^{2+}-binding affinity in the high millimolar range (2-10 mM) could allow for Ca^{2+}-binding in the pro-urine without affecting serum Ca^{2+} levels (1-2 mM). Future studies need to further optimize the Ca^{2+}-binding kinetics of the identified peptide. In order to investigate the biological function of this peptide in healthy mice and in a mouse model with kidney stones, C57BL/6J mice were administrated with 1% (v/v) ethylene glycol (EG) via drinking water and subsequently treated with either a normal Ca^{2+} diet (0.92% (w/w)) or a high Ca^{2+} diet (2% (w/w)) for 28 days. Yet, Ca^{2+} crystal deposition in the kidney was not detected in any of the conditions. **Chapter 3** demonstrated that Ca^{2+}-binding peptides can be used to bind Ca^{2+} in the physiologically relevant range. Optimized Ca^{2+}-binding peptides should be investigated in other mice models than C57BL/6J which better reflect kidney stone disease.

Fine tuning Mg^{2+} reabsorption in the distal convoluted tubule

Previous genome wide association studies (GWAS) identified the *ARL15* locus to be associated with urinary Mg^{2+} excretion in 9.099 individuals in seven European cohorts. ARL15 is localized in the TAL and DCT of the kidney where it could be involved in renal Mg^{2+} reabsorption through regulating the channel activity of the Mg^{2+} channel TRPM6. In order to further understand the function of ARL15, we characterized ARL15 and investigated its role in the kidney by using *Arl15* heterozygous (*Arl15*$^{+/-}$) mice in **Chapter 4**. Results demonstrated that ARL15 belongs to the small GTPase superfamily and it is predicted to bind Mg^{2+}. The tissue expression pattern of *Arl15* showed that it is ubiquitously expressed and predominantly found in lung, inguinal fat, epididymal fat, spleen, testes and kidney. Homozygous *Arl15* knockout mice died after birth. By challenging *Arl15*$^{+/-}$ mice with a high fat diet, we did not detect significant differences in the serum Mg^{2+} concentration and 24-hrs urinary Mg^{2+} excretion between *Arl15*$^{+/+}$ and *Arl15*$^{+/-}$ mice. In addition, there were significant changes detected in the mRNA expression levels of Mg^{2+}-related genes, metabolism-related genes, and membrane trafficking-related genes in the kidneys of either *Arl15*$^{+/+}$ or *Arl15*$^{+/-}$ mice on the high fat or low fat diets. In summary, our results suggest that *Arl15*$^{+/-}$ mice have a normal phenotype, and exhibit no changes in renal Mg^{2+} handling.

ARL15 as a new binding partner of CNNM

By proximity-dependent biotin identification (BioID) and co-immunoprecipitation, we demonstrated that ARL15 binds to proteins of the CNNM family. Interestingly, CNNMs have been reported to regulate Mg^{2+} transport at the basolateral membrane of the DCT. Subsequently, we investigated how ARl15 regulates CNNM activity in **Chapter 5**. Immunostaining indicated that CNNM2 and ARL15 co-localize along the basolateral

membrane of the DCT of mouse kidney. Co-immunoprecipitation demonstrated that ARL15 predominantly binds to the CBS2 domain of CNNMs. Our BioID results indicated that ARL15 is involved in N-linked glycosylation. Transient overexpression of ARL15 in human embryonic kidney 293 (HEK293) cells resulted in an increased N-glycosylation of CNNM3 proteins. The functional consequences of ARL15-dependent glycosylation were examined by $^{25}Mg^{2+}$ uptake experiments. We showed a significant decrease of $^{25}Mg^{2+}$ uptake upon overexpression of ARL15 and a significant increase of $^{25}Mg^{2+}$ uptake upon knockdown of ARL15 in multiple kidney cancer cell lines. Moreover, knockdown of ARL15 in renal cell carcinomas resulted in disturbed glycosylation of CNNM3. Altogether, our results established ARL15 as novel regulator of Mg^{2+} transport in the DCT.

This thesis provided new insights regarding compensatory mechanisms of Na^+ transporters in the PT upon inhibiting SGLT2, made the first step towards testing a novel approach in the treatment and prevention of kidney stones, and further revealed a novel regulatory mechanism of Mg^{2+} transport within the DCT. Together, this will help to understand more on the regulation of electrolyte handling in the various nephron segments.

Nederlandse samenvatting

De natrium- (Na^+), magnesium- (Mg^{2+}), en calcium (Ca^{2+}) -balans is cruciaal voor vele fysiologische processen in het menselijk lichaam. De hoeveelheid Na^+, Mg^{2+}, en Ca^{2+} in het bloed wordt deels bepaald door de nieren. Heropname van deze mineralen vindt plaats in verschillende delen van de nier, waaronder de proximale tubulus, het dikke opstijgende been van de lis van Henle, het distaal convoluut en de verbindingsbuis. Een verstoorde mineraalbalans is geassocieerd met onder meer hoge bloeddruk, diabetes, nierkanker en nierstenen. Het doel van dit proefschrift was om: *I*) te onderzoeken wat het effect is van remming van de Na^+-glucose transporter 2 (SGLT2) op de aanwezigheid van eiwitten betrokken bij de Na^+ heropname in de nier; *II*) Ca^{2+}-bindende eiwitfragmenten te ontwikkelen die zeer specifiek de Ca^{2+} concentratie in de urine kunnen verlagen om niersteenvorming te voorkomen; *III*) het nieuwe Mg^{2+}-gerelateerde gen ARL15 (ADP ribosylation factor like GTPase 15) in de nier te bestuderen; en *IV*) te achterhalen hoe ARL15 de Mg^{2+} heropname in de nier reguleert door middel van de interactie met cyclin en CBS domein divalent metal cation transport mediators (CNNMs).

Compensatoire mechanismen van Na^+ heropname door remming van SGLT2 in de proximale tubulus

De afgelopen decennia is er meer aandacht gekomen voor SGLT2 remmers door hun rol in het verbeteren van de bloedsuikerspiegel en het verlagen van de bloeddruk. SGLT2 remmers verlagen de bloeddruk door een verhoogde uitscheiding van Na^+ in de urine, ook wel natriurese genoemd. In **hoofdstuk 2** kregen muizen met diabetes de SGLT2 remmer dapagliflozin (DAPA) toegediend en werd de aanwezigheid van genen en eiwitten relevant voor Na^+ heropname in de nier bestudeerd. De muizen met diabetes vertoonden een verhoogde glucosewaarde in het bloed die sterk verlaagd was na een 18-daagse behandeling met DAPA. Om de effecten van SGLT2 remmers op Na^+ heropname in de nier te bestuderen, zijn de eiwitten die Na^+ opnemen in de verschillende delen van de nier in kaart gebracht. De aanwezigheid van de genen natrium-waterstof uitwisselaar 3 (*Nhe3*) en natrium-fosfaat cotransporter (*Napi-2a*) in de proximale tubulus was verhoogd in DAPA-behandelde muizen. Er werden geen verschillen waargenomen in de aanwezigheid van de genen *Nkcc2* en *Ncc* (belangrijk voor het transport van Na^+ in de lis van Henle en het distaal convoluut) tussen DAPA-behandelde en onbehandelde muizen met diabetes. De resultaten van deze studie bewijzen dat DAPA-behandeling zorgt voor verhoging van compensatoire eiwitten die betrokken zijn bij Na^+ heropname in de proximale tubulus van de nier in muizen met diabetes.

Ontwikkeling van Ca^{2+}-bindende peptiden om niersteenformatie te voorkomen in de lis van Henle

Nierstenen (nefrolithiase) zijn een wereldwijd toenemend medisch probleem. Patienten die nierstenen hebben gehad, hebben een grote kans op terugkeer ondanks de verbeterde behandeling. Een effectievere methode om nierstenen te voorkomen is dan ook noodzakelijk. In **hoofdstuk 3** zijn Ca^{2+}-bindende eiwitfragmenten ontwikkeld. Hiervoor is gebruikt gemaakt van de structuur van een natuurlijk Ca^{2+}-bindend eiwit, het zogenaamde EF-hand domein. De binding van Ca^{2+} aan deze eiwitfragmenten is onderzocht door gebruik te maken van circulair dichroïsme spectroscopie. Deze metingen lieten een dosisafhankelijk effect zien van de calciumconcentratie op eiwitfragment 4 (Ac-DKNGDGYIDAAE-NH_3). Daarnaast werd aangetoond dat dit eiwitfragment niet resulteerde in cellulaire toxiciteit, en het vertoonde slechts minimale cellulaire opname in proximale tubulus humane nier 2 (HK-2) cellen. Ca^{2+}-binding aan dit eiwitfragment bij concentraties in de hoge millimolaire eenheid (2-10 mM) zou Ca^{2+} weg kunnen vangen in de voorurine zonder de Ca^{2+} waarde in het bloed te beïnvloeden (1-2 mM). Verder onderzoek is nodig om de binding van Ca^{2+} aan het beoogde eiwitfragment te optimaliseren. Om de biologische rol van dit eiwitfragment te onderzoeken, zijn diermodellen met nierstenen nodig. Hiertoe werden muizen behandeld met 1% (v/v) ethyleenglycol (EG) in het drinkwater en eveneens een Ca^{2+}-rijk dieet gevoerd gedurende 28 dagen. Echter, kristalafzetting in de nier werd niet waargenomen. Concluderend, **hoofdstuk 3** laat zien dat Ca^{2+}-bindende eiwitfragmenten gebruikt kunnen worden om Ca^{2+} te binden binnen fysiologische concentraties. Geoptimaliseerde Ca^{2+}-bindende eiwitfragmenten dienen getest te worden in alternatieve muismodellen waarin nierstenen beter vormen dan in de hier gepresenteerde studie.

Het nauwkeurig instellen van de Mg^{2+} heropname in het distaal convoluut

Eerdere genoom-brede associatiestudies (GWAS) hebben een associatie geïdentificeerd tussen ARL15 en de urinaire Mg^{2+} uitscheiding in zeven Europese cohorten van totaal 9.099 individuen. ARL15 is aanwezig in de lis van Henle en het distaal convoluut van de nier, waar het mogelijkerwijs betrokken is bij de heropname van Mg^{2+}. ARL15 behoort tot de superfamilie kleine GTPases en bindt mogelijk Mg^{2+}. Om de functie van ARL15 in de nier beter te begrijpen werden in **hoofdstuk 4** muizen gebruikt die over een heterozygote uitschakeling van het *Arl15* gen beschikken (*Arl15*$^{+/-}$). Muizen zonder het *Arl15* gen sterven na geboorte. *Arl15* wordt aangemaakt in meerdere weefsels, en met name in de longen, buikvet, milt, testis en nieren. *Arl15*$^{+/-}$ muizen die blootgesteld werden aan een vetrijk dieet vertoonden geen significante veranderingen in de hoeveelheid Mg^{2+} in het bloedplasma of in de uitscheiding van Mg^{2+} in de urine gedurende 24-uur, ten opzichte van gezonde muizen. Daarnaast werden er geen significante verschillen waargenomen in aanwezigheid van genen betrokken bij de Mg^{2+}-balans, bij metabolisme of bij membraantransport tussen de nieren van *Arl15*$^{+/-}$ en gezonde muizen op een

vetrijk of vetarm dieet. Samenvattend, onze resultaten tonen aan dat *Arl15*$^{+/-}$ muizen beschikken over vergelijkbare erfelijke eigenschappen als gezonde muizen, en dat zij geen abnormaliteiten vertonen wat betreft de Mg^{2+} heropname in de nier.

ARL15 als nieuwe interactiepartner van CNNM

Door gebruik te maken van biochemische bindingstudies, waaronder de zogeheten (nabijheid-afhankelijke) biotine identificatie (BioID) en co-immunoprecipitatie, hebben wij aan kunnen tonen dat ARL15 aan eiwitten uit de CNNM-familie bindt. CNNMs staan erom bekend het Mg^{2+} transport te regelen aan het basolaterale membraan van niercellen. In **hoofdstuk 5** is onderzocht hoe ARL15 de activiteit van deze CNNM eiwitten reguleert. Met behulp van immunohistochemische kleuringen van nieren van de muis werd aangetoond dat CNNM2 en ARL15 samen aanwezig zijn in distaal convoluutcellen. Uit co-immunoprecipitatie experimenten bleek dat ARL15 voornamelijk bindt met het CBS2 domein van CNNM. Onze BioID resultaten suggereren dat ARL15 betrokken is bij N-gebonden glycosylering. Een verhoogde aanwezigheid van ARL15 resulteerde in een verhoogde glycosylering van CNNM3 eiwitten in humane embryonale niercellen (HEK293). De functionele consequenties van ARL15-afhankelijke glycosylering werden onderzocht middels experimenten met een stabiel ^{25}Mg isotoop. Er was een significante vermindering van Mg^{2+} opname bij verhoogde aanwezigheid van ARL15 in meerdere nierkankercellijnen, en een hogere Mg^{2+} opname wanneer ARL15 was uitgeschakeld. Bovendien was er een verstoorde glycosylering van CNNM3 bij uitschakeling van ARL15. Tezamen suggereren onze resultaten dat ARL15 het Mg^{2+} transport in het distaal convoluut reguleert door de activiteit van CNNM eiwitten te bepalen.

Concluderend hebben de studies beschreven in dit proefschrift geleid tot nieuwe inzichten in de mechanismen achter Na^{+} heropname in de proximale tubulus bij het gebruik van SGLT2 remmers. Daarnaast is een eerste stap gezet in het opzetten van een vernieuwende benadering voor de preventie van nierstenen. Tot slot is er een nieuw regulatiemechanisme van Mg^{2+} heropname in het distaal convoluut aan het licht gebracht.

8

List of Abbreviations

List of Publications

Curriculum vitae

Research data management

RIMLS PhD portfolio

List of abbreviations

A

A	Alanine
ACE	Angiotensin-converting enzyme
Adipor1	Adiponectin receptor 1
Adipor2	Adiponectin receptor 2
Adrb3	Beta-3 adrenergic receptor
Afr1	ADP ribosylation factor 1
Afr6	ADP ribosylation factor 6
ADP	Adenosine diphosphate
AMP	Adenosine monophosphate
ANOVA	Analysis of variance
AQP1	Aquaporin-1
AQP2	Aquaporin-2
ARL15	ADP ribosylation factor-like GTPase 15
Arfgef-1	ADP ribosylation factor guanine nucleotide exchange factor 1
Arfgef-2	ADP ribosylation factor guanine nucleotide exchange factor 2
ATP	Adenosine triphosphate
Atp1a1	ATPase sodium potassium transporting subunit alpha 1
Atp1b1	ATPase sodium potassium transporting subunit beta 1

B

BCA	Bicinchoninic acid
BD	Brownian dynamics
B4GALT1	Beta-1,4-Galactosyltransferase 1
BioID	Biotin identification
BioGRID	Biological general repository for interaction datasets
BP	Blood pressure
BSA	Bovine serum albumin

C

CA	Carbonic anhydrase
CANA	Canagliflozin
Ca^{2+}	Calcium
cAMP	Cyclic adenosine monophosphate
CaP	Calcium phosphate
CaOx	Calcium oxalate
CBS	Cystathionine-β-synthase
CD	Collecting duct

CD	Circular dichroism (Chapter 3)
cDNA	Complementary DNA
Cl^-	Chloride
CNBH	Cyclic nucleotide binding homology
CNNM1	Cyclin and CBS domain divalent metal cation transport mediator 1
CNNM2	Cyclin and CBS domain divalent metal cation transport mediator 2
CNNM3	Cyclin and CBS domain divalent metal cation transport mediator 3
CNNM4	Cyclin and CBS domain divalent metal cation transport mediator 4
CNT	Connecting tubule
CRISPR	Clustered regularly interspaced short palindromic repeat
Cldn16	Claudin16
Cldn19	Claudin19
COM	Calcium oxalate monohydrate
Cpt1	Carnitine palmitoyltransferase 1
Cpt	Carnitine palmitoyltransferase 2
C-terminal	carboxyl terminal

D

D	Aspartic acid
DAPA	Dapagliflozin
DARS	Decoys as a reference state
DCT	Distal convoluted tubule
DMEM	Dulbecco's modified eagle's medium
DPM1	Dolichol phosphate mannosyltransferase subunit 1
DMSO	Dimethyl sulfoxide
DNA	Deoxyribonucleic acid
Dol-Man	Dolichol mannose
Dol-P-Man	Dolichol phosphate mannose
DTT	Dithiothreitol
DUF21	Domain of unknown function-21

E

E	Glutamic acid
EDTA	Ethylene diamine tetra acetic acid
EGF	Epidermal growth factor
GFP	Green fluorescent protein
EGTA	Ethylene glycol tetra acetic acid
EG	Ethylene glycol
Ele	Electrostatic energy of the representative complex
ElDesE	Electrostatic desolvation energy of the representative complex

EMPA	Empagliflozin
EmPAI	Exponentially modified protein abundance index
ENaCα	Epithelial sodium channel α
ENaCβ	Epithelial sodium channel β
ENaCγ	Epithelial sodium channel γ
Endo H	Endoglycosidase H
ER	Endoplasmic reticulum

F

F	Phenylalanine
FACS	Fluorescence activated cell sorting
Fabp1	Fatty acid-binding protein 1
FDA	Food and drug administration
FITC	Fluorescein isothiocyanate
FLS	Fatty liver shionogi
FXYD2	FXYD domain containing ion transport regulator 2

G

G	Glucose (Chapter 1)
G	Glycine (Chapter 3)
G	Glomerulus (Chapter 5)
GDP	Guanosine diphosphate
GTP	Guanosine-5′-triphosphate
GDP-Man	GDP-mannose
GFR	Gomerular filtration rate
GAPDH	Glyceraldehyde 3 phosphate dehydrogenase
GLUT1	Glucose transporter 1
GLUT2	Glucose transporter 2
GK	Goto-kakizaki
GO	Gene ontology
GST	Glutathione S-transferase
GWAS	Genome wide association studies

H

HC	High calcium diet
HbA1c	Hemoglobin A1C
HCO_3^-	Bicarbonate
HDL	High-density lipoprotein
HE	Hematoxylin and eosin
HNO_3	Nitric acid

HF	High fat diet
HK-2	Human kidney-2
H_2O_2	Hydrogen peroxide
HSH	Hypomagnesemia with secondary hypocalcemia
HyDesE	Hydrophobic desolvation energy of the representative complex

I

I	Isoleucine
IPRA	Ipragliflozin
I-TASSER	Iterative threading ASSEmbly refinement

K

K	Lysine
K^+	Potassium
KEGG	Kyoto encyclopedia of genes and genomes
KDa	Kilo Dalton
KK/A^y	Diabetic KK and lethal yellow

L

L	Leucine
ICP-MS	Inductively coupled plasma mass spectrometry
LD	Light-dark
LF	Low fat diet
LMAN1	Lectin, mannose binding 1
LUSEO	Luseogliflozin

M

Mg^{2+}	Magnesium
MQ	Milli-Q water
MC	Metabolic cage

N

N	Asparagine
Na^+	Sodium
NAM	Nicotinamide
NBC	Sodium bicarbonate cotransporter
NC	Normal calcium diet
NADPH	Nicotinamide adenine dinucleotide phosphate
NCC	Sodium chloride cotransporter
NCX1	Sodium calcium exchanger 1

NHE3	Sodium hydrogen exchanger 3
NKCC1	Sodium potassium chloride cotransporter 1
NKCC2	Sodium potassium chloride cotransporter 2
NaPi-2a	Sodium phosphate cotransporter

O

OLETF	Otsuka long-evans tokushima fatty
OPLS	Optimized Potentials for Liquid Simulations
OPN	Osteopontin

P

P	Proline
PBS	Phosphate-buffered saline
PCR	Polymerase chain reaction
P_i	Inorganic phosphate
Pepck	Phosphoenolpyruvate carboxy kinase
PT	Proximal tubule
PVALB	Parvalbumin
PEPCK	Phospho-enolpyruvate carboxykinase
Plin1	Perilipin 1
PNGase F	N-glycosidse F
PMCA	Plasma membrane calcium-ATPase
PNGase F	Peptide N-glycosidase F
PTP	Protein tyrosine phosphatases
PRL1	Phosphate of the regenerating liver1
PRL2	Phosphate of the regenerating liver2

R

R	Arginine
RAAS	Renin-angiotensin-aldosterone system
Repr	Representative chosen
ReprE	Total interaction energy of the chosen representative
RMSD	Root-mean-square deviation
RNA	Ribonucleic acid
ROS	Reactive oxygen species
RPN1	Dolichyl-diphospho-oligosaccharide
RT	Reverse transcriptase
RT-qPCR	Real-time quantitative polymerase chain reaction

S

S	Serine
SBP	Systolic blood pressure
SD	Sprague dawley
SEM	Standard error of the mean
SGLT1	Sodium glucose cotransporter 1
SGLT2	Sodium glucose cotransporter 2
sgRNA	Single guide RNA
Scnn1a	Sodium channel epithelial 1 subunit alpha
Scnn1b	Sodium channel epithelial 1 subunit beta
Scnn1g	Sodium channel epithelial 1 subunit gamma
Slc2a2	Solute carrier family 2 member 2
Slc5a1	Solute carrier family 5 member 1
Slc5a2	Solute carrier family 5 member 2
Slc12a1	Solute carrier family 12 member 1
Slc12a3	Solute carrier family 12 member 3
Slc18a1	Solute carrier family 8 member 1
Slc26a6	Solute carrier family 26 member 6
Slc34a1	Solute carrier family 34 member 1
Slc41a1	Solute carrier family 41 member 1
Slc41a3	Solute carrier family 41 member 3
STT3A	STT3 oligosaccharyltransferase complex catalytic subunits A
STT3B	STT3 oligosaccharyltransferase complex catalytic subunits B
STZ	Streptozotocin

T

TCL	Total cell lysis
T1DM	Type 1 diabetes mellitus
T2DM	Type 2 diabetes mellitus
TAL	Thick ascending limb of Henle's loop
TOFO	Tofogliflozin
TRPM6	Transient receptor potential cation channel subfamily M member 6
TRPM7	Transient receptor potential cation channel subfamily M member 7
TRPV5	Transient receptor potential cation channel subfamily V member 5

U

UT-A1	Urea transporter-A1

V

V	Valine

W

WK	Wistar kyoto
WT	Wildtype
WTD	Western-type diet

Y

Y	Tyrosine

Z

ZDF	Zucker diabetic fatty
Zn^{2+}	Zinc

Protein and gene names used within this thesis are abbreviated and formatted according to the guidelines depicted in the genetic nomenclature guide published by *Trends in Genetics*. An example is depicted below in Table 1, i.e. the gene *ARL15* with its corresponding protein ADP ribosylation factor-like GTPase 15 (ARL15) as example.

Table 1: Gene and protein abbreviations & nomenclature

Species	Gene	Protein
Human (Homo sapiens)[1]	ARL15	ARL15
Mouse (Mus musculus)[2]	Arl15	ARL15
Zebrafish (Danio rero)[3]	arl15	ARL15

1. McAlpine P: Genetic nomenclature guide. Human. *Trends Genet.* 39–42, 1995
2. Davisson MT: Genetic nomenclature guide. Mouse. *Trends Genet.* 35–38, 1995
3. Mullins M: Genetic nomenclature guide. Zebrafish. *Trends Genet.* 31–32, 1995

List of publications

1. **Ma C**, de Baaij JHF, Millar JP, Gault AV, de Galan EB, Bindels RJM, Hoenderop JGJ. Effect of dapagliflozin treatment on the expression of renal Na^+ transporters/channels on high-fat diet diabetic mice. *Nephron* 2019;142:51–60

2. **Ma C**[#], Yevgen Zolotarov[#], Irene Gonzalez-Recio, Serge Hardy, Gijs Franken, Elie Kostantin, Femke Latta, Noriko Uetani, Jean-François Côté, Irene Díaz Moreno, Antonio Díaz Quintana, Joost GJ Hoenderop, Luis Alfonso Martínez-Cruz, Michel L. Tremblay[#], Jeroen HF de Baaij[#]. ARL15 regulates CNNM-dependent Mg^{2+} transport by modulating its N-linked glycosylation. (*Submitted*)

3. Mingxue zhou, Yutong Liu, **Chao Ma***. Distinct nuclear architecture of photoreceptors and light-induced behaviors in different strains of mice. (*Submitted*)

4. **Chao Ma**, Sanédy Simon, Caro Bos, René J.M. Bindels, Joost G.J. Hoenderop,Jenny van der Wijst. Development of Ca^{2+}-binding peptides to control urinary Ca^{2+} concentration to prevent kidney stone formation. (*In preparation*)

5. **Chao Ma**, Ying Bai, Liz Bentley, René JM Bindels, Roger D Cox, Joost GJ Hoenderop, Jeroen HF de Baaij. ARL15 heterozygous mice exhibit normal electrolyte homeostasis. (*In preparation*)

[#]Authors contributed equally to this work; *Corresponding author

Curriculum vitae

Chao Ma was born in Jilin, China, on the 17th of October 1988. After graduating from high school, he obtained his bachelor with a major in Resource and Environmental Sciences at Jilin Agriculture University in Jilin, China. In 2012, he decided to pursue his interest in life science and joined Professor Shuping Zhang's lab at Tsinghua University in Beijing, China. During his master study, he focused on examining the tissue distribution of Renalase in *ApoE*$^{-/-}$ mice fed a high-fat diet and the effect of valsartan on the expression of Renalase. He found that Renalase is a potential-related gene of lipid metabolism and atherosclerosis, and it may be the possible molecular target of valsartan to help stabilize atherosclerotic plaque. His master research consisted of studying the function of a novel Mitochondria-localized Glutamine Acid Rich Protein (MGARP) in the development of the retina, with emphasis on photoreceptor cells, by using in utero electroporation in *Mgapr*$^{-/-}$ embryonic mice. In 2016, Chao joined the department of Physiology at the Radboud university medical center (Radboudumc) as a PhD candidate. Under the supervision of Prof. dr. Joost Hoenderop, Dr. Jeroen de Baaij and Dr. Jenny van der Wijst, his research focused on investigating the effect of dapagliflozin treatment on the expression of renal sodium transporters/channels on high-fat diet diabetic mice. This part of work provides insights on the treatment of both hypertension and diabetes in Type 2 diabetes patients. In another study, he developed several small peptides with optimized Ca^{2+}-binding affinity to act as Ca^{2+} buffers in Henle's loop, without affecting serum Ca^{2+} levels. This may provide the first evidence for an effective approach to further study treatment and prevention of kidney stones. His PhD research work also consists of studying the functional implication of ARL15 for CNNMs-mediated Mg^{2+} transport. Chao presented his work by oral and poster presentations at scientific conferences. In 2019, he received the travel grant to visit the American Society of Nephrology meeting in Washington, D.C., USA. Additionally, Chao successfully completed the PhD training program of the RIMLS graduate school and supervised four master students and five undergraduate students from Biomedical Sciences and Medical Biology studies.

Research data management

The data generated during my PhD project at the Radboudumc were documented according to the Findable, Accessible, Interoperable and Reusable (FAIR) guiding principles.[1] All the primary and processed data obtained during my PhD work are stored on the local digital servers which belong to the department of Physiology and Radboudumc. In addition, all data were accessible on Labguru, an electronic lab book, which is managed and supported by the Information and Communication Technology (ICT) unit of Radboudumc and daily backed-up on local Radboudumc servers. The animal studies described in **Chapter 2, Chapters 3 and 4** were approved by the University of Ulster Animal Ethics Review Committee, the Animal Ethics Board and the Central Animal Laboratory of the Radboudumc and the MRC Harwell Institute Ethical Review Committee and the MRC Harwell Animal Welfare, all in agreement with the Experiments on Animals Act (Wet op de dierproeven, Wod). To make sure the data is accessible to the associated staff, all data (including raw data, descriptive files, figures, and file names) is stored and archived in accordance with the protocols of the department of Physiology.

1. Wilkinson MD, Dumontier M, Aalbersberg IJ, *et al*. The FAIR Guiding Principles for scientific data management and stewardship. *Sci Data* 2016; 3: 160018

RIMLS PhD portfolio

Radboud Institute for Molecular Life Sciences
PhD portfolio

Institute for Molecular Life Sciences
Radboudumc

Name PhD student:	Chao Ma	**PhD period:**	11/01/2016 – 11/01/2020
Department:	Physiology	**Promotor:**	Prof. dr. J.G.J Hoenderop
Research School:	Radboud Institute for Molecular Life Sciences	**Co-promotors:**	Dr. J.H.F. de Baaij Dr. J.A.J van der Wijst

TRAINING ACTIVITIES	**Year(s)**	**ECTS**
a) Courses & Workshops		
- RIMLS Graduate Course	2016	1
- Winterschool Nierstichting	2017	1.5
- Microscopy Imaging Course	2017	1.0
- Within Sight of my PhD Course	2017	1.0
- Scientific Integrity Course	2018	1.0
- How to sell your science	2018	0.5
b) Seminars & lectures		
- RIMLS Radboud Research Rounds / Lecture Series	2016-2019	1.6
- RIMLS Seminars	2016-2019	1.2
- Renal Disorder Theme Meeting	2016-2019	2.2
- Meet the expert	2017-2019	1.0
c) (Inter)national Symposia & Congresses		
- RIMLS Radboud New Frontiers	2016-2019	3.0
- RIMLS PhD retreat #	2016-2019	3.0
- CNNM meeting *#	2019	2.0
- ASN Kidney Week: Washington DC, USA #	2019	2.0
- Radboud Science Day (Molecular Physiology group)	2016-2020	1.5
- Radboud Science Day	2017	1.0
d) Other		
- PhD Thesis Committee Meeting	2016-2019	0.5
- World Kidney Day	2016-2019	1.5

TEACHING ACTIVITIES

e) Students

- Supervision Milou Smits	2018	2
- Supervision Sidra Kashif	2018	2
- Supervision Shirin Moster	2018-2019	2
- Supervision Sanedy Simon	2019	1
- Supervision minor students (5x)	2018-2019	1

TOTAL	34.5

Oral and poster presentation are indicated with * and # after the name of the activity, respectively

9

Dankwoord

Acknowledgements

致谢

Yes, approved, this is the title of the email I got from my supervisor, professor, and also my friend, Prof. Dr. Joost Hoenderop, when my thesis was approved by thesis committee. With some pride, I am very happy with my thesis and my work. In my time in physiology, I have learned and matured a lot both scientifically and personally and I am very grateful to many people who helped me along the way. In this chapter, I would therefore like to express my gratitude to my supervisors, colleagues, collaborators, friends, and family who motivated, helped, and supported me and thus, in their own way, contributed to this thesis.

First and foremost, I would like to express my appreciation to Prof. Dr. Joost Hoenderop, Prof Dr. René Bindels, and my co-promoter Dr. Jeroen de Baaij and Dr. Jenny Van der Wijst for their guidance and support throughout my 4 years work in the physiology department. **Joost**, thank you for helping me so much in these years. Over the years, I learned a lot from you. If I use one word to describe you, I will use discipline to describe you. I always believe that discipline is the most important value and character that a successful man should have. If I use five words to describe you, I will use discipline, hardworking, leadership, determined, and optimistic to describe you. You always start to work early in the morning. Most of the time, I can always receive your email reply very fast wherever you are in the world. We can always get support from you. Whenever we have difficulties, you can always give us useful suggestions and find positive perspectives. You are such a hardworking man who set an excellent role model for us. Every time I feel tired, you motivated me to have the energy to work again and never give up. Thank you for checking my thesis point by point. I feel so touched that you even helped me to find my mistakes in my references, there are around 500 references in total in my thesis. Thanks for the ideas and inputs you provided to my PhD study, and your strong leadership in the work, and your advice to my life. I am very happy to work and talk with you both at work and after work. I never have the feeling that you are my professor or boss, however, I always regard you as a very good friend who always support me, cheer up me, and steer me to the correct direction both scientifically and personally. Therefore, I am not surprised that you won the University Teaching Prize, and you also made a great contribution to the physiology study and published a lot of great papers in top journals. You are a perfect example of showing that you can be excellent in everything you put effort into. **Jeroen**, it's really nice that I start to work together with you in my second year. You are such an amazing and smart guy with unbelievable leadership. Communicating with you is such a cozy thing that I enjoyed a lot. Thank you for guiding me for the ARL15 and CNNM study. We finally made it into a story. You give me so many good ideas and inspired me so much. I still remember in the CNNM meeting, when I was giving a presentation, you and Joost gave me so many eye contacts and inspired me a lot. I have the feeling that you and Joost are even more nervous than me. At that point, I feel so happy and lucky to have two supervisors like you two people. I do enjoy the nice talks with you at the lunch time, work discussion, drinking beers in Nijmegen, having Chinese food, and we had very a nice time in Washington D.C in the ASN meeting. **Jenny**, you started to supervise me in my third

year, you are so nice, patience, and sweet. You are always there to help us and listen to us. I do enjoy the nice talks with you in the coffee break time, lunch time, experiments time, work discussion, and the amazing dinner at your home. You also give me a lot of good ideas on my projects. Now, I also learned a lot of chemistry knowledge through our kidney stone project. We met almost weekly in the last few months to talk about my thesis. Thank you so much for helping me to correct the structure of the thesis, mistakes, and providing great ideas on how to make the figures better. Now, I am much more confident in writing than before. **René**, thank you for your great vision, leadership, and your extraordinary ability to our RIMLS institute and our department. We appreciate the efforts taken by you. We love our human oriented institute and department so much. Especially as foreigners, I never feel lonely. I really enjoy the talks with you in the work meetings and the dinner in the ASN meeting.

Dr. **Jo Zhou**, thank you for mentoring me for four years. In these four years, you gave me a lot of useful suggestions and advices to help me to master my PhD work and my future career choice. I do enjoy the nice talks with you. Thank you very much.

The collaborations with other research groups have been of great benefit for my work in my PhD study. I am grateful to all of the people who were directly or indirectly involved in and contributed to my projects. Prof. Dr. **Michel Tremblay**, thank you for your inputs, ideas, and scientific discussions on the ARL15 and CNNM project! It has been wonderful to work together with your team. Your enthusiasm in science inspired me a lot. Also **Eugene**, it's really nice to collaborate with you for our ARL15 and CNNM story. You are a hard worker and an extremely motivated guy. We finally made our ARL15 and CNNM project into a very nice story and good luck with your PhD in Montreal. **Serge**, you made a lot of unbelievable contributions to CNNM and PRL study, I am really happy to see that you addressed a detailed mechanism study of ATP, PRL, and AMPK/mTORC2 pathway at various levels, which will definitely boost the study of magnesium, PRL, and CNNM. I am looking forward to seeing more and more papers from you. Dr. **Alfonso Martínez de la Cruz**, thanks for all of the works you did for the structure biology part of the ARL15 and CNNM paper. I do enjoy the nice scientific discussion, nice talks with you in our zoom meeting and CNNM meeting. Structure biologists are our best friends, your knowledge and findings on the structure of CNNM, ARL15, and PRL will always be highly appreciated. Dr. **Roger Cox** and Dr. **Ying Bai**, thanks for providing us with *Arl15*$^{+/-}$ mice samples, these samples boost our study and navigated us to the correct direction. We will definitely combine all of our data and make it into a nice story. Prof. Dr. **Roland Brock** and **Sander Van Asbeck**, thanks for your technical supports and suggestions for my kidney stone project.

Luke, it's really nice to meet you in the Netherlands. In the past few years, we went to so many places and had so many nice memories. The nice beer, food, and traveling in Rotterdam, Arnhem, Haarlem, Nijmegen, and Doetinchem. In my first year, you helped me so much in my SGLT2 project, helping me to involve in European lifestyle, and my English. Through time, we develop very good friendships, you became a true friend, and

of course now my paranimf, and we still keep in touch although you left our department. Thanks for your support in these years, especially your help in polishing my cover letter and CV for my postdoc position. Thank you for your nice present which will definitely help me to know more about Los Angeles very fast. By the way, I still remember our plan to travel in the USA and to go to visit Marco in Mexico next year, hope to see you soon. I wish you all the best for your life in the Netherlands with **Emma**. And I am sure that we will keep in touch and keep seeing each other. Mi amigos**, Paco, Juan, Sara, Maria**, you guys have very strong postdoc power. **Paco**, you are a very funny guy, I still remember we can't understand each other's English in the beginning, and we always need Eric V or Caro to be our translator, but this did not affect our friendship. I do enjoy the nice time with you playing football, funny talks, watching the World cup, yearly beer night, and your supports in my PhD study. I am very happy that you are enjoying your nice life with your wife and your son **Daan A**. But, by the way, it seems that we still can't understand each other's English, even until now. **Juan**, I always have the feeling that you are on your way to travelling or on your way back from travelling. We had a nice time in the Düsseldorf Christmas market and enjoyed the nice beer and wine, Germany Schweinhaxen, and Japanese noodles in Düsseldorf. You are my true friend, and of course now my paranimf. I do enjoy the nice talks with you at dinner time after work, and thanks for your traveling suggestions on my tour around Europe. We should always keep in touch, and I am sure I will meet you again in California and China. I hope you will enjoy your life in either Europe or Argentina in the future. **Sara**, I do enjoy the nice talks with you at lunch time, drinking beers at Olivier in Utrecht with the gang and your boyfriend. You are a very outgoing lady who can always cheer people up. I always have the feeling that you can always give me a lot of useful suggestions and helps whenever I need help. Thanks for your useful and good suggestions for my postdoc searching. I am quite happy that you are enjoying a nice time in Switzerland. Like you said science is small, I am sure we will meet each other one day. **Maria**, my neighbor in my last few months in our department. We also had a lot of nice talks at lunch time. Thank you for your supports and kind suggestions for my PhD work and postdoc searching. I wish you all the best for the future; you've been and always will be a great friend to me. **Sami** and **Eric V**, the Cilia Team. **Sami**, we had so many talks outside and inside the lab, you are a very good company after work in the lab. Both of us are foreigners in the lab, so we always support each other and help each other. I do enjoy the travelling with you, playing football with you. Thanks for the nice suggestions you gave me in the Netherlands. In my last few days in the Netherlands, we met in Maastricht and made a lot of nice pictures, all of these are very nice memories of my life. I am very happy with you on your success in your postdoc career by winning many grants and publishing many papers. In the second year of my PhD, we made the plan to travel to Paris, but later, we didn't manage to do it. In two months, you will come to the USA; we should travel in the USA as we planned in Amsterdam. I hope all is going well for you, and we can always have a chat whenever we want to talk to each other. **Eric V**, my dear friend, we had

a lot of nice memories together. Talking together during coffee breaks, drinking beers at Olivier in Utrecht, Arnhem, and my place, attending your marriage party and gender reveal party, and the yearly drink in Arnhem. We also had a very nice time in Washington in the ASN meeting. Thank you for guiding me around Washington, and we made many nice pictures together. All of these consist of my good memories in the Netherlands. I am very happy that you are enjoying your new job, your life with **Mirte** and **Lotte V**. I wish you and your family all the best for the future and I am sure that we will keep in touch and keep seeing each other. You are always welcome wherever I am living. **Hacene**, it's also very nice to meet you in the Netherlands. We both work in the metabolism team. It has been wonderful to work together with you during these past few years although we didn't work together directly. You were a great company inside the lab after work and outside the lab on the weekends. We explored Nijmegen so much and made a lot of nice pictures. Thanks for your support in these years. I am very happy that you are enjoying your time with your family and your work in Algeria. You've been and always will be a great friend to me. I wish you all the best for your PhD and your future and I am always happy to hear from you and talk to you. **Valentina**, a hard worker, and extremely motivated PhD. You were a great company in the lab in the evening and weekend. Although we haven't worked directly together on a project, yet I cherish good memories with you such as the nice talks during the breaks, dinner time, drinking beers at Olivier in Utrecht, and Arnhem. I wish you all the best for your PhD and scientific career. **Marco**, My Spanish learning was initiated by you. I still remember the first word you taught me was Adios, mi amigo. Together with you, and Luke, we went to many bars and restaurants in Nijmegen. Hopefully, Luke and I can manage to go to visit you in Mexico. I wish you all the best for your work and life. **Steef**, we work in the same team, you are a very smart guy with critical thinking. I enjoyed the nice talks with you and thanks for your suggestions on my projects. It has been great to work together with you in the past few years. I had a great time sharing my data and having scientific discussions with you. **Omar**, you are the first people who went to pick me up in Nijmegen, and introduced the people in the lab to me. Your enthusiasm and sense of humor did motivate me a lot at the beginning of my PhD study. It has been nice to work together with you in the sodium team. **Lisanne**, you are a very warmhearted girl. I do enjoy the nice talks with you in the coffee breaks, and I hope that you can find a good job, and always be happy. **Gijs**, you are a very funny guy. I found that you always have a lot of topics to talk with different people. It was nice to work with you to learn more about CNNM protein, and we are making a lot of progress on it. Thank you for your immunocytochemistry results for our ARL15 and CNNM story, and also thanks for giving a lot of good suggestions on improving the manuscript. It was really a lot of fun to have the CNNM meeting with you, drink beers after the meeting, and the nice talks with the collaborators who are working very hard on elucidating the function of CNNM. **Lynette**, ARL15 is a great protein, I am very happy to work together with you to investigate the function of ARL15. It has been a lot of fun to share the data, have scientific dis-

cussion with you. I am very looking forward to seeing your great story on ARL15 kidney-specific knockout mice. **Lotte**, we may not have worked directly together on a project, yet we both study novel genes related to hypomagnesium. I am very looking forward to your pinkbar protein stories. I do like the nice talks with you on the weekend, coffee break time, lunch time, and the glow festival in Eindhoven. You still need to tell more about your stories and experience in China. With many colleagues, I have had the privilege to develop amazing friendships. Just like those people mentioned above, this is also true for **Michael**, **Sjoerd, Mark,** and **Eric B**. Together with you guys, **Luke**, **Paco,** and **Eric V**, we have the yearly beer drink event in Arnhem before Christmas, lots of nice talks, food & drinks together, we had a lot of fun times and I hope they continue!

Femke, thank you so very much for helping me in the molecular works. I do enjoy our nice talks in the coffee break, sharing my data with you, the great inputs from you, and the nice scientific talks in the lab meeting. You've been and always will be a great friend to me. **Caro**, you also helped me a lot on animal studies and the staining. It has been great to work together with you and be your neighbors in my first two years. I do enjoy the nice talks with you at lunch time, coffee break times, and physiology events. You act like a running sun who always bright other people's life. **Irene**, thank you for making our department so organized, and the items we ordered delivered in good condition. I also appreciate the greetings from you through Facebook at the beginning of this year. **Rosanne**, thanks for helping me to arrange everything at the beginning of my PhD work. You made my life much easier. **Rachel**, **Véronique**, **Judith**, and **Janneke**, thanks for arranging the meetings, events, and paperwork for our department. Your contributions are highly appreciated. **Jojanneke**, thanks for organizing the teaching, I feel very happy and honored to be involved in the teaching. **Nicolai,** I enjoy the nice talks with you in the meetings and thank you for your tips and suggestions on my career choice.

Sidra, **Milou**, **Shirin**, and **Sanedy**, you guys are unbelievably good, smart, and hard-working master students. I am so honored to supervise you. Thanks for the contributions you made to the ARL15 and CNNM story, and the kidney stone story.

Furthermore, I would like to express my appreciation to all the rest who bring/brought our department to the 'next level', **Andreas, Elja, Charlotte, Claudia, Mohammad, Daan, Ellen, Frans, Kim, Laura, Niky, Barnabas, Margo, Marjolein, Anique, Lara, Wouter , Peter, Selma, and Theun,** and all the people from Integrative Physiology and anyone that I might have forgotten!

Tommy, my language partner in Tsinghua University, you are the first foreigner I met in Beijing, and I always believed that I wouldn't come to the Netherlands if I didn't meet in China. Our friendship starts in China, and we had a lot of nice talks in Tsinghua University and in Beijing. I wish you all the best for your future and your life in the Netherlands and hope we keep on seeing and messaging each other. You've been and always will be a great friend to me, our time together in China and the Netherlands were unbelievably great! Thank you for recommending me the Dutch universities, then, I have the oppor-

tunities to come to the Netherlands where I met a lot of amazing people and had an incredibly great memory. I will always cherish my memories in the Netherlands in my life.

Brazilian Omar, it was super nice to meet you on the 7th floor of RIMLS. We had a lot of nice talks after work and had a lot of good time in Nijmegen and Maastricht. You are a very hardworking and motivated PhD; I wish you all the best for your life in the Netherlands and your research career.

Hans, my landlord, I am the only guy who stayed at your place for more than one year, and it's 4 years in total in the end. We had a lot of nice memories in Nijmegen and Germany. Thanks for your help, suggestions, nice dinners, and supports in these four years. I wish you all the best for your life. You are always welcome wherever I live.

宋春喜大哥，我常常想，我们是什么样的缘分，能在荷兰交到您这个忘年交，记得一次吃饭，您说过您80年代在我的老家当过兵，我想只有用缘分来解释我们在荷兰的相遇。您通过自己的努力，在荷兰有了今日的成就，祝您的公司更上一层楼。我也随时会支持您并帮助您实现将传统中医发扬光大的梦想。

张老师，感谢您在我读硕士时候的教导，您对科研的严谨认真，一直影响着我，感谢您的培养。周明学师兄，感谢你这么多年来的帮助，是你带我入了生命科学的大门，在后来又给我了很多的帮助，永远都记得当年在北京时候，你给我的帮助。贾利云师姐，感谢你在张老师实验室教我做电转，免疫组化，你是一个好老师，很开心，你在郑州找到了自己的生活和工作方向。杨慧朋师兄，感谢你在分子生物学上对我的帮助，我们一起研究MGARP在视网膜中的作用，与你一起做实验，探讨科研问题，我很开心。李凌丹师姐，虽然我们没有直接的共同做过一个课题，但是，在实验室遇到你这个老乡真的很开心，我很喜欢午饭时，以及平时和你关于人生的探讨。吴放师兄，感谢你在清华对我的帮助，无论是生活上，学术上，你都给了我无尽的帮助。梁桐师兄，我们共同研究MGARP的作用，后来，一起来了欧洲，感谢你在瑞士的照顾，也恭喜你将自己的工作发表在顶级期刊上。李蕊师姐，我和梁桐师兄紧随你的步伐，来了欧洲，很开心你在欧洲找到自己的幸福。刘雨桐师妹，我们一起发表了很多文章，感谢你的帮助以及提供的想法。

苏卫朋，李杨，刘耀先，你们是我多年的挚友，每次有什么不开心的事情都会找你们聊天，你们都会给我很多鼓励与帮助，很感激你们，很开心遇到过你们，希望我们的友谊可以永存。

同时也要感激我的家人们，你们给了我无数的关爱与鼓励，你们也是我努力奋斗的动力源泉。

爸爸，妈妈，谢谢您们，感谢您们为了我的坚持，我的梦想，无条件的支持我。虽然我是家中唯一的孩子，但是，您们从没有限制过我对梦想的追求。虽然，您们担心我在国外会遇到各种坎坷，尤其还在异国他乡，没有父母的陪伴。但是，我已经长大，不能一直像孩童时期依偎在您们的身边，我要独身一人寻找更加宽阔的空间，创造人生的辉煌。正是因为昨天的分离，才有了我今天不一样的人生！感谢你们一直鼓励我，支持我，相信我，由于学习的原因，多年在国外不能在您们身边陪伴，每次想到这里，我都心有愧疚，所以，我常告诫自己要努力变得越来越优秀，成为父母的骄傲，不辜负您们对我的期待。最后，感激所有未能提及的，但是对我直接或间接有过帮助的人，感谢你们。

Institute for Molecular Life Sciences
Radboudumc

Institute for Molecular Life Sciences
Radboudumc